Caractérisation de la forme et de la surface de poudres laitières et céréalières : Relations entre propriétés et réactivité des particules

Ingrid Murrieta-Pazos

École Nationale Supérieure d'Agronomie et des Industries Alimentaires

Ecole Doctorale Sciences et Ingénierie Ressources Procédés Produits Environnement (RP2E)

Laboratoire d'Ingénierie des Biomolécules – LIBio
en collaboration avec le Centre RAPSODEE (Université de Toulouse-Mines, Albi)
Spécialité « Procédés biotechnologiques et alimentaires »

THESE

Présentée pour obtenir le grade de Docteur de l'Université de Lorraine

par

Ingrid MURRIETA PAZOS

Caractérisation de la forme et de la surface de poudres laitières et céréalières : Relations entre propriétés et réactivité des particules

Directeur de thèse: Joël SCHER (LIBio)
Directeur de thèse : Laurence GALET (Centre RAPSODEE)
Co-directeur de thèse : Claire GAIANI (LIBio)

Soutenue publiquement le 16 octobre 2012 devant la commission d'examen

Jury

Mme. I. Pezron (UTC)	Rapporteur
M. D. Poncelet (Oniris)	Rapporteur
M. J. Fages (Centre RAPSODEE)	President
M. B. Cuq (SupAgro)	Examinateur
Mme. C. Gaiani (LIBio)	Examinateur
Mme. L. Galet (Centre RAPSODEE)	Examinateur
M. J. Scher (LIBio)	Examinateur
M. E. Chávez (Nestlé)	Invité

TABLE OF CONTENT

Nomenclature

AFFE	After Free Fat Extraction
AFM	Atomic Force Microscopy
AMF	Anhydrous Milk Fat
AN	Acceptor Number
ASMP	Agglomerated Skim Milk Powder
ASMP	Aglomerated Standard Skim Milk Powder
a_w	Water Activity
AWMP	Agglomerated Whole Milk Powder
AWMP	Agglomerated Whole Milk Powder;
BET	Brunauer–Emmett–Tellet
CGI	Chromatographie Gazeuse Inverse
CLSM	Confocal Laser Scanning Microscopy
CP	Cream Powder
CR	Capillary Rise
DN	Donor Number
DSC	Differential Scanning Calorimetry
DVS	Dynamic Vapor Sorption
EDX	Energy Dispersive X-ray spectroscopy
ESCA/XPS	Spectroscopy for Chemical Analysis
ESEM	Enviromental Scanning Electron Microscopy
FID	Flame Ionization Detectors
GAB	Guggenheim-Anderson-Boer
GC	Gas Chromatography
HPLC	High Performance Liquid Chromatography
IGC	Inverse Gas Chromatography
IGC-ID	Inverse Gas Chromatography Infinite Dilution
ISO	International Organization for Standardization
MET	Microscopie Électronique en Transmission
MFA	Microscopie à Force Atomique
MPC	Milk Proteins Concentration
NL	Neutral Lipids

NMC	Native Micellar Casein
NWI	Native Whey Isolate
PL	Phospholipids
Ra	Mean Roughness
RH	Relative Humidity
RH	Relative Humidity
SCa	Sodium Caseinat
SDV	Sorption Dynamique de Vapeur
SEM	Scanning Electron Microscopy
SMP	Skim Milk Powder
SMPG	Skim Milk Powder Granulated
SPI	Soy Protein Isolate
SSMP	Standard Skim Milk Powder
SWMP	Standard Whole Milk Powder;
TEM	Transmission Electron Microscopy
THF	Tetrahydrofuran
ToF-SIMS	Time of Flight Secondary Ion Mass Spectrometry
TPC	Theoretical Protein Content
WMP	Whole Milk Powder
WMP	Whole Milk Powder
WMPG	Whole Milk Powder Granulated
WPC	Whey Protein Concentrate
XPS/ESCA	X-ray Photoelectron Spectroscopy Electron
CG	Caractérisation par Chromatographie Gazeuse
CGI	Energie de surface par Chromatographie Gazeuse Inverse
HR	Humidités Relatives
MC	Montée capillaire
MEB	Microscopie Electronique à Balayage
MEBE	Microscope Electronique à Balayage Environnemental
MFA	Microscope à Force Atomique
SPX	Mesure de la composition de surface par Spectroscopie des Photons X

LIST OF TABLES

LIST OF FIGURES

LIST OF EQUATIONS

I. INTRODUCTION

Ce travail a été effectué dans le cadre d'un programme ANR "Reactive Powder" ALIA-08 (Alimentation et Industries Alimentaires 2008), comprenant 3 thèses et un post-doctorat. Le projet a été développé au sein d'un consortium scientifique de 7 laboratoires spécialisés dans le domaine général des poudres et des poudres alimentaires (figure 1).

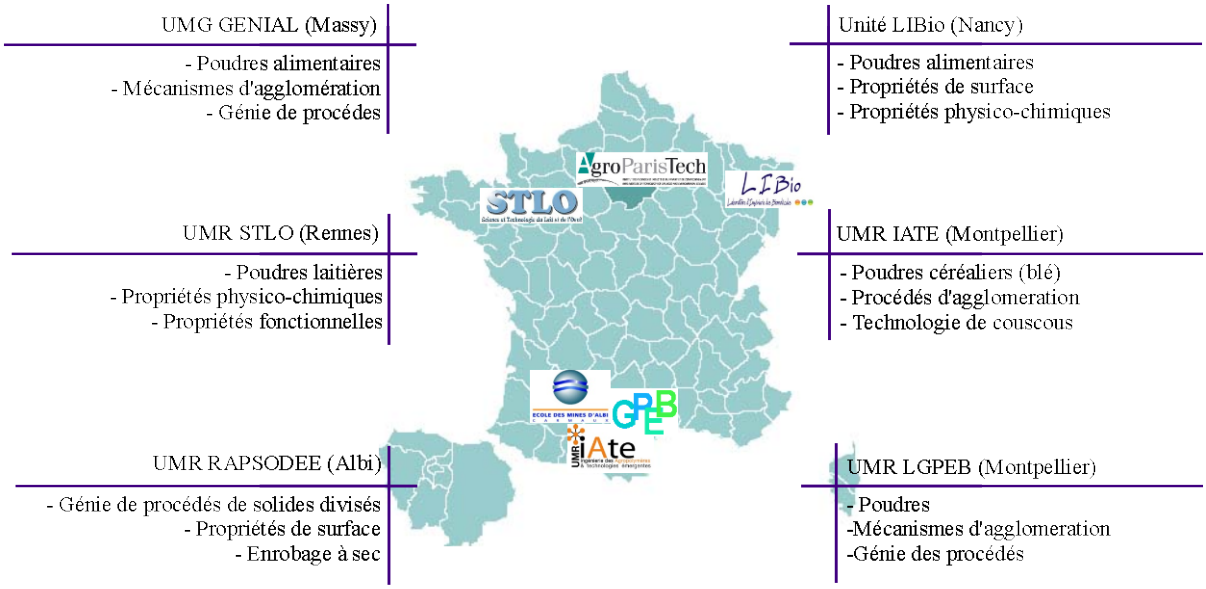

Figure 1. Laboratoires participant à l'ANR "Reactive Powder"

Le programme "Reactive Powder" a pour objectif d'étudier et de relier les propriétés de surface de poudres alimentaires (réactivité de surface) avec le mécanisme d'agglomération, et les principaux procédés d'obtention des poudres alimentaires (figure 2).

Le premier maillon de ce programme WP_1 (figure 2) dont fait l'objet ce travail, a été développé en collaboration entre le LIBio de l'Université de Lorraine-INPL à Nancy et le centre RAPSODEE CNRS Mines à Albi. La thèse s'est déroulée les 18 premièrs mois au LIBio et les 18 dernièrs mois au centre RAPSODEE. Ce travail est consacré au développement et à l'adaptation des techniques de caractérisation de surface aux particules alimentaires, afin d'étudier la réactivité de la surface des poudres alimentaires.

Depuis plusieurs années, de plus en plus d'études sont effectuées sur la caractérisation de propriétés de poudres alimentaires, notamment pour prédire et contrôler les propriétés fonctionnelles au moment de l'utilisation dans l'industrie et pour une meilleure qualité du produit final. La caractérisation des poudres est donc très importante pour l'évolution,

l'innovation et le développement des industries agroalimentaires. Cependant la plupart des études attribuaient les propriétés fonctionnelles à l'ensemble de la poudre. Toutefois, de récentes publications ont démontré que les propriétés fonctionnelles d'une poudre sont fortement reliées à la distribution des caractéristiques individuelles, et plus spécifiquement aux propriétés de surface.

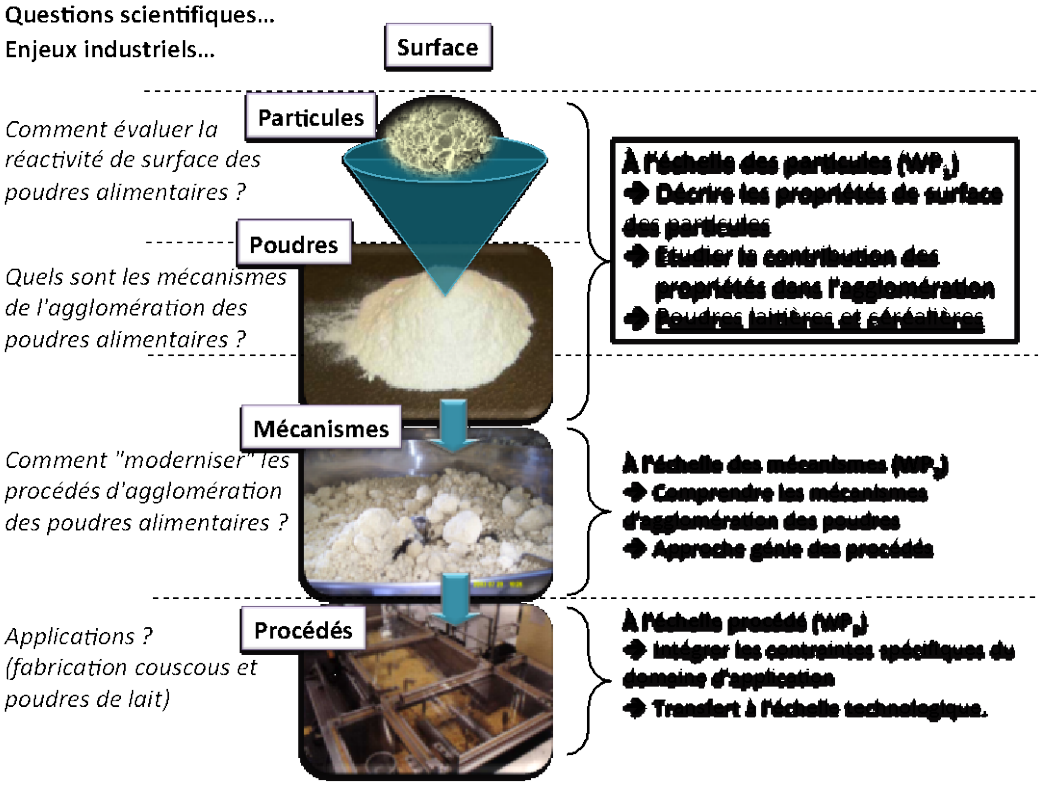

Figure 2. Différentes échelles du projet ANR "Reactive Powder"

C'est ainsi que l'approche au niveau de la surface est développée. Cette approche étant récente et plutôt novatrice ; plusieurs défis se dessinent autour du développement et de l'adaptation des techniques à cette échelle d'analyse, avec toutefois des limites. L'objectif de ce travail est donc de concevoir, d'adapter et de développer des techniques de caractérisation au niveau de la surface qui permettront de décrire la réactivité de surface des particules des poudres alimentaires.

Nous avons choisi les produits provenant de deux familles de poudres: laitières (poudres de lait) et céréalières (semoule). Ce choix a été fait car ces produits sont obtenus de manières assez différentes que ce soit au niveau des matières premières ou des procédés. Ainsi, les résultats peuvent très bien se compléter, une connaissance plutôt générale est obtenue avec l'étude des deux familles de poudres.

Les résultats de ce travail de thèse ont été rassemblés en 6 publications qui ont été intégrées dans ce manuscrit. La rédaction et la publication des différents articles suivent un ordre chronologique avec le déroulement de la thèse. Par contre, dans le manuscrit, ils peuvent être cités dans un ordre différent pour une meilleure organisation des concepts et des idées. Les résultats complémentaires qui n'ont pas fait l'objet de publications sont intégrés dans les différents chapitres.

L'organisation de la thèse dans ce manuscrit consiste d'abord en un premier chapitre contenant l'introduction et un deuxième chapitre consacré à l'étude bibliographique. Le chapitre bibliographique présente les principales techniques expérimentales d'étude de la surface de poudres alimentaires à travers une revue qui a fait l'objet d'une publication acceptée dans Journal of Food Engineering. Ensuite, le rassemblement de l'ensemble des résultats (objet d'article ou pas) est proposé avec une approche multi-échelle (figure 3): échelle atomique, échelle moléculaire et échelle microstructurale. Finalement, un chapitre concentre les conclusions et propose les perspectives pour la suite du sujet.

Le premier chapitre permet de faire l'introduction du sujet et de positionner le travail dans son contexte.

Le deuxième chapitre consacré à l'étude bibliographique a fait l'objet d'une publication (annexe A): Murrieta-Pazos, Gaiani, Galet, Calvet, Cuq & Scher. Food powders: Surface and form characterization revisted. Journal of Food Engineering 112 (2012) 1-21. Dans cet état de l'art, nous citons les principales techniques utilisées pour caractériser les particules des poudres alimentaires en décrivant la technique utilisée, les poudres caractérisées et finalement les propriétés fonctionnelles reliées à la caractérisation obtenue. Les principales techniques utilisées jusqu'à présent pour caractériser les particules ne sont pas très nombreuses. Il y a les facteurs de forme dont les techniques sont limitées aux microscopies et à l'analyse d'images, et la caractérisation de la surface dont les principales techniques sont la Spectrométrie des Photo-électrons X (SPX), la Microscopie Électronique à Balayage en mode Environnemental (MEBE), la Microscopie à Force Atomique (MFA), la Microscopie Électronique en Transmission (MET), la Sorption Dynamique de Vapeur (SDV) et la Chromatographie

Gazeuse Inverse (CGI). Finalement, quelques techniques innovantes sont proposées pour l'étude de la réactivité de surface de poudres alimentaires.

Le troisième chapitre concerne les matériels et méthodes et décrit les produits et les techniques utilisées dans ce travail. Il intègre les matériels et méthodes utilisés dans les articles ainsi que dans les travaux qui n'ont pas fait l'objet de publications. La totalité des publications n'est pas intégrée dans ce travail, seulement les résultats et discussions des articles figurent dans le troisième chapitre. Par conséquent, une description détaillée des matériels, techniques et appareils est développée dans ce chapitre et permet de comprendre le développement des discussions du troisième chapitre.

Le quatrième chapitre est divisé en trois sous-chapitres, la figure 3 montre la répartition des publications et du travail non publié dans les trois sous-chapitres.

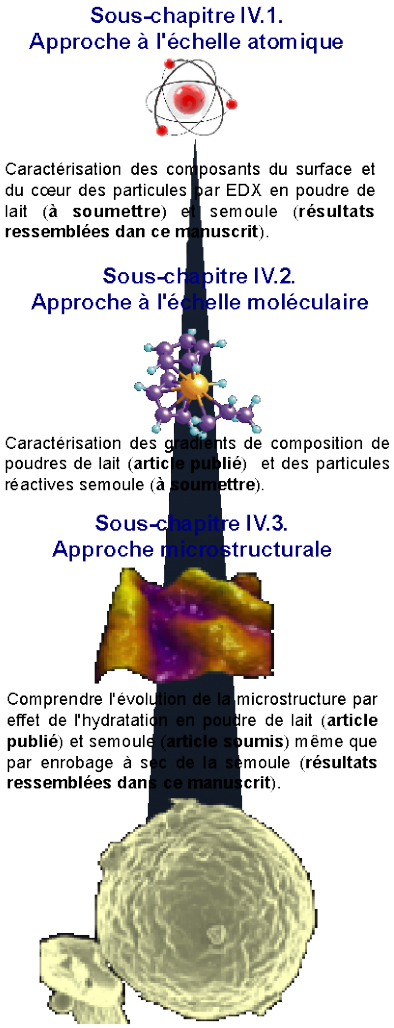

Figure 3. Approche multi-échelle abordée pour présenter les résultats de ce travail.

Le premier sous-chapitre est dédié à l'approche atomique. Dans cette approche, les principales techniques utilisées XPS et EDX (Energy Dispersive X-ray spectroscopy) mesurent la concentration atomique de surface. A partir de ces spectres, il est possible de remonter aux valeurs de concentrations moléculaires, mais l'approche est focalisée sur le détail d'analyse. Le propos de ce sous-chapitre est de caractériser les surfaces des poudres réactives. Pour la poudre de lait, les résultats ont fait l'objet d'une publication, les résultats et discussions sont presentés dans ce manuscrit (IV.1.1). L'article sera soumis en décembre 2012. Murrieta-Pazos, Galet, Rolland, Scher and Gaiani. Energy Dispersive X-ray: Validation of the technique to characterize the surface composition of milk powders. Le même protocole a été développé pour la semoule dont les résultats sont rassemblés dans ce manuscrit (IV.1.2).

Le deuxième sous-chapitre est lié aux techniques qui mesurent des propriétés au niveau moléculaire. Tel est le cas des techniques comme la GC (Gas Chromatography), IGC (Inverse Gas Chromatography) et CR (Capillary Rise). Un premier article est consacré aux propriétés moléculaires des poudres de lait (voir section IV.2.1.) et le deuxième à la caractérisation des poudres réactives en prenant comme poudre modèle la semoule (voir section IV.2.2.). Les deux travaux ont fait l'objet de publications. Le premier article a été publié dans Food Hydrocolloids (Annexe B): Murrieta-Pazos, Gaiani, Galet and Scher, 2012. Composition gradient from surface to core in dairy powders: Agglomeration effect. Food Hydrocolloids 26, 149–158. Le deuxième article que sera soumis en decembre 2012: Murrieta-Pazos, Galet, Calvet, Kaouach, Gaiani & Scher. How to characterize reactive food powders: Particle shape and surface characterization of durum wheat semolina.

Le troisième sous-chapitre est consacré à l'étude des particules modifiées par des contraintes externes au niveau microstructural. Jusqu'à présent, les propriétés mesurées dans le premier et deuxième chapitre permettent de caractériser la particule native (sa structure n'est pas modifiée), cela est diffèrent dans l'approche microstructurale. En effet la réactivité d'une poudre est exprimée quand les particules interagissent avec des contraintes externes. Ainsi, le dernier sous-chapitre intègre des études qui au niveau microstructural modifient la surface. Les axes étudiés sont l'évolution de la surface par humidification et la modification de la surface par enrobage sec des composant purs. Ces études permettent de comprendre la microstructure des particules et comment elles interagissent donnant lieu à la réactivité des poudres.

Pour le premier axe intégrant l'évolution de la surface par humidification, un article a été publié dans Colloids and Surfaces pour la poudre de lait (Annexe C). Les résultats et discussion son intégrés dans ce manuscrit dans la section IV.3.1.: Murrieta-Pazos, Gaiani, Galet, Cuq, Desobry and Scher, 2011. Comparative study of particle structure evolution during water sorption: Skim and whole milk powders. *Colloids and Surfaces B: Biointerfaces* 87, 1–10. . Un deuxième article pour la semoule a été présenté dans le 7ème Colloque Science et Technologie des Poudres, avec avis positif pour une publication dans Powder Technology. Les résultats et discussion sont également intégrés dans ce manuscrit dans la section IV.3.2.: Murrieta-Pazos I. Comparative study of the evolution of particle structure during water sorption in different size classes of durum wheat semolina. *Special volume of Powder Technology*. Submitted.

Finalement pour le deuxième axe concernant la modification de la surface par enrobage à sec, les résultats sont ressemblés dans ce manuscrit (voir section IV.3.3.).

Le cinquième et dernier chapitre concentre les conclusions de ce travail. Ces conclusions sont accompagnées de perspectives et de propositions de développement du sujet pour le futur.

II. BIBLIOGRAPHIC STUDY

II.1. FOOD POWDERS

These last 10 years, a lot of food products have been developed and commercialized in a powdered form. As a consequence, a new branch of science and engineering may be identified. Such discipline deals with the integration of fundamental scientific fields (process engineering, particle engineering, surface physics and chemistry, physico-chemistry) within some applied scientific fields (food biochemistry, food technology, functional properties, and food quality) (Cuq *et al.* 2011; Ortega-Rivas, 2009).

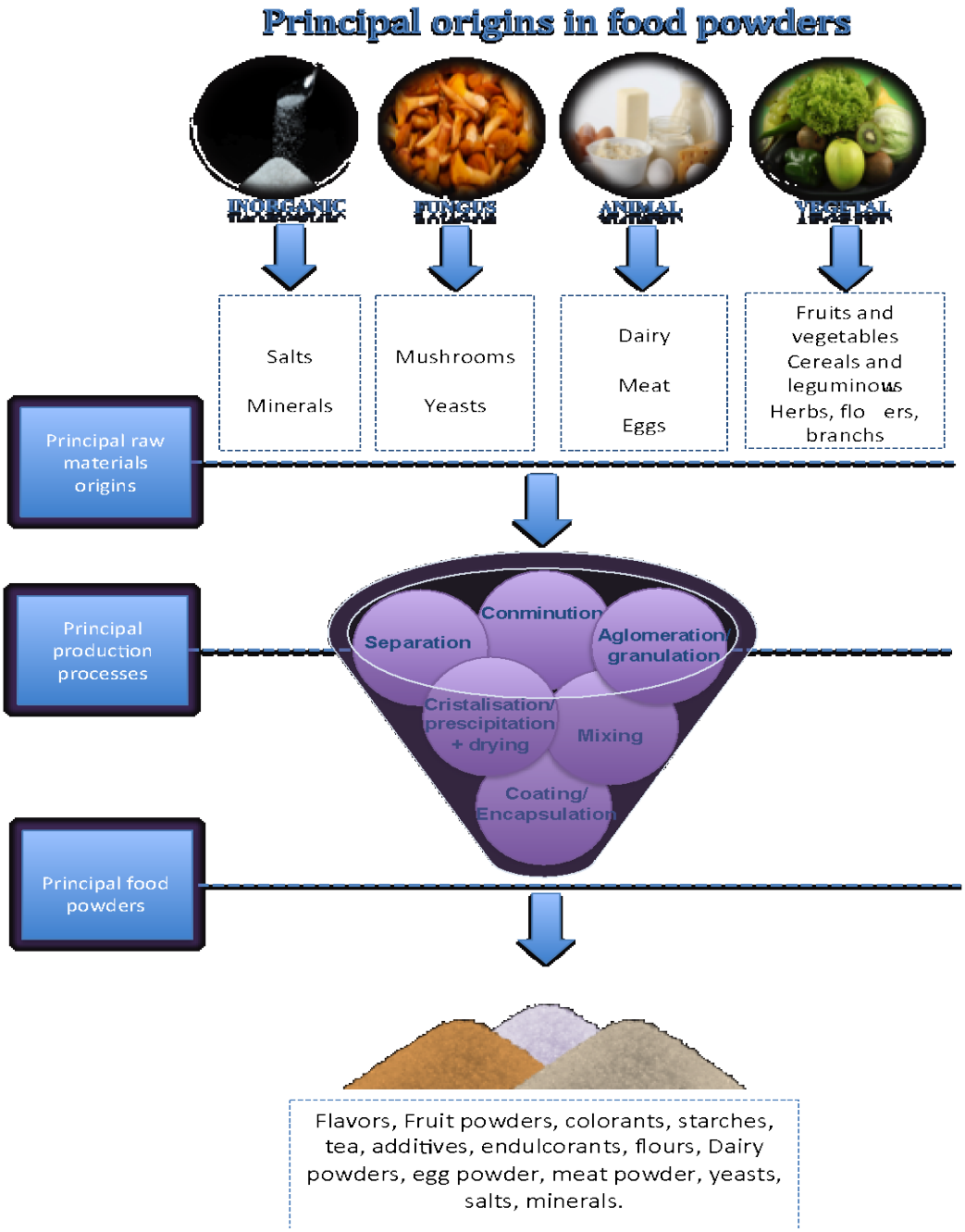

Figure 4. Principal origins of food powders (Murrieta-Pazos 2012a).

For the food industry, the interest with powder forms is mainly linked to their stability (chemical and microbiological), to the reduced transport costs and general convenience. In industry powders can be considered as end products (sugar, salt, coffee, spices, dried milk…) and also as intermediate products between several industries. For example those producing powders and alternatively those using powders as ingredients for food products (fruits, starch, eggs, milk, cereals...).

For consumers, quick and complete reconstitution of these products is one of the main quality indicators (Forny *et al.* 2011). Food powders represent a large variety of powder materials that differ in their chemical composition and physical characteristics. Sources of food powders are as diverse as food in general (Figure 4), therefore differences in forms, structures, composition and behaviors of food powders can be better understood by knowing powders' origins (Cuq *et al*., 2011). It is important to remark that powders can also be a mix of ingredients making its composition and study more complex.

However, scientific and technical descriptions of the food powder properties remain incomplete. It is known that the characteristics and the properties of the particles (and more particularly the surface properties) play a central role in the mechanisms involved during powders production (milling, spray drying, or crystallization), and use (storage, flow, agglomeration, dispersion, solubilisation…). Until now, the properties of food powders are classically described using bulk parameters. Nevertheless, is being recognized that the functional properties of food powders are largely dependent of the surface composition and surface characteristics of the particles (Gaiani *et al*., 2006; Kim *et al.* 2002; Millqvist-Fureby *et al.* 2001). This is one of the reasons why several powder properties may be explained by a better knowledge and characterization of particle surfaces and physical and/or chemical interactions among them and their environment (Gaiani, 2006; Kim, 2008). The characteristics of the particle surface may depend on different factors: bulk composition, operating conditions and storage conditions (figure 5).

Powder surface investigation requires very precise and elaborate techniques. Until now few investigations have been applied to food powder surfaces. Consequently research is still limited and this is the reason why the development of new surface characterization techniques may be an extensive field to exploit with considerable interest to the food industry.

This review is going to highlight the experimental techniques that enable the characterization of food powders surfaces and, when it is reported, to connect this information with their functional properties.

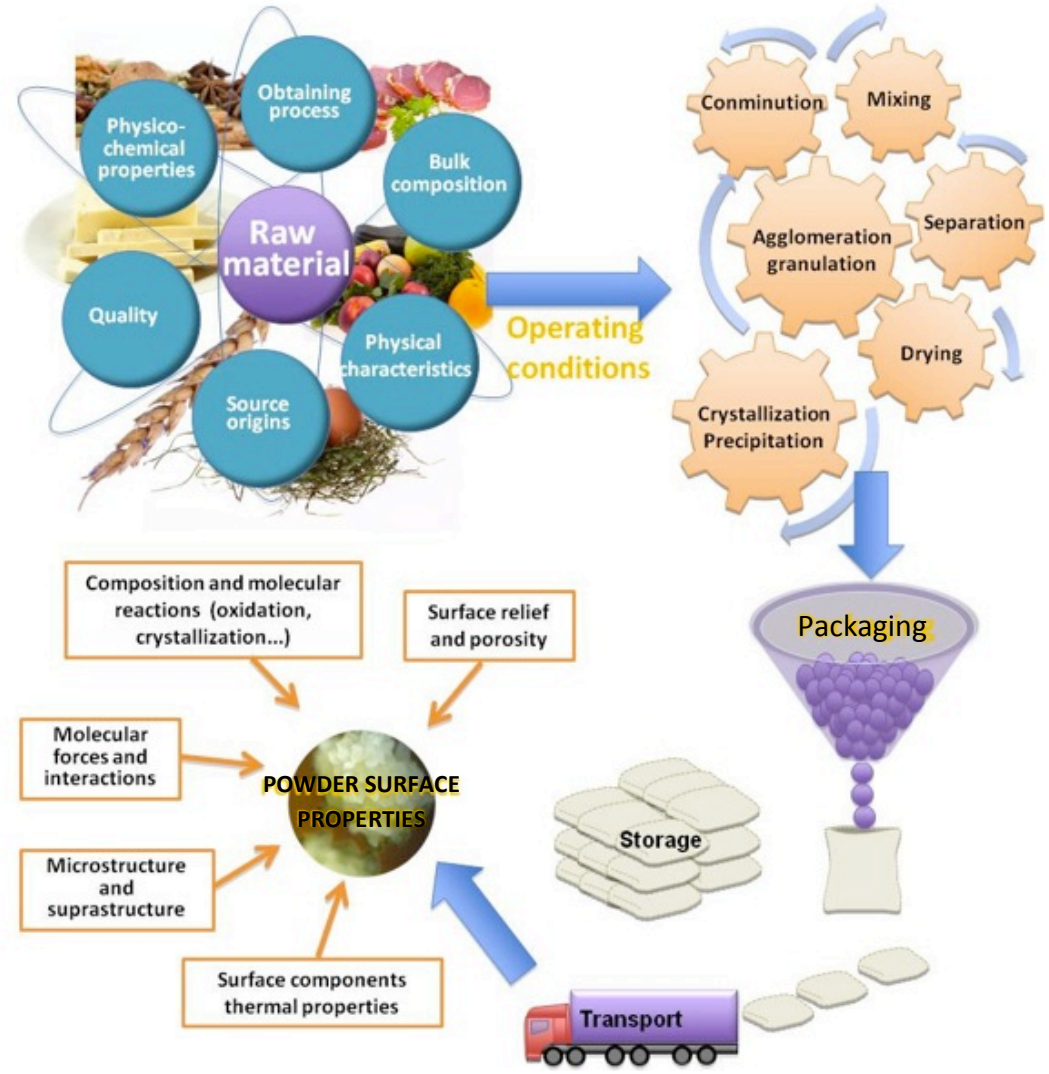

Figure 5. Variable factors affecting the powder surfaces properties (Murrieta-Pazos 2012a).

II.2. X-RAY PHOTOELECTRON SPECTROSCOPY (XPS)

XPS (also called ESCA Electron Spectroscopy for Chemical Analysis) is an analytical technique widely used in surface analysis (Briggs, 1994; Rouxhet & Genet, 2011). It provides elemental and chemical state data from the first nanometers of the surface of solid samples. The sample is placed in an ultra high vacuum and irradiated with photons from a soft X-ray source with a well-defined energy. The method is based on surface irradiation, which causes a complete transfer of photon energy to atomic electrons (Bosquillon *et al.*, 2004). When the electron binding energy (E_b) is lower than the photon energy ($h\upsilon$) the electron is emitted from

the atom with a kinetic energy (E_k) equal to the difference between the photon energy and the binding energy, minus the spectrometer work function Φ:

$$E_k = h\upsilon - E_b - \Phi \quad \text{Equation 1}$$

Because XPS is an ultra high vacuum technique (10^{-8} kPa), it may present limitations for food with water present, but not for powdered food (James & Smith, 2009).

II.2.1. USE OF XPS IN THE DAIRY POWDER FIELD

The first developments using this equipment in the field of dairy powders were done by Fäldt, (1995). Then, the use of XPS was regularly reported for the determination of the surface composition of dairy powders (Gaiani *et al.*, 2006; Gaiani *et al.* 2011b; Gaiani *et al.* 2007b; Kim *et al.*, 2002; Kim *et al.* 2009a, 2009b, 2009c; Millqvist-Fureby *et al.*, 2001; Millqvist-Fureby & Smith, 2007; Shrestha *et al.* 2007), and sugar mixed with dairy proteins powders (Jayasundera *et al.* 2010, 2011a, 2011b, 2011c) at an elemental level. From the C, O and N percentages, surface contents in protein, lactose and lipids were calculated with a matrix formula where the elemental composition in the sample is assumed to be a linear combination of pure components making up the sample (Gaiani *et al.*, 2006; Jayasundera *et al.* 2009; Kim *et al.*, 2002). Milk powders are generally composed of lipids, proteins and lactose but also vitamins and traces of mineral elements. By using the precedent matrix, only lactose, lipids and proteins were taken into account; other components were neglected (Fäldt, 1995; Gaiani, 2006; Kim, 2008).

One of the most important results obtained with this technique concerned the over-representation of some components at the powder surface in comparison with the bulk composition (Gaiani *et al.*, 2006; Kim *et al.*, 2002; Shrestha *et al.*, 2007; Vignolles *et al.*, 2009b). Lipids and proteins (surface active components) were systematically found over-represented at the surface whereas lactose was less represented (table 1, 2 and 3). Indeed when fat is present in the formulation, even in very low quantity, for example the skim milk powder, the fat will cover the surface. Alternatively, protein will govern the surface in absence of lipids or share the surface cover with the fat present. Nevertheless, the lipids cover the majority of the surface in the presence of both components. Finally, lactose was observed in the interior of the particle after free fat extraction industrial (table 3).

Table 1. Bulk composition and surface composition obtained from XPS and linear equation relating elemental components to lactose, protein and fat in milk powders and milk sub-product powders obtained from Lab Scale Spray Dryers.

Powder system	Feed solids (%)	Number of homogenization passes	T_{in}/T_{out} (ºC)	% of surface lactose (Bulk)	% of surface proteins (Bulk)	% of surface fat (Bulk)	Reference
WMP-SMP 1.1% fat	41.2	-	120/80	41* (59.6)	51* (39.3)	8* (1.1)	(Nijdam & Langrish, 2006)
WMP-SMP 1.8% fat	41.2	-	120/80	35* (59.2)	45* (39.0)	20* (1.8)	
WMP-SMP 3.4% fat	41.2	-	120/80	31* (58.3)	38* (38.4)	31* (3.4)	
WMP-SMP 6.7% fat	41.2	-	120/80	29* (56.3)	33* (37.0)	38* (6.7)	
WMP-SMP 14.0% fat	41.2	-	120/80	23* (52.1)	24* (33.9)	53* (14.0)	
WMP-SMP 29.8% fat	41.2	-	120/80	19* (43.0)	21* (27.3)	60* (29.8)	
WMP-SMP 1.1% fat	41.2	-	200/125	52* (59.6)	31* (39.3)	17* (1.1)	
WMP-SMP 1.8% fat	41.2	-	200/125	42* (59.2)	29* (39.0)	29* (1.8)	
WMP-SMP 3.4% fat	41.2	-	200/125	36* (58.3)	28* (38.4)	36* (3.4)	
WMP-SMP 6.7% fat	41.2	-	200/125	35* (56.3)	24* (37.0)	41* (6.7)	
WMP-SMP 14.0% fat	41.2	-	200/125	27* (52.1)	24* (33.9)	49* (14.0)	
WMP-SMP 29.8% fat	41.2	-	200/125	20* (43.0)	16* (27.3)	64* (29.8)	
SMP:Lac (3:1)	35	-	180/80	29 (63)	61 (26)	10 (1)	(Shrestha *et al.*, 2007)
SMP:Lac (1:1)	35	-	180/80	31 (75)	58 (17)	11 (0.8)	
SMP:Lac (1:3)	35	-	180/80	39 (88)	57 (9)	5 (0.25)	
SMP	10	-	145/85	10* (51.0)	46* (36.0)	44* (1.0)	(Kim *et al.*, 2009b)
SMP	20	-	145/85	16* (51.0)	48* (36.0)	35* (1.0)	
SMP	30	-	145/85	51* (51.0)	24* (36.0)	25* (1.0)	
SMP	10	-	205/105	18* (51.0)	48* (36.0)	34* (1.0)	
SMP	20	-	205/105	22* (51.0)	50* (36.0)	28* (1.0)	
SMP	30	-	205/105	29* (51.0)	51* (36.0)	20* (1.0)	
WMP	10	6	145/85	0* (36.6)	3* (27.9)	97* (26.6)	
WMP	20	6	145/85	0* (36.6)	3* (27.9)	97* (26.6)	
WMP	30	6	145/85	0* (36.6)	3* (27.9)	97* (26.6)	
WMP	10	6	205/105	0* (36.6)	3* (27.9)	97* (26.6)	

WMP	20	6	205/105	0* (36.6)	3* (27.9)	97* (26.6)	
WMP	30	6	205/105	0* (36.6)	3* (27.9)	97* (26.6)	
WMP	10	2	145/85	0* (36.6)	2* (27.9)	98* (26.6)	
WMP	20	2	145/85	0* (36.6)	2* (27.9)	98* (26.6)	
WMP	30	2	145/85	0* (36.6)	2* (27.9)	98* (26.6)	
WMP	10	2	205/105	0* (36.6)	2* (27.9)	98* (26.6)	
WMP	20	2	205/105	0* (36.6)	2* (27.9)	98* (26.6)	
WMP	30	2	205/105	0* (36.6)	2* (27.9)	98* (26.6)	
NMC	15	-	-/70	0.8 (0.2)	93.9 (87.3)	5.3 (0.3)	
NWI	15	-	-/70	0.1 (0.5)	66.1 (91.9)	33.8 (0.4)	
NMC+Lac	15	-	-/70	14.3 (26.6)	76.8 (63.1)	8.9 (Tra)	
NWI+Lac	15	-	-/70	9.5 (28.5)	62.9 (64.4)	27.6 (0.5)	
NMC+NWI	15	-	-/70	0.3 (0.3)	89.6 (88.8)	10.1 (Tra)	
NMC	15	-	-/80	0.6 (0.1)	99.4 (86.4)	0.0 (0.8)	
NWI	15	-	-/80	0.0 (0.6)	69.8 (92.2)	30.2 (0.3)	
NMC+La	15	-	-/80	16.0 (26.6)	79.3 (62.0)	4.7 (0.7)	
NWI+Lac	15	-	-/80	12.7 (28.9)	66.3 (65.7)	21.0 (T)	
NMC+NWI	15	-	-/80	0.0 (0.6)	95.6 (86.1)	4.4 (T)	
NMC	15	-	-/110	2.2 (0.1)	97.8 (86.7)	0.0 (0.5)	(Gaiani *et al.*, 2010)
NWI	15	-	-/110	0.0 (0.8)	88.6 (92.2)	11.4 (T)	
NMC+Lac	15	-	-/110	16.5 (26.7)	83.5 (62.7)	0.0 (T)	
NWI+Lac	15	-	-/110	18.8 (28.5)	81.1 (66.1)	0.1 (T)	
NMC+NWI	15	-	-/110	0.2 (0.6)	94.3 (89.1)	5.5 (T)	
NMC	15	-	-/130	1.5 (0.4)	98.5 (87.6)	0.0 (0.5)	
NWI	15	-	-/130	0.0 (1.3)	88.1 (92.3)	11.9 (0.6)	
NMC+Lac	15	-	-/130	19.7 (27.9)	80.3 (63.2)	0.0 (T)	
NWI+Lac	15	-	-/130	20.8 (29.3)	79.2 (65.6)	0.0 (0.5)	
NMC+NWI	15	-	-/130	0.0 (0.5)	92.9 (86.8)	7.1 (T)	
NMC	15	-	-/150	3.5 (0.3)	96.5 (86.5)	0.0 (0.3)	
NWI	15	-	-/150	4.0 (0.7)	85.4 (91.6)	10.6 (0.4)	

NMC+Lac	15	-	-/150	19.7 (25.6)	80.3 (63.3)	0.0 (T)
NWI+Lac	15	-	-/150	19.2 (26.6)	77.0 (67.8)	3.8 (T)
NMC+NWI	15	-	-/150	0.8 (0.5)	99.2 (88.7)	0.0 (0.6)

*Values directly extracted from graphics

Lac: Lactose, NMC: Native Micellar Casein, NWI: Native Whey Isolate, SMP: Skim Milk Powder, T_{in}/T_{out}: inlet temperature/outlet temperature, T: Traces, WMP: Whole Milk Powder.

Table 2. Bulk composition and surface composition obtained from XPS and linear equation relating elemental components to lactose, protein and fat in milk powders and milk sub-product powders from Pilot Scale Spray Dryers.

Powder system	Evaporation capacity ($Kg.h^{-1}$)	T_{in}/T_{out} (ºC)	% of surface lactose (Bulk)	% of surface proteins (Bulk)	% of surface fat (Bulk)	References
NMC	70–120	-	0.0 (0.4)	100.0 (86.7)	0.0 (0.3)	(Gaiani *et al*., 2006)
NMC+Lactose	70–120	-	8.9 (22.1)	89.4 (66.3)	1.7 (0.4)	
NMC+Ultrafiltrate	70–120	-	3.4 (21.3)	91.3 (62.2)	5.3 (0.4)	
NMC	-	215/70	0 (1.5)	94 (80.6)	6 (0.4)	(Gaiani *et al*., 2007)
NMC-A15DS-20ºC-WB	-	215/70	0 (1.5)	94 (80.6)	6 (0.4)	
NMC-A30DS-20ºC-WB	-	215/70	0 (1.5)	94 (80.6)	6 (0.4)	
NMC-A60DS-20ºC-WB	-	215/70	0 (1.5)	89 (80.6)	11 (0.4)	
NMC-A15DS-20ºC-SB	-	215/70	0 (1.5)	94 (80.6)	6 (0.4)	
NMC-A30DS20ºC-SB	-	215/70	0 (1.5)	87 (80.6)	13 (0.4)	
NMC-A60DS20ºC-SB	-	215/70	0 (1.5)	83 (80.6)	17 (0.4)	
NMC-A15DS-50ºC-WB	-	215/70	0 (1.5)	94 (80.6)	6 (0.4)	
NMC-A30DS-50ºC-WB	-	215/70	0 (1.5)	94 (80.6)	6 (0.4)	
NMC-A60DS-50ºC-WB	-	215/70	0 (1.5)	86 (80.6)	14 (0.4)	
NMC-A15DS-50ºC-SB	-	215/70	0 (1.5)	94 (80.6)	6 (0.4)	
NMC-A30DS-50ºC-SB	-	215/70	0 (1.5)	88 (80.6)	12 (0.4)	
NMC-A60DS-50ºC-SB	-	215/70	0 (1.5)	83 (80.6)	17 (0.4)	

AxDS: After x Days of Storage (x = 15, 30 or 60), NMC: Native Micellar casein, SB: standard bag, T_{in}/T_{out}: inlet temperature/outlet temperature, WB: Watertight bag.

Table 3. Bulk composition and surface composition obtained from XPS and linear equation relating elemental components to lactose, protein and fat in milk powders and milk sub-product powders from industrial installations.

Powder system	Storage conditions	Solvent nature	Extraction time (h)	% of surface lactose (Bulk)	% of surface proteins (Bulk)	% of surface fat (Bulk)	References
SMP	-	-	-	36 (51.0)	46 (36.0)	18 (1.0)	(Kim *et al*., 2002; Kim, *et al*. 2005a)
WMP	-	-	-	2 (36.6)	0 (27.9)	98 (26.6)	
CP	-	-	-	1 (12.3)	0 (11.5)	99 (71.5)	
WPC	-	-	-	6 (7.4)	41 (80.4)	53 (5.6)	
SMP	-	-	-	27 (50.0)	61 (34.0)	12 (1.0)	(Shrestha *et al*., 2007)
SMP	after 6 months	-	-	36 (51.0)	44 (36.0)	20 (1.0)	(Kim et al., 2009c)
WMP		-	-	1 (36.6)	0 (27.9)	99 (26.6)	
CP		-	-	0 (12.3)	0 (11.5)	100 (71.5)	
SMP-ASFB	-	-	-	42* (51.4)	40* (35.0)	18* (0.8)	(Kim et al., 2009a)
SMP-A2VFB	-	-	-	40* (51.4)	42* (35.0)	18* (0.8)	
SMP-A3VFB	-	-	-	42* (51.4)	39* (35.0)	19* (0.8)	
WMP-ASDC	-	-	-	3* (26.8)	0* (26.5)	97* (37.5)	
WMP-A3VFB	-	-	-	2* (26.8)	0* (26.5)	98* (37.5)	
IWMP-ASDC	-	-	-	2* (26.8)	0* (28.0)	98* (36.1)	
IWMP-A1VFB	-	-	-	2* (26.8)	0* (28.0)	98* (36.1)	
IWMP-A2VFB	-	-	-	2* (26.8)	0* (28.0)	98* (36.1)	
MPC	-	-	-	1.8* (4.8)	68* (84.7)	30* (1.5)	(Fyfe *et al*., 2011)
MPC-A14DS	20ºC, 44RH%	-	-	1.6* (4.8)	67* (84.7)	32* (1.5)	
MPC-A30DS		-	-	1.2* (4.8)	69* (84.7)	30* (1.5)	
MPC-A60DS		-	-	1.6* (4.8)	68* (84.7)	30* (1.5)	
MPC-A90DS		-	-	3.6* (4.8)	68* (84.7)	28* (1.5)	
MPC-A14DS	40ºC, 44RH%	-	-	1.2* (4.8)	66* (84.7)	32* (1.5)	
MPC-A30DS		-	-	1.5* (4.8)	69* (84.7)	29* (1.5)	
MPC-A60DS		-	-	1.6* (4.8)	70* (84.7)	28* (1.5)	
MPC-A90DS		-	-	3.0* (4.8)	69* (84.7)	28* (1.5)	
MPC-A14DS	20ºC, 66RH%	-	-	3.0* (4.8)	67* (84.7)	30* (1.5)	

MPC-A30DS		-	-	1.8* (4.8)	67* (84.7)	32* (1.5)	
MPC-A60DS		-	-	2.2* (4.8)	67* (84.7)	30* (1.5)	
MPC-A90DS		-	-	3.2* (4.8)	67* (84.7)	29* (1.5)	
MPC-A14DS		-	-	1.5* (4.8)	65* (84.7)	33* (1.5)	
MPC-A30DS	40ºC, 66RH%	-	-	2.2* (4.8)	67* (84.7)	30* (1.5)	
MPC-A60DS		-	-	1.0* (4.8)	69* (84.7)	30* (1.5)	
MPC-A90DS		-	-	3.5* (4.8)	67* (84.7)	29* (1.5)	
MPC-A14DS		-	-	1.6* (4.8)	66* (84.7)	33* (1.5)	
MPC-A30DS	20ºC, 84RH%	-	-	1.7* (4.8)	64* (84.7)	33* (1.5)	
MPC-A60DS		-	-	1.2* (4.8)	75* (84.7)	24* (1.5)	
MPC-A90DS		-	-	4.6* (4.8)	-* (84.7)	-* (1.5)	
MPC-A14DS		-	-	1.8* (4.8)	67* (84.7)	33* (1.5)	
MPC-A30DS	40ºC-84RH%	-	-	2.2* (4.8)	64* (84.7)	30* (1.5)	
MPC-A60DS		-	-	2.2* (4.8)	66* (84.7)	30* (1.5)	
MPC-A90DS		-	-	3.5* (4.8)	67* (84.7)	29* (1.5)	
WMP	-	-	-	0.5 (52.0)	6.2 (37.1)	93.3 (1.4)	(Murrieta-Pazos, *et al*., 2012b)
AWMP	-	-	-	1.3 (36.7)	7.5 (26.2)	91.2 (27.3)	
SMP	-	-	-	30.9 (52.0)	45.1 (37.1)	22.8 (1.4)	
ASMP	-	-	-	36.3 (36.7)	39.3 (26.2)	23.2 (27.3)	
	-		0.17	45 (58)	50 (41)	5 (1)	(Kim *et al*., 2002)
SMP	-	Petroleum ether	24	44 (58)	55 (41)	1 (1)	
	-		48	45 (58)	54 (41)	1 (1)	
	-		0.17	5 (40)	9 (31)	86 (29)	
WMP	-	Petroleum ether	24	9 (40)	10 (31)	81 (29)	
	-		48	10 (40)	22 (31)	68 (29)	
	-		0.17	23 (13)	10 (12)	67 (75)	
CP	-	Petroleum ether	24	24 (13)	12 (12)	64 (75)	
	-		48	26 (13)	15 (12)	59 (75)	
	-		0.17	7 (8)	92 (86)	1 (6)	
WPC	-	Petroleum ether	24	9 (8)	90 (86)	1 (6)	
	-		48	9 (8)	90 (86)	1 (6)	

	-		0.17	44 (58)	53 (41)	3 (1)	
SMP	-	Hexane	24	59 (58)	41 (41)	- (1)	
	-		48	62 (58)	38 (41)	- (1)	
	-		0.17	3 (40)	24 (31)	54 (29)	
WMP	-	Hexane	24	63 (40)	18 (31)	19 (29)	
	-		48	67 (40)	19 (31)	14 (29)	
	-		0.17	4 (13)	0 (12)	96 (75)	
CP	-	Hexane	24	4 (13)	0 (12)	96 (75)	
	-		48	5 (13)	0 (12)	95 (75)	
	-		0.17	8 (8)	92 (86)	0 (6)	
WPC	-	Hexane	24	10 (8)	90 (86)	0 (6)	
	-		48	10 (8)	90 (86)	0 (6)	
WMP	-	Petroleum ether	5 x 0.83	19.3 (52.0)	18.1 (37.1)	62.5 (1.4)	(Murrieta-Pazos, *et al*. 2012b)
AWMP	-	Petroleum ether	5 x 0.83	18.4 (36.7)	8.1 (26.2)	72.8 (27.3)	

*Values directly extracted from graphics

AxVFB: After x vibrating fluidized bed (x = 1, 2 or 3), ASDC: After Spray Drying Chamber, ASFB: After Static Fluidized Bed, AWMP: Agglomerated Whole Milk Powder, ASMP: Agglomerated Skim Milk Powder, AxDS: After x Days of Storage (x = 14, 30, 60 or 90), CP: Cream Powder, IWMP : Instant Whole Milk Powder, MPC: Milk Protein Concentrate, NWI: Native Whey Isolate, RH: Relative Humidity, SMP: Skim Milk Powder, T_{in}/T_{out}: inlet temperature/outlet temperature, T: Traces, WPC: Whey Protein Concentrate, WMP: Whole Milk Powder.

This tendency to observe an overrepresentation of the lipids and then the proteins at the surface, is observed at all production scales, independent of the production conditions. Results for laboratory (table 1), pilot (table 2) and industrial (table 3) dryers are shown confirming this tendency.

In laboratory conditions (table 1), Nijdam & Langrish (2006), studied 2 drying temperatures and 6 formulations, mixing Whole Milk Powder (WMP) and Skim Milk Powder (SMP) in order to change the lipid concentration. A small change in the average fat content results in a large change in the surface fat coverage, however, the surface fat coverage is less affected by increases in the average fat content at higher fat concentrations. Higher temperature resulted in larger fat and lactose cover. Nevertheless, the augmentation of lactose at the surface does not correspond to the protein-lactose proportion in bulk composition. Authors postulate that at lower drying temperatures, protein has more time to migrate to the surface of the droplet before sufficient moisture is evaporated to form a skin. Similar results in terms of lactose-protein surface composition where observed by Shrestha *et al*. (2007), who studied powders conformed by mixtures of SMP and lactose. Later Kim *et al.* (2009b), studied 3 solid concentrations in spray drying feed solutions, 2 drying temperatures for SMP and WMP and 2 homogenization passes for WMP. The author postulated that higher feed solids content would give rise to more viscous droplets, preventing the migration of components and redistribution at the surface. The authors goes on to describe now lactose concentration is stronger at higher temperatures, agreeing with Nijdam & Langrish's (2006) proposal that the fat surface concentration is reduce by high temperatures in SMP and does not present an important influence in WMP. In addition any difference is noted with the increase of homogenization passes performed in WMP feeding solutions.

Gaiani *et al*. (2010), observed an enrichment of the surface in lipids and proteins regardless of the spray-drying temperature (the powder was dried at 5 different outlet temperatures) or the formulation obtained by combinations of Native micellar casein (NMC), Native whey isolate (NWI) and lactose. Furthermore, lipids enrichment is stronger in powders containing NWI than NMC and higher temperatures increase the protein-lactose surface content and reduce the surface fat content.

At pilot scale (table 2), Gaiani *et al*. (2006), produced and analyzed the surface of particles of NPC, and mixtures of NPC with protein ultrafiltrate or lactose, consequently

surface particles was modified. The nature of the ingredient added was determinant in the surface modification. Later the same authors (Gaiani *et al*., 2007) studied the effect of storage in NMC powder at 20 and 50 ºC, stoked in two different package (standard or watertight bags), the storage time was 15, 30 and 60 days each sample. Results reveled significant surface changes only after 60 days of storage, when powder is stocked in watertight bags. When powders are store in standard bags, changes are registered after 30 days of storage. These results suggest that powder conservation is possible before 30 days of storage or more time if they are stocked in watertight bags. Temperature did not demonstrate an effect in surface composition modification.

At industrial scale (table 3), it was observed the surface composition of WMP, SMP, Cream Powder (CP) and Weight Protein Concentrate (WPC) (Kim *et al*., 2002, 2005a), later the same author (Kim *et al*., 2009c), determined the effect of storage (6 months) in these powders, a migration of the fat to the surface was systematically observed in all the powders. WMP, SMP and Instant Milk Power (IMP), were collected in different points of the spray drying and fluidized bed processes (Kim *et al*., 2009a). Surface did not present strong changes in the structure according to the collection point, results suggest that surface characteristics are developed in drying and they are not modified in the subsequently steps.

Murrieta-Pazos *et al*. (2012b), compared the surface composition of WMP and SMP with the agglomerated milk powder versions, WMP granulated (WMPG) and SMP granulated (SMPG). A similar composition was observed between WMP and WMPG, the same effect was observed between SMP and SMPG. The agglomeration process consists in the addition of fine milk particles before draying step, then a suspension of fines and milk is dried. The study demonstrates that this supplementary step does not change the mechanism of surface by draying this suspension. Fyfe *et al*. (2011) studied the effect of storage in Milk Proteins Concentrate (MPC) after 14, 30, 60 and 90 days at 25 and 40ºC, the powders were stocked in recipients with relative humilities at 44, 66 and 84%. No significant changes to the surface composition were observed.

Finally different solvents and treatments are applied to fatty dairy powders (WMP, WMPG, CP) in order to extract the surface free fat (Kim *et al*., 2002; Murrieta-Pazos *et al*. 2012b), the efficiency of the technics can be observed after analysis of surface composition in

"surface fat free" powders, then these powders were used to evaluate the evolution of functional properties.

Different mechanisms of powder surface formation were proposed and discussed from these results summarized in table 1, 2 and 3**,** they all agrees with the formation of a fat surface, then the draying of the next layer forming a skin with a subsequently drying of the core. Recently, this technique (surface composition by XPS) has been successfully applied to investigate links between particle surface chemical composition and particle functional properties.

II.2.1.1. Reconstitution properties

By comparing casein powders containing variable combinations of hygroscopic material (lactose and/or minerals), the presence of lactose at the powder surface calculated by the matrix model from XPS results, was found to improve the wetting properties (Gaiani *et al*., 2010). NMC dried at 5 different temperatures. After addition of 30% of lactose to the formulation lactose present in the surface increase (table 1) and wetting time was reduced from 932, 631, 642, 639 and 623 s to 543, 431, 205, 202 and 201 s respectively. The same study was performed for NWI. After addition of 30% of lactose in the formulation, the surface lactose also increase, showing a wetting time improvement from 1498, 1290, 1120, 1179 and 1131 s to 1085, 991, 66, 557 and 499 s respectively.

Surface fat cover seems to have a very important influence in the powder wetting properties. For the 25 powders studied (Gaiani *et al*., 2010), a direct correlation between fat surface content and wetting time was observed. For example for the surfaces with higher fat content, values obtained by NWI dried at 70 °C (33.8%) gave a maximum registered wetting time of 1498 s. The fastest wetting times (205, 202 and 201 s) were registered using NMC with addition in the formulation of 30% of lactose at 110, 130 and 150 °C; this gave 0% surface fat. These results agreed with those obtained Kim *et al*. (2002), studying WMP and cream powder (CP). Here the wetting times for WMP and CP were in excess of 900 s, and after free fat extraction the wetting times were reduced to 35 and 100 s for WMP and CP, respectively.

Lecithination of powders is a practice recurrent in the food powder industry that improve wetting and rheology of powders, Millqvist-Fureby & Smith, (2007) added lecithin to SMP,

Wey Protein Concentrate (WPC) and lactose in order to adapt the method relating elemental analysis of XPS to surface composition of powders covered with lecithin. This adaptation was developed with a layer model indicating that lecithin would coat the whole particle surface. Surface composition for SMP + Lecithin, WPC + Lecithin and lactose + lecithin was 54.3, 54.8 and 0% of proteins, 17.9, 23.5 and 51.3% of lactose and 27.8, 21.7 and 48.7 % of lecithin respectively.

Authors attribute the low lecithin values to the thickness of the coverage. The lecithin layer thickness is estimated at approximately 2.5 nm. This is thinner than the analysis depth (10 nm). From this value estimation of the surface layer thickness for each powder was calculated: 1.6 nm for SMP + Lecithin, 0.8 nm for WPC + Lecithin and 1.9 for lactose + lecithin.

Another study related the wetting time of ultra-filtrated and spray-dried Native phosphocaseinat with fat migration from the bulk to the surface during storage of casein powders (Gaiani *et al*., 2007). Values grew from 12 s in fresh powders to 35 s (watertight bag) and 73 s (standard bag) after 60 days storage at 20 ºC. Results were more drastic stored at 50 ºC with 148 s (watertight bag) and 265 s (standard bag), This delay in the wetting time was attributed to a larger fat coverage.

For SMP the same phenomenon was observed. The fat surface coverage in fresh powder was determined at 18% and after 6 months of storage at room temperature (10-30 ºC), the fat coverage shifted to 20%. For WMP and CP the fat surface coverage was important even for fresh powder (98 and 99%). However no significant changes were observed after 6 months storage: (Kim *et al*., 2009b).

In order to improve the reconstituted powder properties, others studied the effect of processing parameters on the powder surface. High spray-drying temperatures (Gaiani *et al*., 2010), high solid content and homogenization (Kim *et al*., 2009b) , appear to produce powders with less surface fat (table 1, 2 and 3) allowing shorter wetting times as demonstrated in the work of Gaiani *et al*. (2010).

The influence of the protein denaturation (whey proteins) on components repartition in the dry particle was also studied by Millqvist-Fureby *et al*. (2001). A slight increase in surface

fat was observed with the denaturation percentage whereas the lactose coverage was almost constant and the protein coverage decreased. The wetting time was augmented from 21 to 40.2 s for the corresponding degree of denaturation of 4 and 51% with a consequential increase in the surface fat content.

II.2.1.2. Caking phenomena

Caking is a prevalent situation that can cause problems in operation, equipment surfaces or product yield (Adhikari *et al*. 2001). Nijdam & Langrish (2006), related the degree of caking to the surface composition of milk powders presenting different fat contents. The results indicated that the degree of caking was high (> 90%) for powders containing between 5% and 30% of surface fat. On the other hand, the caking was importantly reduced (< 60%), when surface fat was less than 3% here there appears to be a strong correlation between the caking ability of the powder and the fat surface coverage. Hartmann & Palzer (2011), studied caking kinetics of water-soluble amorphous powders. For these powders, the sinter bridges created in the powders were measured.

II.2.1.3. Lipids oxidation

Surface fat also indicates a susceptibly to oxidation (Kim *et al*., 2002). For example, an oxidation "signature" may be potentially observed by XPS. Kim *et al*. (2002) compared the oxygen peak of various dairy powders to detect an oxidation at the surface. After 2 days storage at 40ºC, the O_{1s} peak had significantly changed in all the powders (SMP, WPC, WMP and CP), with the biggest increase (1.5%) observed in the CP and the smallest observed in SMP.

II.2.1.4. Flowability

The flowability of a powder is an important property in handling and processing operations, such as storage, transportation, formulation, mixing, compression or packaging (Knowlton *et al*. 1994). Flowability is known to be highly dependent on particle size and distribution (Barbosa-Canovas *et al*. 1987), but also on surface chemical composition (Kim *et al*., 2005a). The angle of response was measured to reveal flow properties for different spray-dried powders: SMP, WMP, WPC and CP (Kim *et al*., 2005a). WMP and CP provided surfaces largely covered by fat, WPC gave a medium surface fat coverage and SMP a low surface fat coverage (table 1, 2 and 3). A regular flow was registered for skim milk powder (85º), the rest of the powders did not flow (0º). In order to find if flow difficulties came from

lipid surfaces, free surface fat was extracted. Powders that did not flow before extraction flowed correctly after the procedure, presenting angles of response about 80º (WMP), 60º (CP) and 90º (WPC). Kim *et al*., (2009b) also found some differences in flowability of skim milk powder after 6 months of storage increasing the contact angle from 85º (fresh powder) to 90º.

II.2.2. USE OF XPS FOR NON-DAIRY FOOD POWDERS

The use of XPS in the field of vegetal powders was limited with accessibility onto to pour databases. XPS studies on starch permit elemental composition determination of the outer 5-10 nm of the granule surface. Russell *et al*. (1987) and Baldwin (1995) deduced the percentage of protein surface coverage from nitrogen peak areas. Granule surfaces of cereal starches contain between 1 and 2% nitrogen, whereas potato starch surfaces contain only 0.01% nitrogen. Using the nitrogen peak area technique the percentage of protein surface coverage was revealed as 4 to 12.5% for cereal starches and around 0.5% for potato starches. This protein content apparently varies according to the botanical source of the starch.

Saad *et al*. (2009) performed XPS on wheat flour before and after re-grinding and related the surface flour composition to water sorption properties. After decomposition of oxygen Os1 (O=C, O–C and H_2O**)**, carbon C1s (C–(C, H), C–(O, N), C=O and O–C=O) and nitrogen N1s (C-NH and C–NH_3**)** peaks, C1s peak appear induce a slight decrease of the C–(C, H) bond from 61% in native flour to 60%, 59% and 57% respectively to first, second and thirst re-grinding passes, concurrently the total of C–O functions (C–(O, N), C=O and O–C=O) increased. From the O1s peaks, the O=C functions increased significantly whereas the O–C functions decreased from 82.0 in native flour to 77.5, 76.9 and 75.2, respectively to first, second and thirst re-grinding passes. These results reflect a decrease in the number of hydrophobic bonds and a decrease in the number of hydrophilic bonds, authors attribute this behavior to physical changes induced by re-grinding resulting in starch granule rupture.

The matrix formula developed for dairy powders (Fäldt, 1995) was derived for wheat powders (Saad *et al*., 2011a). Native flours as well as flours reconstituted from pure components were analyzed in order to validate the method. Surface of reconstituted flours was calculated, for example in 90% starch-10% protein mixture, the surface composition resulted between 87.4 and 90.6% of starch and between 12.9 and 10.3% of proteins, depending on the calculus method. These values were consequent with the mixture

composition. A very different result was obtained for native powders, 5 native flours were analyzed: Impression wheat variety flour standard (F1), Peeled flour of crusty wheat variety (F2), Pearled flour of crusty wheat variety (F3), Peeled flour of tiger wheat variety (F4) and Pearled flour of tiger wheat variety (F5). Surface composition obtained for flours F1, F2, F3, F4 and F5 was: 1.7, 1.2, -6.5, -1,3 and -5.7% of starch, 54.2, 53.8, 70.5, 85.6 and 66.5% of protein and 44.5, 45.3, 36.6, 28.9 and 39.6 of lipids, respectively. The composition of the native flour presents an over-representation of lipids and proteins, compared with the bulk composition (81.3% starch, 12.9% protein, 2.3% lipids). After comparison of native and reconstituted flours, native powders resulted more complex materials with a heterogeneous distribution of the components. Authors concluded that surface composition is not a simple transposition of the bulk composition suggesting some mask interactions between the components. The lack of references for cereal products makes difficult to conclude on the reliability of this method applied to characterization of surface cereal products (Saad *et al*., 2011b). The surface of wheat flour fractions was also studied (Saad *et al*., 2011b) the same technique was used to determine the surface composition of fractions. When analyzing fractions, the protein content decreases from 51.9 to 43.5% and the lipid content increases from 46.7 to 51.1% with the augmentation of the particle size, a clearest tendency is observed in ground flour sieved decreasing from 54.8 to 20.9% of protein and 46.3 to 63.4% of lipids with the size particle augmentation. In both cases the starch content was relatively constant (Saad *et al*., 2011a).

The use of XPS in the field of other food powder is infrequent. Stevens & Schroeder, (2009) performed quantitative analysis of saccharides by XPS. They presented the spectra of various carbohydrates. The accuracy of the analysis permits the distinction between mono-, di-, and polysaccharides. Indeed, chemical shifts of the C–O and O–C–O groups increase on moving from monosaccharaides to disaccharides to polysaccharides, actually the rates of Al Kα X-ray-induced degradation are significantly different, specifically the O/C decrease and increase in the peaks at 285 and 289.1 eV. These authors also found a relationship between the caramelization tendency and time of exposure to XPS radiation. The database developed is now a useful tool for surface carbohydrate analysis.

Vega *et al*. (2005) adapted the matrix formula (Fäldt, 1995) for spray dried ice cream mixes, different formulations were tested. Ice cream spray dried powders observed the same over-representation of the fat at the surface (between 81 and 96%) in comparison with bulk

composition (between 19.1 and 44.9% of fat content), powders without emulsifiers and containing casein reduced surface fat (from 85 to 78%) at expense of higher protein coverage (6-11%), powers without emulsifiers not containing casein also reduced fat cover (from 81 to 73%) exchanging this deficit by a gain in protein cover (from 8 to 15%).

Rouxhet *et al*. (2008) analyzed cake ingredients; the authors propose an elaborated model to relate atomic composition to biochemical molecules. In order to achieve this propose they extracted information on chemical functions and refine the results expression in terms of molecular constituents. This model make possible distinguish among proteins, carbohydrates, Phospholipids (PL) and Neutral Lipids (NL) in flour, eggs white, egg yolk and whole egg powders. The results agree with those obtained from the matrix model (Fäldt, 1995), surface molecule distribution is different from bulk composition. The results illustrating similitudes between the both methods are obtained for flour. This powder presents concentrations of PL and NL fewer than 2% in bulk composition in contrast to the surface with approximately 10% and 30% of PL and NL respectively. Even when results are consequent with the others a publication, this method is more detailed, it permits to obtain finest information about the surface by discriminating from different molecules of the same family (lipids).

II.2.3. INTERESTING COMPLEMENTARY TECHNIQUE

The combination of time of flight secondary ion mass spectrometry (ToF SIMS) and XPS has proved to be a valuable tool for the analysis of surfaces. Until now, this combination had never been done for food powders. The ToF-SIMS uses a pulsed primary ion beam to desorb and ionize species from a sample surface. The resulting secondary ions are accelerated into a mass spectrometer and are then mass analyzed by measuring their time-of-flight from the sample surface to the detector. The application of ToF-SIMS in food analysis has been explored only very recently. For example, this method has been applied with success to analyze pesticides on the surface of olives (Focardi *et al*., 2006), the principal component presenting the strongest variance (90.3%) after analysis of 51 samples, was used to determine differences on the surface samples; the study shown signals at $m/z = 31$ (CH_3O^+) and $m/z = 147$ ($C_6H_{14}NOP^+$ or $C_6H_{13}NOS^+$) with higher intensities in native olives ($1.12X10^{-4}$, $2.93x10^{-5}$ respectively) than olives covered with pesticide ($4.23x10^{-4}$, $2.42x10^{-4}$ respectively). (Cliff *et al*., 2003), adapted the technique to monitoring and imaging clofazamine with dominant peaks m/z 184 [$(CH_3)_3NCH_2\ PO_4H_2$] on the surface of yeast cells in the frozen-hydrated state, they demonstrated the absent of clofazamine within molecular information

from a cell fractured in order to reveal the cell ultrastructure. In the therapeutic field, Grenha *et al*. (2007) characterized the surface and the internal structure of microsphere containing chitosan and mannitol. It was possible to investigate the repartition of the components in the particle surface by obtaining the characteristics peaks of each component m/z 193 ($CH_{19}P_2N_6O$), m/z 249 ($C_{10}H_{18}PO_5$), and m/z 281 ($C_4H_{21}N_{14}O$), chitosan nanoparticles being successfully encapsulated in mannitol microspheres. All these works have demonstrated the power of ToF-SIMS spectral analysis and chemical imaging for the study of food and may be an interesting tool for food powders.

II.3. MICROSCOPY TECHNIQUES MAKING SURFACE CHARACTERIZATION POSSIBLE

II.3.1. SCANNING ELECTRON MICROSCOPY

SEM apparatus uses a beam of electrons instead of light to form an image. In some cases, it may be necessary to cover the powders with a thin layer of carbon or gold to give it conductive properties. In food powders, SEM images could detail the particle shape and surface aspect. Powders suprastructure and organization have been widely studied in milk (McKenna *et al*., 1999) and milk-wheat flour mixtures (Al Mahdi *et al*., 2006). For dairy powders, surface dents have been widely registered (Gaiani *et al*., 2006; Haque & Roos, 2006; Kim *et al*., 2009c; Millqvist-Fureby & Smith, 2007).

Lactose mixtures and milk models obtained by freeze-drying (Marabi *et al*., 2008) (table 4), presents the same structure described by Haque & Roos (2006) (table 1), who also noted more bright surfaces in higher surface fat content powders. Different spray dried milk powders (skim milk, whole milk, cream and whey protein concentrate) were treated with petroleum ether and ethanol in order to extract surface free fat (Kim *et al*., 2002). The SEM images obtained from powders before extraction show smooth surfaces and clearly dented surfaces after ethanol extraction; a less affected surface was obtained with petroleum ether, (table 4). Kim *et al*. (2009b) obtained milk powders at two spray-drying temperatures (145/85 and 205/105 ºC). More spherical particles and smoother surfaces were obtained at the higher temperature (table 4). It was also observed that particles bigger than 90 µm are agglomerates. SEM was also used to characterize powder surfaces during storage, thus Gaiani *et al*. (2009) noticed some pores at the surface of casein powders, (table 4).

Cross section analyses of milk and cream powders (table 4) were also performed after free fat extraction (Kim *et al*., 2009c). Here the authors deduced some capillary properties that may interact in the migration of fat into the surface. (Murrieta-Pazos *et al*., 2011) observed the evolution of lactose crystals formed at the surface of WMP and SMP conditioned at different relative humidities (table 4).

Jenni (2007) observed a change in the shape and the surface aspect of wheat flour particles as a function of their size; the particles became less and less rounded and more and more rough as size increased. Partial dissolution of particles surface was observed in MPC stored at 65% RH during 14 and 30 days (table 4) by Fyfe *et al*. (2011).

The starch granule has been also widely studied. (Fannon *et al*., 1993) observed pores at the surface of starch granules of potato, corn and wheat deducing the formation of interior channels in the structure. Later, Gallant *et al*. (1997), observed starch from different botanical sources, meanly wheat and potato (table 4). These particles were characterized as a golf ball shape, where nodules correspond to amylopectin-based blocklets suspended in an amylose-based supporting matrix.

II.3.1.1. Interesting complementary methods

Recently, SEM images were sometimes combined with Energy Dispersive X-ray spectroscopy (EDX) analyses. The EDX analysis system works as an integrated feature of a SEM apparatus and cannot operate on its own. Its characterization capabilities are due in large to the fundamental principle that each element has a unique atomic structure, thus X-ray energy emitted by the atoms after excitation with an electron ray is characteristic of each element's atomic structure. Hence one element can be identified uniquely from one another. To stimulate the emission of characteristic X-rays from a specimen, a high-energy beam of charged particles is focused into the sample. The output of an EDX analysis is an EDX spectrum, which is a plot of how frequently an X-ray is received for each energy level. The higher a peak in a spectrum, the more concentrated the element is in the sample. This technique was used for identifying the elemental composition of the sample, or an area of interest thereof.

Table 4. Surface characterization of food powders by Scanning Electronic Microscopy.

Methods	Powder systems								References
spray drying	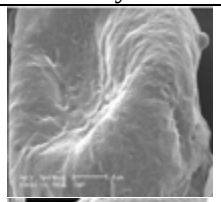	SMP	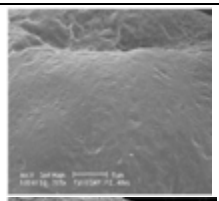	SMP after free fat extraction (petroleum)	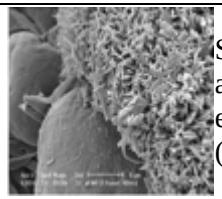	SMP after free fat extraction (ethanol)			(Kim *et al.*, 2002)
	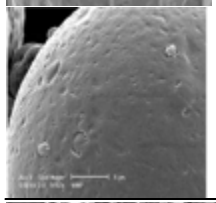	WMP	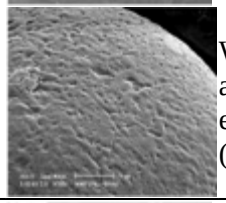	WMP after free fat extraction (petroleum)	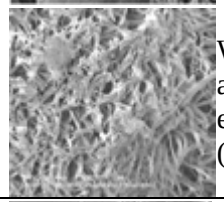	WMP after free fat extraction (ethanol)			
	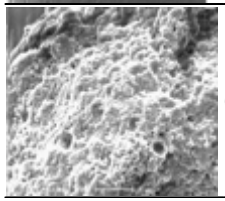	CP	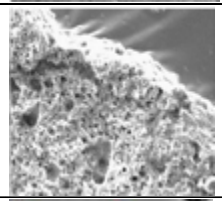	CP after free fat extraction	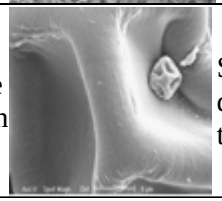	SMP (spray dried at low temperature)	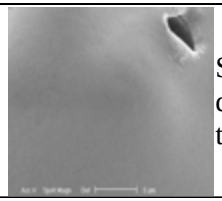	SMP (spray dried at high temperature)	(Kim *et al.*, 2009b) (Kim *et al.*, 2009c)
		fresh NMC	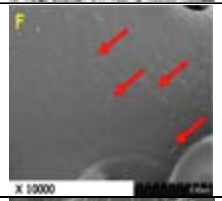	NMC after 60 days					(Gaiani *et al.*, 2009)
	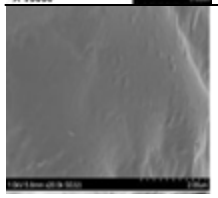	SMP a_w = 0.23	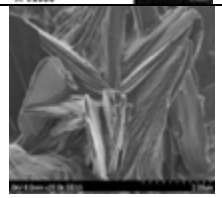	SMP a_w = 0.94	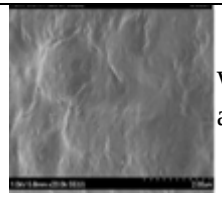	WMP a_w = 0.23	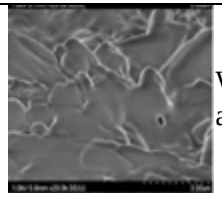	WMP a_w = 0.94	(Murrieta-Pazos *et al.*, 2011)

	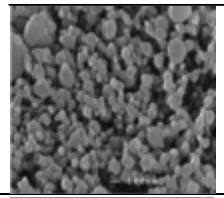	MPC a_w = 0.65	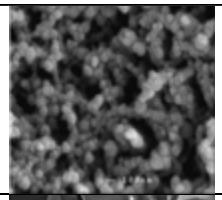	MPC a_w = 0.65 after 90 days			(Fyfe *et al.*, 2011)
freeze drying	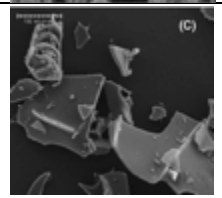	Lactose + WPI	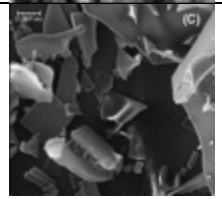	Lactose + NaCa	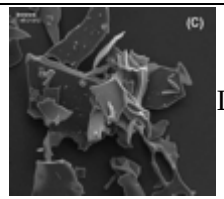	Lactose	(Haque & Roos, 2006)
	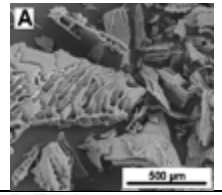	Milk powder (0% fat)	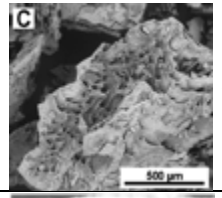	Milk powder (10% fat)	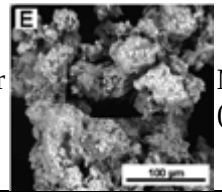	Milk powder (45% fat)	(Marabi *et al.*, 2008)
extraction	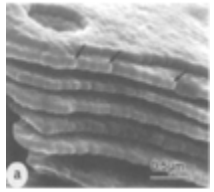	Wheat starch after enzymatic hydrolysis	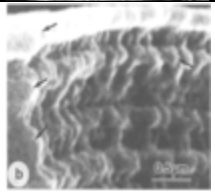	Potato starch after enzymatic hydrolysis			(Gallant *et al.*, 1997)

EDX has been used on vegetal material and food extracts. For example, EDX spectra showed mineral nutrients (P, K and Mg) stored in different tissues of quinoa seeds (Prego *et al*., 1998). Other authors analyzed some protein bodies in tissues of different rice grains by this technique and observed some micronutrienst (Fe, Mn, Zn and Cu) and macronutrients (P, Mg and K) in specific rice genotypes (Prom-u-thai *et al*., 2008). Recently, this technique has also been used for the detection of irradiation treatment on basmati rice by the analysis of minerals extracts (Sanyal *et al*., 2009). In the field of food powder, Murrieta-Pazos *et al*., (2012b), adapted the matrix model in XPS (Fäldalt, 1995) in this case using EDX data to investigate the chemical composition of dairy powders at a depth of approximately 1 µm, surface composition was calculated for WMP and SMP, protein, lactose and lipids content was WMP = 34, 16.8, 46.4% and SMP = 25.8, 13.7, 58.6% respectively (Murrieta-Pazos et al., 2011). The same technique was performed to characterize surface of granulated milk powders, Granulated WMP (GWMP) and Granulated SMP (GSMP). Protein, lactose and lipids content was GWMP = 21.3, 11.9, 65.4% and GSMP = 7.5, 1.3 91.2% respectively. Another analyze was performed in whole milk particles, WMP and GWMP, after extraction of the free fat at the surface, surface composition protein, lactose and lipids obtained was WMP = 30.0, 11.3, 55.5% and GWMP = 31.3, 13.1, 52.3% respectively. By comparing these surface composition with those obtained by XPS (table 3), an interesting gradient model of a milk powder particle was proposed (Murrieta-Pazos *et al*., 2011).

II.3.2. ATOMIC FORCE MICROSCOPY (AFM)

In food science, application of the AFM is quite recent and mostly concerns the study of the structures of biopolymers (mostly polysaccharides including carrageenan, cellulose, pectin, xanthan) as film deposition onto a surface (Funami, 2010; Iijima *et al*., 2007; Kirby *et al*., 2008; Lukasiewicz *et al*., 2007; Olivares *et al*., 2010).

In food powders, AFM can be used to investigate the surface topology of different botanical sources of starch granules at the nanoscale. Some examples are: wheat (Baldwin, 1995; Baldwin *et al*., 1998; Gallant *et al*., 1997), pea (Ridout *et al*., 2004) and also rice (Ohtani *et al*., 2000a), some of these examples are illustrated in table 5. By comparing the difference between the highest and lowest points on a granule surface (measured at a scan size of 1000 nm^2), Baldwin *et al*. (1998) reveals a flatter surface of Riband wheat starch compared to potato starch (table 5). (Ohtani, *et al*., 2000b) observed starch by different methods of

sample preparation as microtome, enzymatic digestion and physical destruction of starch granules (table 5), from five different botanical sources (corn, potato, rice, sweet potato and wheat).

Images revealed different surface roughness depending on the botanical source, but supported a blocklet starch model. The structure of the starch granules after hydration have been studied and showed a banded-ring structure alternating amorphous and crystalline rings (Gunning *et al*., 2010; Parker *et al*., 2008).

The gelatinization of starch (from different sources, pure or blended with other biopolymers, during heating) was also observed, (An *et al*., 2008; Funami *et al*., 2008; Quiroga & Bergenståhl, 2007), some examples are presented in table 5. Some interesting scanning chemical force microscopic investigations have been reported recently, native and hydrolyzed tapioca starch have been imaged with functionalized –OH and $–CH_3$ tip probes in order to study the relationship of the surface structure and the amylose/amylopectin ratio (table 5). However the differences in the chemical domain of the starch were not determined by topographic images (Wuttisela *et al*., 2009).

The majority of food particle powders are multicomponent and rough. In the studies reported in the literature, the food material samples are specially prepared for AFM imaging by either embedding into a resin, slicing, powdering or centrifuging in a suspension to then deposit or fix the sample onto a mica plate. To use the AFM techniques to image the surface of food particles and study their topology is still a challenge. Until now, AFM was rarely tested on flours (Jenni, 2007) or dairy powders (Murrieta-Pazos *et al*., 2011) and/or others food powders than starch (Tomoaia-Cotisel *et al*., 2010; Waduge *et al*., 2010).

Recently, Murrieta-Pazos *et al*., (2011) demonstrated the precision of the technique to characterize the surface of two dairy powders presenting low and high fat surface coverage (table 5).

Table 5. Surface characterization of food powders by Atomic Force Microscopy.

Powder systems						References
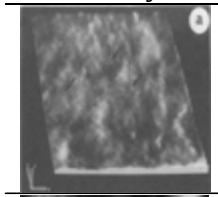	Native wheat starch	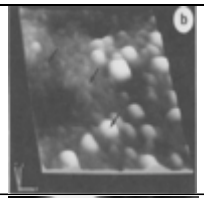	Native potato starch	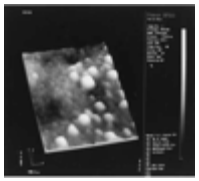	Native potato starch	(Baldwin *et al*., 1998; Gallant *et al*., 1997)
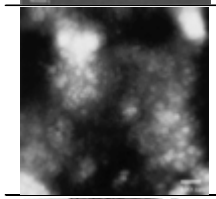	Rice starch after destruction of granules	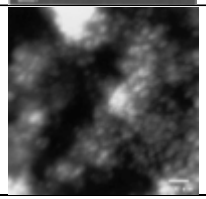	Corn starch after destruction of granules	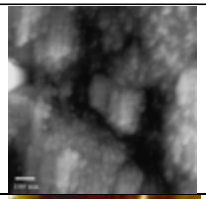	Potato starch after destruction of granules	(Ohtani *et al*., 2000b)
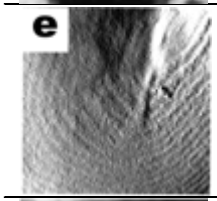	Pea starch after exposure to water	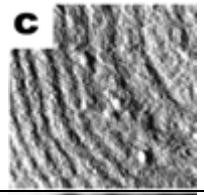	Pea starch after drying	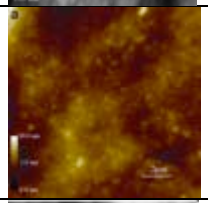	Potato starch gelatinized	(An *et al*., 2008; Ridout *et al*., 2004)
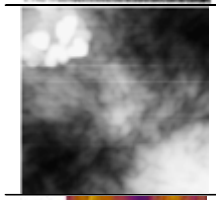	Tapioca starch mapped with -OH	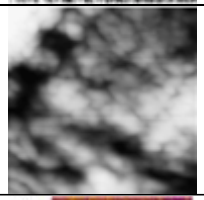	Tapioca starch mapped with -OH after acid hydrolysis	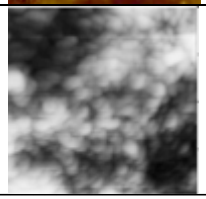	Tapioca starch mapped with $-CH_3$	(Wuttisela *et al*., 2009)
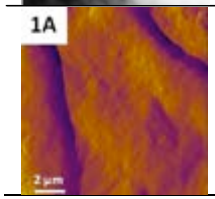	Skim milk powder	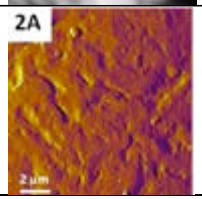	Whole milk powder			(Murrieta-Pazos *et al*., 2011)

AFM images were in agreement with those obtained by SEM, revealing a flat surface for skim milk powder (SMP) and a rough surface for whole milk powder (WMP). In addition, the average surface roughness was determined and was respectively found around 306 nm for SMP and 146 nm for WMP for a definite surface area (10x10 μm).

AFM was also recently used to study the structure of MPC particles as function of the storage in reconstituted milk (fresh and after ageing 30 days at 25ºC and 65% RH) (Fyfe et al., 2011). The AFM measurements permit to conclude that the surface modification of the aged MPC and the increase of the surface hydrophobicity contribute to the decrease of the MPC solubility during storage.

II.3.3. TRANSMISSION ELECTRON MICROSCOPY (TEM)

In TEM, an image is formed from a beam of electrons transmitted through an ultra thin specimen and consequently forms an image at the receiving device. The beam of electrons interacts with the specimen as it passes through.

The application in food powders is not very extensive. Nevertheless, specific details about protein-protein and protein-fat interactions can be observed in milk powder sample (Vignolles *et al*., 2009a). The microstructure of four commercial whole milk powders and their insoluble residuals were observed. Differences were observed depending on the processing conditions (McKenna *et al*., 1999; Qi, 2007), some examples are shown in table 6**.**

TEM has permitted the understanding of the suprastructure of the starch granules. These studies started with (Whistler & Turner, 1955). “Blockets” of granules were later observed in the starch surface structure (Baldwin *et al*., 1997), and more recently, a technique was performed that oxidized the surface of amorphous regions in order to attach silver particles (table 6). The silver helps highlight the starch superstructure and so a model has been developed (Gallant *et al*., 1997).

(Rayas-Duarte *et al*., 1995) used gold-labeling to detect a specific polypeptide by TEM, both in the surface and inside the starch granule in wheat endosperm (table 6).

Table 6. Characterization of food powders by Transmission Electron Microscopy (TEM).

Methods	Powder systems		References
Spray drying	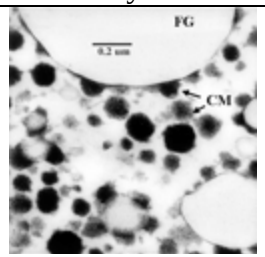 Instant whole milk powder CM: Casein Micelles FG: Fat Globules	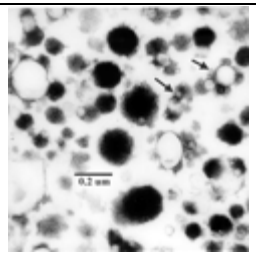 Instant whole milk powder Arrows: Interactions Fat Globules-Casein Micelles	(McKenna *et al.*, 1999)
Extraction	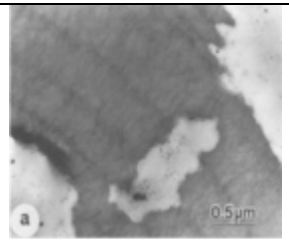 Wheat starch after enzymatic hydrolysis	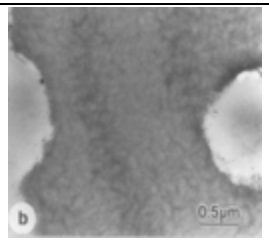 Potato starch after enzymatic hydrolysis	(Gallant *et al.*, 1997)
Natural state	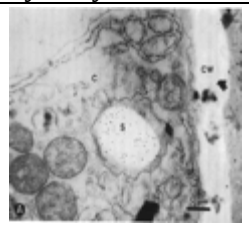 Wheat endosperm S = starch	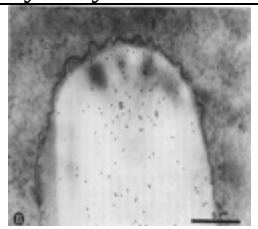 Wheat endosperm Arrow = starch surface	(Rayas-Duarte *et al.*, 1995)

II.3.4. CONFOCAL LASER SCANNING MICROSCOPY (CLSM)

Recently, CLSM was shown to be a helpful tool for internal micro-particle characterization. CLSM enables the production of 3-dimensional optical plan images. It can provide information about particle morphology and the location of fat at the surface of whole milk particles (McKenna, 1997). The work of McKenna *et al*. (1999) for different commercial whole milk powders, was complemented by CLSM observations of differences in fat droplet size and distribution across the surface under different process conditions (table 7). CLSM was also performed on high-fat milk powders after a 6 month storage period, with and without homogenization (table 7) by Vignolles *et al*. (2009a). Differences in fat droplet size were also associated to the process conditions. The distribution of fat within and on the milk powder was also studied by (Kim *et al*., 2002), results are observed in table 7. Chanvrier *et al*. (2005) observed the protein structure in corn flour (table 7). The influence of drying temperatures was investigated by Paramita *et al*. (2010) on microencapsulated limonene. The increase of the feed temperature increased the wall thickness and decreased the diameter of hollow particles. This is found favorable to avoid flavor release and to resist the penetration of both oxygen and water from the surrounding environment. Paramita *et al*. (2010) have also employed the CLSM technique for studding the morphology of spray-dried microcapsules.

Table 7. Characterization of food powders by Confocal Laser Scanning Microscopy (CLSM).

Methods	Powder systems				References
Spray drying	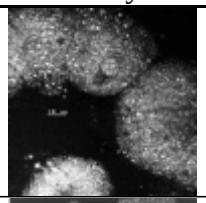	Instant whole milk powder	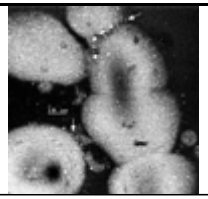	Instant whole milk powder	(McKenna *et al*., 1999)
	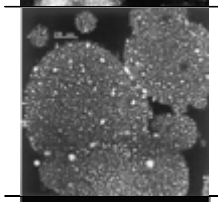	Whole milk powder			(Kim *et al*., 2002)
	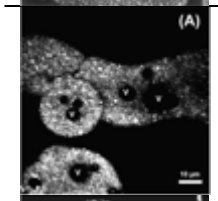	Milk model with low free fat	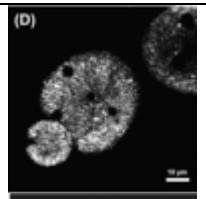	Milk model with low free fat after free fat extraction	(Vignolles, Lopez, Ehrhardt, *et al*., 2009)
	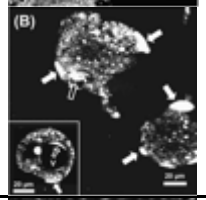	Milk model with high free fat	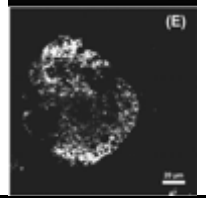	Milk model with high free fat after free fat extraction	
Milling	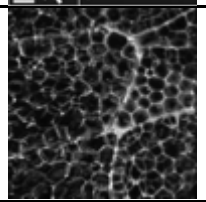	Proteins in corn flour			(Chanvrier *et al*., 2005)

II.4. LASER DIFFRACTION AND DYNAMIC IMAGE ANALYSIS

Until recent years, shape analyses were performed by image processing techniques obtained by CLSM and/or SEM (Du & Sun, 2004). Nowadays, laser diffraction systems coupled with image processing have been developed and permit on line measuring of size and shape in a very high number of particles. A great number of qualitative terms may be used to give some indication of particle shape (Saad *et al*., 2011b). For example, the circularity or sphericity is defined as the ratio of the perimeter or the silhouette and the circumference of a disk that has de same area as the silhouette and the convexity is the ratio of the value obtained by projecting a particle area filling concave zones and the real area. This describes the compactness of a particle (Hentschel & Page, 2003).

Saad *et al*. (2011b), developed a quantitative method to evaluate shape factors (Elongation, Circularity, Compactness and Convexity) of wheat powder particles. The powders studied were, Native Flour, Sieved Flour <125 μm, 125-160 μm and >160μm, Native semolina and Semolina Sieved < 315μm and >315μm. Wheat particle display values of elongation between 2.04 and 2.11, circularity from 1.13 to 1.17, compactness between 0.690 and 0.707 and finally convexity from 0.902 to 0.873.

The wetting behavior of a solid particle may be influenced by the particle size. The wettability time was systematically shorter (88-115 s) for large (~400 μm) particles in the case of casein powders (Gaiani *et al*., 2005). Indeed, faster wetting (4.1 s studying 4g of sieved skim milk powder) is often recorded with large particles (>1000 μm) doe to the formation of large pores, high porosity and small contact angles between the powder surface and the penetrating water (Freudig *et al*., 1999).

Very little work has been carried out for food powders on particle morphology (Gaiani *et al*., 2011a; Perea *et al*., 2009) whereas the literature was very furnished for minerals powders (Chau *et al*., 2009; Ulusoy, 2008). Nevertheless, Perea *et al*. (2009) found some relationships between the morphology of milk powder agglomerates and their rehydration properties. An increase of the solubility and the wettability was related with an increase of the particle compactness and shape factor. The study of Gaiani *et al*. (2011a) showed, for the first time, a correlation between powder rehydration properties and particles shape, in addition to the particle size and color (mainly related to chemical composition). The sphericity was the

shape parameter demonstrating a stronger influence in rehydration properties, sphericity values were registered between 0.5 and 0.9 for dairy powders (NMC, NWI, SMP, WMP and Semi-SMP), small particles presenting high sphericities values (~0.9) obtained lower wetting times, SMP = 1750 s, Semi-SMP = 1650 s, NMC = 2500 s. Furthermore, a regression model was developed to replace time-consuming measurements for dispersibility and solubility.

II.5. DYNAMIC VAPOR SORPTION (DVS)

The DVS apparatus provides fully automated, rapid and accurate measurements of gravimetric moisture uptake in solid materials at a wide temperature range using dynamic environment control and ultra-sensitive recording microbalance. Sorption isotherms were performed for casein powder during storage by Gaiani *et al*. (2009). By applying the model of Guggenheim-Anderson-Boer (GAB), after 60 days of storage, a decrease of the monolayer capacity was registered from 0.0632 to 0.0617 kg/kg at 20ºC and from 0.0632 to 0.0524 kg/kg at 50ºC. This decrease in the water affinity was related to the surface fat increases during storage. It was hypothesized that a layer of fat may progressively cover the surface making it more hydrophobic, the appearance of this fat layer was confirmed by XPS (table 1 2 and 3).

Wheat flour isotherms were also registered by Saad *et al*., (2009). Isotherms were fitted to GAB model, the values shown a slightly increase in the monolayer capacity, from values obtained in native flour (0.085 kg/kg) to those registered after first pass re-grinding (0.084 kg/kg), second pass re-grinding (0.085 kg/kg) and thirst pass re-grinding (0.086 kg/kg), even when XPS presents a decrease in the number of hydrophobic bonds in contrast to hydrophilic bonds. Authors attributed the higher water affinity to a starch granule rupture caused by the re-grinding process. Mathlouthi & Rogé (2003) correlated the water vapor adsorption isotherm to the caking and flowability of sieved and/or pulverized sucrose, studding from amorphous and/or crystalline (RH > 86%) forms.

Flowability measured as friability angle was registered from 35-55º at HR = 30% to 90º at HR = 90% for all the sizes. The caking of crystalline forms does not allow to decaking the powder because of an agglomeration phenomena. Murrieta-Pazos *et al*. (2011) related data obtained from the sorption isotherm to the powder surface composition (EDX, AFM and XPS). The curves of diffusivity were directly correlated to the chemical state of lactose crystallized (HR > 54%) or amorphous (HR < 54%), during water uptake and its localization at the surface. The protein, lactose and lipids composition registered in the first micrometers

(by EDX at ~1μm) was SMP = 34.0, 16.8 and 46.4 respectively and WMP = 25.8, 13.7 and 58.6 respectively, the composition of the first nanometers (by XPS at ~10 nm) is shown in table 3.

The DVS method could not give direct information about the surface but may be used to obtain the following data: monolayer capacity, water binding energy and specific surface area. These data were in turn related to the particle surface characteristics.

II.6. SURFACE CHEMICAL EXTRACTION TECHNIQUES

Different extraction techniques have been developed to obtain surface fat from dairy powders table 8. Vignolles *et al*., (2009a) enhanced one technique by varying the solvent hydrophobicity, the number of extractions, the solvent/powder ratio, the agitation mode and intensity, and also the extraction time. (Kim *et al*., 2009a) precisely described a procedure to selectively collect surface free fat, inner free fat, encapsulated fat and total fat.

After fat extraction, it may be of interest to obtain information about the extracted fractions. DSC and High Performance Liquid Chromatography (HPLC) are the most used in order to compare total fat with surface fat properties.

DSC is one of the most widely used thermal analytical techniques in food research (Farkas & Mohácsi-Farkas, 1996). Vignolles *et al*. (2009a) adapted protocols of DSC to measure the thermal profiles of fat in situ directly in powder samples, and in anhydrous bulk fat extracted from the powders. In a low free fat dairy powder, i.e. less than 5% of the total fat, the crystallization profile of fat in the powder after free fat extraction had a second exothermic peak which enthalpy was higher than in the powder before free fat extraction.

Table 8. Variable fat extraction techniques and quantities extracted in milk powders and milk sub-product powders.

Powders	Free fat		Surface free fat		Inner fat		Encapsulated and total fat			References
	Quantity ($g.g^{-1}$)	Extraction method	Quantity ($g.g^{-1}$)	Extraction method	Quantity ($g.g^{-1}$)	Extraction method	Quantity encapsulated fat ($g.g^{-1}$)	Quantity total fat ($g.g^{-1}$)	Extraction method	
WMP	-	-	0.007	(Buchheim, 1978) Hexane	0.015	(Kim *et al*., 2005b) Hexane	0.235	0.266	(Kim *et al*., 2005b) Hexane/ isopropanol	(Kim *et al*., 2005b)
CP			0.266		0.211		0.228	0.715		
WMP	0.028	(Buma, 1971) Petroleum ether	-	-	-	-	-	-	-	(Kim *et al*., 2005a)
SMP	0.001									
CP	0.490									
WPC	0.002									
WMP after spray drying chamber	0.019	(Kim *et al*., 2009a) Hexane	0.009	(Kim *et al*., 2005a) Hexane	-	-	-	-	-	(Kim *et al*., 2009a)
WMP-A3VFB	0.018		0.007							
IWMP after Static fluidized bed	0.012		0.010							
IWMP-A1VFB	0.012		0.009							
IWMP-A2VFB	0.016		0.012							
WMP after 6 months	-	(Buma, 1971) Hexane	0.010	-	0.034	(Kim *et al*., 2005b) Hexane	0.208	0.261	(Kim *et al*., 2005b) Hexane/ isopropanol	(Kim *et al*., 2009c)
CP after 6 months	-		0.509		0.097		0.033	0.679		
WMP	0.021	(Vignolles *et al*. 2009a) Petroleum ether	-	-	-	-	0.217	0.237	Röse-Gottlieb Petroleum ether	(Murrieta-Pazos *et al*., 2012b)
Agglomerated WMP	0.030						0.206	0.252		

AxVFB: After x vibrating fluidized bed (x = 1, 2 or 3), CP: Cream Powder, IWMP: Instant Whole Milk Powder, SMP: Skim Milk Powder, WMP: Whole Milk Powder, WPC: Whey Protein Concentrate.

The crystallization curves obtained were different and attributed to a difference in fat suprastructure and fat composition. On cooling, different melting profiles were also observed and attributed to different fatty acid organization in total and free fat. Kim *et al*. (2005b), Murrieta-Pazos *et al*., (2012b) and Vega *et al*. (2005) studied dairy powders and ice cream mixture powders and they did not found differences in the melting profiles of free fat and encapsulated fat. It was explained by the need of a very different fatty acid profile to obtain a different melting profile.

Kim *et al*. (2005a) suggested a tendency present among the different milk fat fractions studied by GC, high-melting triglyceride species (saturated fatty acid C6-C18) seem slightly more concentrated in the free-fat fractions and low-melting triglyceride species (unsaturated fatty acid C16-C18) seem more concentrated in the encapsulated fat, this results agree with those obtained by Murrieta-Pazos *et al*. (2012b) for WMP.

No significant differences were observed by GC between fat fractions obtained from standard and agglomerated powder, meaning that functional differences observed between these powders were not due to a different fat compositions (Murrieta-Pazos *et al*., 2012b).

Changes in the surface composition during long-term storage of WMP and CP was studied by gaseous chromatography (GC) and reversed-phase High Performance Liquid Chromatography (HPLC) were studied by (Kim *et al*., 2009c). After 6 months storage was observed in the inner free fat a decrease in the long-chain saturated fatty acids (C16:0 and C 18:0) with concurrent increases in the long-chain unsaturated fatty acids (C16:1 and C18:1-C18:3),. This was in agreement with the triglyceride profile obtained by HPLC. The results showed that inner free fat had higher concentration of low-melting triglycerides (C24-34) and medium-melting triglycerides (C36-C40) compared with other milk fat fractions. High-melting triglycerides were found to be slightly more concentrated in the surface free fat. A release of low-melting triglycerides towards the surface of the powder during storage was observed in both WMP and CP.

II.7. INVERSE GAS CHROMATOGRAPHY (IGC)

The functionality of food powders can be affected by surface property modifications caused by external factors such as ambient humidity, the surface amorphous content generated by the process, or the storage conditions. It is also of interest to modify the surface functionality by addition of a flavor compound or emulsifier. Inverse Gas Chromatography (IGC) appears as an efficient tool to investigate surface modifications of food powders under different parameters.

In contrast to conventional gas chromatography where a known stationary phase separates and identifies various components, IGC uses identified molecules called probes, to determine surface properties of a solid packed into a column. IGC can provide different physical chemistry parameters of the solid surface such as surface energy, thermal transitions, crystallinity, specific surface area, and thermodynamic properties of the probe-solid system including heats of adsorption, free energy and entropy of adsorption.

Depending on the amount of injected probes, two techniques of IGC can be distinguished: IGC at infinite dilution consisting of the injection of a very minute amount of probe vapor corresponding to the beginning of the isotherm, or IGC at finite concentration with injection of some microliters of liquid probe in order to cover approximately the surface of the solid with one monolayer. This second technique permits the plotting of sorption isotherms for different organic probes or water molecules. The theory is already well detailed elsewhere (Conder & Young, 1979).

In the food field, IGC was used for several years mainly to study the influence of moisture on surface properties of food products and to determine their interactions with aroma compounds. As shown in the following paragraphs, different food powders were investigated such as wheat or corn starch, wheat gluten, collagen, soy protein, sugars (lactose, glucose, sucrose, raffinose), chitin, pasta products, dry bakery products, theophylline and caffeine.

II.7.1. IGC AND MOISTURE ADSORPTION ISOTHERMS TO INVESTIGATE INTERACTIONS BETWEEN HUMIDITY AND FOOD COMPONENTS

IGC is a rapid and efficient technique for the determination of moisture adsorption isotherms. Coelho *et al*., (1979a) showed the presence of water-polymer interactions from water isotherms on collagen. The isosteric heat of adsorption is higher at low moisture

content, revealing the adsorption of water molecules on the most active sites. It then drops slightly to a constant value of 6.8 kcal/mol, characteristic of hydrogen bonding.

Table 9. Zimm-Lundberg cluster analysis for two systems: water-raffinose and water-wheat flour at 30°C.

system	a (mg $H_2O.g^{-1}$ solid)	$p.10^3$ (atm)	a_w (p/p_0)	C_1G_{11}	References
water-wheat flour	10	0.37	0.01	-0.35	(Riganakos *et al*., 1989)
	20	1.85	0.04	-0.65	
	30	4.63	0.11	-0.85	
	40	14.80	0.35	-0.60	
	50	23.87	0.57	-0.16	
	60	27.20	0.65	0.05	
	70	29.97	0.72	0.29	
	80	32.38	0.77	0.55	
	90	34.60	0.83	0.85	
	100	36.63	0.87	1.14	
water-raffinose	1.0	7.2	0.17	-0.25	(Demertzis *et al*., 1989)
	2.0	17 .0	0.41	+0.07	
	3.0	22.8	0.52	+0.54	
	4.0	26.9	0.64	+1.28	
	4.5	27.7	0.66	+1.54	
	5.0	28.7	0.69	+1.86	

a: water uptake, , a_w: water activity, C_1G_{11} : cluster function , p: pressure of water.

They also proved the absence of clustering of water molecules in collagen by the calculation of the value of the Zimm-Lundberg cluster function C_1G_{11} (Zimm & Lundberg, 1956), the result was negative. It should be highlighted that if this function has a negative value the water molecules are dispersed and adsorbed on active sites on the solid surface. On the contrary, a positive value of this function indicates the presence of clusters of water molecules.

In the cereals field, IGC was used to study water sorption by wheat flour (Riganakos *et al*., 1989). Two different mechanisms were suggested: at lower water vapor pressures, the water molecules adsorb themselves on the active sites of high binding energies such as C=O, COO^- or NH_4^+, and at higher moisture contents (> 25.10^{-3} atm), water clusters are formed showing that water-water interactions are favored. This is shown by the value of the cluster function C_1G_{11} upper to 0 (table 9).

Water isotherms were successfully fitted to the BET, GAB and Freundlich isotherm models. Riganakos *et al*. (1994) compared the gravimetric (the static method with saturated

salt slurries) with two IGC methods (called IGC and CIGC respectively corresponding to several injections or a single large solute injection) to obtain water sorption by wheat and soy flour. The publication of Coelho *et al*. (1979b) gives the details about the plot of the moisture sorption isotherm with these two methods. There was an excellent agreement between monolayer values using the three methods (table 10).

Table 10. BET and GAB isotherm constants for water sorption in wheat and soy flours using the static gravimetric, IGC and CIGC sorption methods at 30°C (Riganakos *et al*., 1989).

Method	Powder	BET model		GAB model		
		V_m (g /g)	C	W_m (g /g)	C	K
Gravimetric		0.068	36.90	0.065	26.48	0.94
IGC	Wheat flour	0.063	34 .28	0.063	20.28	0.91
CIGC		0.061	30.48	0.062	20.84	0.91
Gravimetric		0.050	15.28	0.048	20.48	0.90
IGC	Soy flour	0.055	20.78	0.050	25.30	0.96
CIGC		0.051	14.04	0.053	17.20	0.94

The same authors also obtained moisture sorption isotherms on polysaccharides such as apple and citrus pectin (Demertzis *et al*., 1991) and also on crystalline raffinose (Demertzis *et al*., 1989). The monolayer values for crystalline raffinose calculated with the BET model at different temperatures are much lower (1.30 mg $H_2O.g^{-1}$ solid at 35 °C) than those reported for other sugars such as lactose (32 mg $H_2O.g^{-1}$ solid at 34 °C) and sucrose (99 mg $H_2O.g^{-1}$ solid at 35 °C). This could be attributed to the high degree of crystallinity of raffinose., the higher is the degree of crystallinity, the higher the hydrophobic character of the sugar and the tendency to form clusters. This leads to a lower water monolayer value. The water-water interactions are favored with regard to the hydrophobic surface-water interaction. Results of the Zimm-Lundberg cluster analysis show that cluster formation is favored on raffinose even at relatively low water pressures (table 9). The cluster function C_1G_{11} is greater than 0 from a pressure equal to 17×10^{-3} atm. If we compare the two powders, wheat flour and raffinose, at any given pressure, the water uptake is much lower for raffinose than for wheat flour. The effect of crystallinity was also reported by (Smith *et al*., 1981) on water sorption isotherms of sucrose (crystalline saccharose) and amorphous glucose. The ability to sorb a given amount of water is greater for the amorphous sugar than for the crystalline one. However the authors overlooked some key aspects during the investigations. The nitrogen specific surface area of the two sugars that can influence water sorption was not taken into account. Also, the BET equation was used to calculate the monolayer coverage with water, however the data did not conform to the linearized BET equation. The authors then interpreted this non-conformity as a

result of a complex sorption mechanism occurring in the very low water activity ranges studied. (Helen & Gilbert, 1985) compared water sorption isotherms of two bakery products: crackers (high in fat and low in sugar) and sweet biscuits. The cracker absorbs significantly more moisture than the sweet biscuit, indicating a higher hygroscopicity of the crackers. The clustering analysis indicated that water-food interactions were favored in the crackers compared with water-water interactions in sweet biscuits. An experiment consisting of adding increasing amounts of crystalline sucrose to crackers leads to a decrease of their hygroscopicity. This favors the formation of water clustering and shows the isotherm of crackers tend to that of the sweet biscuit. This study also confirms that higher is the crystalline character of a powder, smaller is the capacity to absorb water and the formation of water clustering is favored. Pasta products were analyzed by Lagoudaki *et al*. (1993), who compared moisture sorption isotherms of conventional and diet spaghetti. The capacity to sorb water is higher for conventional spaghetti than for diet spaghetti, due to its higher carbohydrate content. The same authors (Lagoudaki & Demertzis, 1994) also compared the effects of moisture and temperature on the water sorption of dehydrated food constituents such as potato starch, egg albumin and wheat gluten. Table 11 gathers the BET and GAP isotherm constants for water sorption at 30 °C on potato starch, egg albumin, wheat gluten and spaghetti.

Table 11. BET and GAB isotherm constants for water sorption in spaghetti, potato starch, egg albumin and wheat gluten at 30°C.

Sample	BET model		GAB model			References
	V_m (g/g)	C	W_m (g/g)	K	C	
Conventional spaghetti	0.0604 ± 0.0018	7.77 ± 4.2	0.0770 ± 0.0112	0.84 ± 0.08	7.48 ± 1.22	(Lagoudaki *et al*., 1993)
Diet spaghetti	0.0548 ± 0.0060	7.13 ± 2.5	0.0589 ± 0.0155	0.84 ± 0.30	6.54 ± 1.37	
Potato starch	0.0675 ± 0.0055	14.04 ± 1.66	0.0906 ± 0.0083	0.73 ± 0.08	10.48 ± 1.72	(Lagoudaki & Demertzis, 1994)
Egg albumin	0.0537 ± 0.0058	7.91 ± 1.73	0.0576 ± 0.0073	0.77 ± 0.08	7.17 ± 1.33	
Wheat gluten	0.0440 ± 0.0048	7.49 ± 1.15	0.0530 ± 0.0055	0.85 ± 0.01	7.32 ± 1.57	

II.7.2. IGC A TECHNIQUE USED TO STUDY SURFACE AMORPHOUS CONTENT

Performance of a solid in different processes can be related to its amorphous content especially located at the surface. So techniques like IGC which are able to quantify amorphous content on a solid surface are of great interest. Different works were carried out on lactose using IGC. Ticehurst *et al*. (1996) examined four batches of lactose (Batches A, B, C

and D), which exhibited variable processing performance but were revealed identical by usual physical and chemical techniques. Only IGC led to different surface properties. Table 12 gathers values of the dispersive component of the surface energy, γ_S^D and specific free energy of adsorption, ΔG^{sp} of different polar probes for the four batches. If the γ_S^D are comparable, the ΔG^{sp} for polar probes exhibit significant differences, indicating variations in the polar surface properties between the batches.

Table 12. Surface properties of α-lactose monohydrate at 30°C after conditioning at 40°C (Ticehurst *et al.*,1996).

Samples	γ_S^D (mJ/m^2)	ΔG^{sp} (kJ/mol)			
		Acetone	THF	Ether	Ethyl acetate
Batch A	44 ± 2	9.1 ± 0.3	7.3 ± 0.2	6.0 ± 0.2	8.6 ± 0.2
Batch B	40	5.7	4.4	2.9	5.4
Batch C	41 ± 3	8.2 ± 0.3	6.6 ± 0.2	5.2 ± 0.2	7.8 ± 0.2
Batch D	42	8.7	6.9	5.4	7.7

The lactose was also studied to show some relationships between IGC parameters and amorphous content on the solid surface (Newell *et al*., 2001a). Three samples of lactose were compared by IGC: a crystalline lactose, a spray dried 100% amorphous lactose and a milled lactose with less than 1% amorphous content by mass. The milled lactose was noted to have a similar dispersive surface energy (41.6 mJ/m^2) to the 100% amorphous lactose (37.1 mJ/m^2), indicating that the amorphous was preferentially located on the surface. This result revealed that milling disrupts the surface more than the bulk. For comparison, the dispersive surface energy value for the crystalline lactose was equal to 31.2 mJ/m^2. The same authors (Newell *et al*., 2001b) also showed that under humid conditions (0-20% RH), the dispersive component of the surface energy of amorphous lactose was reduced to the value of the crystalline one, giving evidence of crystallization.

Ambarkhane *et al*. (2005) compared IGC and gravimetric vapor sorption to study the behavior of amorphous lactose during the water sorption. The data made it possible to determinate: (1) a first transition at low RH (ca. 10% RH) corresponding to the onset of significant molecular mobility in the amorphous material; (2) the glass transition followed by the collapse of amorphous lactose occurring between 30 and 40% RH; and (3) the onset of crystallization above 45% RH. The authors showed that at each temperature T of analysis, the amorphous lactose crystallizes when Tg_{mix} (using the Gordon-Taylor equation taking into account the masses and Tg of water and dry amorphous lactose) is 32 °C below T.

$$\left(\gamma_{Seff}^{D}\right)^{1/2} = \phi_1(\gamma_{S1}^{D})^{1/2} + \phi_2(\gamma_{S2}^{D})^{1/2} \quad \text{Equation 2}$$

where: ϕ_x are the respective surface fractions of each solid.

The values γ_{S1}^{D} and γ_{S2}^{D} are determined by the pure solids reference. This calculation needs crystalline and amorphous references. The authors warned against the reference material; if the amorphous contains other surface disorders (i.e. fractures, defect sites, etc) its energies will be interpreted against amorphous references. The first test reviewed on lactose. Crystalline α-lactose monohydrate and spray-dried lactose were respectively taken as the crystalline and the fully amorphous surface references. From these reference materials, several physical mixtures were prepared in order to measure the difference in γ_{S}^{D} and to compare them with the theoretical values. There is excellent agreement between experimental data and the theoretical prediction based on the surface energies of the crystalline and amorphous references. IGC gives only the surface amorphous content. A bulk technique, DSC, was carried out to evaluate the bulk amorphous content. Comparing the IGC and DSC amorphous content showed how disorder was distributed throughout the particle. For the micronized sample, the disorder resides only at the solid surface. The partially recrystallized spray-dried sample presents an energetic surface as well as bulk corresponding to a significant amorphous percentage (~70%). The ball milled particles lead to very high surface amorphous content while the bulk gives around 5%.

To conclude, IGC appears as an efficient tool to evaluate the surface amorphous content and the amorphous phase, which can be desirable (e.g. to stabilize proteins) or undesirable (e.g. can decrease the stability and induce changes in product performance).

II.7.3. IGC TO INVESTIGATE INTERACTIONS BETWEEN FLAVOR COMPOUNDS AND FOOD COMPONENTS

IGC is also of interest in the food field regarding the study of interactions between flavor compounds and food components. These compounds have a great impact on the flavor of the final food product. IGC is a powerful tool to investigate the adsorption of flavor compounds onto solid support such as proteins, starch and sugars.

One of the first studies on this subject was realized by McMullin, Bernhard, & Nickerson (1975), which demonstrated that lactose has a great ability to adsorb aromas. The heats of adsorption of a large variety of organic compounds (esters, aldehydes, ketones, alcohols and hydrocarbons) on anhydrous lactose were compared (Table 13). For a given number of carbon atoms alcohols have the highest heats of adsorption, hydrocarbons have the lowest, and the other functions adsorb with intermediate strengths. The hydrogen bonds formed between the lactose and the functional groups of organic compounds, such as hydroxyl for alcohols, was supposed to be the major factor involved in the strength of adsorption.

Table 13. Heats of adsorption on two solids: soy protein isolate and lactose obtained by different authors.

-ΔH (kcal/mole)	Soy protein isolate			Lactose
Flavor	(Aspelund & Wilson, 1983)	(Crowther *et al*., 1980)	(Zhou & Cadwallader, 2004, 2006)	(McMullin *et al*., 1975)
n-hexane	-	-	6.8	-
n-nonane	6.52	-	-	9.24
n-decane	8.36	-	-	10.55
Hexanal	8.89	11.1	10.3	11.63
Methyl n-butyrate		-	-	10.65
Methyl n-pentanoate	6.71	-	-	12.14
Methyl n-hexanoate	8.19	-	-	13.57
2-Pentanone	2.92	10.1	-	10.81
2-Hexanone	6.04	11.0	10.5	12.03
2-Heptanone	8.11	12.7	-	13.09
1-Pentanol	11.25	13.1	-	16.03
1-Hexanol	13.89	16.7	16.3	17.57
1-Heptanol	18.06	16.8	-	17.18

Soy protein is also of much interest in the food field. Different authors also studied interactions between soy protein and aroma compounds. Crowther *et al*. (1980) compared adsorption coefficients and heats of adsorption of a number of volatile organics onto soy protein isolate (SPI) after treatments involving different levels of temperature, moisture and shear. They observed changes in adsorption coefficients of the treated samples attributed to a decrease in binding due to the protein denaturation. Aspelund & Wilson (1983), also measured heats of adsorption to determine strengths of adsorption of flavors onto SPI (table 13). They noticed that the hydrocarbons adsorbed the weakest and the alcohols the strongest onto dry soy protein. The former interact only with non-specific interactions (Van

der Waals), the latter interact not only with nonspecific interactions but also with specific ones and especially hydrogen bonds.

Zhou & Cadwallader (2004) also arrived at the same conclusion as (Aspelund & Wilson, 1983). Volatile polar probes such as 1-hexanol and hexanal have higher binding affinities than an apolar one (hexane) due to hydrogen binding interactions with SPI. The retention of these polar probes are weaker at 30% RH, indicating possible competition for binding sites on the SPI surface between these volatile probes and water molecules. The same authors (Zhou & Cadwallader, 2006) completed their first study on SPI by investigating the influence of flavor compound chemical structure, including functional groups (hydrocarbons, esters, ketones, aldehydes and alcohols) and stereochemistry (position of a double bond, or the distance between a double bond and an hydroxyl group) on binding. They compared thermodynamic and sorption data under different relative humidities.

Boutboul *et al*. (2000) investigated the interactions between aromas and native cornstarch. They observed that retention was higher under humid conditions than under dry conditions especially for alcohols. The authors proposed different hypotheses; on one hand a predominant adsorption phenomenon involving hydrogen bonds between aromas compounds such as alcohols, and glucose residues of the starch. On the other hand, a solvation of aroma compounds by water molecules allows for their diffusion through the starch matrix. Boutboul *et al*., (2002) also obtained different sorption isotherms on starch depending on the aroma compounds and the interactions developed between the starch and the aroma compounds (type II for an ester, type III for d-limonene and linear for an aldehyde and an alcohol).

II.7.4. IGC TO ASSESS THE MODIFICATIONS OF SURFACES AFTER COATING BY EMULSIFIERS

IGC is also a useful tool for the assessment of the modifications of surface properties of powders after different treatments. The evolution of surface properties of sucrose coated by emulsifiers commonly used in chocolate, lecithin or polyglycerol polyricinoleate (PGPR), was monitored by IGC (Rousset *et al*., 2002) (table 14).

The adsorption of the emulsifiers decreases the acidic character (Ka parameter) originating from the hydroxyl group and consequently increases the lipophilicity of the

sucrose. The sucrose-sucrose interactions are weaker inducing an increase in the fluidity of fat-based suspensions like chocolate.

Table 14. Effect of adsorbed lecithin and PGPR at the sucrose surface (Rousset *et al*. 2002).

	Granulated sucrose			Jet milled sucrose		
	Without emulsifiers	With lecithin	With PGPR	Without emulsifiers	With lecithin	With PGPR
γ_S^D (mJ/m^2)	30.3	30.6	31.1	36.5	30.9	30.0
$K_A.10^{-2}$	18	15	15	19	16	16
$K_B.10^{-2}$	23	28	33	22	26	29

II.8. PERSPECTIVES

For a better understanding of the relationships between surface properties and functional properties it is absolutely necessary to characterize the powder surface in detail. For this purpose, specific analytical methods (physico-chemistry and surface physics) able to evaluate the surface properties of the food powders are needed. Some techniques are now well developed in the food powder fields (XPS, SEM), however others may need more attention from the scientific community (TOF-SIMS, particle morphology, EDX).

In figure 6, an example of multi-scale surface investigation is presented.

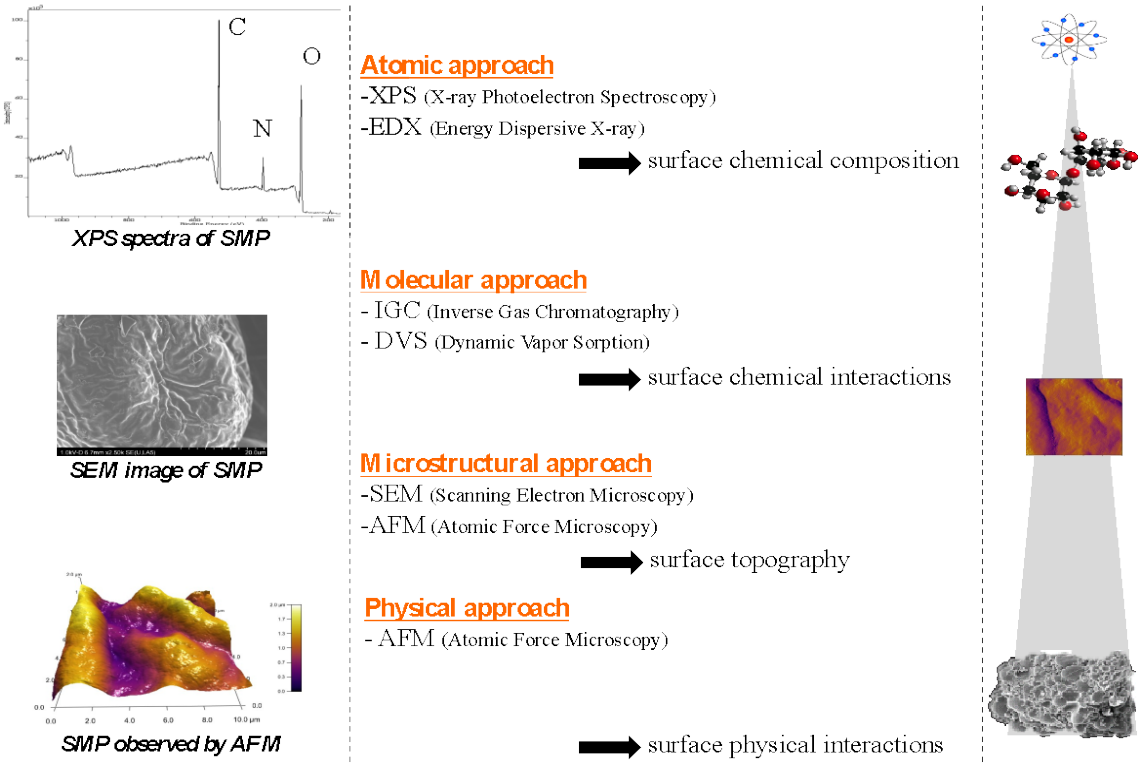

Figure 6. Some techniques allowing the surface characterization.

Coupling atomic, molecular, microstructural and physical approaches may be an interesting option to best understand the surface reactivity. Concurrently, some techniques, like IGC, were rarely used on food powders and may be an efficient tool to evaluate the modifications of surface properties of a powder under wet conditions, or the adsorption of flavor compounds which has a great impact on the flavor of the final product. Recently, IGC was also carried out to quantify the surface amorphous content and the amorphous phase (desirable or undesirable) for the stability of the powder.

Concurrently, research is needed to bind basic approaches with technological applications, while integrating the contribution of both particle surface and process parameters occurring from powder manufacturing to end-products. The principal functional properties of a food powder may be linked to water, thermal and/or mechanical constraints. Figure 7 highlights some links between surface characterization and constraints (hydric, thermal and mechanical).

In conclusion, the surface properties determinations could be of great importance as the surface governs some essential functional properties: wetting, dispersibility, stickiness, flowability, etc. In spite of the only recent use of some techniques, all those presented have been successfully used in the study of food powders.

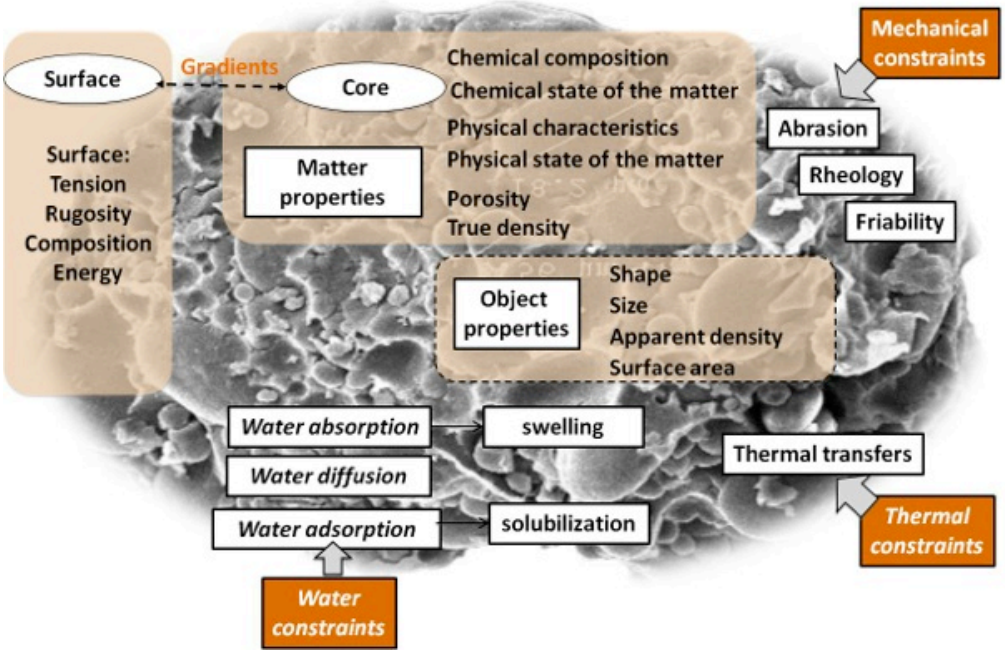

Figure 7. Links between surface characterization and constraints (hydric, thermal and mechanical).

III. MATERIELS ET METHODES

Le présent chapitre introduit tous les matériels et méthodes utilisés dans ce travail de recherche. Ils ont été développés dans deux laboratoires : LIBio et RAPSODEE. Ce chapitre permet aux lecteurs d'avoir une vision générale de la partie expérimentale de l'ensemble du travail de recherche car il inclut les matériels et méthodes utilisés dans les différents articles.

III.1. MATERIELS

Les matériels étudiés dans ce manuscrit de thèse proviennent de deux grandes familles de produits alimentaires: laitières et céréalières. D'un côté, on a la poudre de lait, un produit d'origine animale dont la matière première, le lait, est de nature liquide. Ensuite, il est déshydraté par séchage par atomisation pour obtenir une poudre. De l'autre côté, on a la semoule, d'origine végétale obtenue à partir de grain de blé dur et tout simplement divisé en fines particules par broyage.

Toutes deux sont des poudres de qualité industrielle, intéressantes de par leur complexité et leurs différentes origines d'obtention. Cela se traduit pas une certaine complémentarité.

III.1.1.LES POUDRES DE LAIT

La déshydratation des produits alimentaires permet d'assurer la stabilité du produit par réduction de l'activité de l'eau a_w, ainsi que de frais de transport et de stockage (Schuck *et al*., 2012).

Dans l'industrie agroalimentaire, la méthode de séchage la plus utilisée est le séchage par pulvérisation (charcuterie, produits de la pêche, fourrage, céréales et produits d'origine végétale, fruits, lait, œufs, sang, etc.) (Schuck *et al*., 2012).

L'atomisation (aussi appelée spray drying) est une technique de séchage très courante. Elle consiste à pulvériser le produit, qui est sous forme liquide, dans un courant de d'air chaud. Lorsque le produit humide est placé dans un flux d'air (ou un autre gaz) suffisamment chaud et sec, un gradient de température et de pression partielle en vapeur se produit spontanément entre les gouttelettes et l'air (Schuck *et al*., 2012). Ce phénomène cause:

- un transfert de chaleur de l'air pour le produit en raison de la différence de température.

- un transfert inverse d'eau dû à la différence de pressions partielles de vapeur entre l'air et la surface du produit (figure 8).

L'air sert donc à la fois de fluide de transfert de chaleur et de gaz porteur pour l'élimination de la vapeur d'eau. L'air est chaud et sec quand il pénètre dans la tour de séchage et refroidi et humide quand il la quitte. La température de surface du produit est équivalente à la température de l'air humide soit environ 45 °C obtenu pour une température en air sec de 200 °C.

Le séchage est une méthode d'évaporation de l'eau de surface, cela entraîne une remontée capillaire de l'eau de l'intérieur de la gouttelette vers la surface. Tant que l'humidité moyenne est suffisante pour maintenir la surface assez humide, la vitesse d'évaporation reste constante. Ensuite, une diminution de la vitesse est observée et la température de surface augmente (Schuck *et al*., 2012).

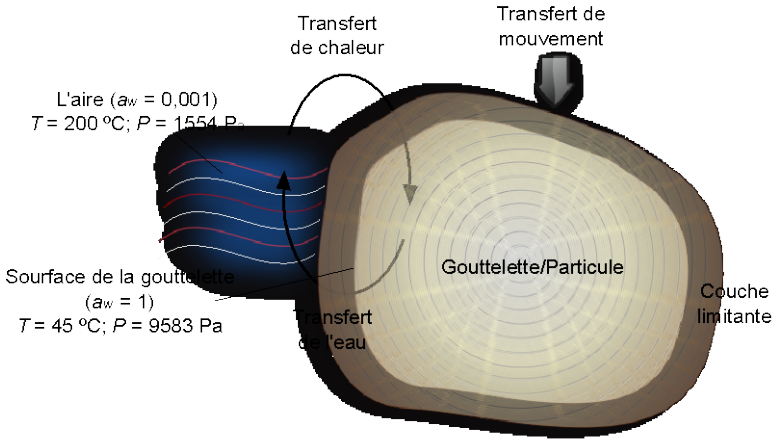

Figure 8. Principe du séchage par atomisation

La vitesse de séchage dépend de trois facteurs:

a) De la surface d'évaporation, qui augmente au fur et à mesure que le diamètre des gouttelettes diminue; la déshydratation s'accélère en même temps que l'interface augmente en taille. Cette interface obtenue par pulvérisation du liquide et de l'air chaud, ainsi que les endommagements du produit par la chaleur sont minimisés (Písecký, 1997; Refstrup, 2003).

b) De la différence de pressions partielles de vapeur d'eau entre la surface de la particule et l'air, qui dépend de l'humidité absolue et de la température d'entrée de l'air.

c) De la vitesse de migration de l'eau de l'intérieur vers la surface de la particule, laquelle peut être réduite par la formation d'une croûte à la surface formée en raison de la transformation des composants par la chaleur.

Le séchage par atomisation consiste principalement en cinq étapes (Písecký, 1997):

a) La concentration: les matières premières sont normalement concentrées avant l'introduction dans le pulvérisateur.

b) L'atomisation: l'étape d'atomisation crée les conditions optimales pour l'évaporation de l'eau dans le produit ayant des caractéristiques souhaitées à la fin du processus.

c) Le contact gouttelettes-air : dans la chambre, le liquide atomisé est mis en contact avec un gaz chaud entraînant l'évaporation de 95% de l'eau contenue dans les gouttelettes en quelques secondes.

d) Séchage des gouttelettes: l'évaporation de l'humidité se déroule en deux étapes. Au cours de la première étape, il y a suffisamment d'humidité dans les gouttelettes pour remplacer le liquide évaporé à la surface et l'évaporation a lieu à un taux relativement constant. La deuxième étape commence lorsque l'humidité n'est plus suffisante pour maintenir des conditions de saturation à la surface des gouttelettes, ce qui provoque une croûte séchée qui se forme à la surface. L'évaporation dépend alors de la diffusion de l'humidité à travers la croûte, qui gagne de plus en plus d'épaisseur.

e) Séparation: des cyclones, des filtres à manches, et des conteneurs à précipitation électrostatiques peuvent être utilisés pour l'étape de séparation finale. Des épurateurs humides sont souvent utilisés pour purifier et rafraîchir l'air de sorte qu'il puisse être libéré dans l'atmosphère.

Le séchage par atomisation (figure 9) présente des avantages certains. Le taux d'alimentation va de quelques kilos par heure à plus de 100 tonnes par heure. Le fonctionnement est continu et adaptable à un contrôle entièrement automatique.

Les poudres standard, en raison de leur taille relativement faible, ne se reconstituent pas bien dans l'eau. A l'inverse, les poudres "agglomérées" et/ou "instantanées" ont été spécifiquement développées pour contrer cela. La fabrication d'une poudre agglomérée suit d'abord le processus classique, décrit ci-dessus. Toutefois, au cours du séchage par atomisation, des petites particules de poudre quittent le séchoir : " les fines ". Les fines sont récupérées dans les cyclones et retournées dans la chambre de séchage à proximité de l'atomiseur. Les gouttelettes du concentré liquide entrent en collision avec les fines et se collent les unes avec les autres, pour former des "agglomérats" de taille plus importante (0,1-0,3 mm) et de forme irrégulière. Les poudres agglomérées se dispersent dans l'eau plus rapidement, elles sont moins poussiéreuses et plus facile à manipuler que les poudres classiques.

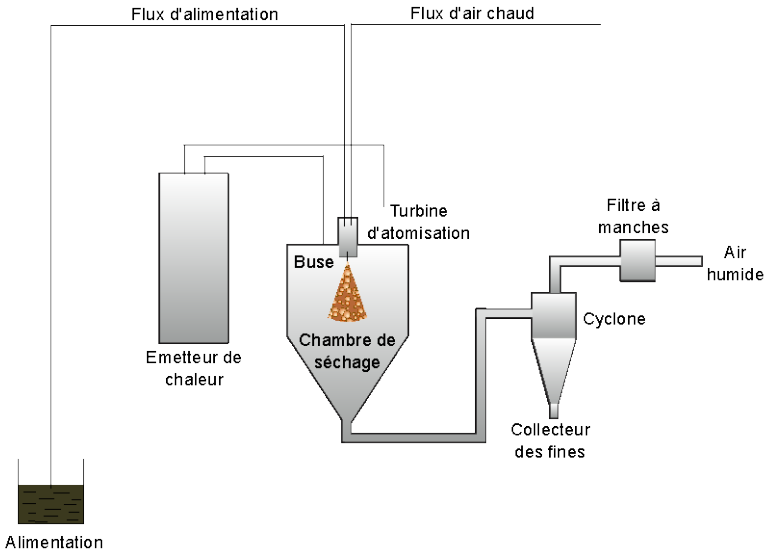

Figure 9. Exemple d'installation d'un équipement de séchage par atomisation.

Pour les poudres de lait entier instantanées, une étape supplémentaire est nécessaire. Après l'agglomération, pour rendre le produit véritablement "instantané" et surmonter l'hydrophobicité ; des traces de lipides sont pulvérisés à la surface des particules. Cette étape supplémentaire consiste à pulvériser la poudre dans un lit fluidisé avec des quantités infimes d'un agent tensioactif naturel : la lécithine de soja. La lécithine de soja est extraite de l'huile

de soja. Les lécithines sont très répandues dans la nature et sont produites naturellement dans le lait.

Quatre poudres industrielles de marque Lactalis (Laval, France) ont été obtenues, dont la composition globale est détaillée dans le Tableau 15. Comme référence, la composition globale du lait entier et écrémé est aussi intégrée.

Tableau 15. Composition globale des poudres de lait.

	Poudre de lait entier standard ou granulé	Poudre de lait écrémé standard ou granulé	Lait éntier	Lait écrémé
Teneur en eau (%)	4	4	87	91
Protéines (%)	26	37	4	4
Lactose (%)	37	51	5	5
Lipides (%)	27	2	4	0

III.1.2.LES SEMOULES

Pour mieux comprendre la structure des particules de semoule, il faut connaître plus en détail la structure de l'endosperme dont la semoule est formée.

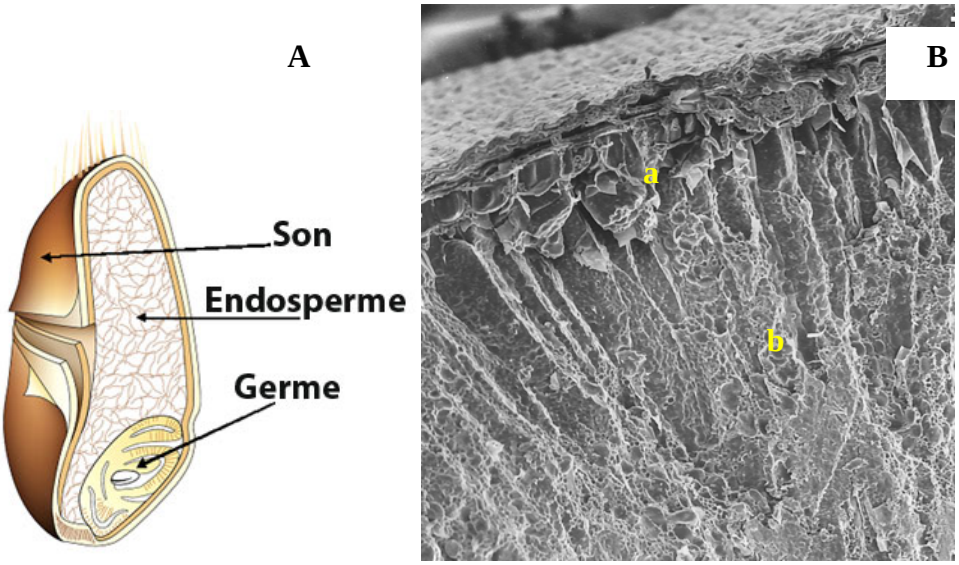

Figure 10. Structure d'un grain de blé (A) et micrographie SEM de l'endosperme de blé dur (B) (Delcour & Hoseney, 2010).

En général l'endosperme est formé par la couche externe d'aleurone (figure 10 B-a) et l'endosperme amylacé (figure 10 B-b). La couche d'aleurone, qui est généralement une couche unicellulaire épaisse, entoure complètement le grain et couvre à la fois l'endosperme amylacé et le germe (Delcour & Hoseney, 2010).

Le broyage est une opération consistant à diviser un solide pour diminuer sa taille et ainsi augmenter sa surface spécifique (surface développée de la poudre par unité de masse) et donc sa réactivité. C'est avec cette opération que les endospermes d'amidon sans le son et le germe sont traités. Un type de broyeur est les plus communément utilisé: à marteaux (figure 11).

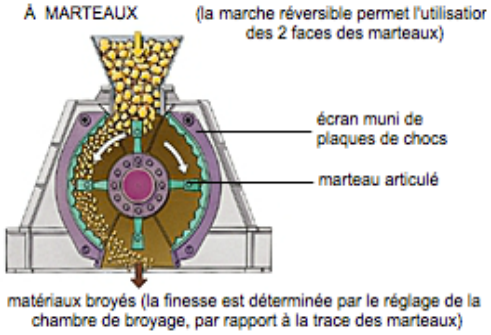

Figure 11. Principal broyeur utilisé dans la production de semoule (Larousse.fr - Types de broyeurs).

Ainsi, lorsque la taille des particules est réduite jusqu'à une taille appropriée, les contenus et les parois cellulaires de l'endosperme produisent de la semoule. Tandis que la farine est généralement un produit réduit jusqu'à atteindre un passage par tamis de 132 μm. La semoule est produite avec des particules de plus grande taille qui sont broyées à partir de *T. durum* (Saad, 2011).

Les raisons des différences de dureté de l'endosperme du blé ne sont pas clairement comprises. Toutefois, les principales différences dans la dureté (texture) des grains de blé tendre et de blé dur, semblent être attribuables à la présence, à l'absence ou la séquence, du polymorphisme dans les protéines puroindoline-a et puroindoline-b. Une théorie dit que ces protéines contrôlent l'interaction du gluten avec la surface des granules d'amidon et cette interaction contrôle la dureté (Delcour & Hoseney, 2010).

Une autre différence entre le blé tendre et le blé dur est la façon dont les cellules se fracturent lorsque les grains sont broyés. Dans les grains de blé dur, le premier point de rupture se produit à niveau de la paroi cellulaire, plutôt qu'à travers l'intérieur des cellules. Cela est particulièrement évident dans les cellules juste en dessous de l'aleurone. Dans l'endosperme de blé tendre, la fracture se produit principalement à travers l'intérieur des cellules. C'est la preuve qu'à l'intérieur des cellules de blé dur la structure est plus solidement liée, résultant en une rupture des parois cellulaires. Bien sûr, comme l'endosperme est réduit à

la taille de la farine, l'intérieur des cellules de blé dur est également fracturé (Delcour & Hoseney, 2010). La figure 12 montre la forte adhésion du gluten (protéines) et de l'amidon dans le blé dur. Le gluten semble enrobé ou adhérer à la surface de l'amidon. Ceci est caractéristique des blés durs. Ainsi, le lien entre les deux est fort. Preuve de la force des liaisons est la tendance des blés durs à casser la paroi cellulaire ou au milieu des granules d'amidon (à noter les granules d'amidon cassé BS) dans la figure 12-A plutôt qu'à l'interface amidon-gluten.

Dans une micrographie similaire de blé tendre figure 12-B, l'apparence est très différente. L'amidon et le gluten présentent le même aspect, mais le gluten n'enrobe pas la surface de l'amidon. Par conséquence il n'y a pas de granules d'amidon fracturés, parce que le lien entre les protéines et l'amidon se casse facilement, cela montre que ce n'est pas une liaison forte. La force de la liaison entre le gluten et l'amidon semble expliquer la dureté du grain, mais la nature de la liaison amidon-protéine n'est pas connue (Delcour & Hoseney, 2010).
Pour développer ce travail une semoule de qualité industrielle a été utilisée (Panzani, Marseille, France).

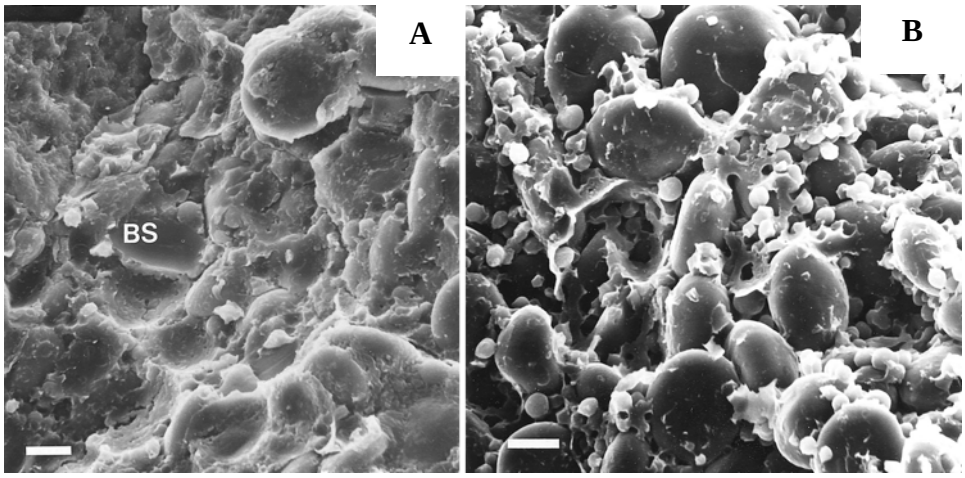

Figure 12. Photo SEM montrant la rupture de l'endosperme de blé dur (A) et de blé tendre (B). (Delcour & Hoseney, 2010).

III.1.3.PREPARATION DES POUDRES PAR TAMISAGE

Avant d'étudier les propriétés de surface des poudres industrielles, il a été nécessaire d'étudier la distribution des caractéristiques individuelles des grains. Pour ce faire, nous avons procédé à l'élaboration du tamisage des particules. Le principe de base du tamisage consiste à diviser un matériau pulvérulent en fractions de tailles différentes en le faisant passer à travers des tamis dont les caractéristiques sont connues. La détermination des

distributions granulométriques par tamisage est réalisée en utilisant une série de tamis dont les mailles sont de taille décroissante et en pesant les fractions retenues sur les différents tamis (Retsch GmbH AS200 digit, Haan, Germany).

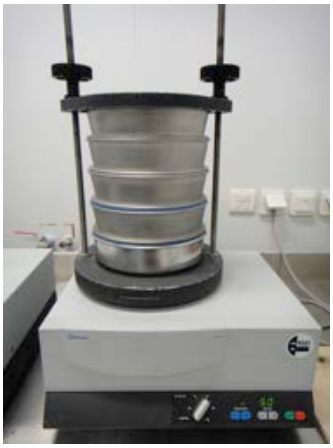

Figure 13. Exemple de tamiseur utilisé.

Dans le cas de la semoule les tamis suivants ont été choisis: 160, 250, 315, 400 et 500 µm pour avoir 5 fractions de taille variable (allant des plus fines jusqu'aux granulées). Pour cela, on a introduit 400 g de semoule dans le tamis supérieur. L'amplitude était fixée à 40 dans l'échelle de l'appareil. Le tamisage durait une demi-journée. Nous avons donc obtenu en tout 5 classes granulométriques: 0-160, 160-250, 250-315, 315-400 et 400-500 µm.

Dans le cas de la poudre du lait, les tamis utilisés ont été les suivants: 40, 80, 125 et 160 µm. Dans la littérature, plusieurs travaux concernant l'étude par la taille des poudres laitières sont disponibles. C'est ainsi que pour ce travail on s'est intéressé à l'étude par la taille que pour les analyses de composition de surface par EDX. La quantité de poudre nécessaire pour ces analyses est de l'ordre de quelques dizaines des milligrammes, par conséquence seulement entre 10 et 20 g de poudre du lait standard (entier et écrémé) ont été tamisés. Le temps de tamisage a été de 20 minutes approximativement à une amplitude de 60 dans l'échelle de l'appareil.

Dans le cas des isothermes de sorption dont la poudre de lait a été analysée, on a conditionné la poudre à une seule taille de particules inférieures à 70 µm, en passant les échantillons par un seul tamis (70 µm).

III.1.4.COMPOSANTS PURS

Pour mieux comprendre les effets de la composition des différentes poudres, les composants purs ont été analysés. Cela a été le cas pour certaines techniques comme la composition de surface par Analyse Dispersive en Energie (EDX), la montée capillaire, l'enrobage ou encore l'agglomération des particules par humidification. Les composants purs utilisés pour les poudres laitières sont les suivants: la matière grasse laitière anhydre (AMF: Anhydrous Milk Fat), le lactose, les caséines micellaires et les protéines sériques. Pour la semoule, nous avons étudié l'amidon et le gluten.

Le β-lactose anhydre à 99 % de pureté, a été acquis chez Sigma-Aldrich, (St. Louis, USA). L'AMF a été prélevée à partir de beurre de la marque "Président". Pour cela, le beurre a été chauffé jusqu'à fondre (sans arriver à l'ébullition). Une fois liquide, le beurre a été centrifugé à 6000 rpm, pendant 10 minutes. La phase liquide (l'eau) est donc décantée et le sédiment solide récupéré correspond à l'AMF.

Les caséines natives micellaires (NCM) de qualité industrielle (Promilk 872B) ont été obtenues par microfiltration à partir de lait par International Dairy Ingredient (IDI, Arras, France). Le produit contient une importante quantité de caséines natives (protéines: 86,9, lipides 0,3, lactose 0.4, cendres 7.6 et teneur en eau 4 %). L'isolat natif de lactosérum à été fourni par Lactalis (Laval, France), il a été obtenu par un processus d'ultrafiltration tangentiel sur membrane suivie d'une diafiltration du micro-filtrat collecté pendant la production de NCM. La composition est la suivante: protéines 87,8, lipides 0,2, lactose 1,0, cendres 2,1 et teneur en eau 4,5 %. L'amidon ainsi que le gluten proviennent tous les deux respectivement de VWR international, LLC, (Darmstadt, Germany) et Sigma-Aldrich, (St. Louis, USA).

III.1.5.POUDRES APRES EXTRACTION DE MATIERE GRASSE LIBRE

La présence ainsi que les effets de la matière grasse à la surface des particules ont été évalué dans les poudres de lait entier (standard et granulé) ainsi que la semoule. Pour cela, il a été appliqué une extraction de la matière grasse libre, dont la technique d'extraction est mentionnée ci-dessous (voir point 2.3.1). La poudre après extraction de la matière grasse libre a été récupérée, séchée et stockée à 4 ºC dans une chambre froide jusqu'à utilisation. L'échantillon récupéré, est donc, une poudre présentant une réduction importante de lipides à la surface. Dans ce travail on l'appellera Poudre Après Extraction de Matière Grasse Libre (Powder AFFE : Powder After Free Fat Extraction).

III.1.6.LES POUDRES MODELES

La technique de caractérisation des composants de surface (1 µm) par EDX a été validée sur des poudres modèles ainsi que des mélanges binaires de lactose-protéines sériques. Deux solutions de lactose et de protéines sériques à 10 % ont été préparées. Ensuite, elles ont été mélangées dans les proportions suivantes: 70-30, 50-50 et 30-50% (lactose-protéines). Pour terminer, elles ont été déshydratés par séchage à froid à l'aide d'un lyophilisateur (Fisher Bioblock Scientific Christ Alpha 1-4, Osterode am Harz, Germany) avec un programme de refroidissement allant à -40 ºC ; une pression de 0,08 mbars pendant 48 heures.

III.1.7.LE COUSCOUS OBTENU A L'ECHELLE LABORATOIRE

Le couscous à l'échelle pilote a été fabriqué et fourni par le laboratoire CIRAD, INRA, Montpellier SupAgro, Universté Montpellier II. La production passe par quatre étapes: le mélange, l'agglomération, la cuisson à la vapeur et le séchage. Le mélange a été préparé dans un mixeur de faible cisaillement LABO 25 (Mahot, France) équipé d'un bol de 10.5 litres. L'eau est ajoutée par pulvérisation directement dans le mixeur à l'aide d'une buse standard pour pulvérisation à plat (TPU 650017, Spraying System Emani, France), connecté directement à la prise d'eau. Ensuite, un rouleur à trois tamis carrés, de 2000, 1500 et 1000 µm de diamètre a été utilisé. L'équipement de cuisson par vapeur (Afrem, Lyon, France) a un compartiment de vapeur de 20 L et un générateur de vapeur de 21 kg/h. Finalement le séchoir à l'échelle pilote (Afrem, Lyon, France) a été utilisé en pour sécher les agglomérats.

III.2. METHODES

III.2.1.CARACTERISATION GLOBALE DES POUDRES

III.2.1.1. Teneur en eau

D'après la norme (AFNOR, 1978), 2 g de poudre sont étuvées pendant trois heures. Après une heure de refroidissement en dessiccateur avec du pentoxyde de phosphore, les échantillons sont pesés. Trois essais par échantillon ont été réalisés.

III.2.1.2. Teneur en cendres

Le taux de cendres a été déterminé par calcination de 2 g de poudre dans des creusets de porcelaine mis dans un four à moufles à 550 ºC. Cette méthode a été développée selon la norme (ADPI, 2002). Trois essais par échantillon ont été réalisés.

III.2.1.3. Teneur en protéines

La teneur en protéines a été déterminée d'après la méthode de l'AOAC (1984). La teneur totale en azote a été obtenue, puis les pourcentages en protéines (g de protéines pour 100 g de poudre), ont été calculés à partir de la teneur en azote total multiplié par un facteur de conversion. Ce facteur représente le rapport entre le poids des protéines et le poids de l'azote. Dans le cas des poudres laitières le facteur correspond à 6,38 et pour les céréalières à 5,70.

III.2.1.4. Teneur en lipides

a) Poudres laitières

La teneur en matière grasse a été déterminée suivant la méthode de Röse-Gottlieb (IDF, 1987). Son principe repose sur une extraction des lipides avec de l'éther diéthylique et de l'éther de pétrole. Le mélange de solvants est ensuite évaporé et les lipides extraits sont pesés. Pour chaque échantillon, trois essais sont réalisés.

b) Semoule

Dans le cas de la semoule la teneur en matière grasse a été déterminée en utilisant l'appareil d'extraction Soxhlet. Pour cette méthode, 5 g de poudre sont placées dans une cartouche pesée au préalable. Le solvant utilisé est un mélange d'éther de pétrole et d'éther diététique (1:1 v/v). Le solvant est placé dans un ballon séché et pesé auparavant. Une fois monté sur l'appareil avec l'échantillon et le ballon contant le solvant le reflux de solvant est attendu pendant 5 heures. Après ce temps, le ballon est récupéré et le solvant évaporé avec un rotavapeur (Heidloph laboratora 4000, Germany) à 40 ºC et 40 rpm. Le gain de poids du ballon représente la quantité de matière grasse dans 5 g de poudre.

III.2.1.5. Dosage des carbohydrates

Le dosage des carbohydrates n'a pas été déterminé par une méthode directe. Le calcul de la quantité de lactose a été fait par soustraction du total des protéines, lipides, teneur en eau et cendres.

III.2.2.PROPRIETES PHYSIQUES

III.2.2.1. Granulométrie

a) Principe

La distribution de taille des particules de poudre a été déterminée par diffusion statique de la lumière grâce à un granulomètre Malvern Mastersizer S (Malvern Instruments Ltd, UK).

Ce type d'appareil est équipé d'un laser de type He/Ne d'une puissance de 5 mW, à une longueur d'onde de 632,8 nm. Une particule diffuse la lumière selon un angle inversement proportionnel à sa taille. Les grandes particules dévient une quantité plus importante de lumière avec des angles faibles et inversement pour les petites particules. Ainsi, nous pouvons obtenir la distribution granulométrique d'un échantillon par la mesure de l'intensité lumineuse diffusée en fonction de l'angle de diffusion.

b) Conditions expérimentales

L'analyse de la granulométrie des poudres a été réalisée selon les cas en voie humide ou en voie sèche. Pour les analyses en voie liquide, la poudre a été dispersée dans l'éthanol. Nous avons utilisé un échantillonneur MS14 dans lequel 1 mg de poudre a été ajouté, sous agitation, dans la cuve d'éthanol, pour obtenir un taux d'obscuration d'environ 30 %. Pour les analyses en voie sèche, la poudre est dispersée sous 3,5 bars de pression. Le mastersizer est alors équipé d'un module de dispersion de l'échantillon à haute pression d'air pour souffler la poudre à travers le rayon laser. Une pression de 3,5 bar a été utilisée, pour la plupart des échantillons. Pour évaluer la qualité d'enrobage, les pressions suivantes ont été utilisées de 0,5, 1,0, 2,0, 3,0 à 3,5 bars.

Cinq mesures ont été effectuées avec chaque échantillon, avec un écart-type de ± 0,5 µm. Les distributions de taille ainsi que les valeurs moyennes D10, D50 et D90 sont récupérées. Ces valeurs correspondent au diamètre moyen en volume, présenté par 10, 50 ou 90% des particules. Les distributions de taille obtenues varient entre 0,05 µm et 878 µm. L'acquisition des données est réalisée à l'aide du logiciel de traitement Malvern (Sizer Sv2.17).

III.2.2.2. Facteurs de Forme : Granulomorphomètre

Les mesures ont été effectuées en utilisant un analyseur QicPic (Sympatec GmbH, Clausthal-Zellerfeld, Allemagne) équipé d'un module de Lixell (Sympatec GmbH) spécifique pour les dispersions en suspension et les émulsions (figure 14).

Les particules granulaires (lait et/ou semoule) passent à travers un faisceau laser qui balaye une zone verticale. La caméra enregistre une séquence d'images correspondant à plusieurs millions de particules. En plus, les données sont enregistrées et traitées

immédiatement pour une évaluation ultérieure supplémentaire. Ce dispositif peut donc fournir des distributions cumulatives de descripteurs de taille et de forme.

Figure 14. Exemple de granulomorphomètre utilisé.

Pour chaque mesure, 0,25 g de poudre ont été dilués dans 75 ml d'éthanol en vue d'atteindre la bonne obscuration et d'éviter la superposition des particules. Trois mesures pour chaque échantillon de poudre ont été effectuées. Le logiciel Windox (5,4 Windox 2007 Sympatec GmbH, Clausthal-Zellerfeld, Allemagne) a été utilisé pour déterminer la taille des particules et la forme des distributions.

La norme ISO (2006), défini certains descripteurs de forme importants dans la projection en 2D d'une particule 3D, afin de mieux comprendre les résultats du QicPic, une liste avec la définition de quelques descripteurs pertinents pour les travaux en cours est donnée:

Diamètre de Feret d_F : c'est la distance entre deux tangentes parallèles au contour de la particule (figure 15-A). Les diamètres de Feret $d_{F_{max}}$ et $d_{F_{min}}$ sont respectivement la plus grand grande et la plus petite valeur de d_F pour un contour donné.

Rapport Hauteur/Largeur (*Aspect Ratio*) est le rapport :

$$AR = \frac{d_{F\,min}}{d_{F\,max}} \qquad \text{Equation 3}$$

La solidité (Solidity) est l'aire de l'objet divisée par la surface délimitée par l'enveloppe convexe, (figure 15-B), soit l'enveloppe convexe minimum contenant l'aire $A \leq A_c$.

$$C_Q = \frac{A}{A_c}$$ Equation 4

La circularité (circualrity) est une évaluation du degré de la façon dont la section projetée de la zone A et le périmètre P est similaire à un cercle :

$$\mathrm{C} = \frac{4\pi \mathrm{A}}{\mathrm{P}^2}$$ Equation 5

Wadell (1933) a proposé une approche de l'équation de circularité appelée *degré de circularité (degree of circularity)* :

$$\mathrm{S_{W2D}} = \frac{\mathrm{C}}{\mathrm{P}} = \frac{\sqrt[2]{\pi \mathrm{A}}}{\mathrm{P}}$$ Equation 6

où *c* est la circonférence du cercle avec une aire *A* projetée de l'aire de la particule, et *P* est le périmètre de la particule effective (figure 15-C).

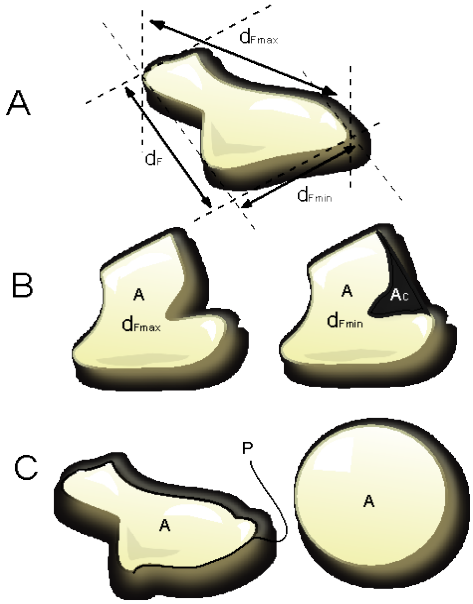

Figure 15. A: Définition des diamètres de Feret dF, dFmax dmin, B: ISO solidité ou convexité par QicPic, C: degrée de circularité ou sphericité par QicPic.

Les descripteurs de forme obtenus avec le QicPic sont le *Rapport Hauteur/Largeur* (*Aspect Ratio*), équation 3, *la convexité* C_Q et *la sphéricité (sphericity)* S_Q. La convexité (C_Q) obtenue par le Qicpic est égale à la solidité ISO (équation 6 et figure 15-B). Sans régions concaves le maximum théorique correspond à une convexité de 1. Enfin, la sphéricité obtenue par le QicPic (S_Q) est égale au degré de circularité, qui pour un aperçu du périmètre P, correspond à la racine carrée de la circularité *C* d'ISO (équations 3, 4 et figure 15-C). Ainsi, cela signifie que la sensibilité de S_Q au changement de la circularité diminue avec l'augmentation de la circularité. Ces précisions doivent être prises en compte lorsque les

valeurs de la sphéricité QicPic (S_Q) sont comparées avec celles de la circularité des autres techniques (Cavarretta, 2009). La valeur de sphéricité est comprise entre 0 et 1 avec des valeurs proches à zéro qui représentent l'irrégularité de forme des particules. En fait, les formes irrégulières se traduisent par une augmentation du périmètre réel.

III.2.3.CARACTERISATION DE LA SURFACE

III.2.3.1. Extraction et analyse de la matière grasse libre, encapsulée et totale

a) Les extractions

Les différences des profils lipidiques et des propriétés thermiques ont été étudiées sur différentes fractions lipidiques présentes dans la poudre du lait. Pour ce faire, les matières grasse libres, encapsulées et totales ont été extraites.

Le contenu de la matière grasse libre d'une poudre alimentaire est défini comme le résidu obtenu après évaporation. Une fois l'échantillon mélangé avec de l'éther de pétrole, il est ensuite filtré et finalement séché.

Les lipides sont extraits de la surface des poudres par des solvants selon la méthode développée par Vignolles *et al*. (2009a) avec quelques modifications. Pour cela, 5 g de poudre ont été placés dans une bécher. L'éther de pétrole est ensuite pesé dans une proportion de 1 à 5 par rapport à la quantité de poudre et ultérieurement ajouté au bécher. La suspension a été mélangée à l'aide d'un barreau magnétique et d'un agitateur électrique à une vitesse de 40 rpm. Après 5 minutes d'agitation, la suspension a été filtrée. Une fois la poudre récupérée, elle est remise en suspension avec une autre dose d'éther de pétrole. Cette opération est suivie d'une autre agitation pendant 5 minutes, cette opération a été faite 5 fois. Après le dernier lavage, le solvant est récupéré, ensuite séparé de la matière grasse par évaporation avec un rotavapeur (Hidloph laboratora 4000, Germany) à 40 ºC et 40 rpm.

La matière grasse encapsulée est récupérée après dissolution de la poudre AEMGL et mélangée avec des solvants. La technique de Röse-Gottlieb (IDF, 1987)a été appliquée. Le produit obtenu est stocké à 4 ºC dans une chambre froide.

Finalement, la matière grasse totale correspond aux lipides contenus dans la totalité des particules. Ici, la poudre native est traitée par la technique de Röse-Gottlieb (IDF, 1987).

Après récupération de la matière grasse libre, encapsulée et totale, les produits ont été stockés à 4 ºC dans une chambre froide jusqu'à utilisation.

b) Caractérisation par Calorimétrie Différentielle à Balayage

La calorimétrie différentielle à balayage (DSC 204 F1, Netzch, Phoenix, USA) a été utilisée pour déterminer les propriétés thermiques de trois fractions de matières grasses (libre, encapsulée et totale). Les fractions analysées sont extraites seulement de la poudre de lait entier (standard et agglomérée). L'étalonnage de la cellule de mesure a été faite avec de l'indium. Environ 10 mg d'échantillon ont été placés dans un creuset en aluminium scellé et perforé manuellement. Les profils de fusion des fractions de matières grasses ont été étudiés en appliquant une rampe de chauffage de 20 °C jusqu'à 70 °C, à 5 °C.min-1 pour l'élimination des cristaux. Puis, le profil thermique global a été enregistré par un refroidissement de 70 °C jusqu'à -80 °C et le chauffage subséquent de -80 °C jusqu'à 100 °C, à 5 ºC min-1. Chaque échantillon a été analysé en double.

c) Caractérisation par Chromatographie Gazeuse (CG)

Les profils lipidiques des fractions de matière grasse extraites ont été évalués par CG après la conversion des acides gras en esters méthyliques correspondants. Chaque fraction de matières grasses (0,1 g) a été dissoute dans 10 ml d'hexane. Un ml de cette solution a été ensuite transféré dans un tube de réaction. L'hexane a été évaporé sous azote. Ensuite, 1 ml de toluène et 1 ml de bore trifluoride-methanol (14 %) ont été ajoutés. Le mélange a été homogénéisé puis mis à réagir à 100 °C pendant 45 min. Après refroidissement à température ambiante, 1 ml d'eau a été ajouté pour arrêter la réaction, suivie par un autre millilitre de cyclohexane. Enfin, 1 ml de la phase organique a été injecté dans la chromatographie en phase gazeuse (Perichrom 2000, Saulx-les-Chartreux, France). La séparation a été effectuée sur une colonne capillaire en silice fondue de 50 m de longueur et 0,25 mm de diamètre interne (CP7419 Varian, Middelburg, Netherlands). Le programme comprend une période initiale à 120 °C pendant 2 minutes et d'une rampe de température (39,9 °C. min^{-1}) pour atteindre le point final.

d) Mesure de la composition de surface par Spectroscopie des Photons X

La spectroscopie des photons X où XPS par son sigle en anglais (X-ray photoelectron spectroscopy), est une technique performante permettant la caractérisation de la surface des

matériaux (0,5 à 15 nm). L'aire analysée est d'environ 1 mm. Donc, dans un lit de poudre, les mesures sont la moyenne de plusieurs particules.

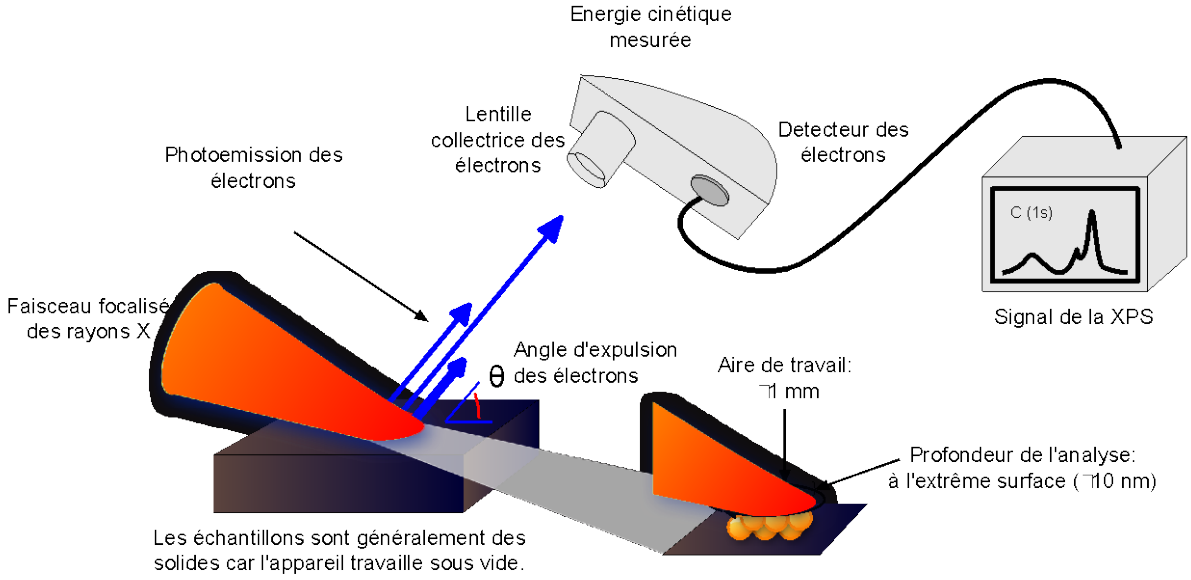

Figure 16. Principe de l'XPS.

La technique est basée sur la photo-émission. Lors de l'irradiation par des photons X, les atomes présents en surface émettent des électrons appelés photoélectrons. La technique consiste à mesurer l'énergie cinétique de ces photoélectrons émis lors de l'irradiation (figure 17). Par la relation de conservation d'énergie, l'énergie de liaison qui caractérise un atome est directement accessible.

Equation de conservation de l'énergie :

$$E_B = hv - E_C - \phi \qquad \text{Equation 7}$$

avec: *hv*, énergie des photons X incidents (eV)

E_B, énergie de liaison (eV)

E_C, énergie cinétique mesurée (eV)

ϕ, énergie nécessaire à l'électron pour franchir la frontière matériel/vide (eV)

h, constante de Planck ($6{,}62.10^{-34}$eV)

v, fréquence de l'onde (s^{-1} ou Hz)

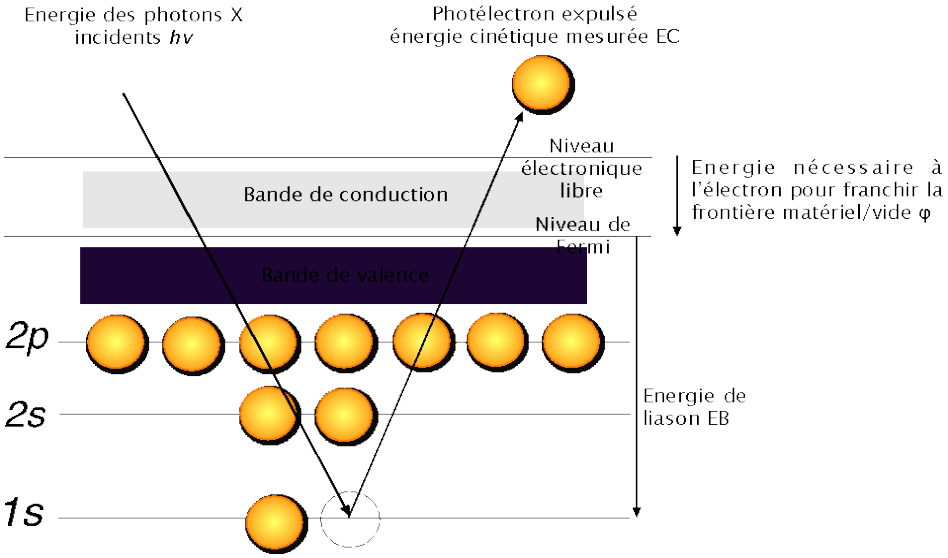

Figure 17. Diagramme de conservation de l'énergie.

Comme toute technique spectroscopique, elle présente l'avantage d'être peu destructive, sensible et applicable à un grand nombre d'atomes. En effet, tout électron dont l'énergie de liaison est inférieure à celle des photons X peut être émis. Ainsi, tous les atomes sont détectables sauf l'hydrogène et l'hélium.

e) Application de la technique à la détermination de la composition de surface des poudres laitières et céréalière.

L'XPS permet tout d'abord une analyse élémentaire. La méthode est décrite en détail par Fäldt (1995) dans son travail de thèse. L'énergie de liaison étant spécifique d'un atome, on peut déterminer les éléments (carbone, oxygène et azote) présents à la surface de la poudre à partir des pics du spectre complet. On peut ensuite déterminer le pourcentage des différents composants (protéine, lactose et lipide) grâce à une matrice à trois inconnues présentée ci dessous:

$$\%C = \alpha_P \cdot C_P + \alpha_L \cdot C_L + \alpha_F \cdot C_F \quad \text{Equation 8}$$

$$\%O = \alpha_P \cdot O_P + \alpha_L \cdot O_L + \alpha_F \cdot O_F \quad \text{Equation 9}$$

$$\%N = \alpha_P \cdot N_P + \alpha_L \cdot N_L + \alpha_F \cdot N_F \quad \text{Equation 10}$$

Avec: % C, % O, % N, les fractions molaires de carbone, oxygène et azote à la surface de l'échantillon (valeurs obtenues à partir des aires des pics C_{1S}, O_{1S} et N_{1S}) C_P, C_L, C_F, les fractions molaires du carbone dans les protéines, le lactose et les lipides. ; O_P, O_L, O_F, les fractions molaires de l'oxygène dans les protéines, le lactose et les lipides et N_F, N_L, N_P, les fractions molaires de l'azote dans les protéines, le lactose et les lipides (valeurs théoriques et

expérimentales obtenues à partir des protéines laitières de la matière grasse laitière anhydre et de lactose monohydraté) αP, αL et αF sont les surfaces relatives en protéines, lactose et lipides déterminées en résolvant la matrice.

La technique a été adaptée pour les poudres céréalières par Saad *et al*. (2011a). Dans ce cas, les valeurs expérimentales des protéines, carbohydrates et lipides sont obtenues à partir du gluten, de l'amidon et de l'huile extrait du blé.

a) Application de la technique à la détermination de la nature des liaisons de surface

La déconvolution des spectres permet une analyse chimique des échantillons. C'est à dire que chacun des pics du spectre global peut être décomposé en plusieurs pics. En effet, dans un composé donné, les niveaux de cœur de l'atome vont réagir à la modification de l'environnement chimique avec des variations de l'énergie orbitale de quelques eV. C'est ce que l'on appelle le déplacement chimique. Ainsi, nous pouvons caractériser la nature de liaisons chimiques de surface et plus particulièrement l'hydrophobicité de la surface de la poudre.

b) Conditions expérimentales

Les analyses ont été réalisées et validées au Laboratoire de Chimie Physique et de Microbiologie pour l'Environnement (LCPME / UMR 7564 CNRS, Université de Lorraine, Vandoeuvre Lès Nancy). Les analyses ont été réalisées avec un appareil Kratos (Axis Ultra, Kratos Analytical, Manschester, UK). La source de radiation est monochromatique (AlK_α) et présentant une énergie incidente de 1486,6 eV. La puissance appliquée à l'anode est réduite à 90 watts pour éviter la dégradation de l'échantillon. L'appareil est calibré pour obtenir une énergie de liaison de 83,96 eV sur l'élément Au $_{4f7/2}$. De plus, la dispersion est ajustée pour donner une énergie de liaison de 932,65 eV sur l'élément Cu $_{2p3/2}$

Les échantillons de poudre sont fixés sur un support en acier (scotch double face conducteur) et dégazés une nuit entière avant l'analyse. Pour permettre une analyse sur une profondeur d'environ 5 nm, l'angle incident du faisceau des photoélectrons détectés est fixé à 90°. L'aire d'analyse est de 700 x 300 µm. Les spectres de survol sont enregistrés avec un pas de 1,0 eV et une énergie passante de 160 eV. Les pics de hautes résolutions (pics de carbone, oxygène et azote) sont enregistrés avec un pas de 0,05 eV pour le carbone et 0,1 pour l'oxygène et l'azote, avec une énergie passante de 20 eV pour chacun.

Les spectres sont analysés avec le logiciel Vision de Kratos (Vision 2,2,6). Une ligne de base, de type Shirley, permet de soustraire le bruit de fond. Les pics sont décomposés à l'aide d'un modèle de distribution Gaussienne – Lorentzienne. La quantification est réalisée avec les coefficients de transmission fournis par le logiciel. Deux points d'analyse sont effectués sur chacun des échantillons avec un décalage de 1 mm sur l'axe des abscisses. Les valeurs des composants purs ont été reportées par Gaiani et al. (2006); ils sont été préalablement analysés comme référence afin de fixer les coefficients expérimentaux de la matrice de calcul.

III.2.3.2. Microscopie Electronique à Balayage (MEB)

a) Principe

La microscopie électronique à balayage repose sur le même principe que la microscopie optique, à la différence près que le rayon incident est constitué par un faisceau très fin d'électrons accélérés sous une tension de 10 à 30 kV au lieu d'un rayon de lumière visible. Les électrons rétrodiffusés et/ou secondaires sont recueillis en synchronisant la détection au balayage du faisceau incident. On obtient ainsi une image de la surface. On distingue deux types de contrastes :

- Le contraste topographique est lié au taux d'électrons rétrodiffusés et à leur accès au détecteur en fonction de la topographie. Cela permet de distinguer la profondeur de l'échantillon.

- Le contraste chimique est lié au facteur de diffusion de l'atome donc à son numéro atomique. Ainsi, on distingue un atome lourd d'un atome plus léger par la présence d'une zone brillante due au nombre élevé d'électrons rétrodiffusés.

b) Analyse Dispersive en Energie

L'analyse dispersive en énergie ou EDX par son sigle en anglais (Energy-dispersive X-ray spectroscopy) implique l'utilisation d'un microscope électronique à balayage. Ce n'est pas un dispositif indépendant, il est systématiquement couplé à un MEB. Il travaille avec le même principe de la conservation de l'énergie que l'EDX. Mais à l'inverse, l'interaction d'un faisceau d'électrons avec l'échantillon provoque l'émission de rayons X, captés ensuite par un détecteur qui traduit l'information en spectres (figure 18).

Dans l'EDX la région d'interaction où les rayons X sont émis est de l'ordre de 1 μm^3. Par contre cette profondeur théorique peut changer en fonction de la sensibilité que peut avoir le matériel au faisceau d'électrons. Dans le cas des poudres organiques, et donc des poudres utilisées dans ce travail, la profondeur réelle peut attendre jusqu'à 5 μm^3 sans qu'il soit possible de mesurer la profondeur exacte. Bien qu'une région plus petite puisse être résolue dans l'imagerie MEB, les rayons X sont détectés dans plusieurs couches minces ou plusieurs régions dans le spécimen. Les photons de rayons X sont analysés par spectroscopie élémentaire pour obtenir des informations sur le spécimen. Les éléments de bore à uranium peuvent être détectés.

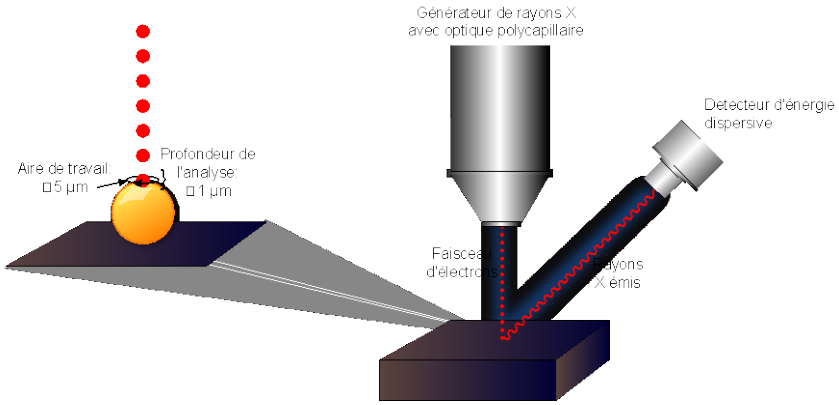

Figure 18. Représentation d'un système EDX.

L'EDX est une méthode de spectroscopie qui est utile dans l'identification des éléments de matériaux. L'EDX ne révèle pas les informations de liaison chimique. Par exemple, si W et Si sont détectés, on ne peut pas dire par EDX si l'échantillon est composé de W enrobé avec de Si ou du WSi_2, ou si l'échantillon contient les trois matériaux. Ainsi l'EDX est plus adapté pour l'analyse des matériaux inorganiques, plutôt que les matériaux organiques lesquels contiennent tous, pour la plupart, les mêmes éléments liés différemment (C, O et N).

c) Mesure de la composition de surface par EDX et gradients de composition

Comme il a été mentionné avant, l'EDX est peu adapté aux matériaux organiques. C'est une des raisons pour lesquelles la technique n'a pas été utilisée dans les poudres alimentaires. Pour la première fois, dans ce travail, une nouvelle approche a été proposée. A partir de la technique développée par Fäldt (1995), la même méthodologie a été adapté à l'EDX, dont les contenus de carbone, azote et oxygène dans les composant purs ont étés mesurés par EDX. Ensuite, le système d'équations a été résolu pour remonter aux valeurs de carbohydrates, protéines et lipides.

La technique a été validée sur des poudres modèles ou des mélanges binaires de lactose-protéines sériques à 30 - 70, 50 - 50 et 70 – 30 %. Cela représente la seule possibilité de produire une poudre modèle pour tester la technique par EDX, car il s'agit d'éléments solubles dans l'eau qui peuvent être parfaitement mélangés. En effet, le mélange de molécules solubles dans l'eau garantie la répartition homogène des ces deux composants dans l'aire de travail de l'ADE (donc 5 μm) contrairement au mélange produit avec des suspensions de caséines ou des émulsions de matière grasse dont la taille des micelles et des gouttelettes est supérieur.

L'intérêt de faire cette adaptation de la technique est motivé par les différences rapportés par les deux techniques: EDX et XPS. Ces techniques peuvent se coupler et ainsi permettre d'avoir des informations complémentaires. Les principales différences entre l'EDX et l'XPS sont la profondeur d'analyse, de 1 μm pour la première et d'environ 5 nm pour la deuxième. Ces différentes profondeurs permettent d'avoir différents niveaux d'analyses. De plus, dans les poudres de lait entier et dans la semoule, ces analyses ont été faites avant et après extraction de la matière grasse. Cela permet d'avoir deux niveaux en plus d'analyse.

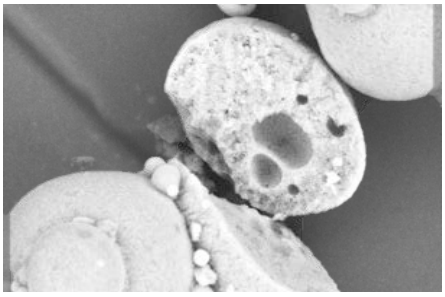

Figure 19. Particule de poudre de lait écrémé coupée avant une analyse EDX.

Une autre différence entre l'EDX et l'XPS est l'aire d'analyse. L'XPS analyse une aire de plus ou moins 1 mm^2, en faisant un balayage de plusieurs particules. De plus, cet appareil ne permet pas de choisir les particules à analyser. L'EDX, à l'inverse, permet de choisir la particule et le point exact d'analyse à l'aide du MEB. Cet équipement travaille dans une aire de 5 μm^2 approximativement. Cela apporte un grand avantage et permet de faire des analyses dans un point précis de la surface, mais aussi au cœur de la particule (si celle-ci a été auparavant coupée). En effet, la poudre peut être prélevée et coupée, ensuite il est possible de chercher les particules coupées par simple observation visuelle avec le MEB (figure 19).

d) Mode opératoire

Sur Nancy, les observations MEB, ont été réalisées au Laboratoire de Chimie Minérale à la faculté des sciences et techniques (UHP Nancy 1, Vandœuvre-Lès-Nancy). Dans ce laboratoire les poudres à analyser ont été fixées sur un ruban adhésif double face puis montées sur un support. Une couche de carbone de 10 nm, puis un mélange or/palladium ont été déposés à la surface des particules de poudre. Cette préparation consiste à rendre l'échantillon conducteur. Les mesures ont été réalisées sous vide secondaire (environ 10^{-5} torr) par rétro diffusion des électrons secondaires avec un microscope électronique à balayage Hitachi S2500, Japon.

Du coté du centre RAPSODEE (Albi), les observations ainsi que les analyses EDX ont été couplées et réalisées à l'Ecole des Mines d'Albi Carmaux. La semoule brute et les fractions tamisées de semoule ont été observées avec un microscope électronique à balayage environnemental (MEBE) XL30 ESEM FEG, Philips, Netherland, fonctionnant à 20 kV en mode vide (figure 20).

Figure 20. MEBE du centre RAPSODEE (Université de Toulouse-Mines, Albi).

Le mode de faible vide (1,4 Torrs) a été utilisé pour les observations faites pour la semoule conditionnées à différentes humidités relatives et les composants purs. Les mêmes conditions ont été mises en œuvre pour les analyses EDX déterminées dans les composants purs, les poudres du lait et la semoule.

Les poudres ont été déposées sur un disque adhésif double-face de carbone fixé sur un support. Pour avoir des analyses au cœur de la particule, quelques échantillons ont été coupés après être placés sur le disque adhésif. Dans le cas des poudres modèles (mélanges binaires), une pastille a été faite pour améliorer l'homogénéité des produits, puis placée sur le disque adhésif.

Les poudres en mode vide ont été enrobées avec un pulvérisateur de marque Polaron (SC7640, Newhaven, UK). Ensuite elles ont été observées avec le détecteur SE. Les poudres en mode faible vide, ont été directement observées avec le détecteur GSE.

Pour les mélanges binaires séchés par lyophilisation, elle sont été préparées des pastilles car les poudres étaient très fines et friables, ne permettant pas l'analyse. Les pastilles ont été fait dans une presse hydraulique manuelle Specac de 25 tonnes, les pastillas ont été formaté avec un moule à pastiller en acier trempé de 13 mm, Perkin Elmer, Wokingham, England. La pression utilisée pour l'élaboration des pastilles fut 10 ton.

III.2.3.3. Microscope à Force Atomique

a) Principe

La microscopie à force atomique AFM par son sigle en anglais (Atomic Force Microscopy) est un outil puissant permettant d'imager une variété de surfaces et de caractériser ces surfaces au niveau atomique. Les images sont obtenues par balayage d'une sonde marquée à travers une surface tout en surveillant et ressemblent les interactions pointe-échantillon.

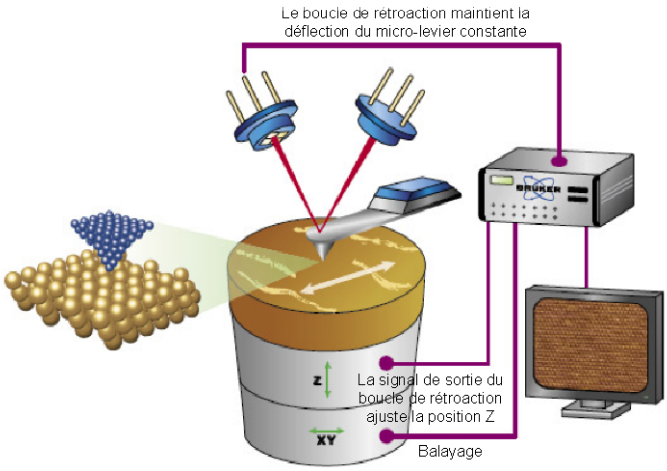

Figure 21. Principe de l'AFM.

L'AFM (figure 21) fournit un certain nombre d'avantages par rapport aux techniques conventionnelles de microscopie. L'AFM sonde l'échantillon et effectue des mesures en trois dimensions, x, y et z (perpendiculaire à la surface de l'échantillon), permettant ainsi la présentation des images tridimensionnelles de la surface d'un l'échantillon. Cela fournit un grand avantage sur n'importe quel microscope disponible auparavant. Avec des échantillons adéquats (propres, pas trop rugueux en surface, pas trop grands), la résolution dans le plan x y

varie de 0,1 à 1,0 nm et dans la direction z de 0,01 nm (résolution atomique). L'AFM ne nécessite ni un environnement sous vide, ni aucune préparation de l'échantillon. Cette technique peut être utilisée dans un environnement ambiant ou liquide. Grâce à ces avantages, l'AFM a des répercussions importantes sur les domaines de la science des matériaux, la chimie, la biologie et encore la physique.

Mode de contact

Le mode contact de l'AFM est l'un des modes les plus couramment utilisés à sonde à balayage. Il fonctionne par balayage de la surface par une extrémité en pointe (fait en nitrure de silicium ou Si_3N_4 attaché à un micro-levier avec un faible module d'élasticité) à travers l'échantillon. Une force extrêmement faible (10^{-9} ~ N, gamme de force interatomique) est maintenu sur le micro-levier, poussant ainsi l'embout contre l'échantillon pour balayer. Ainsi la force de répulsion entre la pointe et l'échantillon ou la déviation effective de la pointe est enregistrée par rapport à la variation spatiale et ensuite convertie en une image analogique de la surface de l'échantillon.

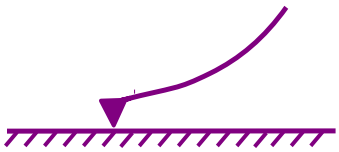

Figure 22 : Mode contact.

Mode de non-contact

Une nouvelle ère en matière d'imagerie a été ouverte lorsque les microscopistes ont introduit un système de mise en œuvre du mode non-contact qui est utilisée dans des situations où la pointe de contact pourrait modifier l'échantillon de manière subtile. Dans ce mode, les pointes sont placées entre 5 et 15 nm au dessus de la surface de l'échantillon. Les forces d'attraction de Van der Waals qui s'exercent entre la pointe et l'échantillon sont détectées. Les images topographiques sont construites par balayage de la pointe au-dessus de la surface. Dans cette mode les forces attractives de l'échantillon sont plus faibles que les forces utilisées par le mode de contact.

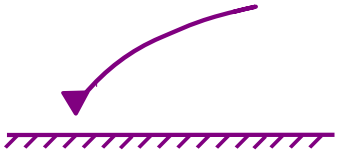

Figure 23. Mode non-contact.

Mode Tapping

Le mode intermittent ou tapping est une avancée majeure dans l'AFM. Cette technique puissante permet l'imagerie à haute résolution topographique des surfaces de l'échantillon qui sont facilement endommagées, mal lié au substrat, ou difficiles à balayer par d'autres techniques AFM. Le mode intermittent surmonte les problèmes liés au frottement, l'adhérence, les forces électrostatiques, et les difficultés rencontrées par les méthodes classiques. Pour ce faire, l'AFM place la pointe en contact avec la surface pour avoir une haute résolution, ensuite la pointe est soulevée de la surface afin d'éviter de traîner la pointe à travers la surface. Le mode intermittent d'imagerie est mis en œuvre au milieu ambiant en faisant osciller l'ensemble du micro-levier ou près de la fréquence de résonance du micro-levier en utilisant un cristal piézo-électrique. Des tubes piézoélectriques provoquent l'oscillation du micro-levier avec une amplitude élevée (typiquement supérieure à 20 nm). Lorsque la pointe n'est pas en contact avec la surface, elle oscille et est alors déplacée vers la surface jusqu'à ce qu'elle commence à la toucher légèrement. Pendant le balayage, la pointe oscillante prend contact avec la surface par intermittence à une fréquence de 50.000 à 500.000 cycles par seconde. Ensuite, l'oscillation de la pointe est nécessairement réduite, à cause de la perte d'énergie causée par le contact de la pointe avec la surface. La réduction de l'amplitude d'oscillation est utilisée pour identifier et mesurer les caractéristiques de la surface.

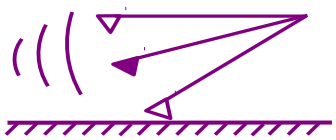

Figure 24. Mode intermittent (Tapping).

b) Mode opératoire

Les images ont été enregistrées à l'aide d'un instrument MFP3D-BIO (Asylum Research Technology, Atomic Force F&E GmbH, Mannheim, Germany) en mode tapping. Un micro-levier de nitrure de silicium de forme conique ont été acquis auprès de Veeco (MLCT-AUNM, Veeco Instruments SAS, Dourdan, France), les modules d'élasticité ont été déterminés en utilisant la méthode d'étalonnage thermique (Lévy & Maaloum, 2002), fournissant des valeurs de ~ 10,4 ± 1,7 pN nm^{-1}. Avant la manipulation, la géométrie de la pointe a été systématiquement contrôlée à l'aide d'une grille commerciale qui permet la visualisation en 3D (TGT1, NT-MTD Compagny, Moscow, Russia). La courbure de la pointe était dans la gamme 20-50 nm. Les expériences ont été réalisées dans l'air à température ambiante. Pour l'immobilisation de la poudre; un morceau de cire (Tempfix mounting

adhésive, Spi Supplies, USA) était placé sur un support disque métallique préalablement chauffé jusqu'à ce que la cire fonde (environ 70 ºC). Une fois la cire fondue et étalée sur le support, le chauffage est arrêté. Finalement, la poudre est saupoudrée à la surface de la cire quand elle commence à se solidifier. Lorsque la cire devient solide, l'échantillon est prêt.

III.2.4.CARACTERISATION DE LA POUDRE REACTIVE

III.2.4.1. Energie de surface par Chromatographie Gazeuse Inverse (CGI)

a) Principe

La CGI apparue en 1967, est une extension de la chromatographie gazeuse classique. En la comparant à cette dernière qui permet la séparation, l'identification et le dosage des constituants d'un mélange volatil. La CGI permet l'analyse des propriétés de surface d'un matériau non volatil placé dans une colonne chromatographique par l'injection d'un mélange gazeux formé du méthane et de molécules organiques parfaitement identifiées, les molécules sondes (figure 25).

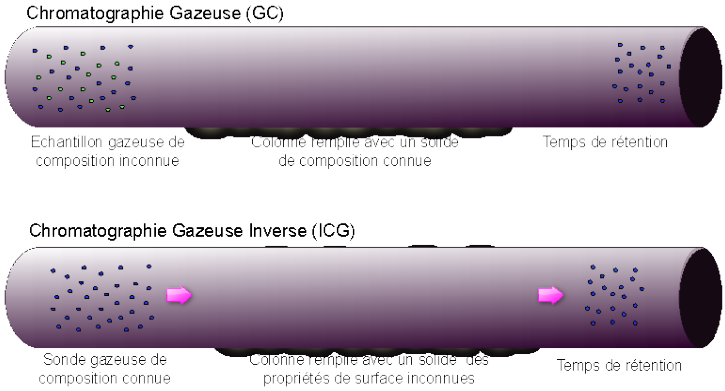

Figure 25. Différences entre la CG et la GCI

En fonction de la nature de la sonde, différentes composantes de l'énergie de surface d'un solide peuvent être calculées. L'injection de sondes alcanes linéaires permet de déterminer la composante dispersive de l'énergie de surface, une mesure des forces de London développées entre les sondes et la surface du solide. La composante polaire de l'énergie de surface du solide peut être évaluée grâce à l'injection de sondes polaires (chloroforme, tétrahydrofurane, acétone, acétate d'éthyle, etc).

La grandeur exploitée en CGI est le temps de rétention t_r de la molécule sonde injectée dans la colonne chromatographique remplie avec le solide d'étude, auquel on a soustrait le temps mort de la colonne, t_0, temps mis par une molécule (le méthane), non retenue par le

solide pour traverser la colonne. On en déduit un volume de rétention V_N, en prenant en compte le débit moyen de gaz dans la colonne.

$$V_N = (t_r - t_0)D \qquad \text{Equation 11}$$

A partir de ces volumes de rétention, deux paramètres ont été évalués au cours de cette étude, la composante dispersive de l'énergie de surface et l'enthalpie libre spécifique d'adsorption de sondes polaires.

b) Composante dispersive de l'énergie de surface

Une observation commune à la chromatographie analytique et à la CGI est qu'au sein d'une famille d'homologues chimiques, le volume net de rétention est une fonction linéaire du nombre de carbone (n_c) pour $n_c > 4$. Ainsi, la démarche consiste à injecter une série de trois alcanes linéaires généralement, de mesurer les temps de rétention (t_N) et enfin de tracer la droite de variation de RT Ln(V_N) en fonction du nombre d'atomes de carbone. On obtient ainsi la droite dite "droite des alcanes" (figure 26).

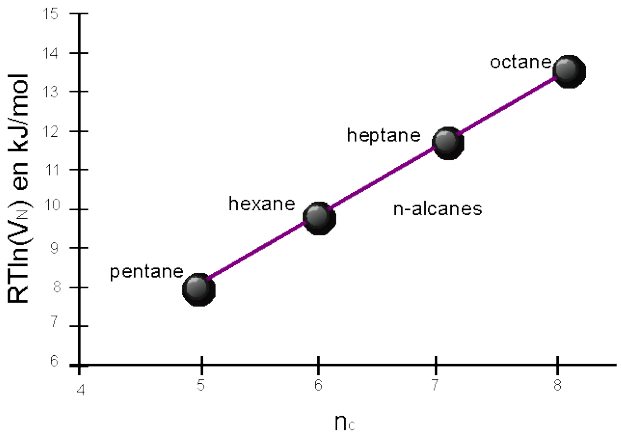

Figure 26. Variation de l'enthalpie libre d'adsorption en fonction du nombre d'atomes de carbones, nc, des sondes n-alcanes

A partir de l'enthalpie libre d'adsorption $\Delta G_a^{CH_2}$ d'un groupe méthylène qui n'est autre que la pente de la droite des alcanes, on détermine la composante dispersive de l'énergie de surface suivant l'équation :

$$\gamma_S^d = \frac{\left(RT\ ln\frac{V_{N(N+1)}}{V_{N(N)}}\right)^2}{4N^2 \cdot a_{CH_2}^2 \cdot \gamma_{CH_2}} = \frac{\left(\Delta G_a^{CH_2}\right)^2}{4N^2 \cdot a_{CH_2}^2 \cdot \gamma_{CH_2}} \qquad \text{Equation 12}$$

Avec N le nombre d'Avogadro (6,022.10^{23} mol^{-1}), a_{CH_2} l'aire occupée par un groupement méthylène adsorbé (0,06 nm^2), R la constante des gaz parfaits, V_N le volume de rétention et γ_{CH_2} l'énergie de la surface d'un solide constitué uniquement de groupements méthylène et déterminée sur le polyéthylène à partir de l'équation 13, à la température T d'analyse.

$$\gamma_{CH_2} = 35{,}6 - 0{,}058\,(T - 20) \qquad \text{Equation 13}$$

c) Enthalpie libre spécifique d'adsorption de sondes polaires ΔG_a^{SP}

L'enthalpie libre d'adsorption d'un solide se décompose en deux termes : $\Delta G_a = \Delta G_a^d + \Delta G_a^{SP}$ où ΔG_a^d est le terme dispersif, évalué par l'injection d'une série homologue d'alcanes linéaires, et ΔG_a^{SP} est le terme spécifique, mesuré par l'injection de sondes polaires, du type chloroforme, dioxanne, acétone, etc.

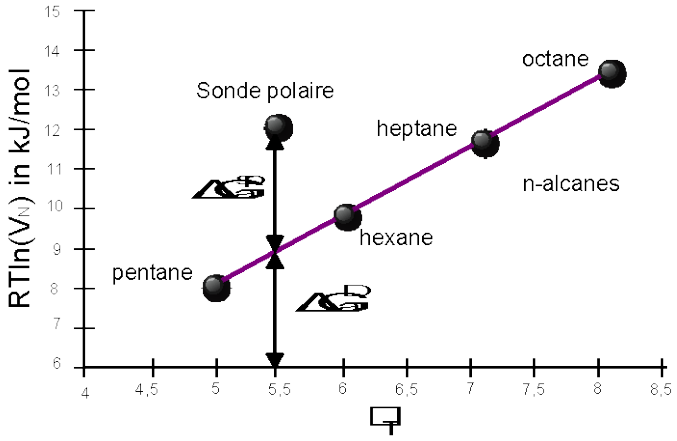

Figure 27. Détermination graphique de ΔG_a^{sp}

Après avoir tracé la droite des alcanes, on reporte, sur le même graphe, un point pour chaque sonde polaire injectée, dont l'ordonnée vaut $RT\ ln\ V_N$ et qui a pour abscisse le paramètre χ_t (Brendlé & Papirer, 1997), qui équivaut à un nombre d'atomes de carbone que devrait comporter un alcane linaire pour interagir avec la surface de la manière façon que la sonde polaire. Ce point se situe au-dessus de la droite des alcanes. La différence d'ordonnée entre ce point et la droite correspond à l'enthalpie libre d'adsorption notée ΔG_a^{sp} (figure 27).

d) Mode opératoire

Pour chaque colonne, la même procédure a été suivie : la poudre a été conditionnée à 60 °C pendant la nuit sous vide à 200 mbar de pression, puis la colonne a été remplie avec de la poudre. Deux chromatographes Agilent 6890 en phase gazeuse ont été utilisés, chacun

équipé de deux détecteurs à ionisation de flamme (FID). Le gaz porteur est l'hélium à un débit d'environ 30 ml / min. L'injecteur et le détecteur ont été chauffés à 150 °C. Les analyses ont été effectuées à 50 °C. L'acquisition des chromatogrammes a été réalisée avec un logiciel RecordView de la société InfoRep (Fontenay-le-fleury, France) et le traitement des données avec un logiciel de la Société Adscientist (Wittelsheim, France). Les sondes utilisées étaient les alcanes linéaires: hexane (C6), heptane (C7) et octane (C8) et des sondes polaires: chloroforme (acide), tétrahydrofurane et dioxanne (basique), acétate d'éthyle et acétone (amphotères). Toutes les sondes utilisées dans cette étude avaient une pureté supérieure à 99 %.

III.2.4.2. Montée capillaire (MC)

a) Principe

Une autre technique utilisée pour caractériser l'énergie de surface libre des poudres est la montée capillaire. Dans cette technique les particules sont en contact avec des liquides mouillants (figure 28).

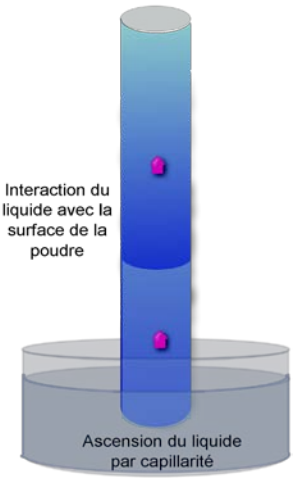

Figure 28. Représentions de la monté capillaire

Washburn (1921) a étudié la pénétration capillaire d'un liquide à travers un réseau poreux, lorsqu'un liquide pénètre dans un tube par capillarité, il y a une relation linéaire entre le carré de la longueur de pénétration et le temps. Dans une analyse théorique de l'écoulement capillaire dans des tubes verticaux et horizontaux, Washburn a développé l'équation différentielle pour laquelle R représente le rayon capillaire formait entre les particules dans le réseaux poreuse :

$$\frac{dl}{dl} = \frac{R\gamma}{\eta 4l} cos\theta \; dt$$ Equation 14

et sa solution :

$$\frac{l^2}{t} = \frac{R_\gamma}{2\eta} cos \qquad \text{Equation 15}$$

Avec :

l = hauteur de liquide qui pénètre dans la colonne de poudre en fonction du temps (t) en m.

R = rayon du capillaire inter-particulaire m.

γ = tension de surface du liquide en N/m.

η = viscosité du liquide en Pa.s

θ = angle de contact en °

L'équation de Washburn est utilisée pour déterminer l'angle de contact dynamique entre une poudre et un liquide. Pour cela un échantillon de poudre est placé dans une cellule cylindrique avec fond poreux est mis en contact avec la surface d'un liquide mouillant et l'on enregistre l'augmentation du poids (m) en fonction du temps. Le poids m de liquide dans l'échantillon est donné par :

$$m = \pi R^2 l \rho \qquad \text{Equation 16}$$

Ou m = masse en g

l = hauteur de liquide qui pénètre dans la colonne de poudre

ρ = masse volumique du liquide en g/m^3

et R = rayon du capillaire inter-particulaire en m.

L'équation de Washburn devient ensuite, où la constante C_w ne dépend que de la géométrie du lit de poudre, elle s'exprime en m^2 :

$$\frac{M^2}{t} = \frac{\pi^2 R^5}{2} \frac{\rho_1^2 2\gamma}{\eta} cos\theta = C_w \frac{\rho_1^2 2\gamma}{\eta} cos\theta \qquad \text{Equation 17}$$

La cinétique de la montée capillaire est liée aux propriétés du liquide et de la poudre aussi qu'aux interactions liquide-solide. A partir de ces interactions les composantes polaires et dispersif (ou non-polaires) de l'énergie de la surface peuvent être déduites. Le solide et le

liquide interagissent l'un avec l'autre, ainsi les valeurs des composantes polaires et dispersives de la matière solide sont fonction des propriétés du liquide.

b) Mode opératoire

Avec la finalité d'étudier les interactions polaires et dispersives, il est nécessaire d'utiliser des sondes ou liquides dispersifes et polaires. Dans le cas de sondes polaires, la plus employée à ce propos est l'eau mais dans le cas de la semoule l'utilisation de l'eau n'est pas possible. L'eau peut pénétrer dans la structure des particules produisant une transformation de la matière, dont les mesures ne sont pas produites uniquement par l'interaction liquide-solide. Par conséquence, d'autres liquides ont été proposés comme sondes polaires. Les liquides polaires utilisés sont l'éthanol et le dioxanne 1.4. Il s'agit des sondes les plus polaires après l'eau, pourtant ce sont des sondes faiblement polaires. L'hexane a été utilisé comme sonde dispersive ou non-polaire qui a une composante polaire égale à zéro. L'isopropanol a été utilisé comme liquide de référence, c'est à dire, comme liquide parfaitement mouillant. Les propriétés des sondes sont décrites dans le tableau suivant :

Tableau 16. Propriétés de différentes sondes utilisées pour la montée capillaire.

	Densité (g/cm^3)	**Viscosité (mPas.S)**	**γ (mJ/m^2)**	**γ^d (mJ/m^2)**	**γ^p (mJ/m^2)**
Isopropanol	0,786	2,390	22,4	19,3	2,1
Hexane	0,660	0,300	18,4	18,4	0,0
Ethanol	0,790	1,074	22,1	17,5	4,6
1,4-Dioxanne	1,034	1,260	33,2	33,2	0,0

Les angles de contact des composants purs et des fractions de semoule ont été mesurés avec un tensiomètre SHGA (GBX, France). Quatre récipients en acier inoxydable ont été utilisés pour préparer le lit de poudre. Le fond des récipients étaient couverts d'un papier filtre, puis l'échantillon a été placé dans le récipient et distribué par une centrifugeuse (32 Rotofix, Hettich, Allemagne) à 4000 rpm pendant 15 minutes. Toutes les expériences ont été réalisées à la température ambiante du laboratoire de 20 °C. Pour s'assurer de la répétabilité des résultats, quatre cellules sont analysées avec un liquide totalement mouillant (isopropanol) pour déterminer la constante *C*. Ensuite, quatre autres cellules sont utilisées pour déterminer l'angle θ. Pour ce faire, la cellule est fixée à la microbalance du tensiomètre. En dessous de cette cellule, on place un réservoir contenant le liquide à analyser sur un plateau amovible. A l'aide de ce plateau, la surface du liquide est amenée au contact de la

cellule. La montée capillaire commence alors ainsi que l'acquisition de la cinétique $m^2 = f(t)$. Les mesures ont été exploitées à l'aide du logiciel Bal285.

Les valeurs d'angle de contact, θ, et la tension de surface, γ_L, des liquides ont été utilisés pour calculer le travail d'adhésion, W_{SL} :

$$W_{SL} = \gamma_L(cos\theta + 1) \qquad \text{Equation 18}$$

Ensuite le modèle d'Owens-Wendt-Kaeble (Eq. 13) a été utilisé pour calculer les composants polaires (γ_S^p) et dispersives (γ_S^d) de l'énergie de surface des poudres (solides), en utilisant les propriétés des sondes polaires (γ_L^p) et dispersives (γ_L^d) (liquides, tableau 16) :

$$W_{SL} = 2\sqrt{\gamma_S^d \gamma_L^d} + 2\sqrt{\gamma_S^p \gamma_L^p} \qquad \text{Equation 19}$$

III.2.5.GRAVIMETRIE D'ADSORPTION DE VAPEUR D'EAU

III.2.5.1. Isothermes de sorption et applications des modèles

a) Principe

Les méthodes de détermination gravimétrique sont basées sur la mesure de la masse de l'échantillon au cours du temps dans des conditions ambiantes fixées. Ainsi, on place l'échantillon dans des conditions de pression relative fixée et on mesure la masse de l'échantillon au cours du temps jusqu'à ce que l'on atteigne un palier dont la détermination est fonction des critères d'équilibre fixés et de la précision de mesure de masse de l'échantillon. Plusieurs méthodes gravimétrique existent comme la méthode statique des solutions salines pour des mesures d'adsorption de vapeur d'eau, ou des méthodes dynamiques, comme celle utilisée sur l'appareillage DVS (Dynamic Vapor Sorption, SMS, UK) pour des mesures d'isothermes d'adsorption de vapeur d'eau ou de vapeur organique.

L'appareillage DVS (figure 29) est constitué d'une microbalance de type Cahn placée dans une enceinte régulée thermiquement.

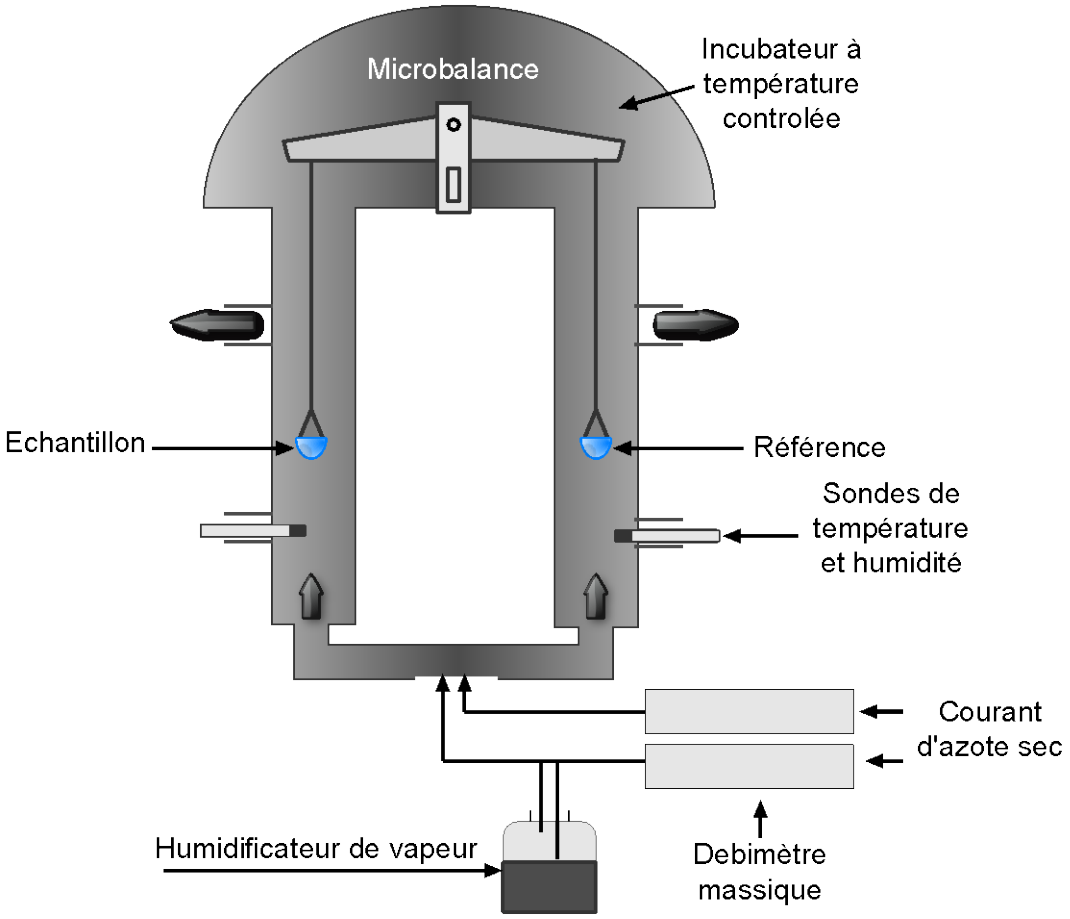

Figure 29. Schéma de principe d'un appareillage DVS.

La plage de températures possibles s'étend de T ambiante à 45°C. Sur un côté de la balance, on place une référence, de l'autre on place l'échantillon à analyser. Les références et les échantillons sont placés sur des plateaux de quartz. Les deux côtés de la balance sont balayés par un flux de gaz constitué par le mélange d'un flux de gaz sec (de l'azote) et d'un flux d'une vapeur d'eau saturée dans les proportions souhaitées, obtenus et régulés à l'aide de fluxmètres de précision. Des sondes combinées d'humidité et de température sont situées juste en dessous des nacelles contenant l'échantillon et la référence, afin de permettre une vérification de l'humidité relative et de la température. Enfin la tête de la microbalance est balayée par un flux constant de gaz sec afin d'éviter les problèmes de dérive ou d'instabilité de la mesure de masse générée par une accumulation d'humidité à cet endroit.

b) Mode opératoire

Deux protocoles et appareils différents ont été utilisés. Pour le premier au LIBio, les isothermes ont été réalisées sur des poudres de lait entier et écrémé. Entre 10 et 30 mg de

poudre est mis dans le porte échantillon de l'appareil. La variation de cette masse due à l'adsorption d'eau est enregistrée à chaque plateau (à l'équilibre) d'humidité relative imposée. Les réglages des paliers d'humidité, les temps d'attente et la température sont fixés. Deux répétitions ont été réalisées pour chaque échantillon. L'humidité varie entre 0% et 95% avec des pas de 10% et un temps d'attente de 720 minutes est fixé pour chaque plateau. Ce temps d'attente permet d'atteindre l'équilibre.

Pour le deuxième appareil du Centre RAPSODEE (figure 30), les isothermes de semoule brute et tamisées ont été analysées.

Figure 30. Appareil DVS au centre RAPSODEE.

L'analyse commence par une série de paliers d'humidités relatives gérés par un critère d'équilibre après un palier de séchage à 0% d'humidité relative pendant 1 heure. Les paliers vont de 0 % à 90 %, avec un pas de 10 % RH puis un palier à 95 % RH. Les échantillons ont été considérés comme étant à l'équilibre lorsque la valeur dm/dt (pente de la mutation de la masse avec le temps) a été fixé à <0,002 mg min-1 ou que le temps d'équilibre dépasse les 300 min.

c) Modélisation des isothermes de sorption

Les isothermes de sorption des poudres laitières et céréalières sont des isothermes de type II. Cela correspond à des milieux granulaires non poreux, selon la classification BET (Brennuer-Emmett-Teller), de forme sigmoïde (figure 31).

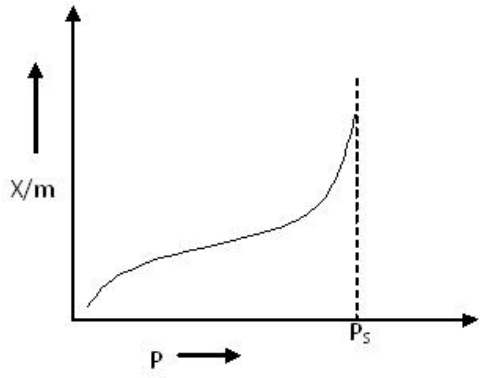

Figure 31. Isotherme de Type II.

Théoriquement trois domaines sont retrouvés:

- Le domaine 1 (a_w = 0 à 0,3) correspond à la fixation d'une couche monomoléculaire d'eau sur les sites les plus hydrophiles. La mobilité des molécules adsorbées en surface est très faible.

- Le domaine 2 (a_w = 0,3 à 0,7) correspond à l'adsorption des molécules d'eau sur des sites moins hydrophiles par liaisons hydrogène, ainsi que par liaisons de type Van-der-Waals, jusqu'à la saturation des sites hydrophiles.

- Le domaine 3 (a_w = 0,7 à 1) correspond à la poursuite de l'adsorption des sites hydrophiles, mais aussi la condensation capillaire.

Les équations GAB (Guggenheim, Anderson et de Boer) et Y & N (Young et Nelson) ont été utilisés pour modéliser les données expérimentales. La qualité de l'ajustement a été évaluée par un coefficient de corrélation linéaire (R^2). Les valeurs de la monocouche ainsi que les propriétés multicouches, qui ont été calculés par les deux modèles et comparés, des plus les propriétés d'absorption ont été calculées par Y & N.

Le modèle GAB (équation 20) est une extension de l'équation BET. Ce modèle est largement utilisé dans les études alimentaires. Ce modèle estime que la chaleur de sorption des multicouches est différente de la chaleur de liquéfaction. L'équation est apte aux isothermes de sorption de 0,1 à 0,8 a_w. Dans cette équation, *C* est la constante de Guggenheim, *k* est la correction permanente impliquant des propriétés multicouches et en vrac propriétés liquides, X_w est la teneur en humidité d'équilibre (% MS), et X_m est la quantité d'eau sur la monocouche (% dm) (Dural & Hines, 1993).

$$X_w = \frac{X_m \cdot C \cdot k \cdot a_w}{(1 - k \cdot a_w) \cdot (1 + (C - 1) \cdot k \cdot a_w)}$$ Equation 20

Y & N est un modèle dérivé du modèle de GAB. Ce modèle considère que, en plus de forces de surface de liaison, les forces de diffusion sont également présentes et cette force pourrait devenir dominante lorsque les couches multimoléculaires de l'eau sont présentes. Puis les forces de diffusion seraient plus fortes avec l'augmentation de l'eau de surface. Enfin, les forces de surface pourraient permettre le mouvement de l'eau dans l'échantillon. C'est le cas d'un grand nombre d'échantillons dans les sciences alimentaires. Les données expérimentales de la sorption et de la désorption peuvent être modélisées avec les équations suivantes:

$$M_S = A(\theta + \alpha) + B\,\varphi$$ Equation 21

$$M_D = A(\theta + \alpha) + B\,\theta\,RH_{max}$$ Equation 22

où M_S et M_D sont des teneurs en humidité d'équilibre pour le cycle respectif à chaque humidité relative, et RH_{max} est l'humidité de l'exposition maximum relative, finalement *A* et *B* sont définis comme suit:

$$A = \frac{\rho_W V_{ads}}{D}$$ Equation 23

$$B = \frac{\rho_W V_{abs}}{D}$$ Equation 24

où ρ_W est la densité de l'eau à la température expérimentale, *D* est le poids de l'échantillon sec, et V_{ads} et V_{abs} représentent les volumes d'eau adsorbée et absorbée (Lyn *et al.*, 2010).

III.2.5.2. Calcul du coefficient de diffusion classique et dynamique

a) Diffusion par la loi de Fick

Le coefficient de diffusion de vapeur d'eau dans les poudres est obtenu à partir de la deuxième loi de Fick. Cette loi peut être utilisée pour calculer la diffusion de particules (Becker, 1959):

$$\frac{M_t}{M_e} = 1 - \frac{6}{\pi^2}\sum_i w(a_i) \sum_{n=1}^{\infty} \frac{1}{n^2} exp\left(\frac{-D \cdot n^2 \cdot \pi^2 \cdot t}{{a_i}^2}\right)$$ Equation 25

où M_t est la teneur en eau (kg d'eau / kg dm) au temps t (min), M_e est la teneur en eau (kg d'eau / kg dm) à l'équilibre (t = ∞), a_i est le rayon (m) de la particule i, $w(a_i)$ est la fraction pondérale de particules qui sont caractérisées par le rayon, n est donc l'incrément du calcule. Aux conditions initiales l'équation peut être exprimé comme suit :

$$M_t = (M_i - M_e) - \frac{6}{\pi^2}\sum_i w(a_i)\sum_{n=1}^{\infty}\frac{1}{n^2}exp\left(\frac{-D\cdot n^2\cdot\pi^2\cdot t}{{a_i}^2}\right) + M_e \qquad \text{Equation 26}$$

où M_i est la teneur en eau dans des conditions initiales (t = 0). Les données expérimentales ont été tracées en changements de masse de l'échantillon (ln M_i-M_e) en fonction du temps d'hydratation, ainsi les paramètres D, M_i, et M_e peuvent être calculés. Le modèle a été confirmé par les valeurs des coefficients de régression et les erreurs résiduelles.

b) Conditionnement à différents Humidités Relatives (HR)

Dans la méthode des solutions salines, des solutions saturées de sels dans des bocaux hermétiques sont utilisées. L'humidité relative de l'atmosphère au dessus de la solution va s'équilibrer à une valeur qui est fonction du sel utilisé (on peut ainsi balayer toute la palette des humidités relatives entre 0,1 et 0,97 à 25 °C). L'échantillon est alors placé dans le bocal et des pesées sont faites à intervalles de temps réguliers, jusqu'à ce que la variation de masse soit considérée comme négligeable. On estimera avoir atteint la masse d'échantillon en équilibre avec l'atmosphère environnante. Pour les poudres alimentaires, le temps d'équilibre peut prendre des mois. De tels temps peuvent permettre la prolifération des microorganismes dans l'échantillon, de plus, la surface de la poudre au contact de l'humide est aussi étudiée. Ainsi, il n'est pas possible d'attendre un temps si long. Dans des analyses préliminaires, on a observé qu'au bout de 3 jours, les échantillons conditionnés à humidités relatives en dessous 85% ont atteint une prise d'eau qui correspond à 98% de la quantité d'eau prise par DVS à la même humidité relative (prise d'eau à l'équilibre). Pour les humidités relatives au-dessus de 85% la prise d'eau a atteint 90%. Par conséquence le temps de conditionnement de 3 jours à été suffisant. De plus, on se sert uniquement d'images de la surface et de la taille des particules après gonflement, qui est presque à 100% après une 90% de pris d'eau. Par conséquence, on a fixé un temps de conditionnement de 3 jours pour les poudres du lait. Cela permet d'éviter le développement des microorganismes. Dans le cas de la semoule, il a été

possible ajouter de toluène (conseillé que pour les échantillons sans matière grasse) cela permet une durée de conditionnement de 7 jours.

Les poudres de lait standard (entier et écrémé) ont été équilibrées à 25 °C pendant trois jours à onze humidités relatives dans des bocaux hermétiques contenant des solutions salines saturées (Sigma-Aldrich) à humidités relatives connues: 11% (LiCl); 22% (CH_3COOK); 33% ($MgCl_2$); 43 % (K_2CO_3); 54 % ($Mg(NO_3)_2$); 69 % (KI); 75 % (NaCl); 79 % (NH_4Cl); 85 % (KCl); 94 % (KNO_3) et 97 % (K_2SO_4).

Dans le cas de la semoule, trois fractions tamisées (0-160, 250-315, et 400-500 μm) ont été équilibrées à 25 °C pendant sept jours à cinq HR % dans des bocaux hermétiques contenant des solutions salines saturées (Sigma-Aldrich) à humidités relatives connus: 11 % (LiCl); 54 % $Mg(NO_3)_2$; 0,75 (NaCl); 85 % (KCl) et 97 % (K_2SO_4). Un millilitre de toluène a été placé dans un récipient séparé à proximité des échantillons pour éviter la prolifération des micro-organismes (Wrolstad *et al*., 2004).

III.2.6.L'ENROBAGE A SEC DE LA SEMOULE DE BLE DUR

a) Principe

L'enrobage à sec est un procédé récent basé sur des méthodes d'association physique de poudres. Cette technique présente les avantages suivants : économie d'énergie (pas d'étape ultérieure de séchage), pas d'utilisation de solvants et simplification des procédés. L'importance de l'enrobage à sec réside dans sa capacité à apporter des changements de propriétés et/ou fonctionnalités des matériaux de base et à améliorer et contrôler les propriétés chimiques et/ou physico-chimiques. Parmi les propriétés de surface qui peuvent être modifiées par l'enrobage, on trouve : la mouillabilité, la coulabilité, la solubilité, la dispersibilité, la saveur et l'arôme, etc.

L'association de particules par enrobage à sec ne signifie pas une simple adhésion entre particules mais de solides liaisons causées par les interactions entre les constituants, comme illustré sur la figure 32.

Il existe quatre facteurs principaux influençant l'adhésion entre particules qui sont: la rugosité de surface, la taille et la forme des particules, la dureté et l'élasticité des matériaux et l'énergie de surface et le travail d'adhésion entre particules.

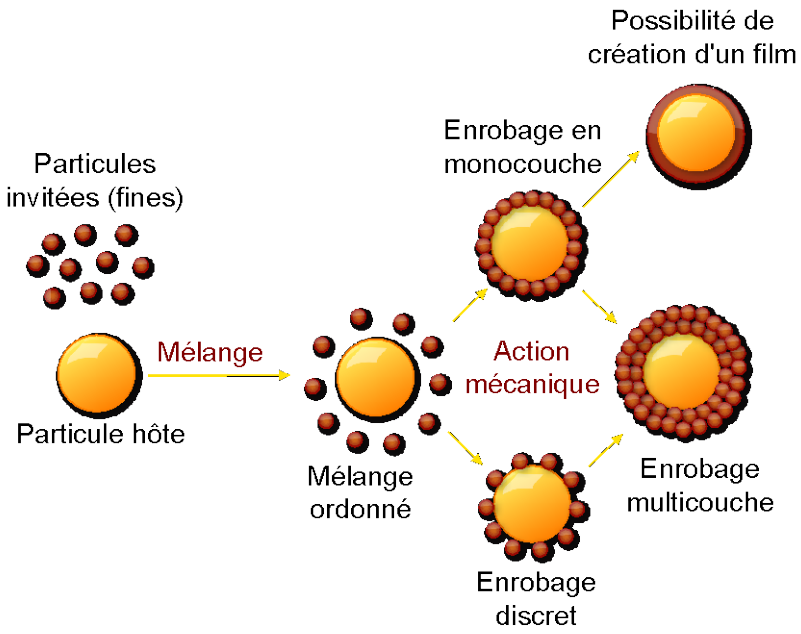

Figure 32. Principe de l'enrobage à sec.

b) Mode opératoire

Dans le cadre de notre étude, nous avons convenu d'enrober la semoule de blé avec trois composés différents (l'amidon, le gluten et l'arabinoxylan) qui ne sont autres que les composés de la semoule de blé dur. En effet, ce choix a pour but de déterminer la contribution de chacun des composés dans les propriétés de surface des particules.

L'appareil utilisé est un mélangeur/granulateur à cisaillement élevé, le Cyclomix développé par la société Hosokawa. Il s'agit d'un pilote de laboratoire qui comprend essentiellement un bol conique de 1 litre de volume représentant la chambre de mélange (figure 33). Celle-ci se fixe sur un couvercle portant un rotor au centre, sur lequel sont fixées 3 paires de pales symétriques et un racleur. L'entrefer entre les pales et la paroi de la chambre est de 3 mm. Ce faible espace génère des interactions spécifiques entre la poudre et la paroi de la chambre distinguant ainsi le cyclomix des autres mélangeurs. Un moteur et une unité de commande permettent de contrôler la vitesse de rotation qui peut aller jusqu'à 3000 tr/min.

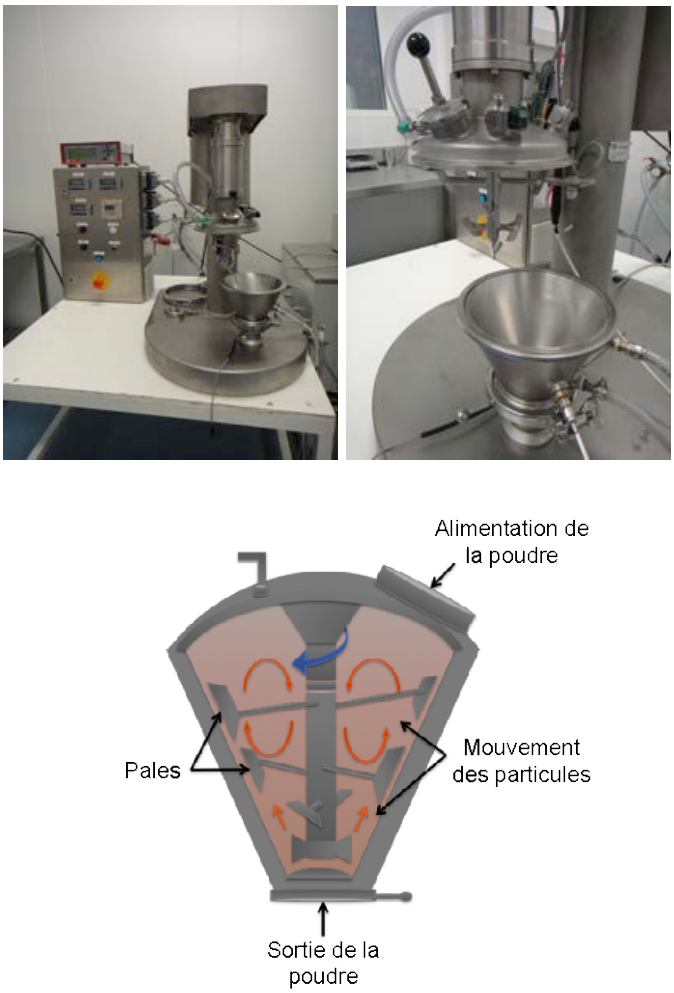

Figure 33. Installation complète du Cyclomix.

Dans cette étude, il a été utilisé une vitesse de 1000 tr/min. L'installation permet par ailleurs un suivi du couple requis pour maintenir la vitesse du rotor. Les durées de traitement requises avec ce type d'installation permettant d'obtenir une bonne homogénéité du produit enrobé sont de l'ordre de la dizaine de minutes. La sélection de la vitesse du traitement a été choisie à partir des tests préliminaires. Le temps de traitement est un temps classique connu en enrobage à sec qui permet un bon degré de mélange. Les tests préliminaires consistaient à traiter au cyclomix la semoule sans particules. Le temps a été fixé à 10 minutes et la vitesse variait de 500, 1000 et 1500 tr/min. La semoule après cyclomix a été observée au SEM et caractérisée en taille par granulométrie lasser. Après caractérisation, une vitesse plus importante et un temps identique n'abimant pas les particules, a été sélectionnée.

Pour calculer la fraction massique (w) de particules invitées (guest particles) nécessaires pour former une monocouche sur la surface des particules hôtes (host particles) (figure 34), nous avons choisi le modèle basé sur les hypothèses suivantes :

- Les particules sont sphériques
- Les particules hôtes et invitées ne subissent aucune déformation (réduction de taille) durant les essais et toutes les particules invitées sont de même taille.

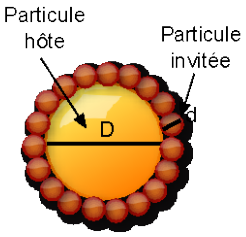

Figure 34. Rapport de taille entre la particule hôte et la particule invitée.

Le modèle utilisé est défini par un arrangement des particules qui conduit à l'équation proposé par (Ouabbas, 2008):

$$\frac{m}{M} = 3.6\left(\frac{d}{D}\right)\left(\frac{\rho}{\rho_h}\right)\left[1+\left(\frac{d}{D}\right)^2\right] \quad \text{Equation 27}$$

$$W_g = \frac{m}{m+M} \quad \text{Equation 28}$$

Avec:

M et m: masse (g) des particules hôtes et invitées, respectivement

D et d: diamètre (µm) des particules hôtes et invitées, respectivement (d/D ≈ 10)

ρ_h et ρ: masse volumique (g.cm^{-3}) des particules hôtes et invitées, respectivement

w_g: le pourcentage massique (%) des particules invitées.

Une simplification des équations permet d'obtenir directement les pourcentage massiques des particules invitées et hôtes à partir du volume de remplissage de l'appareil:

$$M = \frac{V}{\left[\left(\frac{1}{\rho_{hp}}\right)+\left(\frac{\frac{m}{M}}{\rho_{hp}}\right)\right]} \quad \text{Equation 29}$$

$$m = W_h\frac{m}{M} \quad \text{Equation 30}$$

Avec:

M et *m*: masse (g) des particules hôtes et invitées, respectivement

V: volumme de remplissage du cyclomix (mL)

ρ_{hp}: masse volumique de la particule hôte ($g.cm^{-3}$)

La semoule tamisée (315 - 400 μm) avec un D(50) de 374 μm a été utilisée comme particule hôte. Les particules invitées sont: l'amidon avec un D(50) de 20,83 μm, gluten micronisé 6 μm. L'arabinoxylane est une poudre très fine et de consistance très fragile, la mesure de la taille des particules n'a pas été possible ni par granulométrie laser ni par SEM, c'est ainsi qu'une taille approximative de 1 μm été assignée à cette poudre. A partir des équations précédentes et des caractéristiques mentionnées, le pourcentage massique (%) des particules hôtes et invitées a été calculé dans le tableau 17.

Tableau 17. Pourcentage massique et masse des particules hôtes et invitées.

Enrobage	Semoule	Amidon	Semoule	Arab.	Semoule	Gluten micro.
M et *m*(g)	333,65	66,4	383,7	3,2	306,7	85,7
w_h et w_g (%)	83,65	16,6	99,2	0,83	51,4	14,3

IV. RESULTS AND DISCUSSION

IV.1. ATOMIC APPROACH: SURFACE CHARACTERIZATION

The main goal of this thesis work is to characterize the properties of reactive food powders. To achieve this objective, the possible characteristics allowing evaluate the reactivity of a particles were identified. Firstly particles shape and surface chemical composition were taking into a count. It was considered that both properties play an important roll in particle reactivity (interaction particle-particle, interaction particle-extern constraint). However, as it was mentioned in the bibliographic study, very few techniques permit the characterization of the particles surface. Consequently, in a first step, a proposition of methodology to study the surface composition of food powders was developed. The characterization by XPS coupled to EDX analyses was proposed. Both techniques work at atomic level, from this response of analysis a molecular composition was deduced.

XPS has already demonstrated its utility on surface composition determination. Indeed, XPS atomic spectra in combination with the equation system proposed by Fäldt (1995), permit to calculate the percentage of carbohydrates, proteins and lipids in food powder surface. However, XPS is not the only device that can perform an atomic analysis of the particle surface. EDX is a dispositive coupled to the ESEM and it can also analyze the elemental composition in 1 μm depth. Taking into account the potential of this analysis, the technique developed by Fäldt (1995) was adapted to the EDX analysis. The adaptation was performed for both milk powder and semolina.

In the first part of this subchapter, the adaptation of the EDX technique on milk powders was developed. To do it, the composition of milk pure components was determined. Hence the matrix system was fed with the values of pure components. The surface lactose, milk proteins and milk fat of industrial milk particles was then calculated. Part of this work was already communicated in an international congress:

Murrieta-Pazos I., Rolland C., Galet L., Gaiani C. and Scher J. Development of a methodology to determinate the gradient distribution of lactose, milk fat an milk proteins in milk powder particles by EDX coupled to XPS. The 5th International Symposium on Spray Dried Dairy Products. Juin 19-21, 2012, St-Malo, France.

This integral study was written as a paper and will be submitted on December 2012. Results and discussion of this paper is integrated in this manuscript in section IV.1.1 (Energy

dispersive X-ray: validation of the technique to characterize the surface composition of milk powders).

In the second part of this subchapter, the same technique adaptation was performed in semolina. The pure components of semolina were analyzed by EDX, later the matrix system was fed to obtain the values of wheat carbohydrates (starch + arabinoxylan), wheat lipids and gluten at the surface of semolina particles. The methodology was compared and coupled with XPS done on raw semolina and raw couscous as well as semolina and couscous after free fat extraction (AFFE). The gradient composition and the effect of the agglomeration process on the particles were studied. Semolina is a complex powder, making difficult to give convincing conclusions and validate the technique, consequently this study didn't make the object of a publication. However results are of interest and they are discussed in the section IV.1.2. (Gradient composition in semolina and couscous by coupling EDX and XPS analysis).

IV.1.1. ENERGY DISPERSIVE X-RAY: VALIDATION OF THE TECHNIQUE TO CHARACTERIZE THE SURFACE COMPOSITION OF MILK POWDERS.

Milk powders are produced by spray drying assuming that milk components (lipids, proteins, lactose and minerals) are distributed uniformly in the solution fed. Nevertheless, during the process (physical configuration of the dryer, feed characteristics or also the operation conditions) the components get redistributed in the droplet, this claim is supported by a considerable quantity of authors (Gaiani *et al*., 2006; Kentish *et al.*, 2005; Kim *et al*., 2002; Murrieta-Pazos *et al.*, 2012b; Nijdam & Langrish, 2006; Shrestha *et al*., 2007). The resulting particles present heterogeneity between the surface and the core of the particle. In addition, this surface/core differences may be accentuated by packaging, storage and/or transport conditions (Fitzpatrick *et al*., 2007; Gaiani *et al*., 2009; Kim *et al*., 2009c). Recently it has been concluded that the particle surface composition had a strong impact on powder functional properties, for example reconstitution properties (Forny *et al*., 2011), stickiness (Shrestha *et al*., 2007), flowability (Kim *et al*., 2005a), floodability, oxidation (Vignolles *et al.*, 2007), etc. As the food powder production increases more and more, it is the time to use new and innovative methodologies to understand the behavior of food powders functional properties. Consequently a growing number of interesting methods allowing the surface characterization of milk powders have been developed recently (Murrieta-Pazos *et al.*, 2012a).

During the two last decades, the most used technique to characterize the surface of dairy powders was the X-ray Photoelectron Spectroscopy (XPS). XPS provides elemental (atomic percentages) and chemical (binding percentages) information of the first five to ten nanometers of the powder (Fäldt *et al*., 1993; Gaiani *et al*., 2006, 2010; Kim *et al*., 2009a, 2009b, 2009c; Millqvist-Fureby, 2003; Murrieta-Pazos *et al.*, 2012b; Shrestha *et al*., 2007). From the atomic values, the determinations of the principal components percentages (protein, lactose and lipids) on the powder surface were done with the help of a matrix formula. Another classical approach was also possible with the Scanning Electron Microscopy (SEM). However, investigations performed by SEM may present some disadvantages: information about components is difficult to obtain (if not used in conjunction with EDX), samples have to be coated with a conductive material (creation of artifacts), finally the vacuum conditions could alter the powders. Differences in surface composition (lactose, lipids and/or protein) were related to differences in surface topography. For example the powders were more or less shriveled, smooth… (Mistry *et al.*, 1992); but quantitative information are impossible to obtain by this way. An evolution of these investigations was possible using solvent extraction to alter the surface of the particles, but protocol was only interesting for fat coted powders, for example whole milk powder (Vignolles *et al*., 2007).

Energy Dispersive X-ray (EDX) is another powerful technique allowing an elemental analysis of the surface (as well as XPS). This technique, contrary to XPS, allows the surface characterization at a deeper level from the first micron to the five first microns. In addition, EDX allowed a very localized characterization in the particle whereas the area of XPS analysis was larger (300 x 700 µm) (Briggs, 1994). Recently, Environmental Scanning Electron Microscopy (ESEM) images were combined with EDX analyses. The technique was used for identification of elemental components on the sample. The EDX analysis system works as an integrated feature of an ESEM equipment and cannot operate on its own. Their characterization capabilities are due to the fundamental principle that each element has a unique atomic structure. After ejection of an electron, an X-rays is emitted which frequency is exclusive of each element. To stimulate the emission of the characteristic X-rays from a specimen, a high-energy beam of charged particles is focused into the sample. An EDX spectrum is obtained, which is a plot of the frequency of X-ray for each energy level. The higher a peak in a spectrum, the more concentrated the element in the sample. In the field of food powders, EDX was rarely used (Laskin & Cowin, 2001; Murrieta-Pazos *et al.*, 2012a, 2012b). Only few authors used this technique to investigate the chemical composition of dairy

powders. Comparing surface composition obtained by XPS and data collected by EDX, the authors proposed models of powder gradients for skim and whole milk powders (Murrieta-Pazos *et al.*, 2012b). Even if this technique seems to be very promising, these results are the first one and they need to be validated. On biomaterials applications, the technique was rarely used because the depth of analysis exceeds the thickness of the surface layers that determine biocompatibility (Kingshott *et al.*, 2011).

For this purpose, industrial skim and whole milk powders (containing 1 and 28% of lipids, respectively) were used. In addition, pure components (native whey protein isolate, native micellar casein, lactose and anhydrous milk fat) were use as reference to validate the methodology. The aim of this paper is to test and validate the EDX as a technique that can be used to characterize the surface of dairy powders. The results were of EDX were coupled to those of XPS to study the gradients composition at the surface of milk powders.

IV.1.1.3. Powders characterization by ESEM-EDX

a) Pure milk components

ESEM images of pure milk components are shown in figure 35 A, B, C and D. The structure of Native Wey Isolate (NWI) in figure 35 A and Native Micellar Casein (NMC) in figure 35 B are typical of spray dried powders. NWI present agglomerated particles whereas individual spherical structures can be appreciated in NMC sample. The largest NWI particles (around 100 µm) and NMC particles (around 50 µm) are in agreement with the values found by static light scattering (data not shown). In addition, ESEM images performed on NWI powders show a higher heterogeneity in particle size in comparison with NMC powders. All the particles present a smooth surface and the presence of dents is also observed. Typical structures were observed for lactose particles (figure 35 C). Small crystals are observed at the particles surface. In addition, the particles are less spherical and more irregular. In the case of Anhydrous Milk Fat (AMF) in figure 35 D, a drop of the molten fat was placed on the support. Hence the temperature in the ESEM chamber was placed around 5ºC, the liquid fat got solid and a film was formed. No additional specific details were observed.

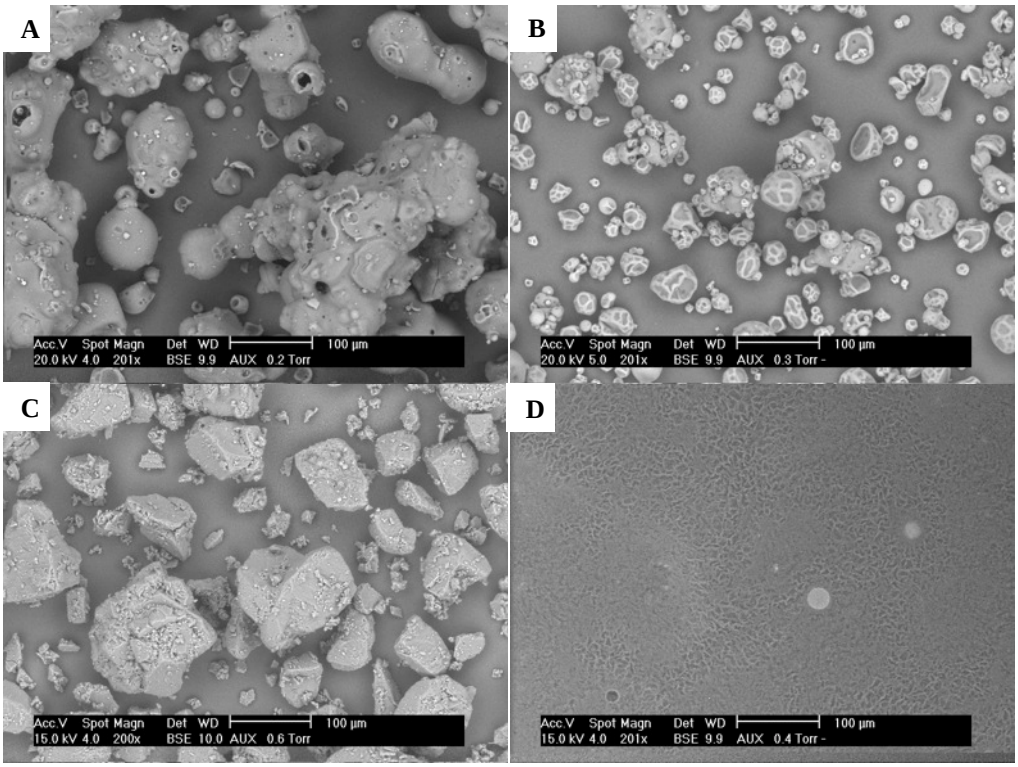

Figure 35. Scanning Electron Micrographs (x200) of reference pure components (native whey isolate powders (A), native micellar casein powders (B), alpha-lactose (C) and anhydrous milk fat (D).

Pure components analyses are shown in figure 36. For lactose, three points (red arrows) were performed on the same particle (figure 36). After analysis (figure 36 B1), it can be observed the local degradation of the lactose at the 3 points, showing the fragility of the lactose structure. This degradation may also cause problems during the analysis of the particle. Indeed, the EDX analysis is sensitive to the angle of analysis with respect to the detector in the apparatus chamber. Such penetration of the electron beam into the particle could avoid a good spread of X-rays to the detector. The particle shape can be also a parameter of influence. Ideally, the sample should be analyzed as a tablet, to get a flat and not-hilly surface. This permit an ideal angle response aligned to the X-ray detector. However, the aim of this work is to study the surface of the particles, as such, the powder should be directly placed in the support. This condition of the sample (powder) creates some difficulties in the analysis, for example a poor repeatability of results and also a limitation on the number of tests per particle.

The results of the points of analysis a, b and c, are shown in table 18. The results present only carbon and oxygen peaks, proper of a carbohydrate. By consequence the analysis confirms the efficacy of the EDX technique to detect the elements that make up organic particles.

Table 18. Atomic composition (%) of the reference powders analyzed in 3 points (represented by a, b and c in Figure 2) for NWI, Lactose and AMF and in 2 points for NMC.

Powder	Atomic Composition (% in mass)	Points of analyze			Average	S.D.
		a	b	c		
Native whey isolate powder	C	74.37	77.96	75.67	76.0	1.9
	N	11.80	10.35	12.58	11.6	1.1
	O	11.17	9.06	10.12	10.1	1.1
	P	0.30	0.30	0.20	0.3	0.1
	S	1.37	1.45	0.96	1.3	0.3
	K	0.52	0.43	0.25	0.4	0.1
	Ca	0.47	0.45	0.22	0.4	0.1
Lactose	C	80.71	81.75	81.22	81.2	0.5
	O	19.29	18.25	18.78	18.8	0.5
Native micellar Casein powder	C	75.15	75.15	-	75.1	0.0
	N	9.41	9.52	-	9.5	0.1
	O	10.67	10.74	-	10.7	0.1
	P	1.45	1.23	-	1.3	0.2
	S	0.70	0.71	-	0.7	0.3
	K	0.24	0.28	-	0.3	0.0
	Ca	2.38	2.37	-	2.4	0.0
Anhydrous milk fat	C	94.58	94.91	94.96	94.9	0.3
	O	5.42	5.09	5.04	5.1	0.3

When looking the carbon value for lactose in table 18; an overestimation of this element is immediately observed. However, the atomic concentration ratios were not in full agreement with the expected stoichiometric values. This overestimation of carbon is known in the use of X-ray techniques (Gerin *et al.*, 1995; Rouxhet & Genet, 2011). The C peak intensity was more important and may be due to carbon contaminant and impurities collected from the atmosphere during the sample transfer into the EDX chamber or during product manufacturing. The percentages obtained for C and O for the three points of analysis are similar and the standard deviation does not vary significantly. This means that there is a good reproducibility of the results done in one particle.

The points of analyzes performed on the Native Way Isolated (NWI) particles are presented in figure 36 A2 and figure 36 B2 before and after analysis respectively. The structure of NWI seemed to be more resistant than lactose and was not affected by the X-ray beam. This resistance can help to reduce variations on the results and also permit to make several analyzes in one single particle.

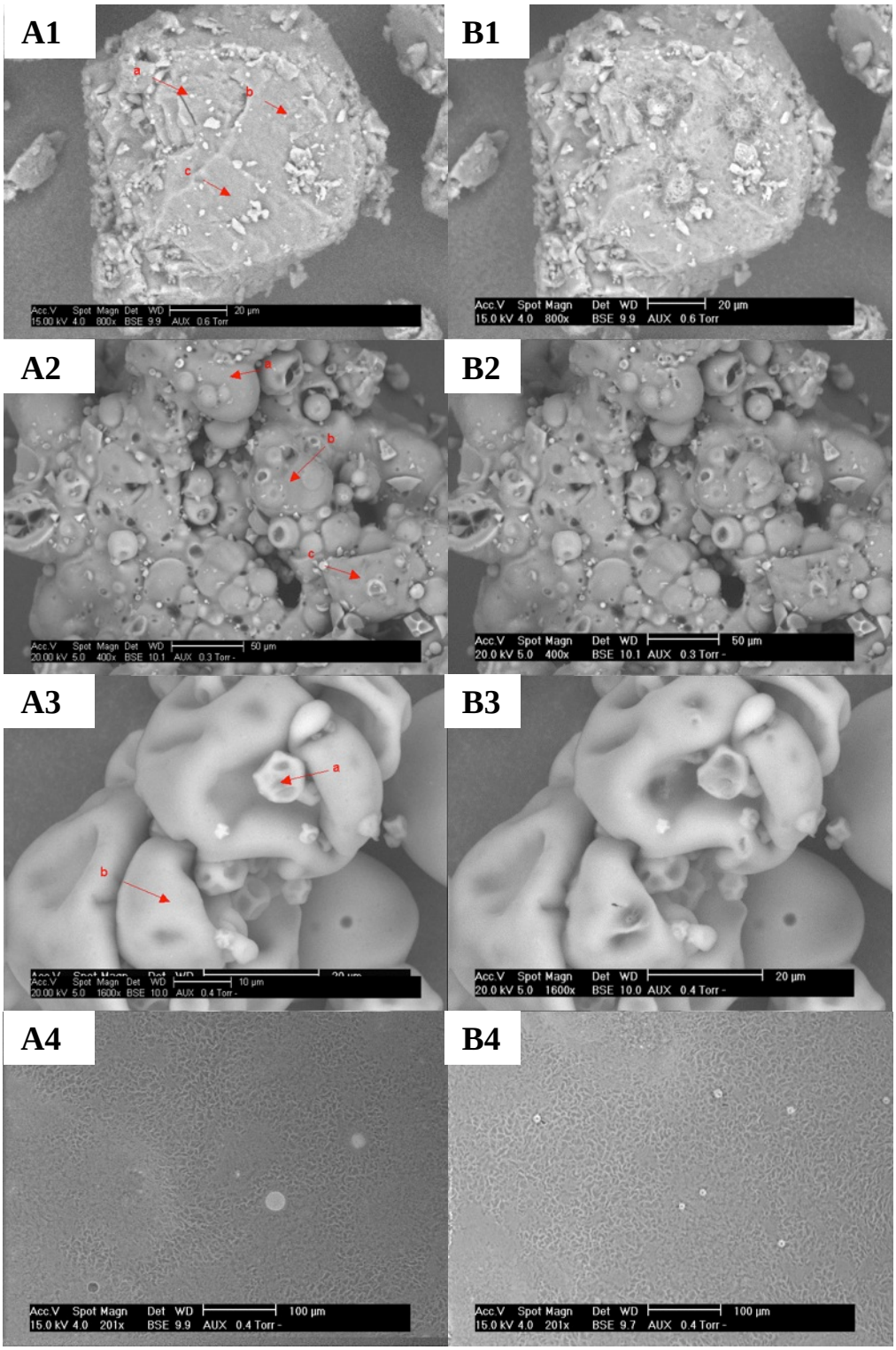

Figure 36. Scanning Electron Micrographs before (A) and after (B) EDX analysis of lactose monohydrated (x800) (1), native whey isolate (x400) (2), native micellar casein (x1600) (3) and anhydrous milk fat (x200) (4).

In table 18, the atomic concentrations obtained at the surface of Native Whey Isolate (NWI) are presented. In addition to C and O elements, it is observed the presence of nitrogen (expected since NWI is a protein) and the presence of minerals. In milk powders, proteins are the only molecules that can have nitrogen element in their composition. Consequently, the N

percentage is directly proportional the protein percentage in the powder. Minerals are not part of the protein molecules but often associated. Sulfur is the most abundant mineral in NWI. As expected, the atomic concentration in NWI do not vary significantly, this confirms a more resistant material allowing a better reproducibility of the analysis.

For NMC powders, the figure 36 A3 and B3 show the same particle before and after 2 points of analysis. The dot a was performed on a small particle close to a bigger one. After the analysis, there is not visible degradation of the material. In general, proteins present a good resistance to the electron beam. Atomic concentrations at the two points are shown in table 18. In this sample, carbon, oxygen and nitrogen are observed, the quantity of minerals is higher than these observed in micelle casein, probably because NMC is richer in calcium and phosphorus than NWI (Gaiani *et al*., 2010). The standard deviation is small, by consequence a good reproducibility is concluded.

Finally, the analysis was also performed on the Anhydrous Milk Fat (AMF). This component (figure 36 A4 and B4) is not a particle but a thin film. It can be observed the degradation caused by the analysis in figure 36 B4, due to a very soft texture. The AMF present a melting point around 40 °C, consequently it can easily become liquid. However, a film instead of a particle (presenting an irregular surface and shape) helps to achieve a good reproducibility in the analysis. The standard deviation for the 3 points of analysis is very small (table 18). Only carbon and oxygen are detected in the analysis, hydrogen is not detected by the technique. As expected, the atomic concentration of carbon is very high. Consequently a little difference is observed according to the theoretical values observed in table 20.

b) Industrial milk powders

Figure 37 shows the general structural aspect of whole (figure 37 A) and skim milk powders (figure 37 B). A smooth surface is appreciated in whole milk particles due to a surface covered by free fat (Vignolles *et al*., 2007). On the opposite, a more rigid and wrinkled surface is observed for SMP due to the presence of a lactose-protein matrix and the absence of visible surface fat. These appearances are characteristic and widely observed (Gaiani *et al*., 2006; Kim *et al*., 2002; Murrieta-Pazos *et al*., 2011; Nijdam & Langrish, 2006).

.

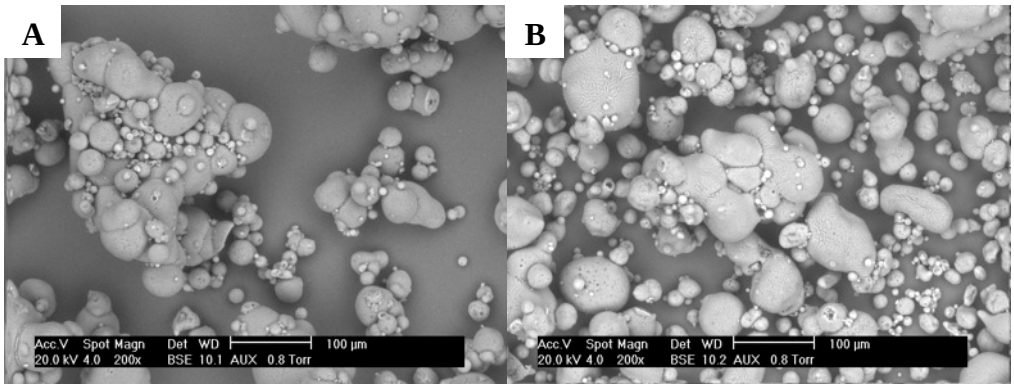

Figure 37. Commercial powders, whole milk powders (A), skim milk powders (B).

c) Results variation analysis (by particle and by day)

The EDX analysis is not typically use in organic samples like dairy powders. Up to now, it is not really clear if different particles could have different atomic elements at the surface. Indeed, contrary to the XPS technique where the area of analysis (700 x 300 µm) covered a huge number of particles; EDX analysis was very local, around 2-5 µm (as seen in figure 36). In order to produce a correct interpretation of results, it is important to obtain a good repeatability.

Table 19. EDX average per particle and average per day of analysis in each pure component.

		Atomic concentration for various pure components (%)			
		Lactose	NWI	NMC	AMF
Average on different particles (more than 10)	C	74.0 ± 7.3	72.4 ± 2.2	73.5 ± 1.5	94.9 ± 0.3
	O	20.6 ± 3.1	12.8 ± 2.8	12.2 ± 1.2	5.1 ± 0.3
	N	-	13.8 ± 1.4	10.7 ± 1.0	-
	P	-	0.2 ± 0.1	1.2 ± 0.1	-
	S	-	0.8 ± 0.3	0.5 ± 0.1	-
	K	-	0.2 ± 0.1	0.2 ± 0.1	-
	Ca	-	0.2 ± 0.1	1.7 ± 0.5	-
Average on different days (4 days)	C	77.9 ± 2.7	73.0 ± 2.7	73.5 ± 1.5	93.9 ± 1.4
	O	22.1 ± 2.7	13.4 ± 1.8	10.7 ± 0.7	6.1 ± 1.4
	N	-	12.3 ± 1.9	12.2 ± 1.4	-
	P	-	0.2 ± 0.1	1.2 ± 0.1	-
	S	-	0.9 ± 0.3	0.5 ± 0.1	-
	K	-	0.3 ± 0.1	0.2 ± 0.0	-
	Ca	-	0.3 ± 0.1	1.7 ± 0.4	-

Consequently, measures on different particles as well as different days were performed. The mean of more than 10 analyses on different particles and the mean of more than 4 different days for each pure component are presented in table 19.

The influence of the particle (more than 10 particles) on the reproducibility was correct for NMC, NWI and AMF. Only the results for lactose present high standard deviation.

Concerning the day of analysis, the repeatability was very good whatever the pure component analyzed. So, the variations in the results seem to be slightly more linked to the particles than to the day of analysis. The variations according to the day of analysis can be explained by the pollution in the microscope chamber. It happens after the analysis of samples with high content on carbon, but in the case of this samples, the regular pollution of the chamber does not affect the repetability.

IV.1.1.4. Validation of the EDX method

a) Determination of theoretical values on pure components

The atomic percentages were calculated theoretically from the chemical composition of lactose, whey, casein and fatty acids present in milk (table 20). EDX determine and quantify the atoms present at the surface of the samples. In the case of organic samples (therefore in milk powders), the principal atoms detected correspond to carbon, oxygen and nitrogen. Some minerals are also detected, but in very small quantities. Hydrogen is also part of the elments present in organic samples, however this elment cannot be detected by EDX. By consequence, the atomic percentage should consider only carbon, oxygen and nitrogen. The teoretical calculus is done in table 20 from the chemical equations of the components. The quantity of atoms (C, O, N) is then expressed in percentage. Finally, the values are adjusted to the quantity of each molecule in milk.

For lactose, which is the principal sugar component in milk, the molecule is mostly monohydrated. Consequently, the calculus of the theoretical atomic percentages was done including a water molecule as other studies (Fäldt & Bergenståhl, 1994; Gaiani *et al*., 2006; Kim *et al*., 2002). For proteins (casein and whey proteins), the amino-acid compositions were used to determine the atomic percentages (Sindayikengera & Xia, 2006). The final percentages: C:64; O:21 and N:15 are very close to those already find in the literature which are C:65; O:19; N:16 (Fäldt *et al*., 1993; Fäldt & Bergenståhl, 1994; Gaiani *et al*., 2006; Kim *et al*., 2002). Finally, the theoretical fatty acid percentages (C:89; O:11) was also calculated from Kim *et al*. (2005b); Murrieta-Pazos *et al.*, (2012b). These percentages are exactly those found in literature (Fäldt *et al*., 1993; Fäldt & Bergenståhl, 1994; Gaiani *et al*., 2006; Kim *et al*., 2002).

Table 20. Theoretical values of atomic percentage contained in protein, sugar and lipids of milk.

		µg/g Pur comp.	Total (%)	Formula[1]	Number of atoms C	O	N	Atomic (%) C	O	N	Total (%) C	O	N
LACTOSE	Lactose	1000.0	73.4	$C_{12}H_{22}O_{11}$	12	11	0	52.2	47.8	0	52.2	47.8	0
	Lactose Monohydrate	-	21.5	$C_{12}H_{22}O_{11} * H_2O$	12	12	0	50.0	50.0	0	-	-	-
CASEINATE	Aminoacids				C	O	N	C	O	N	C	O	N
	Glutamic acid	218.4	21.8	$C_5H_9NO_4$	5	3	1	55.6	33.3	11.1	12.1	7.3	2.4
	Phenilalanina	101.4	10.1	$C_9H_{11}NO_2$	9	1	1	66.7	16.7	16.7	6.8	1.7	1.7
	Proline	93.3	9.3	$C_5H_9NO_2$	5	1	1	71.4	14.3	14.3	6.7	1.3	1.3
	Leucine	88.9	8.9	$C_6H_{13}NO_2$	6	1	1	75.0	12.5	12.5	6.7	1.1	1.1
	Lysine	77.5	7.8	$C_6H_{14}N_2O_2$	6	1	2	66.7	11.1	22.2	4.7	5.2	0.9
	Aspartic acid	75.7	7.6	$C_4H_7NO_4$	4	3	1	50.0	37.5	12.5	3.8	2.8	0.9
	Valine	56.4	5.6	$C_5H_{11}NO_2$	5	1	1	71.4	14.3	14.3	4.0	0.8	0.8
	Serine	55.4	5.5	$C_3H_7NO_3$	3	2	1	50.0	33.3	16.7	2.8	1.8	0.9
	Isoleucine	45.9	4.6	$C_6H_{13}NO_2$	6	1	1	75.0	12.5	12.5	3.4	0.6	0.6
	Threonine	40.5	4.1	$C_4H_9NO_3$	4	2	1	57.1	28.6	14.3	2.3	1.2	0.6
	Arginine	33.5	3.4	$C_6H_{14}N_4O_2$	6	1	4	54.5	9.1	36.4	1.8	0.3	1.2
	Methionine	32	3.2	$C_5H_{11}NO_2$	5	1	1	71.4	14.3	14.3	2.3	0.5	0.5
	Alanine	27.6	2.8	$C_3H_7NO_2$	3	1	1	60.0	20.0	20.0	1.7	0.6	0.6
	Histidine	25.4	2.5	$C_6H_9N_3O_2$	6	1	3	60.0	10.0	30.0	1.5	0.3	0.8
	Glycine	17.3	1.7	$C_2H_5NO_2$	2	1	1	50.0	25.0	25.0	0.9	0.4	0.4
	Tryptophan	10.4	1.0	$C_{11}H_{12}N_2O_2$	11	1	2	78.6	7.1	14.3	0.8	0.8	0.1
	Amino acids total	**999.6**	**100.0**	**-**							**62.7**	**21.6**	**15.7**

		µg/g Pur comp.	Total (%)	Formula[1]	Number of atoms			Atomic (%)			Total (%)		
	Aminoacids				C	O	N	C	O	N	C	O	N
WHEY PROTEINS	Glutamic acid	158.3	15.8	$C_5H_9NO_4$	5	3	1	62.5	25.0	12.5	9.9	4.0	2.0
	Leucine	106.6	10.7	$C_6H_{13}NO_2$	6	1	1	75.0	12.5	12.5	8.0	1.3	1.3
	Aspartic acid	91.8	9.2	$C_4H_7NO_4$	4	3	1	50.0	37.5	12.5	4.6	3.4	1.1
	Lysine	88.1	8.8	$C_6H_{14}N_2O_2$	6	1	2	66.7	11.1	22.2	5.3	5.9	1.0
	Methionine	79.7	8.0	$C_5H_{11}NO_2$	5	1	1	71.4	14.3	14.3	5.7	1.1	1.1
	Threonine	68.7	6.9	$C_4H_9NO_3$	4	2	1	57.1	28.6	14.3	3.9	2.0	1.0
	Proline	66.6	6.7	$C_5H_9NO_2$	5	1	1	71.4	14.3	14.3	4.8	1.0	1.0
	Phenilalanina	58.2	5.8	$C_9H_{11}NO_2$	4	1	1	66.7	16.7	16.7	3.9	1.0	1.0
	Alanine	55.5	5.6	$C_3H_7NO_2$	3	1	1	60.0	20.0	20.0	3.3	1.1	1.1
	Glycine	53.2	5.3	$C_2H_5NO_2$	2	1	1	50.0	25.0	25.0	2.7	1.3	1.3
	Serine	53.0	5.3	$C_3H_7NO_3$	3	2	1	50.0	33.3	16.7	2.7	1.8	0.9
	Isoleucine	49.7	5.0	$C_6H_{13}NO_2$	6	1	1	75.0	12.5	12.5	3.7	0.6	0.6
	Arginine	27.1	2.7	$C_6H_{14}N_4O_2$	6	1	4	54.5	9.1	36.4	1.5	0.2	1.0
	Valine	18.4	1.8	$C_5H_{11}NO_2$	5	1	1	71.4	14.3	14.3	1.3	0.3	0.3
	Tryptophan	17.3	1.7	$C_{11}H_{12}N_2O_2$	11	1	2	78.6	7.1	14.3	1.3	1.4	0.1
	Histidine	7.8	0.8	$C_6H_9N_3O_2$	6	1	3	60.0	10.0	30.0	0.5	0.1	0.2
	Amino acids total	**1000.0**	**100.0**	**-**							**63.6**	**20.3**	**16.1**

		µg/g Pur comp.	Total (%)	Formula	Number of atoms			Atomic (%)			Total (%)		
	Fatty acids				C	O	N	C	O	N	C	O	N
LIPIDS	Palmitic	369.60	36.96	$C_{16}H_{32}O_2$	16	2	0	88.9	11.1	0.0	32.9	4.1	0.0
	Oleic	249.40	24.94	$C_{18}H_{34}O_2$	18	2	0	90.0	10.0	0.0	22.4	2.5	0.0
	Stearic	120.7	12.07	$C_{18}H_{36}O_2$	18	2	0	90.0	10.0	0.0	10.9	1.2	0.0
	Myristic acid	120.7	12.07	$C_{14}H_{28}O_2$	14	2	0	87.5	12.5	0.0	10.6	1.5	0.0
	Capric	37	3.7	$C_{10}H_{20}O_2$	10	2	0	83.3	16.7	0.0	3.1	0.6	0.0
	Lauric	33.7	3.37	$C_{12}H_{24}O_2$	12	2	0	85.7	14.3	0.0	2.9	0.5	0.0
	Linoleic	24.00	2.4	$C_{18}H_{32}O_2$	18	2	0	90.0	10.0	0.0	2.2	0.2	0.0
	Palmitoleic	16.9	1.69	$C_{16}H_{30}O_2$	16	2	0	88.9	11.1	0.0	1.5	0.2	0.0
	Caprylic	10.7	1.07	$C_8H_{16}O_2$	8	2	0	80.0	20.0	0.0	0.9	0.2	0.0
	Margaric	7.5	0.75	$C_{17}H_{34}O_2$	17	2	0	89.5	10.5	0.0	0.7	0.1	0.0
	Linolenic	5.8	0.58	$C_{18}H_{30}O_2$	18	2	0	90.0	10.0	0.0	0.5	0.1	0.0
	Pentadecylic	4	0.4	$C_{15}H_{30}O_2$	15	2	0	88.2	11.8	0.0	0.4	0.0	0.0
	Fatty acids total	**1,000.00**	**100.00**	**-**							**88.8**	**11.2**	**0.0**

[1]By taking into account the peptide binding in proteins between two amino-acid.

b) Determination of experimental values on pure components

Experimental EDX values obtained after analysis of at least 13 points are presented in table 21. It can be observed that values of carbon are overestimated in comparison with theoretical values. Consequently, the nitrogen and oxygen were underestimation. Nevertheless, this carbon overestimation is well known for XPS technique (Gaiani *et al*., 2006; Kim *et al*., 2002; Rouxhet & Genet, 2011). This is why it is necessary to integrate the experimental values of each pure component in the equation system, thus the error is taken into account in each component as well as in the samples.

Table 21. Theoretical and experimental values for XPS and EDX measures on pure components.

	Theoretical values (%) from table 20			Experimental values for the atomic composition (%)					
				EDX			XPS		
	C	O	N	C	O	N	C	O	N
Lactose	50	50	0	79.2	20.8	0.0	62.7	37.3	0.0
Caseins	65	19	16	76.0	12.8	11.2	69.8	16.3	13.9
Whey proteins	65	19	16	73.3	12.8	13.9	68.0	18.0	14.0
Total milk proteins*	65	19	16	75.5	12.8	11.7	-	-	-
Anhydrous milk fat	89.1	10.9	0.0	93.8	6.2	0.0	87	12.3	0.7

* calculated by taking into account 17% NWI and 83% NMC

Lactose values are particularly far from the theoretical ones, contrary to proteins and anhydrous milk fat. As seen in figure 36, lactose is also the only sample presenting degradation after analysis. It could sugest chamber pollution by carbon or a deviation of the X-ray that cannot be finaly registered by the detector. By performing the analyisis in pure components the error is taken into account.

The experimental values of pure components by XPS and EDX present also some differences. XPS values are closer to theoretical atomic concentrations than EDX. This could be explained by a less precision of the EDX analysis and a biger sensibility of the technique to carbon pollution.

c) Analysis of binary mixtures

To corroborate the prediction of the calculated values by EDX, it was necessary to test mixes wich composition was known, thus compare the obtained results with the real composition. Consequently binary mixtures of lactose and whey proteins were prepared and

dried by freeze draying, then analyzed by EDX in pellet form. As the area of analysis is small (5 µm2), the sample must be homogeneous enough at that scale. The choice of lactose and whey proteins was done for this reason. Both compounds are soluble in water and permit good homogeneous solutions. Figure 38 shows the aspect of the three pellets observed by ESEM. Images are quite similar whatever the composition.

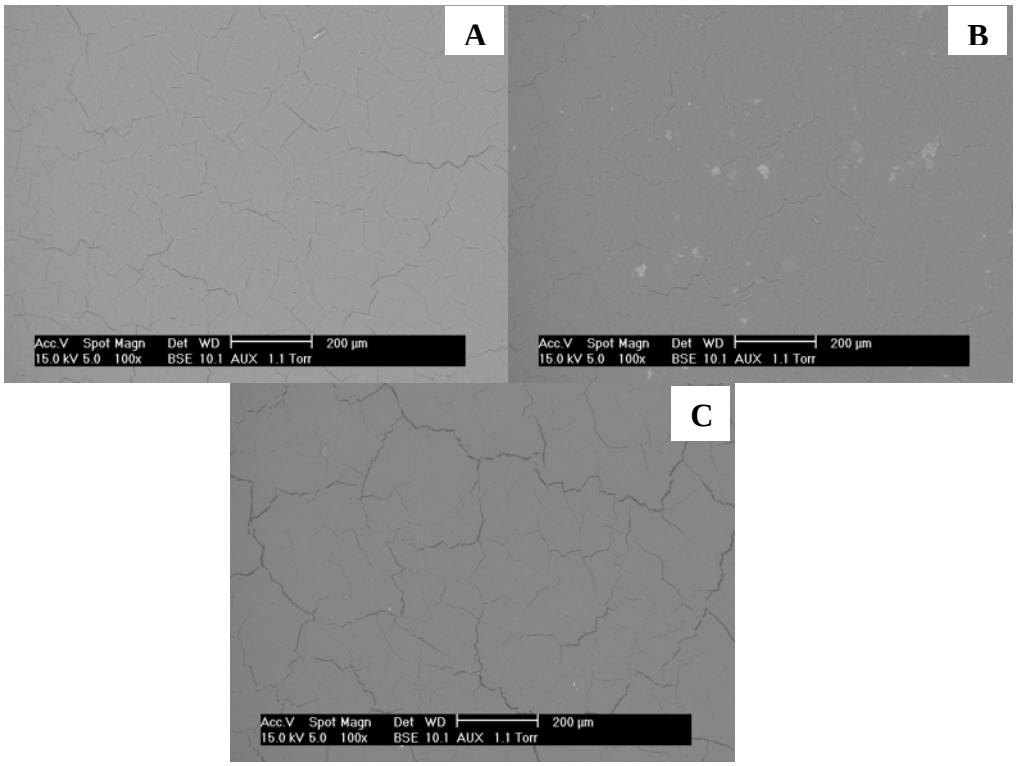

Figure 38. ESEM (x100) of tablets made with binary mixtures of lactose/native whey proteins: 30/70 (A), 50/50 (B) and 70/30 (C).

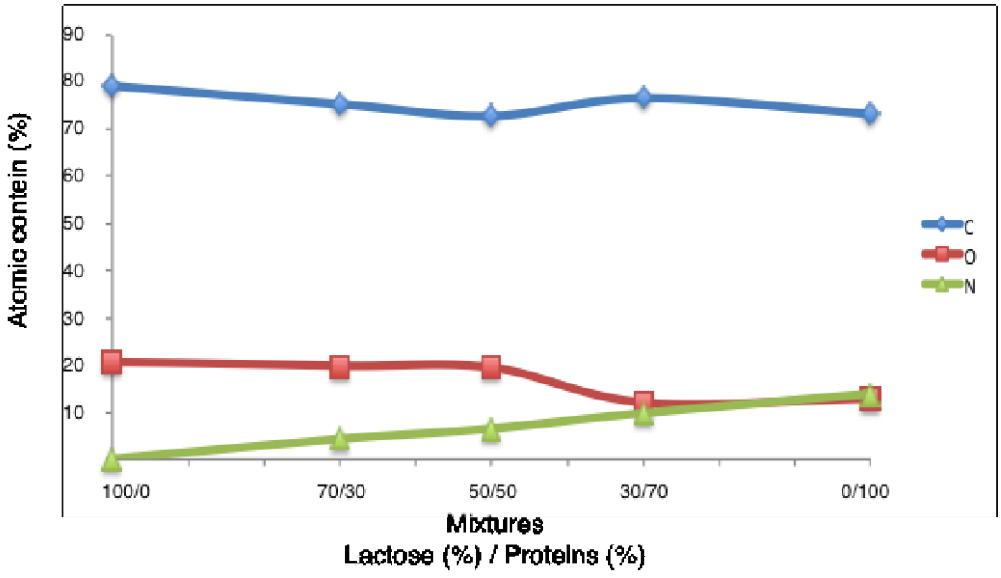

Figure 39. Atomic percentage (in C, O, N) obtained by EDX for variable lactose / whey protein ratio.

The corresponding atomic percentages are presented figure 39. The first point (0/100) and the last point (100/0) are respectively pure lactose and pure NWI. It can be observed that nitrogen values are directly proportional to the protein concentration whereas the values of oxygen and carbon present a more complex behavior.

The molecular composition was obtained from the equations 8, 9 and 10, fed by the atomic percentages (table 22). The three equations system considers three atoms (O, C and N) and three molecules (sugars, protein and lipids). This is the reason why two types of results were presented. If three elements are calculated (lactose, proteins and lipids) by the use of the three equations (presented in the Material and Method part), it can be observed that lactose is systematically underestimated and fat is present (whereas AMF was not added in these mixes). Two explanations are possible for these results. First, the overestimation of fat already observed with the XPS technique, as well as the underestimation of polysaccharide are due to an aerror on the equation system considerations or NWI powder contains residual lipids due to the way of production. These residual lipids may be located at the surface of the tablets increasing fat percentage.

Table 22. Composition of binary mixtures calculated from A% and the equation system.

Equation	Ratio Lactose/Protein	70/30	50/50	30/70
Equations 8, 9 & 10	Lactose	62 ± 6	40 ± 6	13 ± 5
	Protein	34 ± 3	54 ± 2	74 ± 5
	AMF	4 ± 3	6 ± 5	13 ± 3
Equation 8 & 10	Lactose	67 ± 4	46 ± 1	28 ± 5
	Protein	33 ± 4	54 ± 2	74 ± 6

If only equation 8 and 10 are used, as theoretically fat is not present and all the nitrogen present comes from NWI; a correct prediction is done for the 3 mixtures. These results are in agreement with an error in the considerations of the equation systeme.

In order to obtain a better corroboration of the results, three components mixtures, containing also fat need to be produced. However, homogeneous pellets were impossible to

obtain with AMF (data not shown). Indeed, the analysis was performed in a zone containing some parts of lactose/protein matrix and other parts of fat globules.

IV.1.1.5. Application of the technique to the surface and core composition of milk powders.

a) Skim Milk Powder

After validation of the methodology EDX, this technique was used to investigate the surface and core of SMP. In order to do it, the industrial SMP were sieved in five different fractions. The objective of this size classification was to keep a standard deep of analysis. As it was already mentioned, the analysis works in a depth of 1-5 microns approximately. Hence the particle diameter could influence the results of analysis. From the literature is already known the structure of milk particle surface. Firstly the surface is cover by a a thin layer of fat, immediately a skin rich in lactose-protein is found, finally a lactose-protein matrix including some fat globules is observed (Murrieta-Pazos *et al*. 2012a). The thickness of the layers (fat and skin) is unknown. As the layers could have different thickness according to the particle size, a classification by size was pertinent.

An example of the analysis is shown in figure 40 A, the analysis was performed in a skim milk particle at the surface (e and f in red arrows) and the core (a,b,c and d in reed arrows) sieved in a fraction of 125-165 mμ. The results of the analysis are shown in table 23.

An example of particle analysis corresponding to a sieve fraction between 125 and 165 μm is shown in figure 40 A. Two points of analysis were performed at the surface (red arrows e and f) whereas four dots were done on the core (reed arrows a, b, c, d). The atomic percentages are presented in table 23. These results shown differences among the analysis in the same particle, differences seems to come from the point of analysis and not from the surface or the core. This behavior was expected. Indeed milk particles are complex structures, thus the point of analysis could be performed in the lactose-protein matrix. The structure contains more or less concentration of one of the compounds. Traces of lipids may also be present and it may be possible to point out in a fatty area (arrow b). Consequently, a great number of dots within the particle is necessary to obtain an accurate average.

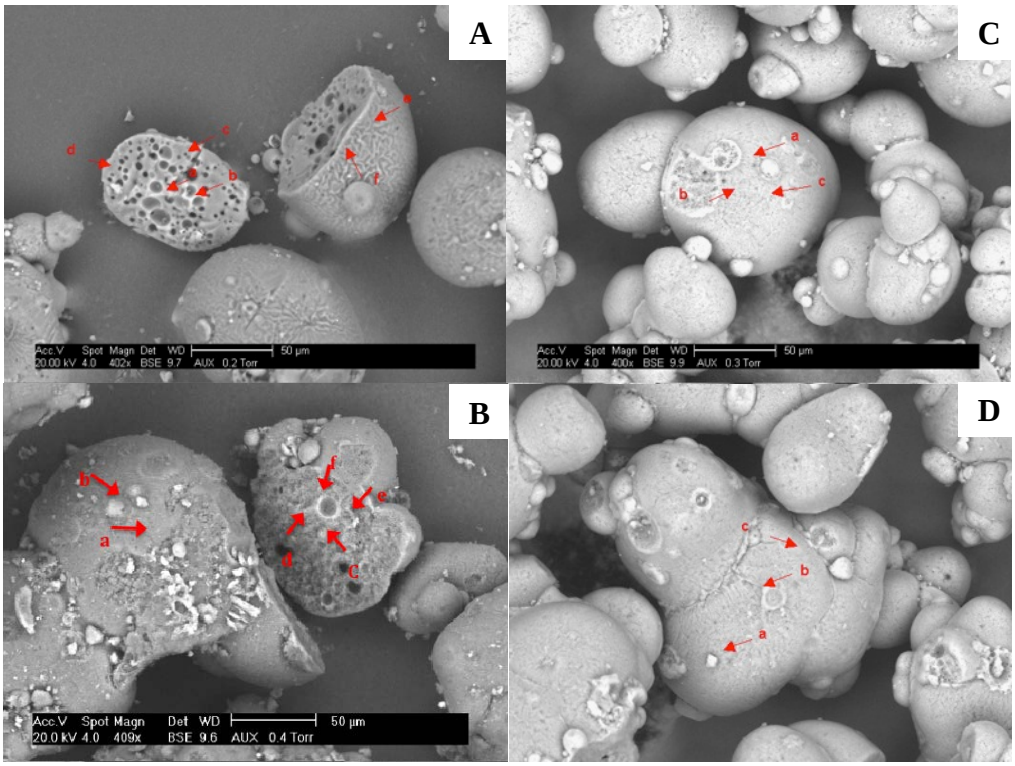

Figure 40. Example of surface and core analysis on variable particles: SMP sieved 125-160 µm (A), WMP sieved at 125-160 µm (B), AFFE sieved at 80-125 µm (C) and AFFE sieved at 125-160 µm (D).

Table 23. Example of raw EDX data obtained for SMP and WMP sieved at 125 – 160 µm.

		SMP						WMP					
		Core				Surface		Core				Surface	
	Point	a	b	c	d	e	f	a	b	c	d	e	f
Atomic percentages	C	73.9	74.6	75.4	69.4	74.8	75.6	76.5	76.5	69.0	70.4	78.3	78.5
	O	13.3	11.5	12.2	16.0	13.8	12.0	14.1	14.2	18.4	18.4	11.9	11.3
	N	7.3	5.3	8.2	8.0	7.6	6.3	5.1	4.6	7.3	4.6	7.0	4.7
	Na	0.6	0.3	0.5	0.3	0.4	0.6	0.3	0.3	0.3	0.1	0.3	0.3
	Mg	0.2	0.1	0.1	0.1	0.1	0.2	0.1	0.2	0.1	0.0	0.1	0.2
	P	1.0	1.7	0.9	1.2	0.8	1.2	0.9	1.0	0.9	0.7	0.6	1.1
	S	0.3	0.6	0.2	0.4	0.2	0.3	0.3	0.4	0.4	0.4	0.2	0.4
	Cl	1.0	1.6	0.7	1.0	0.6	1.0	0.7	0.7	0.8	1.0	0.4	0.8
	K	1.5	2.4	1.0	1.9	0.9	1.6	1.1	1.1	1.5	2.1	0.7	1.5
	Ca	1.0	1.9	0.8	1.7	0.7	1.2	0.9	0.9	1.2	2.2	0.5	1.1
Components percentages	Lac.	23	19	11	39	24	18	36	39	57	68	13	19
	Prot.	62	47	70	68	67	53	43	39	62	39	62	40
	AMF	9	27	14	-13	7	22	16	17	-25	-14	24	35
	Min.	6	9	4	7	4	6	4	5	5	7	3	5

Details of repetition for different sieved fractions are presented in table 24. At least four measures were done at the surface and in the core of the particles. But some clear tendencies

appeared. Differences between surface and core are not significant. For example, lactose is no more present at the core as observed by XPS (Fäldt & Bergenståhl, 1996a; Gaiani *et al*., 2006; Kim *et al*., 2009a). By XPS opposite localization for fat where observed, but these differences are not observed by EDX. Probalby analysis by EDX was much deeper than surface analysis by XPS. So the surface analysis may be very close to the core analysis by EDX. Concerning the effect of particle size, a tendency was observed. Big particles presented more lactose at the surface and small particles presented more fat in the core.

Table 24. Core and surface composition determined by EDX on different size fractions (0-40; 40-80, 80-125 and 125-160 µm) of SMP.

	Surface composition (%)					Core composition (%)				
	1	2	3	4	Average	1	2	3	4	Average
Particle size	0 - 40 µm									
Lactose	30	19	14	18	**20 ± 5**	23	40	23	8	**23 ± 11**
Proteins	75	48	81	70	**68 ± 12**	53	49	45	79	**52 ± 13**
AMF	-9	27	1	7	**-2 ± 7**	19	0	22	11	**13 ± 8**
Minerals	4	6	4	5	**4 ± 1**	6	10	11	2	**8 ± 3**
Particle size	40 – 80 µm									
Lactose	33	37	33	5	**27 ± 12**	5	25	17	11	**24 ± 16**
Proteins	81	53	61	41	**59 ± 14**	71	43	80	49	**62 ± 15**
AMF	-17	6	1	44	**8 ± 26**	23	23	-2	34	**9 ± 19**
Minerals	3	7	3	5	**5 ± 1**	1	9	5	6	**5 ± 3**
Particle size	80 - 125 µm									
Lactose	32	30	24	18	**26 ± 6**	40	19	11	18	**29 ± 12**
Proteins	54	54	65	54	**57 ± 6**	54	45	70	54	**54 ± 8**
AMF	10	10	7	22	**12 ± 7**	2	27	15	22	**12 ± 9**
Minerals	4	6	4	6	**5 ± 1**	4	9	4	5	**6 ± 2**
Particle size	125 - 160 µm									
Lactose	37	44	24	18	**31 ± 19**	23	19	11	39	**27 ± 10**
Proteins	88	53	65	54	**65 ± 16**	62	45	70	68	**59 ± 12**
AMF	-29	-1	7	22	**0 ± 22**	9	27	15	-14	**8 ± 16**
Minerals	4	4	4	6	**4 ± 1**	6	9	4	7	**6 ± 1**

b) Whole Milk Powder

An example of analysis in a particle of WMP sieved at 125-160 mµ is shown in figure 40 B, four dots were performed in the core and two at the surface. Details of atomic percentage and components percentages obtained by the equation system are presented in table 25. From this example results depend on the analysis point selection. As it was observed for SMP, heterogeneity from the distribution of the components on the particle is evident. For example, the quantity of lipids increases in comparison with SMP, probably the method is

sensible to the variation in lipids content. Aberrant values are found, a zone of analysis containing only one or two components could explain these values.

The surface and core composition of the sieved particles are shown in table 25. No differences are observed between the surface and the core. Fat seems to be slightly more present at the surface in comparison with the core in particles over 40 µm. With this technique, the surface analyzed is around 1-5 µm and not 5 nm like for the XPS methods. So, the strong overrepresentation of lipids at the surface of WMP observed by others may be linked to the thickness of fat. Probably nanometric fat layer covers the surface, thin enough to be detected by XPS, contrary to EDX.

Table 25. Core and surface composition determined by EDX on different size fractions (0-40; 40-80, 80-125 and 125-160 µm) of WMP.

	Surface composition (%)							Core composition (%)						
	1	2	3	4	5	6	Average	1	2	3	4	5	6	Average
Particle size	0 - 40 µm													
Lactose	21	30	26	16	15	5	**19 ± 9**	29	28	9	17	11	0	**16 ± 11**
Proteins	29	29	24	33	76	69	**43 ± 23**	23	25	40	45	56	76	**44 ± 20**
AMF	50	39	47	48	8	24	**36 ± 17**	45	44	49	35	30	22	**38 ± 10**
Minerals	3	2	3	3	2	2	**3 ± 1**	3	3	3	3	3	2	**3 ± 0**
Particle size	40-80													
Lactose	42	28	41	30	23	17	**30 ± 10**	28	22	11	18	14	15	**18 ± 6**
Proteins	26	27	25	28	70	45	**37 ± 18**	30	25	71	41	92	66	**54 ± 26**
AMF	29	42	31	40	5	35	**30 ± 13**	39	50	14	37	-7	19	**25 ± 21**
Minerals	3	3	3	3	2	4	**3 ± 1**	3	3	3	4	1	1	**3 ± 1**
Particle size	80-125													
Lactose	36	38	44	42	21	26	**34 ± 3**	33	33	76	25	28	60	**42 ± 12**
Proteins	29	26	27	32	43	47	**34 ± 9**	23	23	39	49	36	47	**36 ± 12**
AMF	32	33	26	23	33	23	**28 ± 5**	41	41	-21	22	31	-11	**17 ± 27**
Minerals	3	4	4	4	4	3	**3 ± 0**	4	4	6	4	6	4	**5 ± 1**
Particle size	125 – 160 µm													
Lactose	60	56	45	47	13	19	**40 ± 20**	46	49	36	39	57	69	**49 ± 12**
Proteins	35	33	27	25	60	40	**37 ± 13**	31	37	44	40	63	39	**42 ± 11**
AMF	1	9	24	24	24	35	**19 ± 12**	19	11	16	17	-25	-15	**4 ± 19**
Minerals	4	3	3	4	3	6	**4 ± 1**	4	4	5	5	6	7	**5 ± 1**

Differences are observed concerning the particle size. Whatever the localization of analysis (surface or core) the fat percentage decreased with the increment in size whereas lactose percentage increased.

c) Analysis of defatted powder

Since the binary mixtures did not validate fat detection, it was necessary to corroborate the sensibility of the analysis on fat. As an alternative, the WMP was treated to change its lipid surface composition. The surface fat was extracted according to the technique developed by Vignolles *et al*. (2007).

Sieved at 80 - 125 µm or 125 - 160 µm, WMP without free fat were analyzed. Measured zones are shown on figure 40 C and figure 40 D. The surface compositions calculated from the atomic percentages are presented in table 26. As expected, the fat content decreased significantly. On the contrary, proteins and lactose increased. This is a very important point to validate the method, even if lipids are generally overestimated the trends between surface and core and the proportion of this element on the particle can be estimated.

Table 26. Surface composition of WMP before and after free fat extraction.

	Before free fat extraction							After free fat extraction						
	1	2	3	4	5	6	Average	1	2	3	4	5	6	Average
Particle size	80-125													
Lactose	36	38	44	42	21	26	**34 ± 3**	46	38	36	41	39	46	**42 ± 4**
Proteins	29	26	27	32	43	47	**34 ± 9**	42	30	39	41	29	41	**37 ± 5**
AMF	32	33	26	23	33	23	**28 ± 5**	8	27	20	15	28	8	**17 ± 8**
Minerals	3	4	4	4	4	3	**3 ± 0**	5	4	4	4	5	5	**4 ± 1**
Particle size	125 – 160 µm													
Lactose	60	56	45	47	13	19	**40 ± 20**	46	38	36	45	46	46	**42 ± 4**
Proteins	35	33	27	25	60	40	**37 ± 13**	36	44	41	39	45	42	**41 ± 6**
AMF	1	9	24	24	24	35	**19 ± 12**	17	9	17	6	6	5	**9 ± 9**
Minerals	4	3	3	4	3	6	**4 ± 1**	4	5	5	3	3	3	**4 ± 1**

d) Interest of the technique for milk powder

Dissimilar results in the core of particles were expected. The core of milk powders presents a complex structure with a lactose-protein matrix and more or less lipid deposits. Nevertheless, it was expected to find more repeatable values at the surface as they are observed in XPS. The principal explanation is that surface measurements by EDX were deeper consequently a similar results is find on measures done in the core (by cutting the particles). Most of the EDX analyses are performed at a theoretical 1-5 µm from surface, this depth is important on a milk particle and depending on the zone analyzed, different results may be obtained. In addition, if the sample is fragile (a lot of lactose) a degradation of the structure may occur adding some noise to the precision of the results.

IV.1.1.6. Interest of coupling XPS and EDX for the determination of milk powder gradient composition

a) Objectives

The methodology presented before permits to characterize the surface and the core of milk powders by EDX. But these results can be enriched by another technique: XPS. Figure 41 summarizes the principal differences and complementarities between these two techniques. Since the deeper and area of analysis are different, coupling of both techniques allows the study of the powder gradients.

Table 25 detailed the atomic and component percentages for WMP and SMP. The surface was determined by XPS (5-10 nm) and EDX (1-5 µm). The core was determined only by EDX by cutting one particle. In order to obtain more information, results for WMP without free fat were also added (surface by XPS and EDX; core).

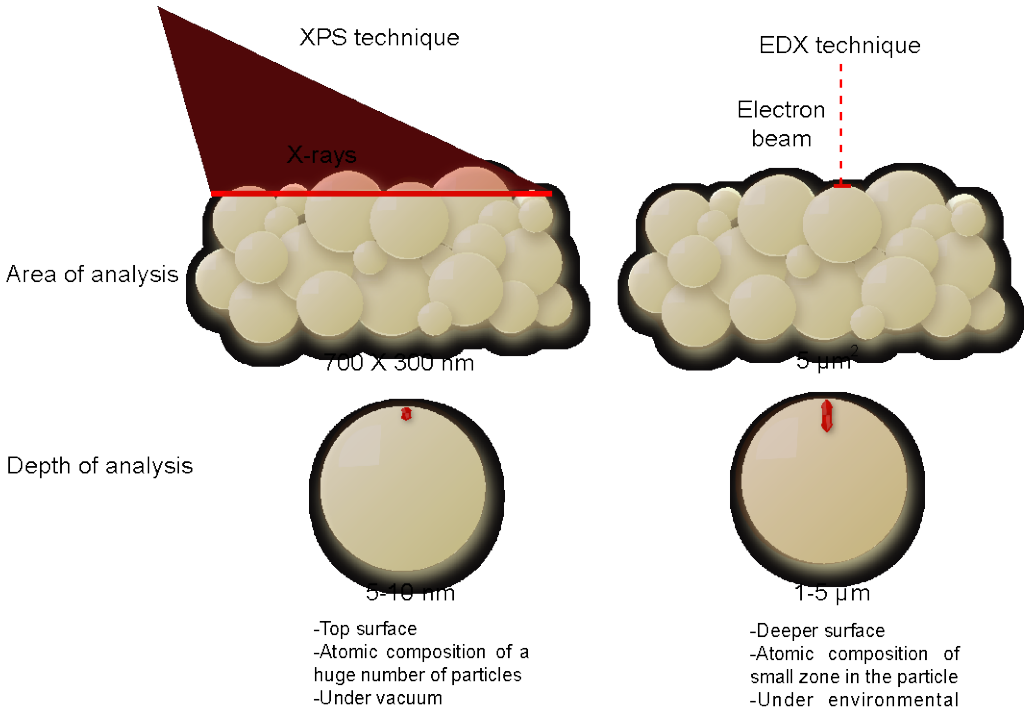

Figure 41. Main differences between XPS and EDX techniques.

To obtain the values of EDX, an average was done with all the analysis (mean for different particles and different sieves). For XPS, these results are the mean of three independent experiments.

b) Gradients for skim milk powders

By observing the atomic percentages (table 27), it can be remarked the mineral gradient. A significant increase of mineral percentage is observed from the surface (XPS), to the narrow surface (EDX) and finally the core (EDX cut particle).

c) Gradients for whole milk powders

Again a clear trend appears for minerals in WMP (table 27). At the surface (XPS), minerals are not detected. At the narrow surface (EDX), several minerals appeared. After free fat removing analyzed by XPS, few minerals, only K, Ca, are present. After free fat extraction and EDX analysis all minerals appear in a higher quantity. This distribution corresponds with the abundance of molecules containing these minerals. For example, potassium and calcium are related to the caseinats, the most abundant molecules containing minerals, thus they are detected first. The surface (XPS) is totally covered by lipids. At the narrow surface (EDX), less fat (29 %) and more lactose (36 %) and proteins (32 %) appeared. In the core by EDX (after cutting the particle), the same percentages were mostly observed.

The free fat extraction completed the information about the validity of the technique. The surface by XPS of the defatted particle was different in comparison with the raw particle. As expected, less fat, more lactose and proteins were observed. By EDX (narrow surface), the tendency is the same but the percentages are closer to the core composition with less fat.

Table 27. Gradients in WMP and SMP by coupling XPS (surface depth around 5 nm), EDX on raw particles (surface depth around 1 μm) and EDX on cut particles (core).

		Whole Milk Powder					Skim Milk Powder		
		Before Free Fat Extraction		After Free Fat Extraction			Raw powder		
		Surface				Core	Surface		Core
		XPS (10 nm)	EDX (1 μm)	XPS (10 nm)	EDX* (1 μm)	EDX (1 μm)	XPS (10 nm)	EDX (1 μm)	EDX (1 μm)
Atomic concentration (%)	C	87.4 ± 1.8	79.6 ± 1.9	77.1 ± 1.1	77.1 ± 1.70	78.8 ± 4.2	65.1 ± 0.5	73.6 ± 2.3	73.7 ± 2.6
	O	11.6 ± 1.2	13.0 ± 1.5	19.9 ± 0.6	14.5 ± 0.8	13.5 ± 2.7	26.5 ± 0.3	13.9 ±2.0	13.6 ±1.7
	N	1.0 ± 0.6	4.4 ± 1.9	2.9 ± 0.2	4.3 ± 0.6	5.2 ± 2.1	7.2 ± 0.1	7.7 ± 2.3	6.6 ± 1.4
	K	-	0.8 ± 0.1	0.2 ± 0.0	1.0 ± 0.2	1.0 ± 0.5	0.5 ± 0.4	1.3 ± 0.6	1.6 ±0.8
	Ca	-	0.6 ± 0.0	0.1 ± 0.0	0.8 ± 0.2	0.8 ± 0.5	0.2 ± 0.0	1.0 ± 0.5	1.3 ±0.7
	Cl	-	0.5 ± 0.2	-	0.7 ± 0.1	0.6 ± 0.2	0.2 ± 0.2	0.8 ± 0.4	1.0 ±0.5
	S	-	0.2 ± 0.1	-	0.3 ± 0.0	0.3 ± 0.1	0.1 ± 0.0	0.4 ± 0.2	0.4 ±0.2
	P	-	0.6 ± 0.2	-	0.9 ± 0.1	0.6 ± 0.2	0.1 ± 0.0	1.2 ± 0.5	1.0 ±0.5
	Na	-	0.3 ± 0.2	-	0.3 ± 0.0	0.3 ± 0.1	-	0.5 ± 0.1	0.4 ±0.1
	Mg	-	0.1 ± 0.0	-	0.3 ± 0.4	0.1 ± 0.1	-	0.2 ± 0.0	0.2 ±0.1
Component composition (%)	Lactose	-3.2 ± 2.5	30.8 ± 14.3	24.7 ± 1.0	41.7 ± 3.8	31.3 ± 19.7	42.2 ± 1.1	26.0 ± 10.1	27.5 ± 12.5
	Proteins	2.2 ± 2.7	37.8 ± 15.8	18.8 ± 1.5	37.2 ± 4.7	44.2 ± 18.2	54.0 ± 1.5	62.3 ± 16.7	56.8 ± 12.1
	AMF	101.0 ± 1.7	28.4 ± 13.2	56.4 ± 0.7	17.5 ± 7.9	19.9 ± 22.5	2.66 ± 0.8	6.8 ± 17.3	9.6 ± 13.9
	Minerals	-	3.2 ± 0.7	0.3 ± 0.0	4.3 ± 0.6	3.6 ± 1.4	1.1 ± 0.7	5.0 ± 1.8	6.1 ± 2.5

* Performed in milk particles sieved at 80-125 μm.

d) The performance of ESEM-EDX as a surface characterization method

The ESEM-EDX technique is a good choice to study the structure of milk powders and images are easily obtained (without vacuum and labeling). In addition, it is possible to focalize the analysis on a zone of interest thanks to the microscope. Coupling the EDX and XPS technique seems to be also very interesting and promising for SMP and WMP. More powders will be analyzed in the future to see if it is possible to generalize the technique to other dairy powders. Information on the surface gradients was obtained and the repartition was coherent with expected results and literature.

EDX technique presents some problems of repeatability. But these problems are inherent to the technique since the zones analyzed are very small. Consequently, depending on the localization of the analysis zone very different results may appear. However, it is possible to minimize this repeatability by analyzing a great number of particles at different locations.

The C, O and N elements were more informative when they were inserted in the equation system. The lactose gradient is also evident with a decrease from the surface (42 %) to the narrow surface (28 %) and the core (27%). Fat was more important in the core in comparison with the surface and no real tendency was observed for proteins.

IV.1.2. GRADIENT COMPOSITION IN *WHEAT DURUM* SEMOLINA AND COUSCOUS BY COUPLING EDX AND XPS ANALYSIS

The surface composition of wheat powder is a domain of interest, it permits to characterize the reactivity of the powder. Nevertheless very few techniques are available in literature. Moreover the only technique available was proposed by Saad *et al*. (2011a).

The author adapted the technique proposed by Fäldt, (1995), this technique deduced molecular surface composition from atomic composition using an equation system. The atomic composition was determined by XPS in diary powders.

Saad *et al*. (2011a) used wheat pure components (starch, gluten and extracted oil) analyzed by XPS, the atomic concentrations of pure components fed the equation system, then wheat flours and semolina surface composition could be characterized.
In this section of the work, EDX is proposed to determine the atomic composition instead of XPS. Then pure components were analyzed by EDX in order to feed equation system and

deduce surface composition of sieved semolina. The results were coupled to XPS analyisis in order to obtain gradient composition information on different depths of the surface, 10 nm in the case of XPS and 1 μm in the case of EDX.

IV.1.2.1. Characterization of pure components by ESEM

In figure 42, pictures obtained by ESEM show the aspect of pure components making up the semolina structure.

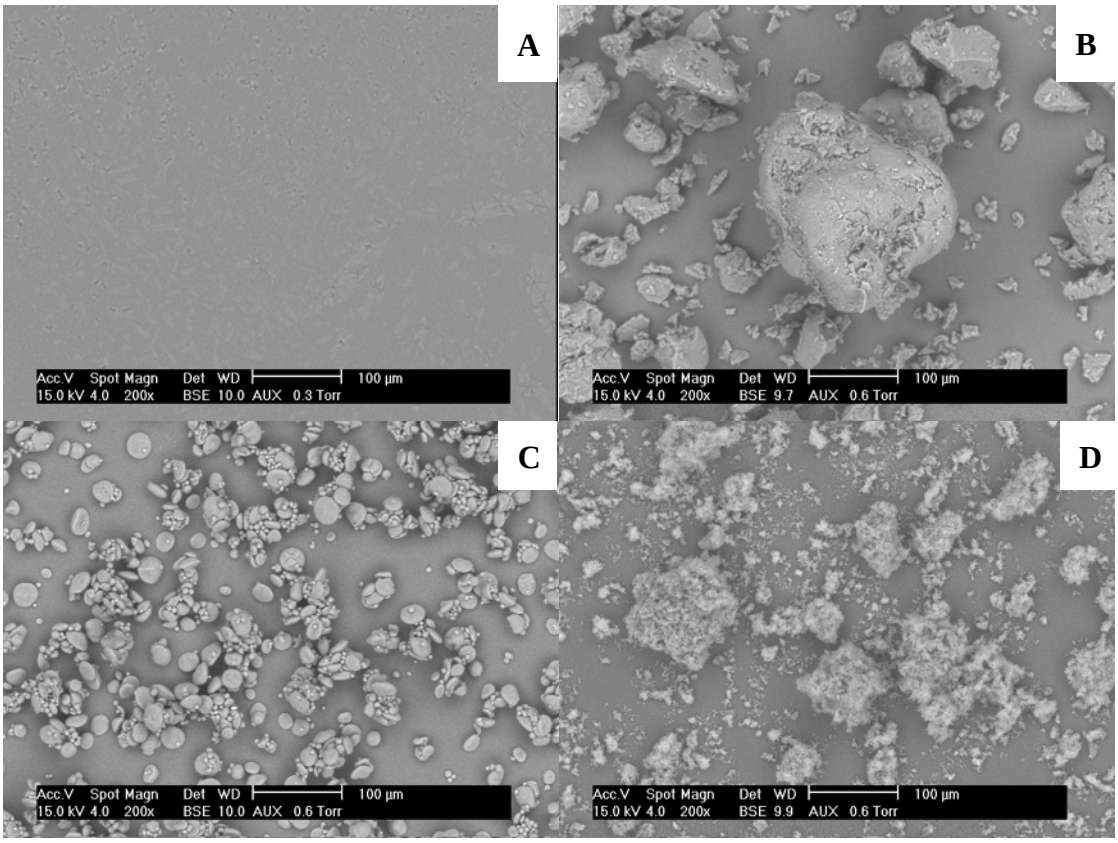

Figure 42. Scanning electron micrographs of the reference semolina particules (pure components) at 200X: Extracted oil (A), Gluten (B), Starch (C), Arabinoxylan (D).

The extracted oil (figure 42 A), is liquid at room temperature. Inside the microscope chamber the temperature was fixed near to 5ºC, then the oil got solid. Gluten particles (figure 42 B) present several sizes and shapes. The structure is different from the original on semolina particles (protein matrix). It was probably modified after the extraction process, however, compositions is considered the same. In the picture (figure 42 C) two populations of particles can be appreciated. One group of small and spherical grains mixed with other group of big round and flat grains. The starch grains conserve the same structure after extraction from semolina. Consequently the same two populations of starch grains can be found in semolina particles. Besides some damage starch can be observed as a result of milling process. Finally Arabinoxylane (figure 42 D), have an structure really fine, light and fragile,

this fragility permits the pass of the beam throughout the sample, consequently the reproducibility of EDX analysis is not good. Several points (20) were measured to obtain a correct value.

IV.1.2.2. Energy-Dispersive X-ray Spectroscopy

a) Pure components

In a first step pure components were analyzed by EDX. EDX analysis is dependent on X-ray detector position on the microscope chamber, in an ideal analysis the sample should be plate and smooth, the elaboration of a tablet is recommended, however the interest of the present work is study particles in their raw state. Consequently EDX analysis was then performed directly in the particles, but not always was possible to perform several analyses in the same particle, the quantity of x-ray detected by the detector depended on the particle shape. Indeed the average for particle was 2 point of analysis.

Gluten

In the picture (figure 43 A,B) an example of analysis in a gluten particle is presented, the average of different analysis on gluten particles is shown in table 28. The picture with red arrows (figure 43 A) corresponds to the selected point of analysis marked with a later (a, b or c). The analyses are then represented with the same letters in the table. The figure 4 B represents the pictures of the particle after EDX analysis. The same procedure was done for all the pure components analyzed.

The gluten spectra show repeatable values of the analysis. Carbon, oxygen and nitrogen are present as well as some minerals (sodium, phosphorus, sulfur and chlorine). Carbon and oxygen are present in all the organic molecules whereas nitrogen is directly related to proteins. Hydrogen is not detected by X-ray techniques, so it cannot be detected in the spectra of EDX. Finally minerals are very often present and associated to protein molecules.

The structure of the gluten after analysis figure 43 B seems not to be affected by the electron beam. It means that the structure of gluten is not fragile. This property turns easier the analysis and also allows several analyses on one particle.

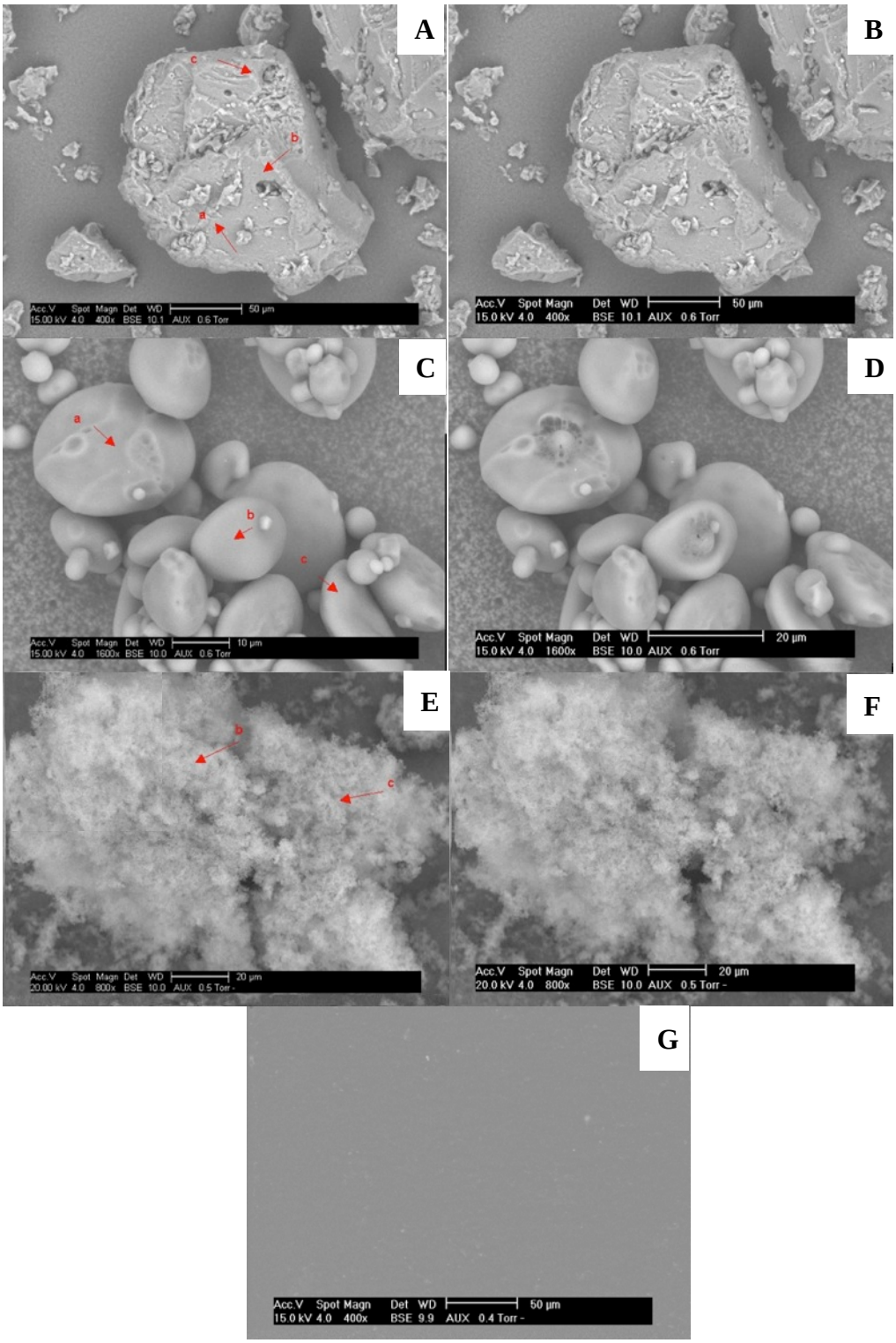

Figure 43. Example of EDX analysis pointing in a gluten particle.

Starch

In the figure 43-C,D, it can be appreciated the analysis performed in starch particles, in this case the size of the particles do not allow the performance of several analysis. Moreover, the electron beam degrades their structure figure 43-D. It turns difficult a second analysis in the same particle. This is a typical degradation observed in carbohydrate particles after EDX analysis, probably due to the fragility of carbohydrates molecules.

Table 28. EDX analysis in the pure components particles

	Gluten			Starch			Arabinoxylan		Extracted wheat oil		
Point	a	b	c	a	b	c	b	c	A	b	c
C	73.35	73.77	71.74	83.39	83.85	83.05	74.14	76.05	94.32	94.46	93.07
O	11.07	11.65	12.63	16.61	16.15	16.95	25.42	23.5	5.29	5.07	5.76
N	14.82	13.85	14.9	-	-	-	0.19	0.17	-	-	-
Na	0.12	0.15	0.13	-	-	-	0.14	0.15	-	-	-
P	0.09	0.07	0.07	-	-	-	0.11	0.12	-	-	-
S	0.39	0.4	0.34	-	-	-	-	-	-	-	-
Cl	0.17	0.11	0.18	-	-	-	-	-	-	-	-
Si	-	-	-	-	-	-	-	-	0.39	0.47	1.17

In table 28 are shown the results of the EDX analysis of starch. In this case, the spectra analysis detects only two elements, carbon and oxygen because it is a carbohydrate molecule, principally formed by carbon and oxygen. An interesting point is the performance of the technique to detect only the elements expected, results are repeatable even in different particles.

Arabinoxylan

The analyses points in arabinoxylan are presented in figure 43 E,F, even if arabinoxylans are sugar molecules as well as starch, the analysis (table 28) detected also some minerals, probably due to deficiencies in the extraction process arabinoxylan. After the analysis it can be observed the degradation of the arabinoxylan (figure 43 E,F), it was completely expected because of the fragile structure formed by these molecules, very crumbly and porous. The repeatability of the analysis was affected because of the fragility of the particles, consequently a high number of analysis were done in arabinoxylan.

Extracted Wheat Oil

Picture of the solid oil layer is shown in figure 43 G. The results of analysis are presented in table 28, three elements were detected, oxygen carbon and silica. The carbon and oxygen

are molecules also found in lipids, the difference between carbohydrates is due to the proportion of carbon and oxygen in the molecules. The other element detected is silica, it must be analyzed on the support of the sample, it means that the analysis can pass trough the sample. Hence the depth of analysis may depend on the sample structure, fragile samples will allow the pass of the beam electrons throughout them and shift a more profound depth. In the case of milk powder and semolina the beam does not penetrate until the support because of the solid state of the sample and the size of the particles. The heterogeneity of the oil permitted a good repeatability of the analysis.

Atomic concentration of pure components: theoretical and experimental values

Table 29 shows atomic theoretical values calculated from the lipid, sugar and protein molecules. Concentration in semolina powders was determined by Beleggia *et al*. (2009). From (table 29) it can be observed that atomic percentages are similar among molecules of the same group, it means for sugars, amino acids, or fatty acids. Amino acids are the molecules with more variation. It could be due to the interaction of 3 elements (C, O and N), in contrast with the homogeneous values in sugars and lipid that contain only 2 elements (C and O). The hydrogen is not taken into account in the theoretical atomic percentage calculation. As it has been explained X-ray technique cannot detect the hydrogen, consequently the theoretical calculation was done in the same conditions to compare both results.

Average of at least 13 analyses are presented in table 30. Comparing table 29 and table 30. It can be observed that carbon is overestimated, a consequent underestimation of the nitrogen and/or oxygen was registered. Experimental atomic percentage (table 30) presents an error in detection of carbon. It is known that carbon is usually overestimated in X-ray analysis, in the case of EDX this error could overestimate the carbon by 60% of its value. Because of that, experimental values obtained from pure components are necessary, the error can then be considered in the calculation of the surface composition.

The O/C ratio was calculated for experimental values, the influence of the overestimation in carbon is reflected in the differences between theoretical (table 29) and experimental (table 30) O/C ratio. The average of theoretical O/C ratio was 0.90, 0.20 and 0.11 for sugars, amino acids and fatty acids respectively whereas the values obtained for theirs experimental homologous, carbohydrates, gluten and extracted oil are 0.20, 0.15 and 0.06, even if the

experimental values have been clearly affected by the overestimation of carbon, it is still possible to remark differences among the molecules by compering their O/C ratios. The atomic percentage values were corrected to obtain 100% in composition when carbon, oxygen and nitrogen are summarized. This correction was done because the equations system considers only 3 principal components in the molecules (C, O and N), consequently minerals are not counted in the total of atomic percentage.

Other correction in experimental values was made for carbohydrates. The equation system also considers that only three molecules are contained in the semolina: carbohydrates, proteins and lipids, thus, the value of carbohydrates was calculated with a combination of starch and arabinoxylan. Arabinoxylans are sugars present in the cellular walls, mostly concentrated in the endosperm. These sugars represent the ~5 % of the dry weight in semolina. Starch is the other carbohydrate present in semolina, it is the principal component of the powder, with a concentration of ~70 % of dry weight in semolina (Sissons, 2008). These concentrations correspond to 6.7 and 93.3 % of carbohydrates for arabinoxylan and starch respectively. Finally the carbohydrate value was calculated with these proportions.

The experimental corrected values (table 30) of carbohydrates, gluten and extracted oil, will feed the equation system in order to determine the molecular surface composition from EDX analysis performed in semolina particles.

Table 29. Theoretical values of atomic percentage contained in protein, sugar and lipids of semolina.

	µg/g SEM**	Total (%)	Formula	Atom Number			Atom %			Total %			
				C	O	N	C	O	N	C	O	N	O/C
							Sugars						
Raffinose	36.9	73.4	$C_{18}H_{32}O_{16}$	18	16	0	52.9	47.1	0.0	38.8	34.6	38.8	0.89
Maltose	10.8	21.5	$C_{12}H_{22}O_{11}$	12	11	0	52.2	47.8	0.0	11.2	10.3	11.2	0.92
Fructose	1.0	1.9	$C_6H_{12}O_6$	6	6	0	50.0	50.0	0.0	1.0	1.0	1.0	1.00
Glucose	0.8	1.6	$C_6H_{12}O_6$	6	6	0	50.0	50.0	0.0	0.8	0.8	0.8	1.00
Sucrose	0.5	1.1	$C_{12}H_{22}O_{11}$	12	11	0	52.2	47.8	0.0	0.6	0.5	0.6	0.92
Arabinose	0.3	0.5	$C_5H_{10}O_5$	5	5	0	50.0	50.0	0.0	0.3	0.3	0.3	1.00
Sugars total	**50.2**	**100.0**	-							**52.6**	**47.4**	**52.6**	**0.90**
							Amino acids						
Leucine	424.1	69.3	$C_6H_{13}NO_2$	6	1*	1	75.0	12.5	12.5	52.0	8.7	8.7	0.17
Arginine	54.6	8.9	$C_6H_{14}N_4O_2$	6	1*	4	54.5	9.1	36.4	4.9	0.8	3.2	0.17
Gamma-Aminobutyric acid	51.9	8.5	$C_4H_9NO_2$	4	1*	1	66.7	16.7	16.7	5.7	1.4	1.4	0.25
Threonine	17.7	2.9	$C_4H_9NO_3$	4	2*	1	57.1	28.6	14.3	1.7	0.8	0.4	0.50
Isoleucine	14.7	2.4	$C_6H_{13}NO_2$	6	1*	1	75.0	12.5	12.5	1.8	0.3	0.3	0.17
Serine	14.1	2.3	$C_3H_7NO_3$	3	2*	1	50.0	33.3	16.7	1.2	0.8	0.4	0.67
Proline	13.3	2.2	$C_5H_9NO_2$	5	1*	1	71.4	14.3	14.3	1.6	0.3	0.3	0.20
Homoserine	5.6	0.9	$C_4H_9NO_3$	4	2*	1	57.1	28.6	14.3	0.5	0.3	0.1	0.50
Alanine	4.6	0.7	$C_3H_7NO_2$	3	1*	1	60.0	20.0	20.0	0.4	0.1	0.1	0.33
Aspartic acid	4.0	0.7	$C_4H_7NO_4$	4	3*	1	50.0	37.5	12.5	0.4	0.3	0.1	0.75
beta-alanine	3.9	0.6	$C_3H_7NO_2$	3	1*	1	60.0	20.0	20.0	0.4	0.1	0.1	0.33
Glycine	2.8	0.5	$C_2H_5NO_2$	2	1*	1	50.0	25.0	25.0	0.3	0.1	0.1	0.50
Valine	0.9	0.2	$C_5H_{11}NO_2$	5	1*	1	71.4	14.3	14.3	0.1	0.0	0.0	0.20
Amino acids total	**612.1**	**100.0**	-							**70.7**	**14.0**	**15.4**	**0.20**

	µg/g SE*	Total (%)	Formula	Atomic number			Atomic %						
				C	O	N	C	O	N				O/C
								Fatty acids					
Linoleic acid	4,281.5	45.1	$C_{18}H_{32}O_2$	18	2	0	90.0	10.0	0.0	40.6	4.5	0.0	0.11
Palmitic acid	2,527.4	26.6	$C_{16}H_{32}O_2$	16	2	0	88.9	11.1	0.0	23.6	3.0	0.0	0.12
Oleic acid	1,029.3	10.8	$C_{18}H_{34}O_2$	18	2	0	90.0	10.0	0.0	9.7	1.1	0.0	0.11
Elaidic acid	847.1	8.9	$C_{18}H_{34}O_2$	18	2	0	90.0	10.0	0.0	8.0	0.9	0.0	0.11
Linolenic acid	378.8	4.0	$C_{18}H_{30}O_2$	18	2	0	90.0	10.0	0.0	3.6	0.4	0.0	0.11
Stearic acid	289.7	3.1	$C_{18}H_{36}O_2$	18	2	0	90.0	10.0	0.0	2.8	0.3	0.0	0.11
Behenic acid	68.2	0.7	$C_{22}H_{44}O_2$	22	2	0	91.7	8.3	0.0	0.6	0.1	0.0	0.09
Tetracosanoic acid	39.2	0.4	$C_{24}H_{48}O_2$	24	2	0	92.3	7.7	0.0	0.4	0.0	0.0	0.08
Palmitoleic acid	16.9	0.2	$C_{16}H_{30}O_2$	16	2	0	88.9	11.1	0.0	0.2	0.0	0.0	0.12
Myristic acid	16.5	0.2	$C_{14}H_{28}O_2$	14	2	0	87.5	12.5	0.0	0.2	0.0	0.0	0.14
Fatty acids total	**9,494.5**	**100.0**	**-**							**89.7**	**10.3**	**0.0**	**0.11**

** SE = Semolina.

* One oxygen is lost in the peptide bond.

Table 30. Experimental atomic concentration by EDX in pure components.

	Atomic %				Corrected values		
	C	O	N	O/C	C	O	N
Starch	83.6 ± 2.4	16.1 ± 2.7	0.0 ± 0.0	0.19	83.8	16.2	0.0
Arabinoxylan	78.4 ± 3.3	20.4 ± 3.2	0.0 ± 0.0	0.26	79.3	20.7	0.0
Carbohydrates*	-	-	-	0.20	83.5	16.5	0.0
Extracted oil	94.00 ± 0.7	5.5 ± 0.5	0.0 ± 0.0	0.06	94.5	5.5	0.0
Gluten	75.8 ± 3.25	11.0 ± 1.2	12.3 ± 2.4	0.15	76.4	11.1	12.4

*Carbohydrates = Starch (93.3%) + Arabinoxylan (6.7%)

b) EDX analysis and surface composition semolina

After analysis of pure, it was obtained the atomic concentration of carbohydrates, proteins and extracted lipids. Later it was possible to calculate the surface composition from analyses performed on semolina. The analyses were done at the surface and the core of cut particles, the center of the particles was found with the help of the ESEM.

Results of each particle are discussed next. In the first particle (figure 44) the points of EDX analysis before (figure 44 A) and after analysis (figure 44 B) are presented.

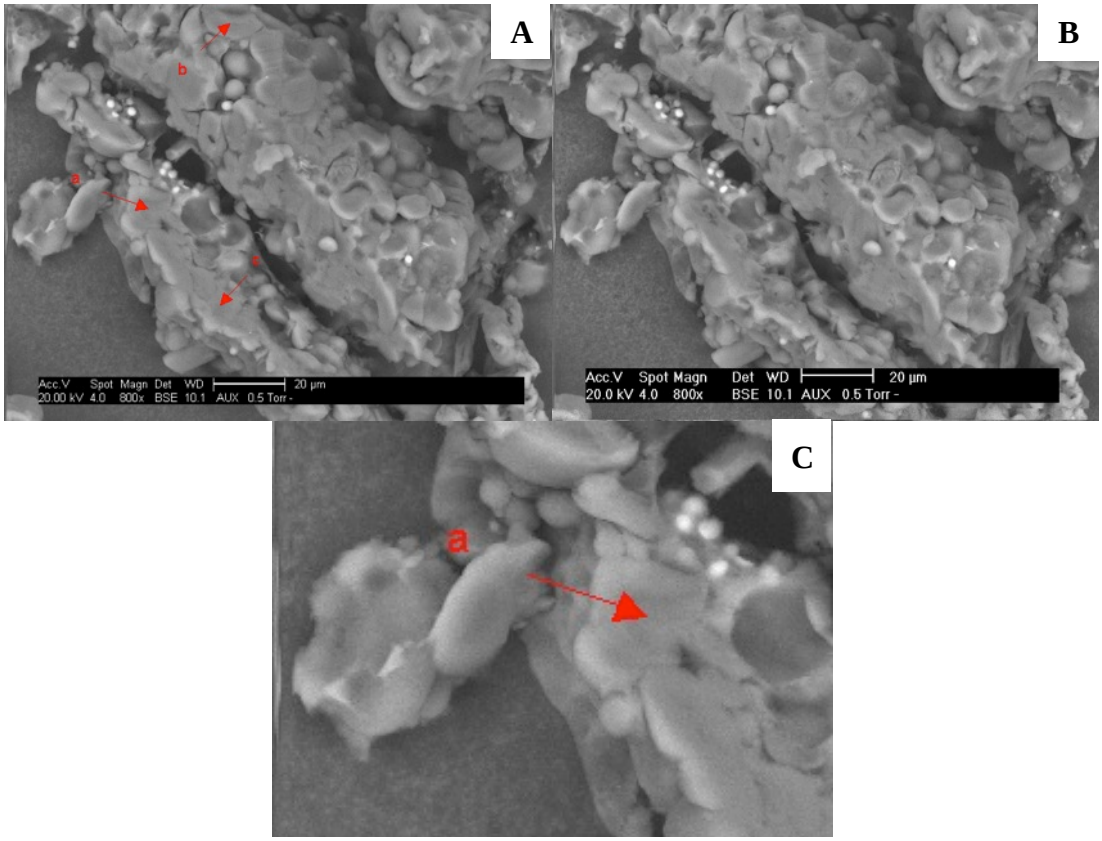

Figure 44. EDX analysis in a semolina particle analyzed at the surface and at the core.

The results of analysis are presented in table 31. The structure of the semolina does not seem to be damaged after analysis. Observing the atomic concentration in table 31, the first point to remark is that nitrogen is missing on the analysis, nitrogen is related only to protein molecules, by consequence this non-detection of nitrogen can be related to the absence of proteins at the surface, however theoretically, gluten that is a protein, is present in the whole particle and it is expected to be at the surface. In fact this three analysis were probably performed in a broken starch, even when the analysis points were selected by randomize, a coincidence happened, all the points were performed in broken starch grains. As it was

explained in the chapter of materials and methods in figure 12, the semolina particles present broken starches due to the strong gluten-starch bond, consequently the milling process breaks the starch grain before the gluten-starch bond (Delcour & Hoseney, 2010). Indeed if we zoom one of the analysis point (figure 44 C), the broken starch grain can be appreciated.

The broken starch granules are not easy to identify performing a simple view at the ESEM, it is necessary to observe very carefully to distinguish broken starches from protein matrix.

In complement the O/C ratio presents values around 0.22, this value is near to the pure starch O/C ratio, it confirms that the analysis was performed in a starch grain. Some minerals were found indicating some traces of minerals, proteins or arabinoxylans.

Table 31. Surface and core EDX analysis and molecular composition in semolina particle

	Point a	Point b	Point c
Element	Atomic %		
C	81.3	80.4	82.5
O	17.5	19.2	17.1
N	0.0	0.0	0.0
P	0.4	0.0	0.1
S	0.2	0.2	0.1
K	0.7	0.2	0.2
O/C	0.22	0.24	0.21
Molecule		%	
Carbohydrats	127.6	124.8	105.7
Proteins	0.0	0.0	0.0
Lipides	-29.6	-25.2	-6.1

Finally the surface composition was obtained by solution of the equation system (equation 8, 9 and 10) and is presented in table 31. Results present aberrant values, calculus gives more than 100% of the concentration for carbohydrates and negative values for lipids. To explain this results it is postulated that the equation matrix result in aberrant values when the conditions of the mathematical model are not accomplishment. One possibility is that principal components are not starch and/or arabinoxylan, lipids and gluten. Other possibility is that summarize of the three components concentration is not linear. However it is possible to have an idea of the principal components at the surface even if these results are not quantitative.

In the particle shown in figure 45, different atomic concentrations are obtained in each point of analysis (table 32). Carbon concentration in point a is less important than point b whereas oxygen and nitrogen are more important in point a than b, more minerals are found in point a. In the zoomed picture after analysis (figure 45 b), both point of analysis seam really similar. It is difficult to distinguish if the analysis was performed in a broken starch grain or in the gluten-starch matrix. According to the atomic concentration, the point b is an analysis performed in the gluten-starch matrix because nitrogen is found. In the case of point b, the analysis seems to indicate that the analysis was done in a broken grain, because no nitrogen was found, thus protein was not detected. The O/C ratio also presents differences in the both analysis. The higher value of the point could be due to an area conformed by molecules other than gluten, starch, arabinoxylan and/or lipids. The O/C ratio of point b correspond to those obtained for starch in pure components (table 30).

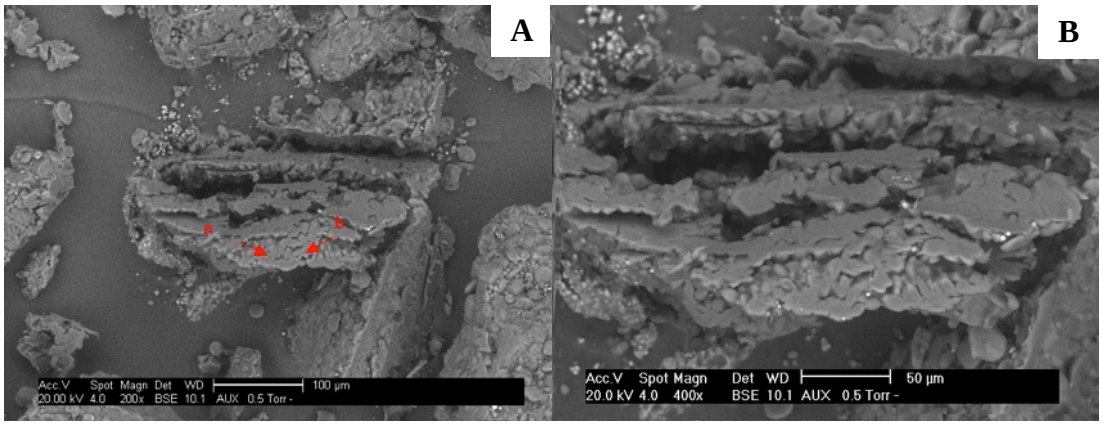

Figure 45. EDX analysis in a semolina particle analyzed at the core.

Table 32. Core EDX analysis and molecular composition in semolina particle

	Point a	Point b
Element	Atomic %	
C	71.2	82.0
O	22.9	17.6
N	5.5	0.0
P	0.3	0.1
S	0.4	0.1
K	0.3	0.1
O/C	0.32	0.21
Molecule	%	
Carbohydrates	108.1	88.1
Proteins	44.6	0.0
Lipids	-52.0	11.7

The molecular surface composition deduced from equation system (table 32), presents aberrant values for the point a, but coherent values for the point b. It seems consistent that concentration of the three components (C, O and N) is not made in a linear relation. Consequently the calculation of the surface composition is not correctly deduced. Nevertheless in some cases, it seems that the equation is capable to calculate coherent values, probably in these points of analysis the component concentration presented a linear interaction, this is the case of the point b. From the last result, a high quantity of carbohydrates and some lipids are found, this analysis seam in agreement with bulk composition in the proportion of carbohydrates and lipids contain (humidity 12, carbohydrates 73, proteins 12, lipids 2 and ashes 1 %).

The analyses in third particle are shown in figure 46. The first analysis was performed in the point b that looked like a starch grain, in this case the starch grain was not broken, it came from the gluten matrix entirely. The point c was selected because it looked like protein matrix.

In the picture after analysis (figure 46), it can be observed that point b presents a degradation of the structure as it was observed in pure starch. Point c analysis didn't affect the structure of the surface. It could confirm that point b analysis was performed in a starch grain.

Table 33 shown the result of the analysis points. In this case nitrogen is found in both analysis, it means that protein is present in both points, however a difference in the carbon and oxygen as well as the O/C ratio is observed. The point b presents a high value of O/C ratio. Again, it can be explained by the presence of other molecules than gluten, starch, arabinoxylan or lipids. In the point c the O/C ratio is more proximate of pure component values. When the molecular formulation is resolved, aberrant values are obtained for the point b whereas coherent values are observed for the point c. The values of point a are not coherent for carbohydrates and lipids, but proteins seams correct, the aberrant values are more often found in carbohydrate-lipid distribution.

Even when a starch grain was pointed, some proteins were present, an explanation is that probably starch grain was not broken, thus it was came out from the protein matrix, consequently some residues of protein could stay at the surface of this starch grain. The values of the point c present a distribution of the components in agreement with the bulk composition, it appears that it was effectively pointed the starch-gluten matrix.

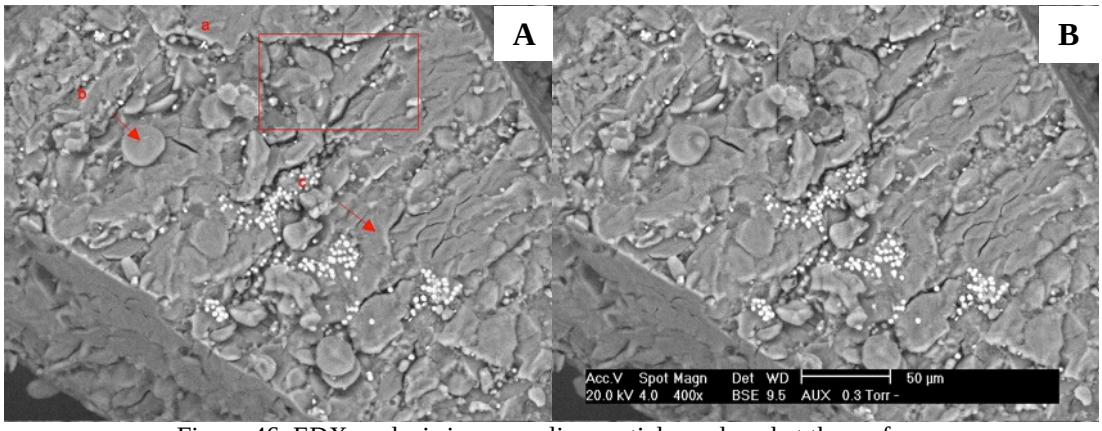

Figure 46. EDX analysis in a semolina particle analyzed at the surface

Table 33. Core EDX analysis and molecular composition in semolina particle

	Point b	Point c
Element	Atomic %	
C	73.2	78.6
O	23.2	18.3
N	2.8	2.8
P	0.3	0.1
S	0.1	0.1
K	0.4	0.1
O/C	0.32	0.23
Molecule	%	
Carbohydrats	119.75	83.92
Proteins	22.73	22.73
Lipids	-43.21	6.72

This results support the claim that aberrant values are probably related to a more complex composition than gluten, starch, arabinoxylan and lipids keeping a linear relation. It seems that analyses performed in areas accomplishment the conditions of the model results are correct whereas areas without with different conformation present aberrant values. It confirms the heterogeneous structure of the semolina surface and core.

Molecular composition from EDX atomic spectra

The technique of Fäldt (1995), cannot be adapted to the wheat powder in a 100%, aberrant values are observed also when XPS is used to obtain the atomic spectra (Saad *et al*., 2011a). This is not the case in other powders as dairy powders where this technique permits a quite good prediction of the molecular composition (Murrieta-Pazos *et al.* 2012a). This can be explained by the structure of the semolina particle. Even if dairy powder and semolina are both food powders, their structure is completely different. The raw materials as well as the

production process influence the structure of each powder. In the case of semolina, the structure is as complex as a tissue, due to its vegetal origin. Indeed, semolina presents a heterogeneous distribution of the components at the surface and this distribution depend on the characteristics of the endosperm section that is later milled to obtain each particle.

Even if the molecular composition calculated with the EDX spectra cannot be validated as a quantitative technique, it provides very interesting information. It is possible to class the points of analysis in points with aberrant values (which probably have a more complex compositions) and points with coherent values (which composition most follow quite well the two conditions considered in the mathematical model, the structure is formed only with starch-arabinoxylan, gluten and lipids in a linear relation). Moreover, just the EDX spectra give interesting information combined with the O/C ratio. From this data, it is possible to corroborate if the point of analysis is done in a broken starch (nitrogen not detected), in a complex composition (O/C values over 0.30), or if it corroborates an excess of proteins and/or lipids (O/C values under 0.20). Minerals give information about the kind of tissue analyzed; hence it was possible to observe some mineral deposits with the analysis. The degradation of the particles by the electron beam as well as the ESEM photos are tools that combined with the molecular composition, the O/C ratio and the atomic spectra can describe the structure of the semolina particle surface.

Molecular composition from XPS atomic spectra

The surface composition of raw and sieved semolina was determined by XPS. Elemental composition of C, O and N amounted at least 99.5% of the detected elements. A typical XPS spectra example is shown in figure 47 for raw semolina.

The XPS works in an area of 1mm, measuring the surface of several particles in a depth of 5 μm. The XPS survey scans of principal components were analyzed and decomposed to obtain chemical functions (Rouxhet *et al*., 2008; Saad *et al.* 2011a). The peak decomposition was performed according to a model for biochemical compounds (Gerin *et al*., 1995).

The C_{1s} peak was decomposed into 4 peaks. The peak at 284.6 eV is attributed to C making a single bond with C or H (C-C, C-H) found in lipid or protein side chains. The peak at 286.0 eV is related to C single bonded to O or N (C-O, C-N). This kind of bonds can be found in alcohol, amine or amide functions in proteins. The peak detected at 287.5 eV is

attributed to C making two single bonds or one double bond with O (O-C-O, O=C-N, O=C-O) present in acetal and hemiacetal functions in polysaccharides or in amide functions in proteins. The peak at 288.6 eV is attributed to C making one double or simple bond with O (O=C-OH, O=C-OR) in ester and carboxyl functions in proteins and cell-wall polysaccharides.

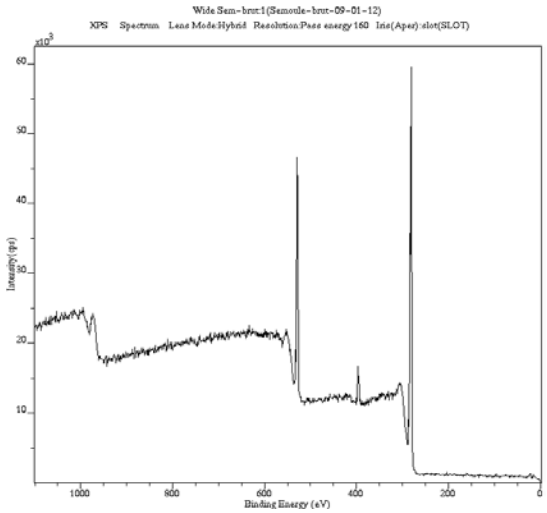

Figure 47. Survey scans obtained from XPS analyses for raw semolina.

The O_{s1} peak was decomposed into 3 sub-peaks. The peak at 531.2 eV is attributed to O doubly bound to C (O=C-O, O=C-OH) these bonds correspond to amide, ester and carboxyl in cell-wall polysaccharides. The peak at 532.5 eV is attributed to O making single bonds with C (C-O-H) in alcohol and (C-O-C) in acetal and hemiacetical functions in polysaccharides. The peak at 533.6 eV is attributed to O bond with hydrogen in water (H_2O).

N_{1s} peak was not decomposed because the possibilities of decomposition were not clear. The registered peak was attributed to uncharged N in amine (C-NH_2) or in amide (O=C NH_2, O= NH-C). N is a component exclusively attributed to protein molecules.

A precedent work gave some evidence to conclude that surface of semolina is rich in lipids (Saad *et al*., 2011a), then in order to confirm the presence of this lipid cover, semolina and semolina after free fat extraction (AFFE) was analyzed by XPS. In addition the effect of agglomeration was also studied analyzing agglomerated semolina, it means couscous and couscous after free fat extraction.

In the table 34 are shown the atomic concentration determined by XPS as well as the molecular surface composition calculated from the XPS results. In the atomic concentration,

raw semolina presented higher values of carbon, whereas raw couscous, couscous AFFE and semolina AFFE presented similar values. Semolina AFFE observed the higher concentration of nitrogen at the same time, raw semolina, raw couscous and couscous AFFE observed similar values. Finally oxygen presented higher values in couscous and couscous AFFE that are similar between them. Raw semolina presents the slower value and a little increment in oxygen concentration is observed in semolina AFFE. These result shown an effect of the fat extraction as well as the agglomeration in the XPS result. The decomposition of the peaks permits to understand the results and the phenomena produce after free fat extraction and after agglomeration.

For the bonds related to lipids C-C, C-H, a clear decrease after free fat extraction in both semolina and couscous is observed, however values of raw couscous was already lower than those measured in raw semolina, hence a possible pert of lipids is produced after agglomeration process. In addition these results confirm that a surface rich in lipids is found at the surface of raw semolina. By its part, couscous also presents a surface rich in lipids, nevertheless these lipids are in lower quantity than semolina.

The bond related to proteins C-N, increased only AFFE of couscous, whereas O=C-N as well as the atomic concentration of nitrogen increment AFFE of both semolina and couscous. These differences are probably due to some protein molecules found in one of the powder that is not present in the other, lost or gain in the agglomeration process, however it is not possible to know what kind of proteins are. The augmentation of the proteins (N) at the surface is evident AFFE.

The carbohydrates can be related to bond of polysaccharides (O-C-O/C=O, O-H/O-C and O-H, O-C) and to wall cell polysaccharides (O-C=OH/O=O-OR and O=C). The concentration of the bonds for polysaccharides increment AFFE of semolina and couscous that was expected, because after extraction of lipids at the surface, the polysaccharides can be better detected. One of the polysaccharides detected (O-H, O-C) presents a clear decrement AFFE of semolina as well as an increment AFFE of couscous. These polysaccharides could be lost by the agitation in the technique of fat extraction. This phenomenon is not happening in the couscous where the grains are more consistent and contains better the elements on the matrix.

The O-C=OH/O=O-OR representing wall cell polysaccharides, observed similar values for all the powders whereas O=C present an increment AFFE only in semolina, probably these wall cell polysaccharides are lost in the agglomeration process consequently they are found in a very less quantity in couscous, in addition the quantity does not increment AFFE. Finally the bond related to H_2O, presents a decrement AFFE in semolina and couscous, probably the petroleum ether dehydrates the particles, in addition values for couscous are lower than values for semolina, this result agree with the lost of water due to heat treatment in the couscous process.

In table 34 the O/C ratio and the molecular surface concentration deduced from the equation system, were calculated by using the experimental values for proteins, carbohydrates and lipids determined by Saad *et al*. (2011a).

Table 34. XPS atomic spectra and calculated surface composition

			Atomic Concentration %			
Binding Energy (eV)	**Functions**		**Semolina**		**Couscous**	
			Raw	**AFFE**	**Raw**	**AFFE**
133.0	P		-	-	0.19	-
163.0	S		-	0.31	-	-
284.6	**C**		**80.21**	**73.72**	**76.53**	**76.5**
284.6		C-C, C-H	60.57	52.77	57.14	50.23
286.0		C-O, C-N	28.77	28.31	30.87	35.12
287.5		O-C-O, C=O	6.99	14.95	7.5	10.01
288.6		O-C=OH, O=C-OR	3.66	3.97	6.5	4.64
399.6	**N**		**3.47**	**8.89**	**2.56**	**3.19**
399.7		NH, NH2	100.0	100.0	100.0	100.0
532.5	**O**		**16.64**	**17.09**	**20.7**	**20.31**
531.2		O=C	12.93	42.05	8.93	8.31
532.5		O-H, O-C	72.63	45.92	79.15	81.4
533.6		H_2O	14.43	12.03	11.92	10.29
	O/C ratio		0.21	0.23	0.27	0.27
	Molecule			%		
	Carbohydrates		-3.13	5.15	23.43	21.15
	Proteins		25.12	128.94	14.95	26.10
	Lipids		78.32	-34.38	61.40	52.74

From these values the O/C ratio for gluten, starch and extracted lipids are 0.22, 0.49 and 0.21 respectively. By observing the O/C ratio in table 34, it can be concluded that semolina presents a value very similar to pure extracted lipids (0.21), this result could confirm that semolina surface is principally covered by lipids at 10 nm. After free fat extraction, an increment in the O/C ratio is appreciated; this augmentation can be produced by a higher concentration of starch at the surface (pure starch O/C ratio = 0.49). It is possible that protein concentration had also increase, but the O/C ratio of protein is very near to O/C ratio of extracted lipids, consequently an increment of protein at the surface will not increment the O/C ration in semolina.

In the case of couscous, the O/C ratio keep the same value AFFE, it can be easily explained by a lower quantity of lipids at the surface than semolina, hence the extraction of those lipids does not reflect a difference in the O/C ratio. More over, the O/C ratio was already higher in raw couscous than semolina and semolina after free fat extraction, it means that lipids at the surface had been already lost in the agglomeration process. It seems that a re-arrangement of the surface in couscous process encapsulate the lipids and it does not permit the migration of oil to the surface.

In fact surface molecular concentration (table 34), complement the information. Semolina, present aberrant values of carbohydrates, a negative number is presented, nevertheless this value can be considered as cero, it is important to remember that this deduction from the equation matrix is not exact, however it can give information about the proportion of the molecules at the surface, in this case carbohydrates can be considered cero.

Even if one negative value is presented, the values are in agreement with the atomic and bonding spectra as well as with the O/C ratio, a high quantity of lipids is present at the surface. After extractions of the lipids at the surface (AFFE), values get more aberrant, this can be due to the not linear relation between the protein and carbohydrates after the extraction, however, the value of lipids decrease whereas the values of proteins and carbohydrates increase, this confirms that the technique is sensible to the modification of composition at the surface and it is also in agreement with the results indicating that proteins and carbohydrates are more abundant after free fat extraction.

Finally, the values deduced for raw couscous and couscous AFFE confirm a diminution of lipids after agglomeration at the surface (raw couscous), and even more AFFE, this diminution on surface lipids presents a consequent increment in the protein and starch concentration after agglomeration. An increment of protein after free fat extraction is also observed. The results deduced from equation system in raw couscous and couscous AFFE seams very correct, no aberrant values are observed, this is a very interesting effect. To explain this change in the values, we postulate that surface of raw semolina and semolina AFFE is very complex as well as heterogeneous, their complexity is very high since they are coming from tissues, thus the assumptions of mathematical model are not accomplished. In the other hand, couscous has been modified by the agglomeration and cooking processes. This could form a more homogeneous surface with a consequent accomplishment of the assumption of the mathematic model. Probably, soluble components get out from the surface as well as lipids, the surface, more homogeneous seams to encapsulate the core of the particle and limit the lipid migration.

Composition from the core to the surface

From EDX results surface and core are not different. These results were expected because milling of *wheat durum* endosperm produces the particles of semolina, hence semolina particle will have the characteristics of the endosperm, the difference between surface and core is only the cut surface, but composition stays the same.

The differences in atomic concentration are related to the analysis point in the protein-starch matrix, this confirms that the surface is very heterogeneous.

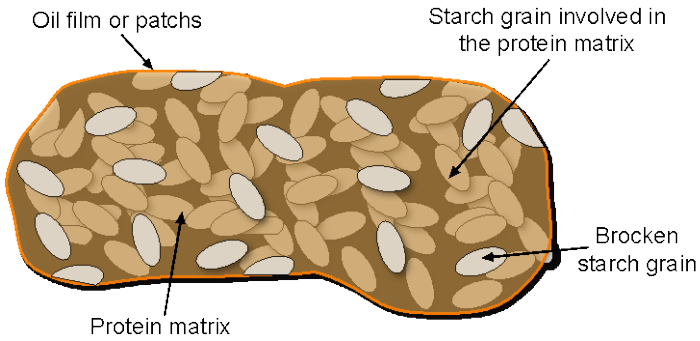

Figure 48. Structure of the semolina particle

Considering the EDX and XPS results, the surface of the semolina is very reach in lipids (around 78 %) at 10 nm at the extreme surface but when the analysis is performed by EDX in

a depth of 1μm the lipid content is reduced (~ 6.1-11.7 %). The quantity of lipids is not exact, but a proportional distribution of the molecules is highlighted. A layer or some patches of lipids are probably placed at the surface, the rest of the lipids are then distributed in the protein-starch matrix. By XPS the second more abundant molecules are the proteins (~ 25.12 %) whereas carbohydrates are present in very few quantities. This can be explained by grain of starch wrapped by a protein layer. Moreover, the liquid state of the lipids could form a film at the surface covering the broken starch grains. Hence at 10 nm it is detected the layer of lipids with some proteins. By EDX is not possible to observe a gradient in proteins and carbohydrates because the concentration of molecules depends on the analysis area. However it can be concluded that semolina presents a surface rich in lipids and a heterogeneous distribution of the proteins and starch grains. A proposition of the structure of the semolina is shown in figure 48.

From the XPS results it is postulated that the surface of couscous is also cover by lipids but in a low quantity than semolina, in addition the protein and starch matrix appear more homogeneous, due to the process of agglomeration (humidification and mechanical work) and cooking.

IV.1.3. Contributions of surface and gradient composition obtained by EDX on powder food knowledge

An original technique to study the surface composition of milk powders and semolina was developed. The technique was more adapted to dairy powders than semolina. It is due to the differences in the surface structure of both powders.

The principal differences are related to the origin of the powder, milling of durum wheat kernel produces the semolina, its vegetal origin make the surfaces as complex as any vegetal tissue. On the other hand, the milk powder is produces by spray draying, it seems that previous processes turn the surface of the powders more homogeneous, this permit a correct analysis at the surface. This phenomenon was also appreciated for the surface characterization of couscous. XPS results seem correct, implying that agglomeration process transforms the structure at the surface, soluble components as well as lipids get re-arranged, surface became homogeneous and it seam to envelope the core and limited the lipid migration.

The differences of core and surface between semolina and milk powders are explained next: Milk powders present an homogeneous surface, this surface seem to be covered by lipids, these lipids are abundant in WMP and reduced in SMP. A skin is formed next the fat layer. It is not clear if the analysis done by EDX is performed at these level or deeper including a piece of core matrix. However analysis present a higher content of lactose at the surface in comparison with the core, next of the lipids layer in whole milk powders, or directly at the surface for skim milk powders. These results suggest that the skin could be richer in lactose than the core. Inside the skin a lactose protein matrix is presented with some lipid deposits of fat that are more abundant in WMP than in SMP.

On the other hand, semolina particle is connected from the inside to the surface of the particle. A protein matrix contains starch grains, these starch grains can be completed enveloped by gluten, or can be broken exposing the pure composition of the starch. Lipids are present in the porous gluten matrix in a liquid state. This state permits the oil to migrate throughout different points of the surface. It seems that lipids could migrate to the particle surface and form a very thin film that is detected only at 10 nm (by XPS). After this film, it can be found starch grains, broken starch grains or the protein matrix. The core and the center are similar, no differences where appreciated inside or outside of the particle.

IV.2. MOLECULAR APPROACH: COMPONENTS GRADIENT DISTRIBUTION AND CHARACTERIZATION OF REACTIVE POWDERS

The present subchapter continues with the development of techniques to characterize the surface of the powders and the gradient distribution of the components. The techniques used in this section work at the molecular scale. DSC, CG, CGI and RC techniques are performed to characterize the molecules at the surface. As size and shape particle properties are also a characteristic participating in the reactivity of the powder, these characterizations are included in this section.

In the first part of this subchapter, the gradient distribution of the elements was studied by coupling EDX and XPS analysis. Milk powders present a gradient composition in terms of lipids and from literature it is known that the lipids are mostly located at the surface and are separated from the lipids inside the particle by a skin. Then, the characteristics of the fat at the surface, as well as inside the particle, were studied. Thermal properties were studied by DSC wheras the fatty acid profile was studied by CG. The objective of this work was to compare the properties of the standard and the agglomerated powders. These results were coupled with the surface composition deduced with the equation system and the XPS and EDX spectra. In addition, the size and shape of particles by SEM were done.

This study is already published: Murrieta-Pazos I., Gaiani C., Galet L. and Scher J., 2012. Composition gradient from surface to core in dairy powders: Agglomeration effect. *Food Hydrocolloids* 26, 149–158. The results and discussion of the publication was integrated in this manuscript in section. IV.2.1.

In the second part of this subchapter, a methodology to characterize reactive properties on powders is proposed. The size and shape of the particle is then determined as an important parameter in the interaction of the particles. In addition two innovative techniques to determine the surface free energy of the powders are proposed: the IGC and the CR. The use of these techniques in food powder is very limited as it was constated in the bibliographic study. The challenge of these methodologies was the adaptation of the techniques to the complex food powder. The results of free energy were related to the surface composition determined by XPS. The study was performed in raw and sieved semolina in order to study the distributions of the properties in the whole powder and relaite it to a possible increment or deacrement on reactivity.

This section was written as a publication and will be submitted on December 2012: Murrieta-Pazos I., Galet L., Calvet R., Kaouach F., Gaiani C. and Scher J. How to characterize reactive food powders: Particle shape and surface characterization of durum wheat semolina. Results and discussion of this article are integrated in this manuscript in section IV.2.2.

Due to the difficulty and the length to adapt these techniques (CGI, RC), only one food powder was studied. The semolina was chosen to keep the balance in the quantity of studies performed in both powders.

IV.2.1. GRADIENT COMPOSITION FROM SURFACE TO CORE IN DAIRY POWDERS: AGGLOMERATION EFFECT

IV.2.1.1. Milk fat fractions characterization

a) Quantification

Table 35 presents the fat fractions percentages obtained for SWMP and AWMP. The free fat was found higher for AWMP in comparison with SWMP.

Table 35. Percentages (g.100g-1 powder) of the three different fractions (total, encapsulated and free fat) in whole milk powders.

Powder[1]	Total fat	Encapsulated fat	Free fat
SWMP	23.75 ± 0.15	21.74 ± 2.55	2.08 ± 0.30
AWMP	25.17 ± 0.04	20.61 ± 0.05	2.97 ± 0.09

[1]SWMP: Standard Whole Milk Powder; AWMP: Agglomerated Whole Milk Powder.

As already noticed by Vignolles *et al*. (2007), the porosity and the powder structure may influence the quantity of free fat. Furthermore, it was reasonable to surface fat for agglomerated powders certainly due to the structure of the agglomerate allowing a better penetration of the solvent in the matrix. The total of the free fat and the encapsulated fat was supposed to be equal to the total fat. It is the case for SWMP. However, a difference was observed for AWMP and could be attributed to the inexactitude of the methods (Buma, 1971).

b) Thermal properties

Thermal properties of the three precedent fat fractions were determined by DSC. The melting profiles of SWMP and AWMP are respectively presented in figure 49 and figure 50.

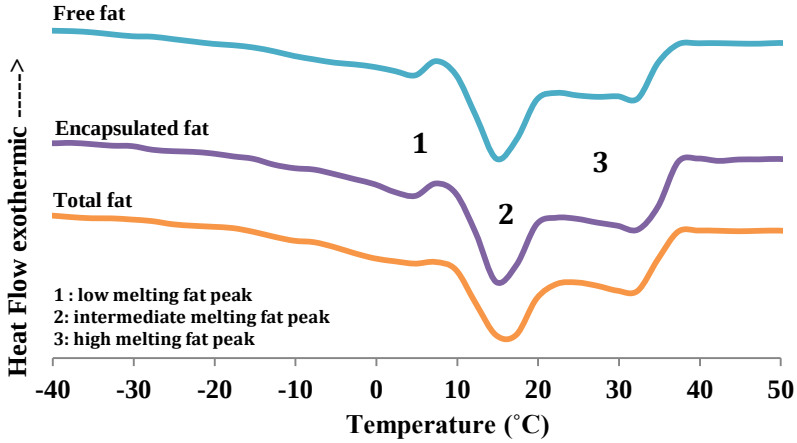

Figure 49. Example of thermogram presenting the fusion of three different fat fractions (free, encapsulated and total) obtained from standard whole milk powder.

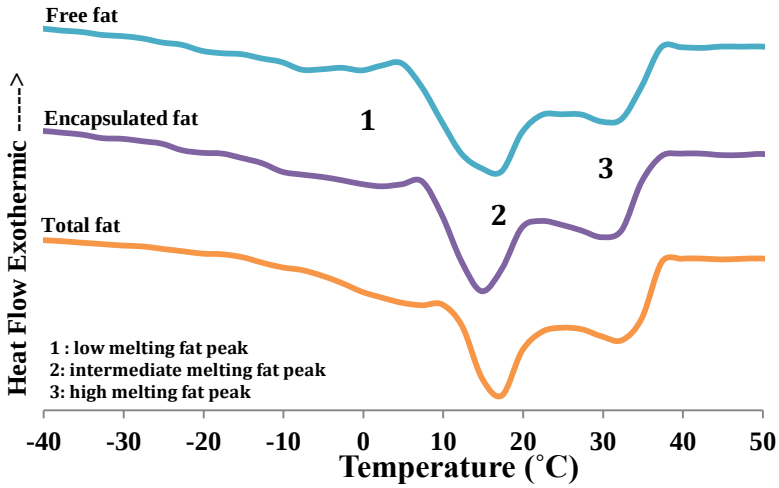

Figure 50. Example of thermogram presenting the fusion of the three different fat fractions (free, encapsulated and total) obtained from agglomerated whole milk powder.

From the XPS results, it can be observed that the surface atomic composition of whole milk powders was only focused on C, N and O elements, indicating the absence of minerals. On the opposite, skim milk powders presented traces of minerals (K, Ca, Cl, S and P) in addition to C, O and N atoms. From the EDX results, minerals were detected at the surface of the four powders. Nevertheless, the percentages were still higher for SMP than WMP. The C, O and N percentages were also significantly different for the same powder between XPS and EDX measures. These differences may be explained by the difference of depth of the analyses. XPS measures were focalized at the first 5 nm whereas EDX measures were at the first micrometer. No significant differences were observed between agglomerated and standard powders presenting the same chemical composition.

Table 36. Transition temperatures of fusion and crystallization of different milk fat fraction.

			Peaks temperature (ºC)			Area	Temperature (ºC)	
	Powder	**Fat fraction**	First	Second	Third	($J.g^{-1}$)	Initial	Final
Crystallization	SWMP	Free	12.6	7.6	-	60.5	18.4	-35.0
		Encapsulated	14.9	7.6	-	67.9	20.3	-32.9
		Total	12.9	7.4	-	62.8	15.2	-32.0
	AWMP	Free	14.3	5.9	-	63.1	20.0	-32.6
		Encapsulated	13.2	7.0	-	59.4	17.0	-29.2
		Total	13.0	7.9	-	63.6	16.3	-34.0
Fusion	SWMP	Free	5.3	15.5	32.2	-69.8	-23.1	37.3
		Encapsulated	4.9	15.7	32.1	-82.1	-22.0	38.6
		Total	5.5	16.1	31.4	-74.0	-20.2	37.7
	AWMP	Free	0.2	16.6	30.4	-72.09	-23.8	38.2
		Encapsulated	3.4	15.2	29.5	-73.99	-24.3	36.4
		Total	6.8	16.6	32.6	-74.9	-24.4	38.2

Three endothermic peaks (1, 2 and 3) are observed with a typical melting behavior starting around -40 ºC and finishing at 40 ºC. These melting peaks (1, 2, 3) may be related to low, intermediate and high melting fat on the basis of their melting points. The independent melting of these three fractions was assumed to be the reason for the three endothermic peaks in the heating curve of milk. This aspect was supported by Ambarkhane *et al.* (2005) and Deffense (1993). Additional interpretations were developed by Ten Grotenhuis *et al*. (1999). Variable fat fractions (low, medium and high) and also variable polymorphic forms of fat were taken into account to explain the presence of these three melting peaks. Consequently, the first endothermic effect in the DSC curves (peak 1) could be explained by the melting of the first amount of α-crystals (mainly composed of low and intermediate melting triglycerides). This peak was only observed after cooling at high cooling rates (Ten Grotenhuis *et al*., 1999). Around 7-8 ºC, a part of the α-crystals transforms into β'-crystals, which leads to the small exothermic effect between peaks 1 and 2. The second endothermic peak (2) has a maximum around 15-16 ºC and is the result of further melting crystals of higher melting triglycerides (mainly in the α-form). The last peak (3) may be caused by melting β'-crystals of high melting species. Because milk fat has many different triglycerides, they do not form pure crystals but tend to crystallize in groups of similar size and structure. So, it is not just the polymorphic forms that are important but also the composition of these mixed crystals. Detailed data of melting and crystallization are summarized in table 36 for the three fractions and also for the two powders (agglomerated and standard). These observations are in agreement with (Kim *et al*., 2005b) which observed a similar behavior in fractions of cream and whole milk powders. They explained the similarity of results by the fact that the thermal behavior may present differences only when important variations in the fatty acid

composition occurred. For example, differences were observed after fragmentation of milk far (Bhaskar *et al*., 1998). The agglomeration process did not affect the thermal properties of the different fat fractions obtained from A and S powders.

c) Fatty acid composition

The three fat fractions were finally analyzed by GC to obtain the fatty acid profiles (table 37). Milk fatty acids can be classified in short chains (4-8 carbon atoms), medium chains (10-12 carbon atoms) and long chains (14-18 carbon atoms).

Table 37. Fatty acid composition determined by gaz chromatogrphy for standard and agglomerated whole milk powder.

Powder	Fatty acid composition		Total fat (area %)	Encapsulated fat (area %)	Free fat (area %)
STANDARD WHOLE MILK POWDER	C8	Caprylic	1.07 ± 0.03	1.12 ± 0.00	1.27 ± 0.07
	C10	Capric	3.70 ± 0.76	3.57 ± 1.82	3.40 ± 0.10
	C12	Lauric	3.37 ± 0.19	3.21 ± 0.04	4.45 ± 0.15
	C14	Mystiric	12.07 ± 0.33	12.65 ± 0.19	12.95 ± 0.64
	C15	Pentadecylic	0.40± 0.01	0.43 ± 0.00	0.46 ± 0.09
	C16	Palmitic	36.96 ± 0.43	37.62 ± 0.44	37.47 ± 0.30
	C16.1	Palmitoleic	1.69 ± 0.01	1.69 ± 0.01	1.58 ± 0.28
	C17	Margaric	0.75 ± 0.01	0.77 ± 0.01	0.74 ± 0.00
	C18	Stearic	12.07 ± 0.16	12.43 ± 0.23	11.73 ± 0.40
	C18.1	Oleic	24.94 ± 0.94	24.32 ± 0.98	23.61 ± 0.10
	C18.2	Linoleic	2.40 ± 0.45	1.71 ± 0.01	1.95 ± 0.29
	C18.3	Lionlenic	0.58 ± 0.04	0.50 ± 0.01	0.43 ± 0.05
Powder	Fatty acid		Total fat	Encapsulated fat	Free fat
AGGLOMERATE WHOLE MILK POWDER	C8	(area %)	(area %)	5.11 ± 3.02	6.85 ± 3.47
	C10	Capric	3.42 ± 0.10	3.18 ± 0.22	3.39 ± 0.09
	C12	Lauric	4.04 ± 0.39	4.20 ± 0.12	4.33 ± 0.20
	C14	Mystiric	12.16 ± 0.26	12.77 ± 0.52	12.80 ± 0.50
	C15	Pentadecylic	0.46 ± 0.03	0.44 ± 0.02	0.40 ± 0.10
	C16	Palmitic	34.48 ± 0.54	35.20 ± 1.18	34.78 ± 1.17
	C16.1	Palmitoleic	1.55 ± 0.09	1.47 ± 0.02	1.51 ± 0.08
	C17	Margaric	0.89 ± 0.14	0.85 ± 0.02	0.85 ± 0.06
	C18	Stearic	11.89 ± 0.90	12.87 ± 1.62	11.68 ± 0.51
	C18.1	Oleic	22.57 ± 0.18	21.25 ± 0.98	20.84 ± 0.93
	C18.2	Linoleic	2.53± 0.09	2.16 ± 0.15	2.09 ± 0.22
	C18.3	Lionlenic	0.77 ± 0.09	0.50 ± 0.19	0.48 ± 0.03

In addition, they can also be saturated and unsaturated. Whatever the powder size (agglomerated or standard), fatty acids with long chains (>14 carbons) were more present in the encapsulated fat fractions. Concurrently, fatty acids with short and medium chains (<14 carbons) were more present in the free fat fractions. Gray colors were used in table 37 to better visualize the differences. Even if the differences were small, there were repeatable and observable for each powder. Similar results were also obtained by Kim *et al*. (2005a, 2005b) for whole milk powders. Nevertheless, they proposed a distribution of high melting fatty acid species at the surface of the particle, whereas the longer of the chain was not taken into account by these authors

d) Milk fat fractions distribution within the particles

From quantification, thermal properties and composition of the fat fractions, the process of agglomeration did not affect the fatty acid distribution in the different fractions. Similar results were obtained for agglomerated and standard powders presenting the same chemical composition. But differences were observed between the fat fractions. From GC results, it may be possible that fatty acids with long chains were less prone to attain the surface of the particle at classical spray-drying temperatures resulting to the presence of more fatty acid with short chain at the surface (free fat) of the particles. Indeed, at classical spray-drying temperatures all the fat fractions are in a mobile fluid form Nijdam & Langrish (2006); the fusion of all the fat elements being obtain around 40 ºC (Jouppila & Roos, 1994; Kim *et al*., 2002). These observations were also confirmed in figure 49 and figure 50; the totalities of the fractions being in a fluid form at temperatures higher than 40 ºC.

IV.2.1.2. Powders size and shape characterizations

a) Microscopy

SEM observations of the four industrial powders were per- formed at two scales (figure 51). The differences between agglomerated and standard powders were very clear. Standard powders were spherical with individual particles whereas agglomerated powders presented agglomerates of spherical particles pasted ones with others. Surface differences were also observed between whole milk powders and skim milk powders.

The first ones had a smooth and homogeneous surface, related to the presence of free fat at the surface (Vignolles *et al*., 2007).

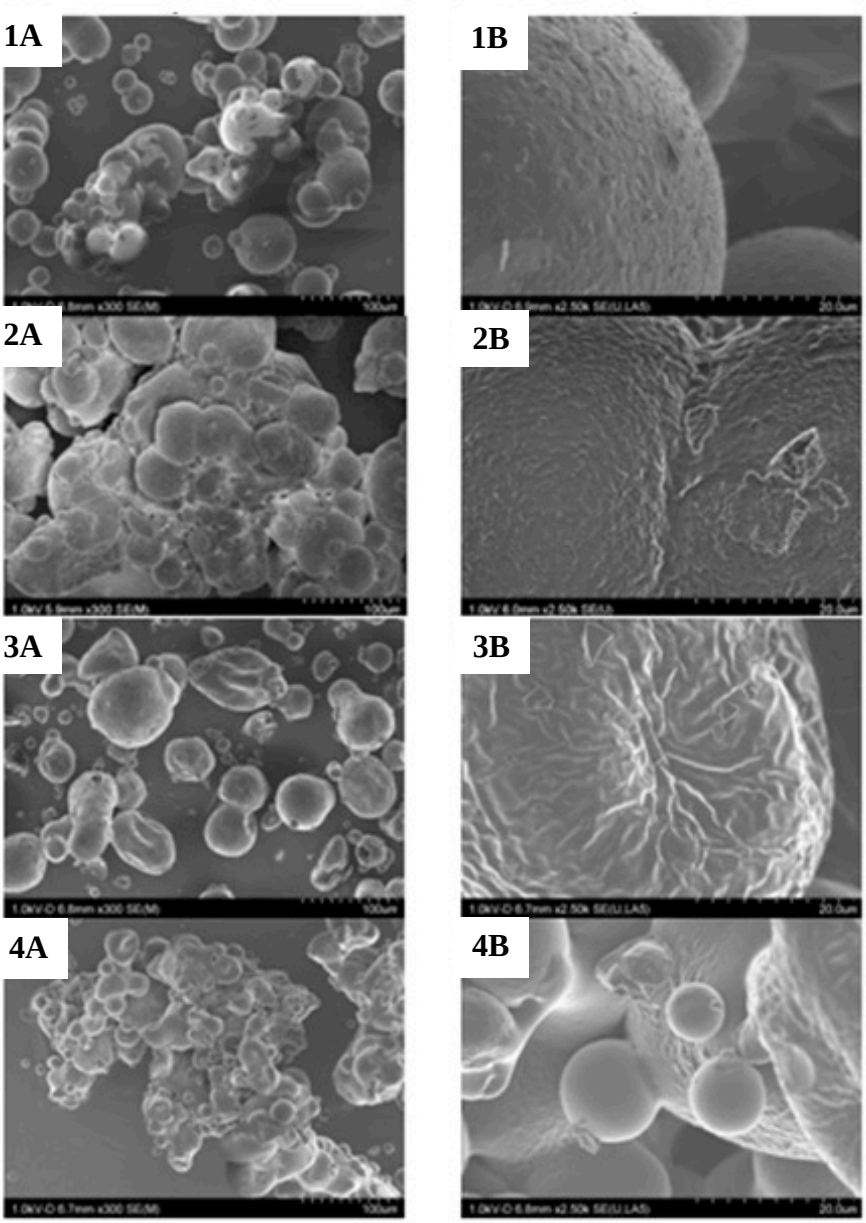

Figure 51. . Scanning Electron Microscopy of the four industrial powders (1: standard whole milk powder; 2: agglomerated whole milk powder; 3: standard skim milk powder; 4: agglomerated skim milk powder). Scale x300 (A) and x2500 (B).

The seconds presented a more wrinkled or "brain surface", related to a lactose-protein matrix with low fat (Gaiani *et al*., 2006; Kim *et al*., 2002; Nijdam & Langrish, 2006; Vega *et al*., 2005). In addition, the drying temperature and the size of the droplet produced by the nozzle were also found responsible of the smooth or wrinkle aspect of the powders. Wrinkled particles were related to low temperatures and important droplet size whereas high temperatures and small droplets allowed a faster evaporation of water inducing a smoother surface (Hassan & Mumford, 1993; Walton, 2000). At the opposite, low temperatures as well as important droplets produced a slow evaporation of water and a slow conformation of skin.

These conditions allowed the particle to deflate and shrivel (Hecht & King, 2000; Kim *et al*., 2009a; Nijdam & Langrish, 2006).

e) Particle size

The sizes of all the powders were determined before and after free fat extraction. Examples of particle size profiles are presented for SWMP (figure 52 A) and SSMP (figure 52 B) before and after free fat extraction.

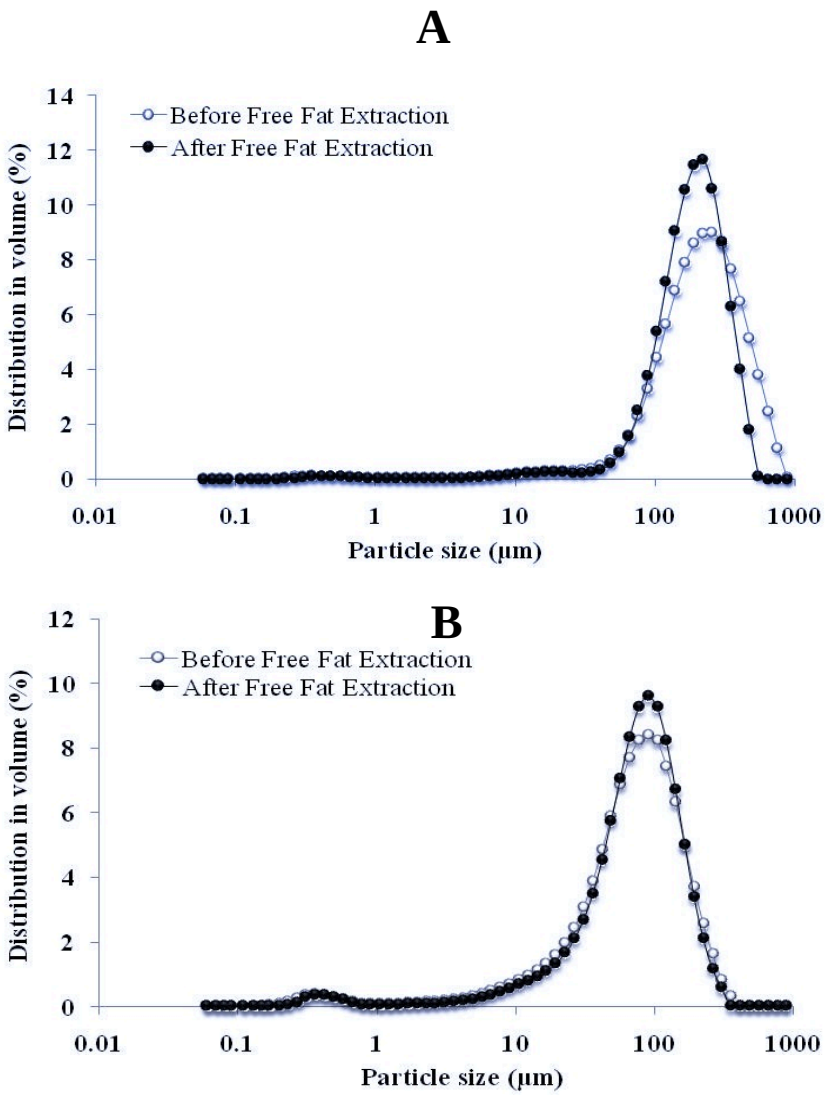

Figure 52. Examples of particle size distribution obtained before and after free fat extraction for standard whole milk powder (A) and standard skim milk powder (B).

Similar profiles were obtained for SSMP whereas a shift in the peak was observed for SWMP when comparing before and after free fat extraction. The shift was observed only for whole milk and may be logically attributed to the fat extraction. The totality of the results is summarized in table 38 under different diameters (D10, D50 and D90). After agglomeration,

the ratio of size increased was around 3 whatever the composition (skim or whole). As consequence, the size of the agglomerated powder was proportional to the size of the standard particles size.

Table 38. Particle size distribution in skim milk and whole milk powder, each standard or agglomerated. For each powder, t-Test comparisons between powders size before and after free fat were performed.

		$D_{(v,0.10)}$ µm	$D_{(v,0.50)}$ µm	$D_{(v,0.90)}$ µm
Before Free Fat Extraction	SWMP	40.4	125.6	291.6
	AWMP	123.6	360.2	674.6
	SSMP	17.3	68.6	158
	ASMP	74.7	201.1	439.4
After free fat extraction	SWMP	39.4^{NS}	116.64^{*}	236.2^{**}
	AWMP	123.9^{NS}	245.42^{**}	403.0^{**}
	SSMP	20.4^{NS}	71.39^{NS}	149.4^{NS}
	ASMP	77.3^{NS}	173.98^{*}	316.2^{*}

$^{***}P < 0.001$, $^{**}P < 0.01$, $^{*}P < 0.05$ and $^{NS}P > 0.05$

Comparison between particle size before and after free fat extraction shown that SWMP presents a significant size reduction after free fat extraction (from 125 to 116 µm). A particle size decrease was also noticed for AWMP (from 360 to 245 µm). Logically, no significant differences were noticed for SSMP (from 68 to 71 µm), as there is no significant free fat extracted from this powder. Surprisingly, a difference was measured for ASMP (from 201 to 173 µm), whereas this powder did not contain surface fat. The differences observed for whole milk powders may be plausibly attributed to the free fat extraction. But the diameter decrease observed for ASMP may be explained only by an eventual particle breakage in ethanol. In addition, it can be clearly observed that the size distribution of whole milk powder was completely moved, confirming that the size of the particle has changed due to the free fat extraction (figure 52).

IV.2.1.3. Powders surface characterization

a) Surface atomic composition before free fat extraction

The surface elemental atomic composition (C, O, N and minerals) was determined by XPS and EDX. These determinations were performed for skim milk powders (table 39) and whole milk powders (table 40).

Table 39. Atomic surface composition (wt %) obtained by XPS and EDX in standard and agglomerated skim milk powder.

Atomic Element	Before Free Fat Extraction			
	XPS		EDX	
	SSMP	ASMP	SSMP	ASMP
C	65.1 ± 0.5	65.1 ± 0.5	71.7	70.7
O	26.5 ± 0.3	26.5 ± 0.3	20	21.2
N	7.2 ± 0.1	7.2 ± 0.1	5.5	4.7
K	0.5 ± 0.4	0.5 ± 0.4	0.7	0.9
Ca	0.2 ± -	0.2 ± -	0.5	0.5
Cl	0.2 ± 0.2	0.2 ± 0.2	0.5	0.6
S	0.1 ± 0.0	0.1 ± 0.0	0.6	0.5
P	0.1 ± 0.0	0.1 ± 0.0	0.1	0.2
Na	-	-	0.3	0.3
Mg	-	-	0.1	0.1
Al	-	-	-	0.3

ASMP: Agglomerated Skim milk Powder; SSMP: Standard Skim Milk Powder.

From the XPS results, it can be observed that the surface atomic composition of whole milk powders was only focused on C, N and O elements, indicating the absence of minerals. On the opposite, skim milk powders presented traces of minerals (K, Ca, Cl, S and P) in addition to C, O and N atoms. From the EDX results, minerals were detected at the surface of the four powders. Nevertheless, the percentages were still higher for SMP than WMP. The C, O and N percentages were also significantly different for the same powder between XPS and EDX measures. These differences may be explained by the difference of depth of the analyses. XPS measures were focalized at the first 5 nm whereas EDX measures were at the first micrometer. No significant differences were observed between agglomerated and standard powders presenting the same chemical composition.

IV.2.1.4. Surface atomic composition after free fat extraction

Interesting results were also obtained from the surface of WMP after free fat extraction (table 40). From XPS results, two minerals (K and Ca) appeared at the surface of WMP in addition to C, O and N elements. This observation suggested the presence of minerals just under the free fat layer. In addition, the percentage of carbon decreased whereas the percentages of oxygen and nitrogen significantly increased. These results are logical with a removing of fat (C decrease) and the apparition of proteins (N increase) and lactose (O/C increase). From EDX results, a new mineral appeared (Mg) after free fat extraction and all the others were present in higher quantities. Similar tendencies were observed for EDX and XPS when comparing the powders before and after free fat extraction. Again, no differences in

atomic surface composition (from EDX and XPS) were observed between agglomerated and standard powders presenting the same chemical composition.

Table 40. Atomic surface composition (wt %) obtained by XPS and EDX in standard and agglomerated whole milk powder before and after free fat extraction.

Atomic Element	Before Free Fat Extraction				After Free Fat Extraction			
	XPS		EDX		XPS		EDX	
	SWMP	AWMP	SWMP	AWMP	SWMP	AWMP	SWMP	AWMP
C	87.4 ± 1.8	86.8 ± -	75.8	78	77.1 ± 1.1	79.4 ± 5.2	74.6	73.5
O	11.6 ± 1.2	12.0 ± -	18.2	17.1	19.9 ± 0.6	18.7 ± 4.3	17.4	18.2
N	1.0 ± 0.6	1.2 ± -	4.1	3.4	2.9 ± 0.2	1.3 ± 0.5	4.8	5.0
K	-	-	0.6	0.4	0.2 ± -	0.5 ± -	0.9	1.0
Ca	-	-	0.3	0.2	0.1 ± -	0.4 ± 0.0	0.6	0.5
Cl	-	-	0.3	0.3	-	-	0.5	0.6
S	-	-	0.3	0.1	-	-	0.2	0.2
P	-	-	0.3	0.3	-	-	0.6	0.5
Na	-	-	0.1	0.2	-	-	0.3	0.4
Mg	-	-	-	-	-	-	0.1	0.1

AWMP: Agglomerated Whole Milk Powder; SWMP: Standard Whole Milk Powder

a) Surface composition in milk components before free fat extraction

With the theoretical matrix developed by others (Fäldt, 1995; Gaiani *et al*., 2006; Kim *et al*., 2005a; Nijdam & Langrish, 2006), the percentages of surface proteins, lactose, fat and minerals were calculated and presented in table 41 for SMP and table 42 for WMP. The theoretical values used in the matrix were obtained from the theoretical composition of lactose (C:50, O:50), proteins (C:65, O:19, N:16) and lipids (C:89.1, O:10.9).

Table 41. Surface composition in components (proteins, lactose, lipids and minerals) obtained from the matrix developed by Faldt (1995) for standard and agglomerated whole milk powder before and after free fat extraction.

Component (%)	Before Free Fat Extraction			
	XPS		EDX	
	SSMP	ASMP	SSMP	ASMP
proteins	45.1	39.3	34.4	29.4
lactose	30.9	36.3	16.9	21.2
lipids	22.8	23.2	45.9	46
minerals	1.2	1.2	2.8	3.4

AWMP: Agglomerated Whole Milk Powder; SWMP: Standard Whole Milk Powder

From XPS results, the surface of WMP was found largely covered by lipids (more than 90%). The surface of SMP presented proteins (around 40%), lactose (around 30%) and lipids. Nevertheless, the latest were still largely over represented (around 20%). These results were

consated by several authors (Gaiani *et al*., 2006; Kim *et al*., 2002; Nijdam & Langrish, 2006; Vega *et al*., 2005).

From EDX results (by using the matrix used for XPS), the surface composition of WMP was found totally different (table 42). Indeed, at 1 mm depth, the surface of WMP presents around 14% of lactose instead of 0% at 5 nm of depth. Lipids were still present but at a lower percentage and proteins percentage were significantly higher at 5 nm depth. For SMP, the differences between the first 5 nm and the first micrometer were less important (table 41). Nevertheless, lactose and proteins were more present at the first 5 nm whereas lipids and minerals were more present just under. Up to now, any comparison with dairy powders was impossible due to lack of EDX data in this field. However, these EDX results were logical and in agreement with the observations done by XPS. Again, no evident differences in surface compositions were measured between agglomerated and standard powders.

Table 42. Surface composition in components (proteins, lactose, lipids and minerals) obtained from the matrix developed by Fäldt, (1995) for standard and agglomerated whole milk powder before and after free fat extraction.

Component(%)	Before Free Fat Extraction				After Free Fat Extraction			
	XPS		EDX		XPS		EDX	
	SWMP	AWMP	SWMP	AWMP	SWMP	AWMP	SWMP	AWMP
Protein	6.2	7.5	25.6	21.3	18.1	8.1	30	31.3
Lactose	0.5	1.3	13.9	11.9	19.3	18.4	11.3	13.1
Lipids	93.3	91.2	58.6	65.4	62.5	72.8	55.5	52.3
Minerals	-	-	1.9	1.4	0.1	0.7	3.3	3.3

AWMP: Agglomerated Whole Milk Powder; SWMP: Standard Whole Milk Powder

b) Surface composition in milk components after free fat extraction

Interesting complementary information was obtained from the analyses of WMP after free fat extraction (table 42). From XPS results, proteins and lactose were more present at the surface of powder after free fat extraction. Lipids were still largely present but the percentage was lower. These results may be explained by the extraction of the lipid layer present at the surface and allowing the apparition of proteins and lactose. The minerals percentages were significantly higher after free fat extraction. By comparing the results of XPS and EDX before and after free fat extraction variables localization of lipids were noticed. Two localizations were also observed in the literature for dairy powders. The first one concerned lipids at the surface, easily removed by solvents and also called “free fat” (Kim *et al*., 2005a; Vignolles *et al*., 2007, 2009a). The second one was located just under this layer and was not easy to

remove. This fraction was called “inner fat” (Kim *et al*., 2005a). The combination of XPS and EDX with free fat extraction allows us to confirm these two localizations.

IV.2.1.5. Gradients of composition in dairy powders

By coupling XPS and EDX, the particle surface was observed at two different levels, respectively the first 5 nm and the first micrometer. In addition, for WMP, surfaces comparisons before and after free fat extraction allowed the characterization of the particles at four different levels. These variable scales of observation permitted a better understanding on how the components were distributed from the surface to the bulk. From these results, two models (for SMP and WMP) were postulated and presented in figure 53.

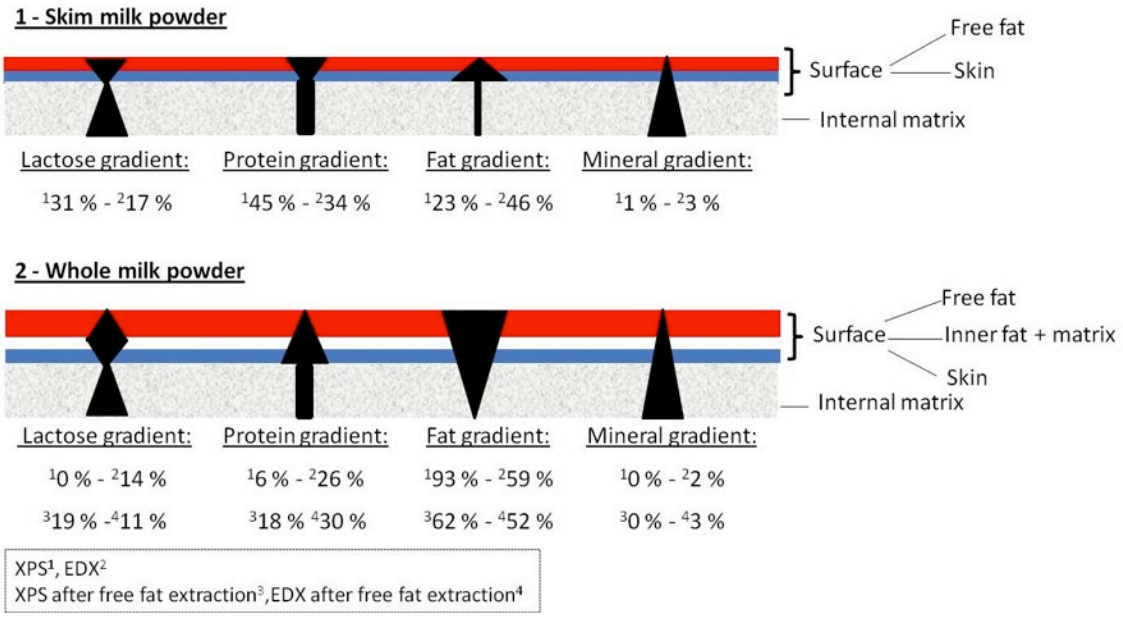

Figure 53. Gradient of composition proposed for a particle of skim milk powder and whole milk powder.

For whole milk powder, the fat gradient decreased significantly from the first nanometers to the first micrometers. Furthermore, the same gradient was observed after free fat removing by solvent extraction. These results suggested a concentration of fat at the surface as already noticed by some authors (Gaiani *et al*., 2006, 2010; Kim *et al*., 2002, 2005a, 2005b; Vignolles *et al*., 2007). An opposite behavior was observed for proteins, a small quantity was found at the extreme surface getting more concentrated throughout the depth of the particle. The powder skin seems to be mainly composed by a matrix of lactose and protein. These components were in higher quantities after free fat removing. Proteins were found more concentrated at core of the particle than at the level of the powder skin. For lactose, the concentration was almost inexistent at the extreme surface. A significant augmentation after

free fat extraction appeared. Finally, after a deeper analysis (EDX) a diminution of lactose was found. These results may be associated to the presence of the powder skin. From these observations it was suggested that the powder skin was constituted by a higher lactose concentration in comparison with the particle core presenting a lactose-protein-mineral matrix.

Finally, a clear mineral gradient appeared from the surface to the core. A link also was observed between the mineral concentration and the order of apparition in the surface gradient. The milk composition in minerals (mg L^{-1}) was details by Fox and McSweeney (1998) as follow: K (1400), Ca (1200), Cl (1000), P (950), Na (500), Mg (130) and S (100). Calcium and potassium were the first elements to appear at the surface after free fat extraction. As expected, these elements were the more abundant in milk. Then, from EDX results, Cl, P, S and Na were detected. These arrangements were still logical with the milk composition. The sulfur presence may be more related to the presence of proteins (whey proteins presenting sulfur) than the mineral element. Finally, Mg element was observed and was one of the less abundant minerals in milk. Interestingly, the order of apparition was also correlated with the mineral molecular weight (g mol^{-1}) as follow: Ca (40), K (39), Cl (35.5), S (32), P (31), Mg (24.7), Na (23). From these observations, the distribution of the components in the WMP may be resumed as:

- an important free fat layer present at the surface of the particle and removed by short-time treatment with solvent,
- an inner fat layer present just under the free fat layer and removable after long-time treatment with solvent,
- a skin mainly composed by a matrix of lactose and proteins,
- and finally a core matrix containing more proteins than lactose
- and including minerals as well as deposits of globular fat.

For skim milk powder, only two levels of composition were investigated, as free fat extractions were not possible for these powders. There is again evidence of components gradients. The protein content at the first 5 nm was more important than at the first micrometer. The same tendency was observed for the lactose gradient with an important decrease between these two depths of analysis. As observed by others (Kim *et al*., 2002; Millqvist-Fureby & Smith, 2007; Nijdam & Langrish, 2006; Vignolles *et al*., 2007), the

presence of a skin (located just under the free fat layer) may explain these observations. This skin may present a higher lactose concentration in comparison with the matrix inside the particle. An opposite gradient was observed for fat. Indeed, the fat may be mostly located just under the powder skin. Even if the fat is still over represented at the surface, we postulated that the skin may be formed faster in these particles and that fat could not migrate in totality to the surface. Afterward, the fat may be localized just under the skin. Finally, a gradient in minerals was also remarked. The same distribution as observed for whole milk particles was noticed; supporting the theory that minerals may be distributed according to their composition in milk and/or the mineral molecular weight. From these observations, the distribution of the components in the SMP may be resumed as:

- a thin free fat layer at the surface (traces),
- a skin mainly made of lactose, proteins and minerals,
- a fat layer just under the skin,
- and finally a core matrix containing proteins-lactose including minerals as well as traces deposits of globular fat.

Concerning agglomerated powders, it can be noticed that globally the gradients were similar for standard and agglomerated powders presenting the same chemical composition. Agglomerated powders are well known to shorten the wetting time of powders in comparison with standard (Gaiani *et al*., 2007). From these results, it can be assumed that the reconstitution enhancement observed for agglomerated powder was not linked to a difference of powder surface composition and/or gradients. In agreement with Forny *et al*., (2011), the improved reconstitution properties of these powders may be more related to the presence of inter-particle pores available for capillary rise.

IV.2.2. HOW TO CHARACTERIZE REACTIVE FOOD POWDERS: PARTICLE SHAPE AND SURFACE CHARACTERIZATION OF DURUM WHEAT SEMOLINA

IV.2.2.1. Environnemental Scanning Electron Microscopy (ESEM)

In figure 54 the general aspect of the raw and sieved semolina at 100X and 800X is shown, raw semolina seems heterogeneous in contrast with sieved powders observing a size augmentation with a homogeneous distribution.

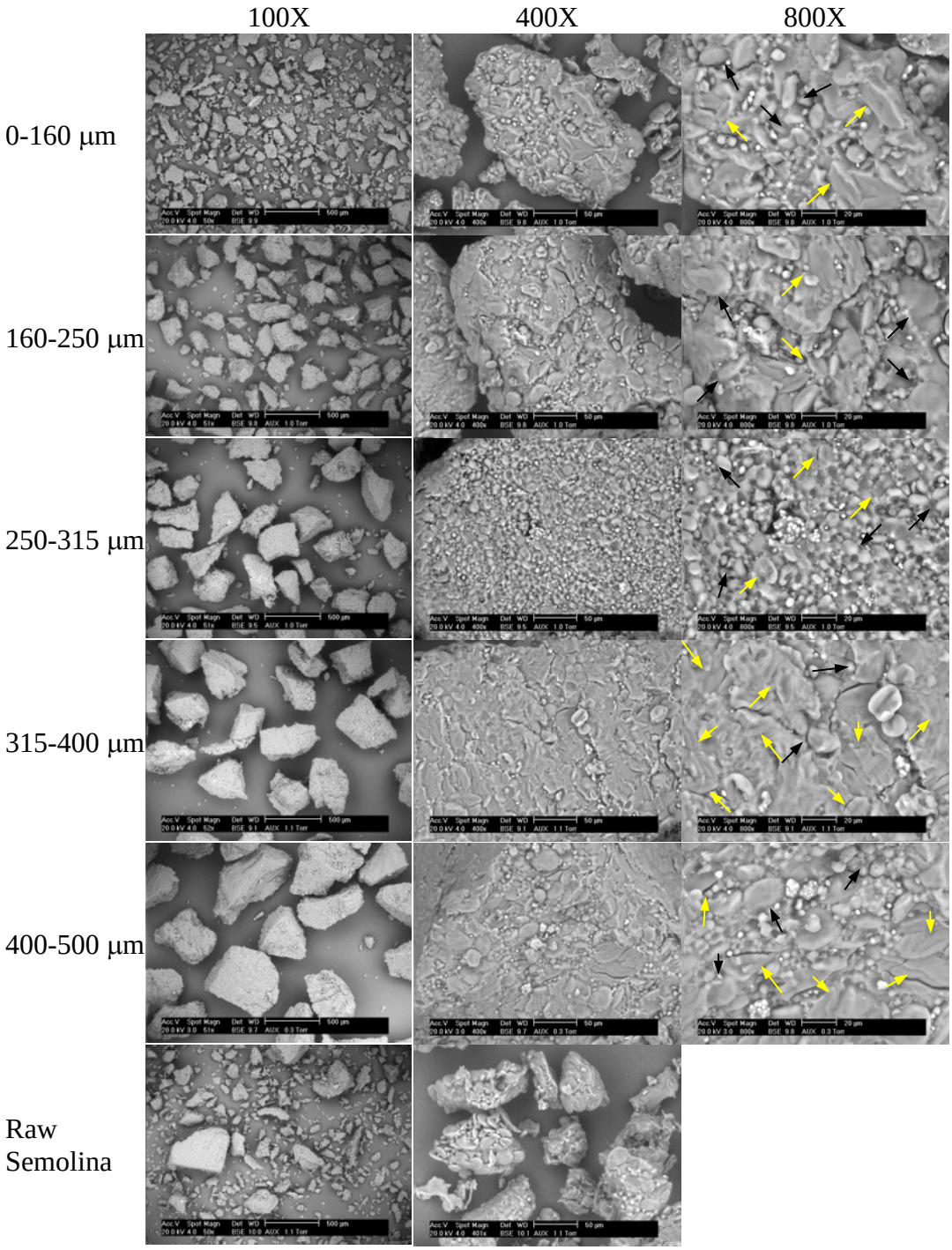

Figure 54. ESEM images at 100 (particles) and 400, 800X (surface) of raw and sieved semolina particles (0-160,160-250, 250-315 315.400 and 400-500µm).

At 400X, the surface of raw semolina particles was observed as being consistent with the heterogeneity of the powder. More specifically, smaller size classes (0-160 and 160-250 µm) present an irregular surface with few broken starch granules (yellow arrows) and some complete starch granules out from under the gluten matrix (black arrows). The biggest size classes (315-400 and 400-500 µm) present a straight surface and more broken starch granules can be observed (yellow arrows). The 250-315 µm class seems to be a transition from one

texture to the other. The evolution of the structure could be related to the milling process and forces applied to the kernel. Saad *et al*., (2011a) proposed that milling conditions could apply different rupture mechanisms through the grain and produce some powders broken at the edge and others broken through the starch particle.

IV.2.2.2. Particle size distribution

The weight of retained powder after sieving was registered for the 5 semolina fractions (figure 55). Retained weight is expressed in percentage of mass: 18.8, 25.3, 26.7, 25.7 and 1.7 corresponding to fractions 0-160, 160-250, 250-315, 315-400, 400-500 μm respectively.

The 0-160 rank is found in a lower proportion of the three central fractions (25.3-27.5 %) but it is still abundant (18.8 %). The 400-500 μm class is present in a very low quantity (1.7 %). Even in a low quantity bulk properties can be influenced for a marked difference in few non-characteristic particles.

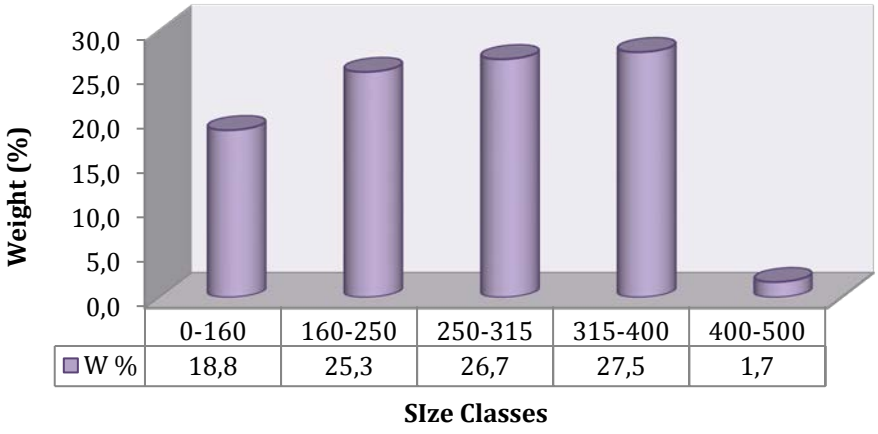

Figure 55. Weight distribution of particle size classes of semolina.

Size distribution curves are presented in figure 56. Raw semolina presents a typical bimodal curve with two populations: a principal one including big and medium particles and a smaller curve containing the fines particles. As expected the curve is situated at the middle of the other curves, it confirms that raw semolina is a mix of the fractions. Bimodal curves are also observed for fractions at 0-160 and 160-250 μm still containing fines whereas biggest fractions (250-315, 315-400, 400-500 μm) present an unimodal curve. The size of particles in volume represented by D(50) is 298 μm for raw semolina and 136, 219, 288, 374, 439 μm for fractions 0-160, 160-250, 250-315, 315-400 and 400-500 μm respectively.

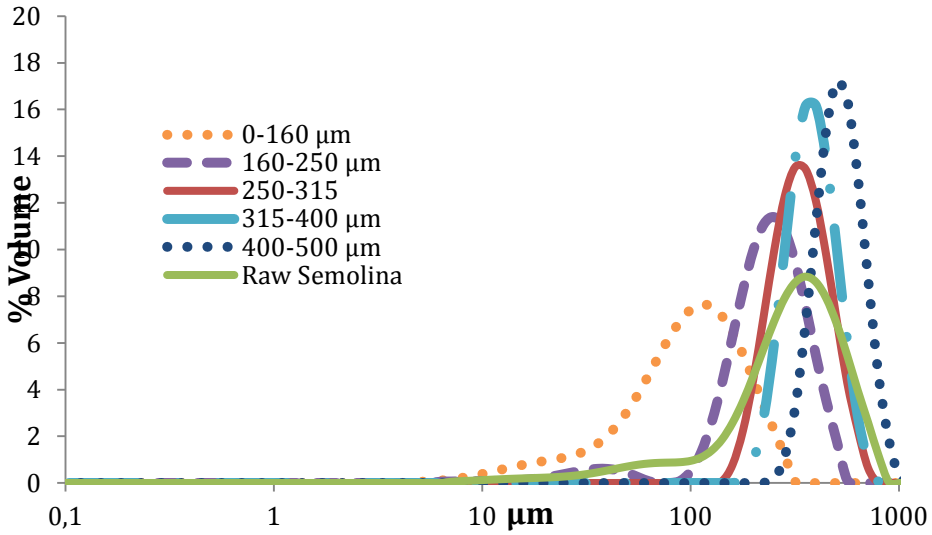

Figure 56. Size distribution of sieved semolina measured by granulometry laser at air pressure of 3.5 bars.

IV.2.2.3. Particle size and shape distribution

The distribution shape parameters (Aspect Ratio, Convexity and Sphericity) observed along the size distribution of semolina is represented in figure 57.

The Aspect ratio parameter showed values from 0.63 to 0.70, with a maximum of this parameter being observed in the small and big particles. It is possible that the smallest particles (16 µm) represent detached starch grains. Semolina particles (more than 100 µm) present a clear tendency: the aspect ratio increases with the particle size, except for the biggest particles (> 500 µm).

Convexity represents the irregularity of a particle. This irregularity is clear when convexity value is near to zero. For semolina particles convexity is directly proportional to the particle size with an increment from 0.79 to 0.89. Bigger particles present a shape less irregular than smaller particles.

Finally a value of one in sphericity represents a perfect sphere. Here a clear tendency can also be noted: the sphericity is inversely proportional to the particle size. Values decrease from 0.80 to 0.72. These results agree with the Aspect Ratio factor showing big particles more elongated. Sphericity is clearly higher in fine particles.

Results are in agreement with the morphology observed by ESEM (Fig. 54). The biggest

particles present an elongated form. A more rectangular form is observed for the 400-500 µm fraction whereas a squared form is observed in the middle size fractions.

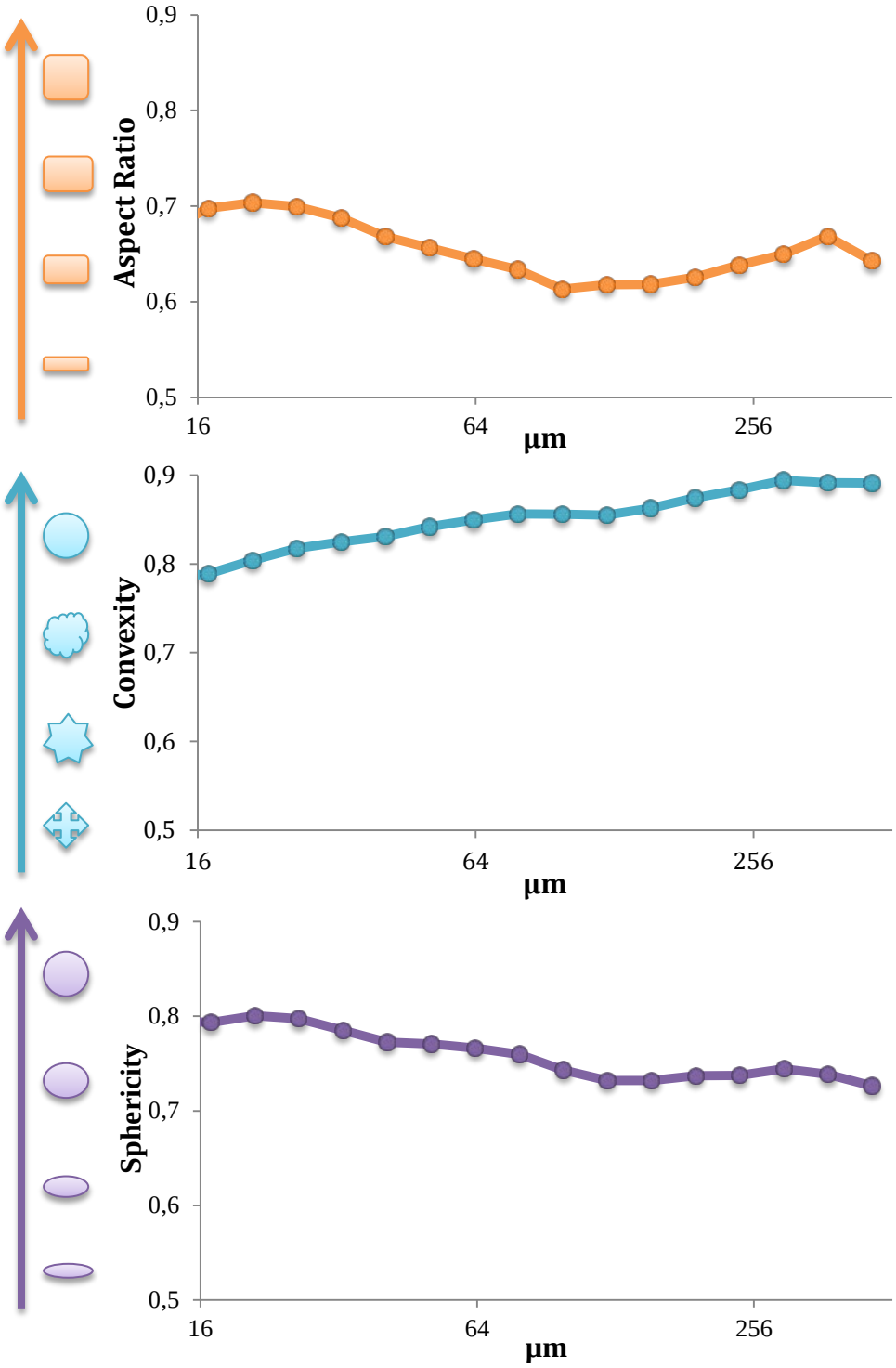

Figure 57. Shape parameters observed in raw semolina: Aspect Ratio (above), Convexity (middle), Sphericiy (down).

Small particles are flatter and spherical whereas big particles are more irregular. This could be explained by the milling process mechanism (Saad *et al*., 2011b). Cutting and/or crushing of durum wheat endosperm kernel produced geometric big particles, then crushing and erosion of big particles, produced irregular medium particles, here the rupture of the particle is more abrupt producing an irregular shape. Finally friction produce detached particles with a more irregular shape for the smallest particles. Indeed reactivity of semolina increases with the diminution of the size.

The shape distribution of semolina in relation to the particle size was also studied by (Saad *et al*., 2011b). The authors determined the elongation (a parameter more used to describe fibers), the circularity (that is similar to the sphericity), the compactness and the convexity. Two semolina fractions were studied < 315 μm and > 315 μm, the authors observed a diminution of convexity from 0.902 to 0.899 and circularity from 1.13 to 1.15 with the augmentation of the size. Differences in these results are subtle contrary to results of this work. Discrepancy could be explained by a different classification of the powder (only two fractions). The apparatus used to take measurements (that was not the same) could also have an influence.

In comparison with other food powders semolina presents subtle differences. Gaiani *et al*., (2011a) studied the shape factors of 35 dairy powders. Authors observed a decrement of the sphericity from 0.88 to 0.55 with the increase of the size from 50 to 450 μm. On the contrary to semolina, convexity values also decrease from 0.91 to 0.75 for the same size evolution. From this comparison it can be observed that tendencies in semolina are clear but subtle.

IV.2.2.4. Bulk composition

The physicochemical bulk composition of raw and sieved semolina is shown in table 43. In these results, a higher content of ashes in fine powders is found (0-160 and 160-250 μm) also a decreasing tendency is observed when particle size increases. For lipids and proteins, an increasing tendency is present with particle size augmentation. Concerning the humidity and carbohydrates no differences were found. Similar values where observed in different wheat flours compositions reported elsewhere (Ocieczek, 2007; Roman-Gutierrez *et al*., 2003). Results are in the same rank of those obtained by Hébrard *et al*., (2003) in raw semolina and fractions, however the authors found a lower content of protein and lipids

related to the increment of particle size. It can be explained by the differences in fractions rank and the fact that differences in the physicochemical composition can be due to several parameters, simple reduction of size and consequent differences in the specific surface, differences in the milling mechanism or a real change on the composition.

Table 43. . Chemical composition (g/100 g dm) of raw semolina and fractions.

Fractions	Ashes %	Proteins %	Lipids %	Humidity %	Total %	Carb.*%
Raw Semolina	0.91 ± 0.02	11.51 ± 0.36	1.52 ± 0.26	12.99 ± 0.05	26.93	73.07
0-160 μm	1.36 ± 0.03	10.62 ± 0.35	0.92 ± 0.18	12.40 ± 0.05	25.30	74.70
160-250 μm	0.94 ± 0.02	11.04 ± 0.2	0.97 ± 0.21	12.63 ± 0.02	25.58	74.42
250-315 μm	0.76 ± 0.01	11.05 ± 0.73	1.25 ± 0.12	12.21 ± 0.01	25.27	74.73
315-400 μm	0.70 ± 0.02	11.13 ± 0.34	1.16 ± 0.13	12.88 ± 0.14	25.87	74.13
400-500 μm	0.70 ± 0.03	11.92 ± 0.61	1.73 ± 0.22	11.76 ± 0.00	26.11	73.89

IV.2.2.5. X-ray photoelectron spectroscopy (XPS)

The surfaces composition of raw and sieved semolina was determined by XPS. Elemental composition of C, O and N amounted to at least 99.5% of all detected elements. The XPS survey scans of principal components were analyzed and decomposed to obtain chemical functions (Rouxhet *et al*., 2008; Saad *et al*., 2011a). The peak decomposition was performed according to a model for biochemical compounds (Gerin *et al*., 1995). The functions formed by molecules can be deduced from the binding energy registered. The carbon, oxygen and nitrogen decomposition of raw semolina is shown in figure 58 as an example. The functions formed by molecules can be deduced from the binding energy registered.

The C_{1s} peak was decomposed into 4 peaks. The peak at 284.6 eV is attributed to C making a single bond with C or H (C-C, C-H) found in lipid or protein side chains. The peak at 286.0 eV is related to C single bonded to O or N (C-O, C-N). This kind of bonds can be found in alcohol, amine or amide functions in proteins. The peak detected at 287.5 eV is attributed to C making two single bonds or one double bond with O (O-C-O, O=C-N, O=C-O) present in acetal and hemiacetal functions in polysaccharides or in amide functions in proteins. The peak at 288.6 eV is attributed to C making one double or simple bond with O (O=C-OH, O=C-OR) in ester and carboxyl functions in proteins and cell-wall polysaccharides. The O_{s1} peak was decomposed into 3 sub-peaks. The peak at 531.2 eV is attributed to O doubly bound to C (O=CO, O=C-N, O=C-OH) these bonds correspond to amide, ester and carboxyl in proteins and cell-wall polysaccharides. The peak at 532.5 eV is attributed to O making single bonds with C (C-OH) in alcohol and (C-O-C) in acetal and

hemiacetical functions in polysaccharides. The peak at 533.6 eV is attributed to O bond with hydrogen in water (H2O).

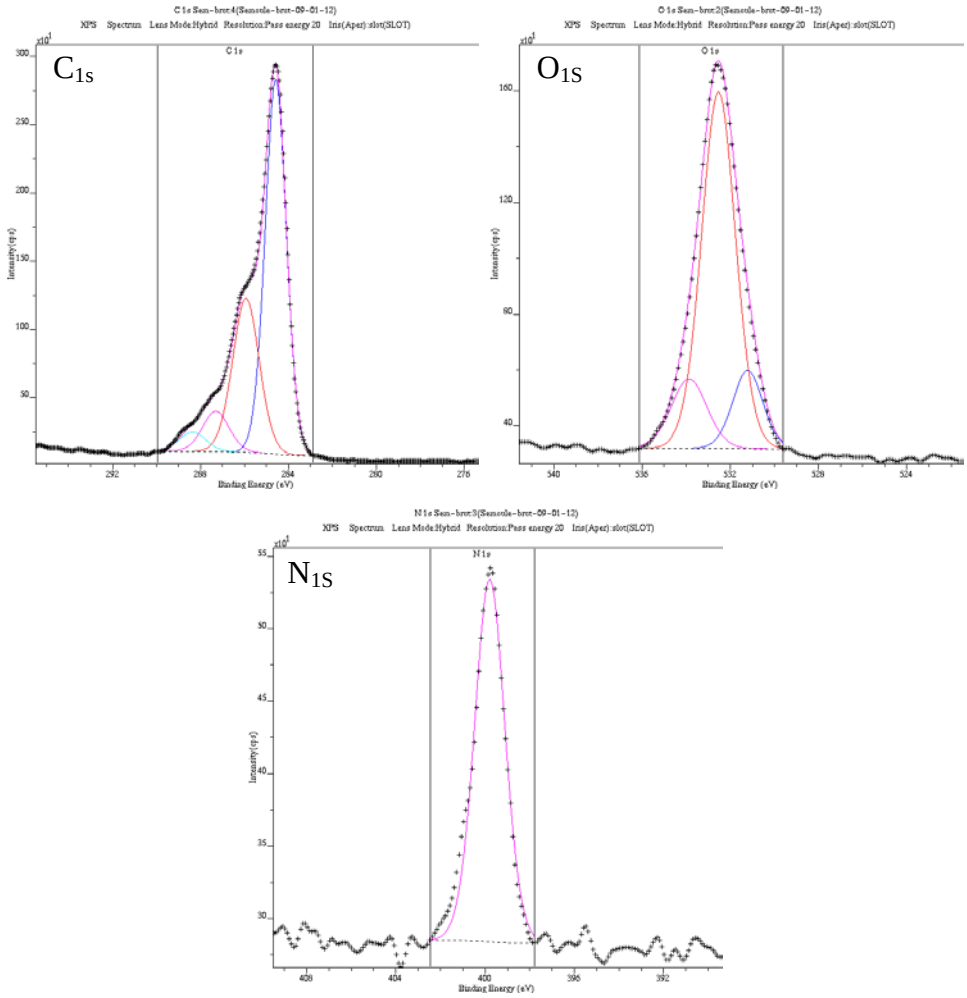

Figure 58. Peak decomposition for C1s (left), O1s (center) and N1s (right) in raw semolina.

N_{1s} peak was not decomposed because the possibilities of decomposition were not clear. The registered peak was attributed to uncharged N in amine (C-$\underline{N}H_2$) or in amide (O=C $\underline{N}H_2$, O= $\underline{N}$H-C). N is a component exclusively attributed to protein molecules.

Atomic abundances of elements (C, N and O) at the surface of the components samples expressed in atomic concentration (%) are presented in table 44.

As expected raw semolina atomic concentrations of C, N and O are an average of the fractions results. For the fractions, C concentration present similar results for middle sizes (160-250, 250-315 and 315-400 µm), but some differences are observed in the extreme fractions presenting the smallest value for 0-160 µm and the biggest value for the fraction 400-500 µm. When peaks are decomposed, differences are not really clear for the smallest

fraction (0-160 μm) however the biggest fraction (400-500 μm) shows a higher intensity for the peak at 284.6 and 288.6 with a consequent reduction of peaks at 286.0 and 287.5. This could be interpreted as a higher presence of lipids in the surface of these fractions.

Table 44. Surface atomic composition by XPS of raw semolina and sieved fractions.

Binding Energy (eV)	**Functions**	**Atomic Concentration % Semolina**					
		Raw	**0-160**	**160-250**	**250-315**	**315-400**	**400-500**
133.0	P	-	0.19	0.22	0.20	0.18	0.21
163.0	S	-	0.21	0.15	0.14	0.13	0.14
284.6	**C**	**80.51**	**78.72**	**79.69**	**80.85**	**79.35**	**82.08**
284.6	C-C, C-H	58.17	63.58	62.17	61.01	63.62	65.03
286.0	C-O, C-N	30.14	26.15	26.77	26.59	26.39	25.09
287.5	O-C-O, C=O	7.90	7.75	6.80	10.18	7.29	6.40
288.6	O-C=OH, O=C-OR	3.80	2.52	4.26	2.21	2.70	3.48
399.6	**N**	**3.5**	**3.96**	**3.56**	**3.31**	**3.44**	**2.7**
399.7	NH, NH2	100	100	100	100	100	100
532.5	**O**	**15.99**	**16.91**	**16.38**	**15.5**	**16.9**	**14.87**
531.2	O=C	13.97	15.66	14.31	15.16	14.13	10.48
532.5	O-H, O-C	71.34	75.29	73.58	71.80	74.48	76.66
533.6	H_2O	14.69	9.05	12.12	13.03	11.39	12.86

N concentration presents a clear tendency, the concentration of the peak decrease with the size of the particles. N is directly related with protein content; hence, a diminution of lipids could explain the augmentation in proteins.

Finally in the oxygen concentration we can observe similar results for all the fractions except for 400-500 μm that presents the smallest concentration. However, after peaks decomposition, the peak 531.2 eV for 0-160 μm fraction shows the strongest value whereas 400-500 μm fraction the presents the smallest concentration. These results reflect a more significant presence of hydrophobic bonds in the small fraction (0-160 μm) opposed to the 400-500 μm fraction that reflects the lower presence of hydrophobic bonds (hydrophobic bonds can be related to lipids or non-damage starch) (Saad *et al.*, 2011a). Consequently surface of the particles in the 400-500 μm fraction might contain either less lipids or more damaged starch. The peaks at 232.5 eV values are more dispersed for all the fractions but the 400-500 μm fraction presents a clearest difference presenting the highest value. The bonds at

this binding energy are related to polysaccharides. This could confirm a more significant presence of damaged starch at the surface. These results are in accordance with the microscopy observations (figure 54), where a higher quantity of broken starch is observed in 400-500 μm fraction.

The surface of sieved semolina is similar in the three middle fractions; differences are observed only in the extreme fractions (0-160 and 400-500 μm). Surface composition does not seem to follow the same tendency as the bulk composition (table 43). The bulk composition presents a clear augmentation of lipids and proteins concentrations with the increase of size. Consequently the structure of the surface is probably not related to the bulk composition.

Saad *et al*., (2011a) studied the surface composition of sieved wheat flours but any tendency was identified. The surface composition did not present diversity in XPS values even when the bulk composition was supposed to be different. On the other hand, a grinding process permitted the authors to obtain different particle sizes with a similar bulk composition. In this case differences in the surface were identified. An evolution related to the diminution of the size due to the grinding process was registered for C from 77.4 to 74.8%, for O from 17.9 to 19.6% and for N from 4.52 to 5.22% in a flour obtained from grinding of ”Impression” wheat variety. Results agree with those obtained for the same authors from commercial flour (Saad *et al*., 2009). They obtained values for C from 77.4 to 74.7%, for O from 18.0 to 19.3% and for N from 4.1 to 5.5%. Authors concluded that differences in semolina surface are related to the grinding process.

As complementary information, it is possible to deduce surface composition from atomic concentration Saad *et al*., (2011a). Protein (gluten), carbohydrates (starch) and lipids (oil) at the surface was estimated after feeding the equation system presented in equation 8, 9 and 10**.** To feed the equation system the atomic composition of pure components is necessary. These values were measured by Saad *et al*., (2011a). The model considers that a linear relation of the components (C, O and N) is equal to 1 or 100%. The values were then recalculated to adjust the addition of the values to 100%. Values are presented in table 45. The adjusted values of pure components fed the equation system from the first expression of the equations; the second expression is fed with the atomic composition of the studied powder (semolina).

Table 45. XPS atomic composition of semolina pure components1 (above), data adjusted to 100% as considered by model (below).

	Gluten	Starch	Oil
Original values			
C (A%)	75.80	66.40	77.70
O (A%)	16.50	32.70	16.60
N (A%)	7.40	0.70	1.30
Si (A%)	0.19	0.00	0.00
S (A%)	0.00	0.27	0.00
P (A%)	0.00	0.00	0.24
Adjusted to 100%			
C (%)	76.03	66.7	80.7
O (%)	16.55	32.6	17.2
N (%)	7.42	0.7	2.1
Other paramters			
O/C ratio	0.22	0.49	0.21

The method adapted by Saad *et al*., (2011a) demonstrated some inaccuracies, consequently the O/C ratio was calculated in order to complement the information. The O/C ratio seems to be characteristic of each component and it can help to deduce the composition at the surface. This parameter was calculated for pure components and it is presented in table 45. After feeding of the equation system, proteins (gluten), carbohydrates (starch) and lipids (oil) percentage was deduced and is shown in table 46 as well as the O/C ratio.

Table 46. Surface composition of raw and sieved semolina deduced from XPS analysis by Saad *et al*. (2011a) method (above) and estimated calculus from N, P, O and C XPS peaks.

Semolina	Raw	0-160 μm	160-250 μm	250-315 μm	315-400 μm	400-500 μm
Proteins (%)	24.84	35.34	26.87	20.66	25.41	8.07
Carbohydrates (%)	-7.01	-0.09	-3.97	-10.00	-0.72	-14.65
Lipids (%)	82.17	64.33	76.72	89.00	74.99	106.22
O/C ratio	0.20	0.21	0.21	0.19	0.21	0.18

Surface composition presents some aberrant values for carbohydrates and lipids calculation. Negative values or values exceeding 100% are obtained, these values can be interpreted as a low (negative values) or high (values exceeding 100%) content of components. That kind of results (negative values or exceeding 100%), are produced for an interaction of the elements (O, N and C) that is not linear. It is possible that the heterogeneous composition of the semolina particle surface not accomplish this condition, hence the system equation present some deficiencies in the calculus. However it is necessary to make remark

that quantity must not be even near to the real value but results can still estimate the molecules proportion at the surface.

Proteins gave values from 8.07 to 35.34 a tendency is observed; the quantity of proteins decreases with the augmentation of the particle size. Nitrogen is a good marker of proteins; from the three principal components only proteins contain this element, and it can be directly related to the protein content. The content of carbohydrates (negative values) can be interpreted as a very low quantity or even an absence of the component at 10 nanometers below the surface.

Lipids are overrepresented (64.33-106.22%) in comparison to bulk composition in table 44 (0.92-1.73%). To confirm this lipid overrepresentation the O/C ratio was analyzed. Pure components table 45 highlights a difference between starch and the other two components (gluten and oil). The value of the starch ratio is 0.49 whereas the value for protein (gluten) and lipids (oil) are similar (0.22-0.21). If these values are compared to the ratios obtained for raw and sieved semolina, it can be assumed that the influence of the starch is not present in the O/C ratio, hence a surface of protein and lipids is supported, as it is suggested by the equation system.

Finally a tendency is observed in the values obtained for surface composition of semolina. The carbohydrate as well as protein contents decrease with the increment of the particle size whereas the lipids increase. These tendencies are in agreement with the bulk composition for carbohydrates and lipids. However, the proteins present an inverse tendency. This would be due to the augmentation of the lipids at the surface. Consequently these lipids could cover the surface making more difficult the access to the proteins.

On balance, the carbohydrates (starch) seem to not be present at 10 nm at the surface, whereas proteins are found and lipids are overrepresented. These results are similar to those observed by Saad *et al.*, (2011a) and they are also in agreement with dairy powders, whole milk powder presents a surface almost totally cover by lipids (>93 %) for a bulk lipid content of 26 %. In Skim Milk Powder lipids are also overrepresented (~22 %) in comparison with bulk lipid compositions (< 2 %) (Murrieta-Pazos *et al*., 2012a).

IV.2.2.6. Inverse gas chromatography (IGC)

The table 47 gathers the γ_s^d and ΔG_{sp}^a values obtained for three semolina fractions of diameters range 0-160, 315-400, 400-500 µm. These values were an average between the values obtained on two columns and three injections per column.

For a given probe, the γ_s^d values obtained on the different particles size are similar. The surface free energy is then similar for any particle in the powder. These results are in agreement with those found in cotton fibers (Rjiba *et al.*,2007), a vegetal material, as it is semolina.

Table 47. Values of γ_d^s and ΔG_{sp}^a of sieved semolina.

	Probes	Probe Nature	0-160 µm	315-400 µm	400-500 µm
γ_d^s (mJ/m^2)	Alkanes	Linear	39 ± 3	38 ± 2	39 ± 2
ΔG_{sp}^a (kJ/mol)	Chloroform	Acid	10.3 ± 0.3	10.1 ± 0.4	10.0 ± 0.4
	Acetone	Amphoteric	10.8 ± 0.4	8.3 ± 0.2	9.2 ± 1.1
	Ethyl acetate	Amphoteric	4.2 ± 0.2	4.2 ± 0.5	4.0 ± 0.1
	1,4-dioxanne	Basic	5.8 ± 0.2	5.5 ± 0.3	5.5 ± 0.2
	THF	Basic	5.8 ± 0.2	6.0 ± 0.3	5.8 ± 0.4

When the surface is investigated with basic and acid probes, the surface is sensitive to the nature of these probes. On one hand, chloroform and acetone lead to similar ΔG_{sp}^a (~ 10 kJ/mol), on the other hand, the ΔG_{sp}^a obtained with ethylacetate, tetrahydrofuran and 1,4-dioxane are halved (~ 5 kJ/mol). Chloroform and acetone present a higher acid character according to the Gutmann scale (respectively 5.4 and 2.5 kcal/mol for the electron acceptor numbers AN) (table 48). On the contrary the ethylacetate, tetrahydrofuran and 1-4 dioxane, are characterized by higher electron donor numbers (17.1, 20.0 and 14.8 kcal/mol respectively for the donor numbers DN) and consequently present higher basic character.

Table 48. The Gutmann electron acceptor (AN) and donor number (DN) for different polar probes.

Probe	Character	AN (kcal/mol)	DN (kcal/mol)
Chloroform	Acidic	5.4	0.0
Acetone	Amphoteric	2.5	17.0
Ethylacetate	Amphoteric	1.5	17.1
Tetrahydrofuran	Basic	0.5	20.0
1,4-dioxane	Basic	0.0	14.8

The semolina surface has more affinities with the acid probes than with the basic ones. This affinity can be explained by the surface composition observed by XPS. One of the

components on the semolina surface deduced from matrix model was lipids. This deduction is also supported by the functions obtained after peak decomposition where peak 284.6 is attributed to C making a single bond with C or H (C-C, C-H) found in lipid or protein side chains. An example of fatty acid profiles of free lipids extraction in wheat durum (semolina) was determined by Konopka *et al*. (2005). They reported this composition: linoleic acid 58.35 %; oleic acid 20.22 %; palmitic acid 16.9 %; linolenic acid 4.16 %; palmitoleic acid, 0.6 %; stearic acid 0.35 %; and others 0.67 %. From the fatty acid profile, it is observed that the principal components in free fat are unsaturated fatty acids (linoleic and oleic acids). This unsaturation present in the fatty acids has a Lewis basic character; this could explain the affinity of the acid probes observed by IGC to the semolina surface. In addition this affinity was also observed for carbohydrate polymers (cellulose) in cotton fibers (Rjiba *et al.*, 2007). Indeed the structures of sugar polymers such as cellulose (in the case of cotton fibers) or starch (in the case of semolina) contain O-H or C-O-C groups in their structure of Lewis basic character, these groups are detected by XPS in the peak 532.5.

The information about the surface, in terms of energy, permits to understand the surface of semolina particles. Nevertheless, the most interesting information is figured out from the basic and acid probes. Indeed, the nature of the probe may give information about the nature of the components at the surface, consequently the presence of one or some component at the surface can be confirm. Further investigation about pure components (starch, gluten and lipids), is necessary in order to couple the information obtained by the basic and acid probes. The development of this technique in flours is still limited because of their thermal sensitivity.

IV.2.2.7. Capillary rise (CR)

Contact angles calculated with Hexane, Ethanol and 1,4-Dioxane as wetting liquid probes for raw semolina, the size fractions and pure components are presented in table 49.

The properties of the wetting liquids used to measure the contact angle are shown in table 50**.** From this data (angles and properties of the liquids), the polar and non-polar surface forces were calculated table 51.

Table 49. Contact angles obtained for raw semolina, fractions and pure components

	Contact Angles (º)		
	Hexane	Ethanol	1,4-Dioxane
Semolina			
Raw	67.9	45.7	64.4
0-160 μm	41.0	43.3	56.0
160-250 μm	23.7	42.2	65.1
250-360 μm	36.6	55.5	67.0
315-400 μm	51.4	44.2	56.4
400-500 μm	4.9	0.0	62.8
Pure Components			
Starch	13.5	50.5	0.0
Gluten	54.4	34.6	29.0

Table 50. Dispersive and polar surface energy components of solvents.

	γ^d(mJ/m^2)	γ^p(mJ/m^2)	γ(mJ/m^2)
Ethanol	17.5	4.6	22.1
Hexane	18.4	0.0	18.4
1,4 Dioxane	33.0	0.0	33.0

Table 51. Dispersive, polar and total forces.

	Surface Energy (mJ/m^2)					
	Ethanol-Hexane			Ethanol-Dioxane		
	γ^d	γ^p	γ	γ^d	γ^p	γ
Semolina						
0-160 μm	20.83	0.04	20.86	20.83	0.34	21.17
160-250 μm	21.14	0.06	21.21	21.14	0.06	21.20
250-315 μm	17.12	0.12	17.24	17.12	0.23	17.35
315-400 μm	20.57	0.03	20.60	20.57	0.40	20.97
400-500 μm	27.91	0.03	27.93	27.91	0.03	27.93
Raw	20.13	0.02	20.15	20.13	0.08	20.21
Pure Components						
Starch	18.68	0.34	19.01	18.68	-0.02	18.66
Gluten	23.19	0.02	23.21	23.19	-0.05	23.15

Dispersive forces (non-polar) are clearly stronger than polar forces. It can be explained by the low polar component of the liquids. Consequently the polar-polar interaction cannot be totally estimated. For a better measure of the polar component, it is necessary to use a higher polar liquid, unfortunately the only liquid with a very high polar component is water (51.0 and 21.8 polar and dispersive components respectively) (Galet *et al*., 2004).

The dispersive forces of raw semolina result in an average of the fractions values. The fractions are similar except for the 400-500 μm fraction, showing a stronger dispersive force. Polar forces are similar. Indeed the results do not permit a differentiation between different size fractions.

In the literature there is no information about surface free energy in semolina or wheat products. Some data is available for materials studied as a surface and not as a powder. Dispersive-polar components (in mJ/m2) are respectively: 28.8-19.2 for wood, 23.1-15.1 for human skin, 32.0-1.1 for polyethylene and 25.4-0 for paraffin wax (Nguyen & Johns, 1978). Hence a better interaction with external constraints as wetting liquids can be deduced from the free energy. By capillary rise the only food powder studied is cocoa (15.9-11.4 mJ/m2), Dispersive constant agrees with semolina but a higher value of polar component is observed. Cocoa is not soluble in water, consequently water was used as polar probe obtaining higher values of the polar component.

Differences between dispersive values in IGC and CR, are due to the differences techniques operation. IGC retention time is conditioned by the residence time visiting the more energetic points at the surface, in the opposite CR is a technique that average the dispersive forces in the whole surface powder, consequently, the dispersive forces value obtained by IGC is higher.

The dispersive forces of raw semolina result in an average of the values of the fractions. The fractions present similar values except for the fraction 400-500 μm with the stronger dispersive force value. Polar results present very low values, and there is no difference between the raw powder and the size fractions. These results do not permit a differentiation between the different size fractions.

In the literature there is no information about surface free energy in semolina or wheat products. Nevertheless some data is available for some material studied as a surface and not in a powder. Dispersive and polar components (in mJ/m2) are respectively: 28.8 and 19.2 for wood, 23.1 and 15.1 for human skin, 32.0 and 1.1 for polyethylene and 25.4 and 0 for paraffin wax (Nguyen & Johns, 1978). By capillary rise the only food powder studied is cocoa where the free surface energy is 15.9 and 11.4 mJ/m^2 for dispersive and polar components

respectively, in this study water was used as polar probe, that is why a high value of polar component was obtained. The polar component depends on the polarity of the probe.

IV.2.2.8. Characterization of reactive powders

After characterization of reactive powders, a protocol is proposed in figure 59.

The separation in size of the powder in different fractions allows determination of the particularities of the powder through the evolution of the particle size. Middle sizes fractions (160-250, 250-315 and 315-400 μm) have similar structures and surface properties. The extremes of the powder (0-160 and 400-500 μm) present the particles with a more reactive morphology and subtle differences in the surface composition; these differences could affect the interaction with external constraint. A greater or lesser reactivity would be conditioned to the constraint nature. The 400-500 μm fraction presents clearest differences than smallest particles but it correspond only to the 1.7%, their properties can be easily masked by the ensemble of the powder than in the case of 0-160 μm fraction, which correspond to the 18.8%.

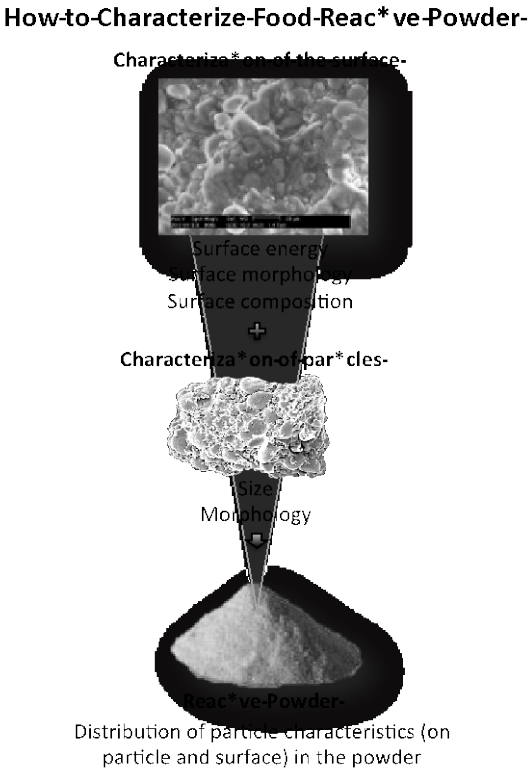

Figure 59. Characterization of reactive powders (Protocole)

Surface free energy proportioned by IGC and capillary rise give useful information to know how reactive is the surface in terms of molecular interaction, this reactivity is the same for all the particle sizes. In food powders other data is almost inexistent not having a reference to deduce a greater or lesser reactivity. Further investigation is necessary to enlarge database.

Results proportioned by IGC and capillary rise give useful information. The surface free energy is the same for any particle size. Therefore the surface free energy in the whole powder is the same. Differences between dispersive values in IGC and CR, are due to the differences in the operation of both techniques. IGC retention time is conditioned by the residence time visiting the more energetic points at the surface, in the opposite CR is a technique that average the dispersive forces in the whole surface powder, consequently, the dispersive forces value obtained by IGC is higher. Obtaining of this data was extremely complicated. IGC and CR techniques are not completely adapted to food materials.

The surface free energy is an interesting parameter when it is compared with other results. However in food powders other data is almost inexistent. Further investigation is necessary to adapt the models applied and analyze the effect of operational conditions on food powders in order to obtain more reliable results as well as a daase allowing the comparison of properties.

IV.2.3. CONTRIBUTIONS GRADIENT STUDY AND CHARACTERIZATION OF REACTIVE POWDERS TO THE SURFACE CHARACTERIZATION KNOWLEDGE IN FOOD POWDER.

In the first section, the study permit to confirm that the granulated milk powders present a similar surface composition with standard powders. The composition of the lipids is similar at the surface and the core. However, the migration of the short chain fatty acids to the surface is a little but clear tendency.

In the second section, the adaptation of the powders to the free energies techniques (GCI and CR) was very complicated. Further investigations are necessary to adapt completely these techniques to semolina and then to other food powders. However, new information about the surface was obtained. A development of the free energy data is necessary for food powders and could permit the comparison with other particles. In addition, these properties could be related to the particle-particle and particle-extern constraints interactions. A key point is the study of the powder with basic and acid probes by GCI. These results appear to

give interesting information about the surface component nature. Finally, it was demonstrated that coupling different surface techniques as the XPS, CGI and CR, permit to integrate results and to figure out interesting theories.

It is important to insist on the originality of the techniques developed in this thesis work, especially in this section. The adaptation of these techniques is really complex and difficult to figure out. Nevertheless, a little step to extend the knowledge of the surface food powders was given.

IV.3. MICROSTRUCTURAL APPROACH: REACTIVITY OF FOOD POWDERS INTERACTING WITH WATER AND SURFACE MODIFICATION BY DRIED COATING.

In this third subchapter the modification of the surface microstructure was studied and two external constraints were evaluated, i) the surface hydration with water, ii) the surface coating with pure components.

In the first part, the reactivity of the particles was studied in presence of water. As it was mentioned in the bibliographic study, the reactivity is done by the powder properties but these powder properties take importance when interact with external constraints. In the food powders, the most common constraint is water. Indeed, most of the characteristics studied in food powders are related to the interaction with water. The main objective of this work is the study of the particles surface. Consequently the interaction with water is done by humidification of the surface (low quantities of water) and not by hydration (high quantities of water).

The surface structure of standard whole milk powder and standard skim milk powder were characterized by classic microscopy (SEM) and Atomic Force Microscopy (AFM). Hydration of the powders was then studied by DVS and the evolution of the surface structure at each relative humidity was followed by SEM. Lactose crystallization was then observed at the surface of the particles in some relative humilities. Information about the nature of the surface is related to the humidity effect with the help of the BET and GAB model. The innovative point of this study was to calculate a dynamic diffusion coefficient. It was done by measuring the particle size at each relative humidity. To do it, the powders were conditioned at different relative humidities in hermetic recipients with saturated salts solutions.

This study is already published: Murrieta-Pazos I., Gaiani C., Galet L., Cuq B., Desobry S. and Scher J., 2011. Comparative study of particle structure evolution during water sorption: Skim and whole milk powders. *Colloids and Surfaces B: Biointerfaces* 87, 1–10. The results and discussion of this publication were integrated to this manuscript in the section IV.3.1.

In the second part, another study of surface evolution after hydration was done, this time in sieved semolina. The same procedure was followed. The powders were conditioned at different relative humilities; then observed by SEM and measured in size. These data were

used to calculate the dynamic coefficient diffusion. The sorption isotherms were fitted to the G.A.B and Y & N models.

This part was presented in the 7ème Colloque Science et Technologie des Poudres, with a favorable recommendation of publication in the special edition of Powder Technology: Murrieta-Pazos I., Patry S., Galet L., Gaiani C. and Scher J. Comparative study of the evolution of particle structure during water sorption in different size classes of durum wheat semolina. *Special volume of Powder Technology*. Submitted. The results and discussion of this publication were integrated to this manuscript in the section IV.3.2.

In the third part of this subchapter (section IV.3.3.), the modification of the semolina surface was developed by dry coating. This is another innovative proposition to modified the surface of food particles. The main goal of this modification is to add some extra-molecules of the pure components (starch, gluten or arabinoxylan), with extra-molecules at the surface; the effect of one of the components being studied.

This work was dedicated to the adaptation of the technique to food powders, different conditions were tested and the results obtained are presented. The optimal conditions were not obtained, however the effect of the surface modification was measured by GCI. These results are not published, since further investigation is necessary. However, the first steps to develop this procedure are discussed here.

IV.3.1. COMPARATIVE STUDY OF PARTICLE STRUCTURE EVOLUTION DURING WATER SORPTION: SKIM AND WHOLE MILK POWDERS

IV.3.1.1. Surface and size characterization of powders freshly manufactured

Whole milk and skim milk powders were observed by SEM. Due to the particle sieving, the particle size was relatively homogeneous (figure 60 1A and figure 60 2A). As observed in figure 60 1B and 2B the average size of each sample was 50 m. Nevertheless, the surface microstructure of the powders was totally different depending on the powder composition (figure 60 1C and 2C). WMP particles presented a regular surface whereas SMP particles were characterized by a “brain type” surface with some deep and shallow folds. The lactose was in an amorphous state as no sharp crystals were noticed for each powder (and confirmed by DSC, data not shown). All these features were typical for fresh whole and skim milk powders (Wrolstad *et al*., 2004).

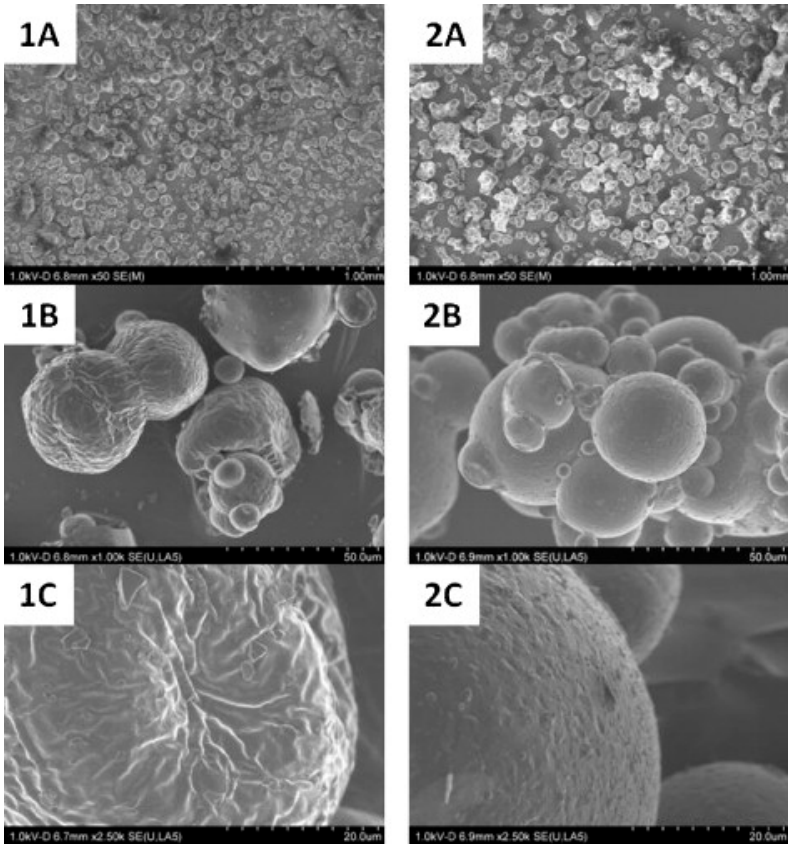

Figure 60. Scanning electron microscopy of skim milk powder (1) and whole milk powder (2). A: ×50, B: ×1000, C: ×2500.

Concurrently, AFM was performed on the same powders to better analyze the particles surfaces (figure 61). Up to now, AFM imaging in tapping-mode has never been realized on dairy powders.

The AFM images obtained by 3-D projection were in total agreement with those obtained by SEM. In addition, the average surface roughness (Ra) was determined and was respectively found around 306 nm for SMP and 146 nm for WMP for a definite surface area (10 × 10 μm). The smoother visual aspect of WMP surface in comparison with SMP surface (a "brain" type surface) was associated with the lower Ra value. The surface composition was determined by XPS with the matrix formula develop in detail for milk powders (Fäldt & Bergenståhl, 1994; Gaiani *et al*., 2006, 2010; Kim *et al*., 2002). It was measured that the surface of WMP was composed at 91.8% of fat, 7.2% of proteins and 0.8% of lactose.

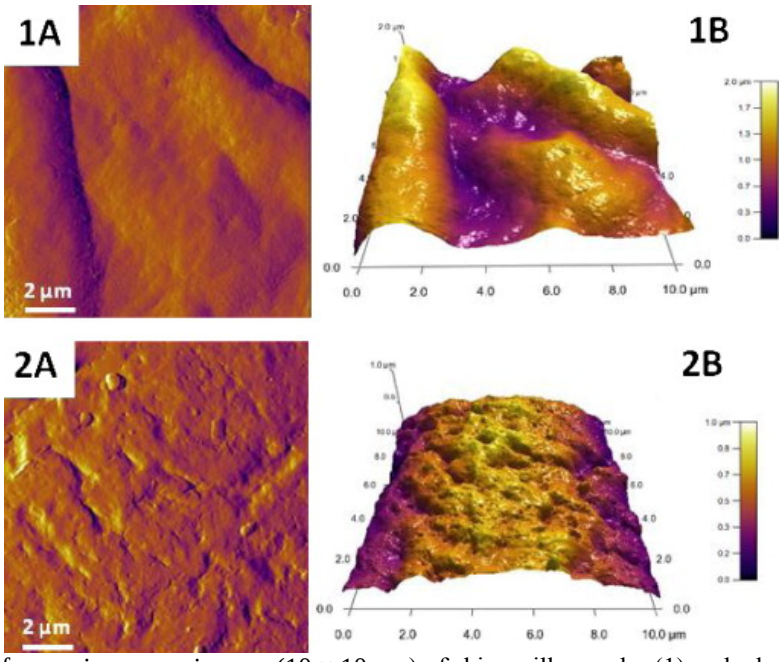

Figure 61. Atomic force microscopy images (10 × 10 µm) of skim milk powder (1) and whole milk powder (2) at high resolution (A) and the 3D projection (B).

The SMP surface presented more proteins and lactose at the surface (45.8% and 30.8% respectively) and less fat (22.3%). Trace minerals were measured at the surface of each powder. These surface compositions were in total agreement with others studies done by XPS on milk powders (Kim *et al.*, 2002, 2009c). The over-representation of fat at the surface in comparison with the bulk composition of the powders is now generally accepted and well understood (Gaiani *et al.*, 2009, 2010; Kentish *et al.*, 2005; Kim *et al.*, 2009b). It is postulated that, during the spray drying of fat-containing materials (e.g. whole milk) larger fat globules are preferentially present at the surface of droplets and so fat appears in high concentration on the powder surface (Kim *et al.*, 2009b). In addition, during spray drying, there is a further increase in the amount of fat probably due to segregation of components within the drying (Gaiani *et al.*, 2010). It is assumed that, even when fat is present at low concentrations (e.g. skim milk) in the milk droplet, residual fat may be preferentially present at the air/droplet interface, and thus may appears at relatively high concentration on the powder surface after complete drying (Gaiani *et al.*, 2009; Kim *et al.*, 2003; Nijdam & Langrish, 2006). This phenomenon may explain the presence of 22% fat at the surface of SMP whereas the particle bulk was composed of only 1.5%. In the presence of surface-active components (such as proteins), it appears that this component accumulates at the surface of a milk droplet/particle at the expense of lactose during drying (M. Jayasundera *et al.*, 2009; Kim *et al.*, 2002; Özkan, Walisinghe, & Chen, 2002; Shrestha *et al.*, 2007). Indeed, only 30% of lactose was observed at the surface of SMP instead of 54% in the bulk. In complement to XPS, EDX analyses were

performed. These two techniques were for the first time coupled to analyze the surface of dairy powders at different deepness. Therefore, EDX analyses were performed to evaluate the surface at 1 m depth whereas XPS was operating at 5–10 nm depth.

Table 52. Composition (%) of milk powders: bulk composition, surface composition calculated from XPS analyses (≈5 nm) and surface composition calculated from EDX (≈1 µm). Mean of at least two independent analyses.

	Lactose	Proteins	Lipids	Minerals	Water
Bulk composition (%)					
Skim milk powder	34.1 ± 0.2	53.9 ± 0.3	1.5 ± 0.0	6.5 ± 0.0	4.0 ± 0.1
Whole milk powder	25.2 ± 0.3	38.8 ± 0.1	26.2 ± 0.1	5.0 ± 0.5	3.8 ± 0.1
First 5 nm composition from XPS (%)					
Skim milk powder	45.8 ± 1.4	30.8 ± 1.2	22.3 ± 1.1	1.1 ± 0.1	–
Whole milk powder	7.2 ± 0.5	0.8 ± 0.1	91.8 ± 2.1	0.2 ± 0.0	–
First 1 µm composition from EDX (%)					
Skim milk powder	34.0 ± 1.8	16.8 ± 0.8	46.4 ± 2.3	2.8 ± 0.6	–
Whole milk powder	25.8 ± 0.9	13.7 ± 1.3	58.6 ± 2.8	1.9 ± 0.4	–

It was observed in table 52 that under the surface established by XPS, the WMP presented proteins (25.8%), lactose (13.7%), lipids (58.6%) and minerals (1.9%). In comparison with the first 5 nm, EDX measurements suggested that the surface of WMP may be externally covered by a thin layer of fat (observed by XPS) with a matrix of proteins, lactose and minerals under this layer. For SMP, EDX measures gave the following percentages: proteins (34.0%), lactose (16.8%), lipids (46.6%) and minerals (2.8%). Contrary to WMP, the lipids were more present in the first micrometer layer in comparison with the five first nanometers. These results may be explained by the dominance of proteins at the surface (more surfactant); more fat being located just under. For each powder, minerals were more located in the first 5 nm.

IV.3.1.2. Effect of water uptake on dairy powder structure and particle size

a) Powder structure

Each powder was introduced in saturated atmospheres during 4 days allowing water exchanges between the powder of low water activity (a_w) and the relative humidity of the surrounding air. SEM was performed on powders equilibrated at 11 aw ranging between 0.11 and 0.97. For WMP, figure 62 indicates that some changes in surface structure with relative humidity occurred.

Between aw = 0.11 and 0.33, the surface was relatively smooth and regular. From aw = 0.43, an irregular surface appears corresponding to lactose crystals formation. It was assumed that crystals are localized just under the surface. As reported previously (Fäldt & Bergenståhl, 1996b; Özkan *et al*., 2002) and in agreement with the XPS results (Table 52), it was not possible to observe sharp lactose crystals at the surface of WMP certainly due to the fact that the surface was mainly covered with a layer of fat. At higher aw values, lactose crystals were more present but still localized under the surface. Surface evolution of SMP with the relative humidity was totally different (figure 63). A substantial amount of needle like lactose crystals was observed on the surface, which confirmed that the lactose was transformed from the rubbery state to the crystalline state around a relative humidity of 54%. Then, the number of dents at the particle surface increased regularly from aw = 0.54 until 0.75. The relationship between the extent of crystallization and relative humidity was found parabolic with the maximum crystallization at a relative humidity around 0.7 (Jouppila *et al*., 1997). Nevertheless, these assumptions are not obvious on our SEM images.

In freshly spray-dried milk powders (figure 60) and at low relative humidity (figure 62 and figure 63) lactose was in the metastable amorphous state. In this state, lactose is hygroscopic and forms a continuous matrix containing embedded fat globules, protein, minerals and air vacuoles. In contact to a high relative humidity and/or an increased temperature, the amorphous state present in the powder may progress into a stable crystalline state. Moreover, previous research has shown that crystallization of lactose may be delayed in the presence of proteins (Hogan & O'Callaghan, 2010; Nasirpour *et al*., 2007), preferential sorption of water by non-amorphous constituents was found to delay the rate at which lactose endured a change from the glassy to the rubbery form (Hogan & O'Callaghan, 2010). It may also be the case with WMP and SMP (figure 62 and figure 63). In SMP, the total protein content was higher (table 52) and the presence of crystal was observed for slightly higher relative humidity than WMP. Hypothesis for this delay was also supported by the fact that proteins may significantly lower the availability of water for plasticization and crystallization of lactose (Hogan & O'Callaghan, 2010; Shrestha *et al*., 2007).

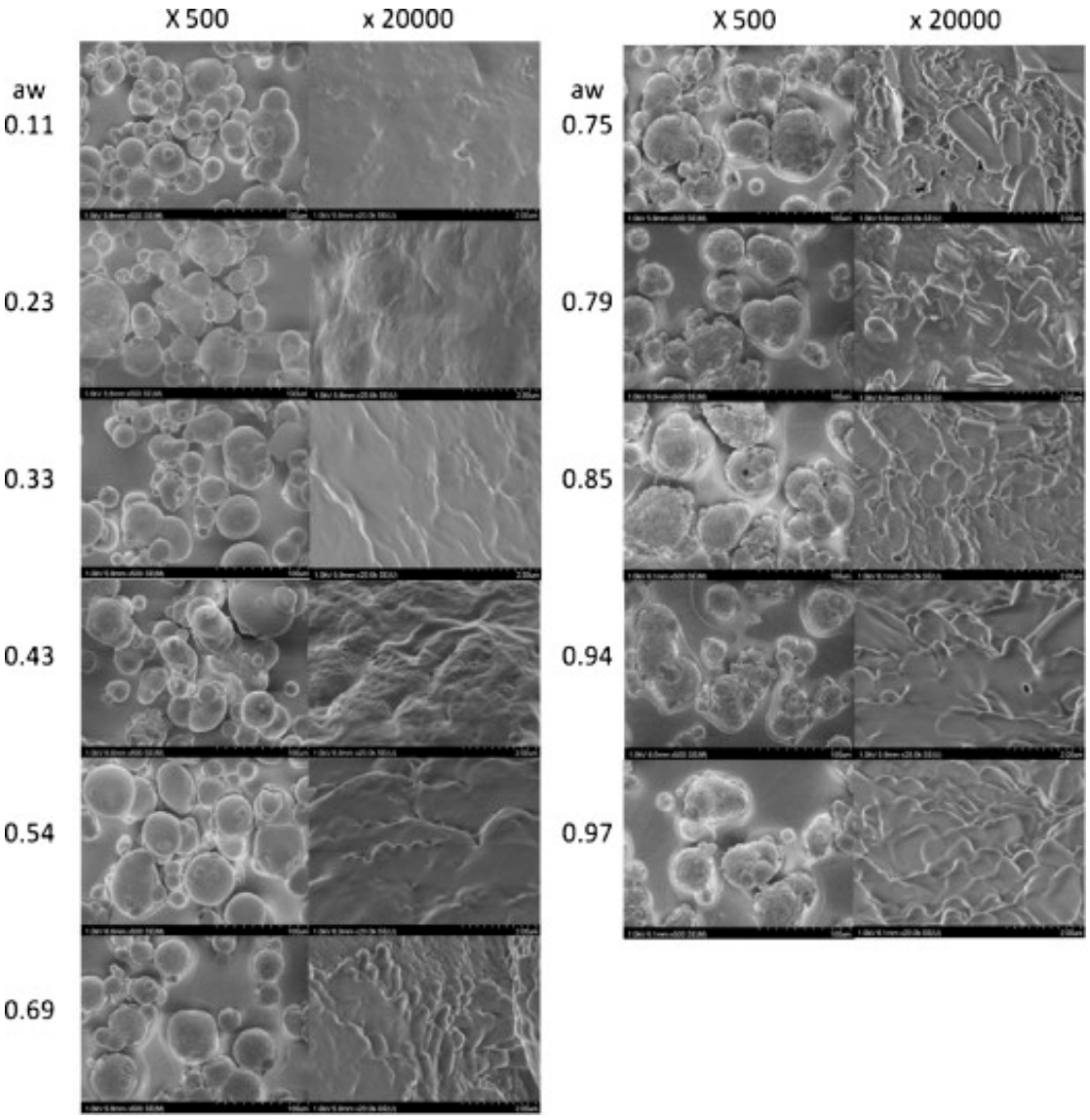

Figure 62. Surface characterization of whole milk particles observed by scanning electron microscopy at variable relative humidity (from 0.11 to 0.97).

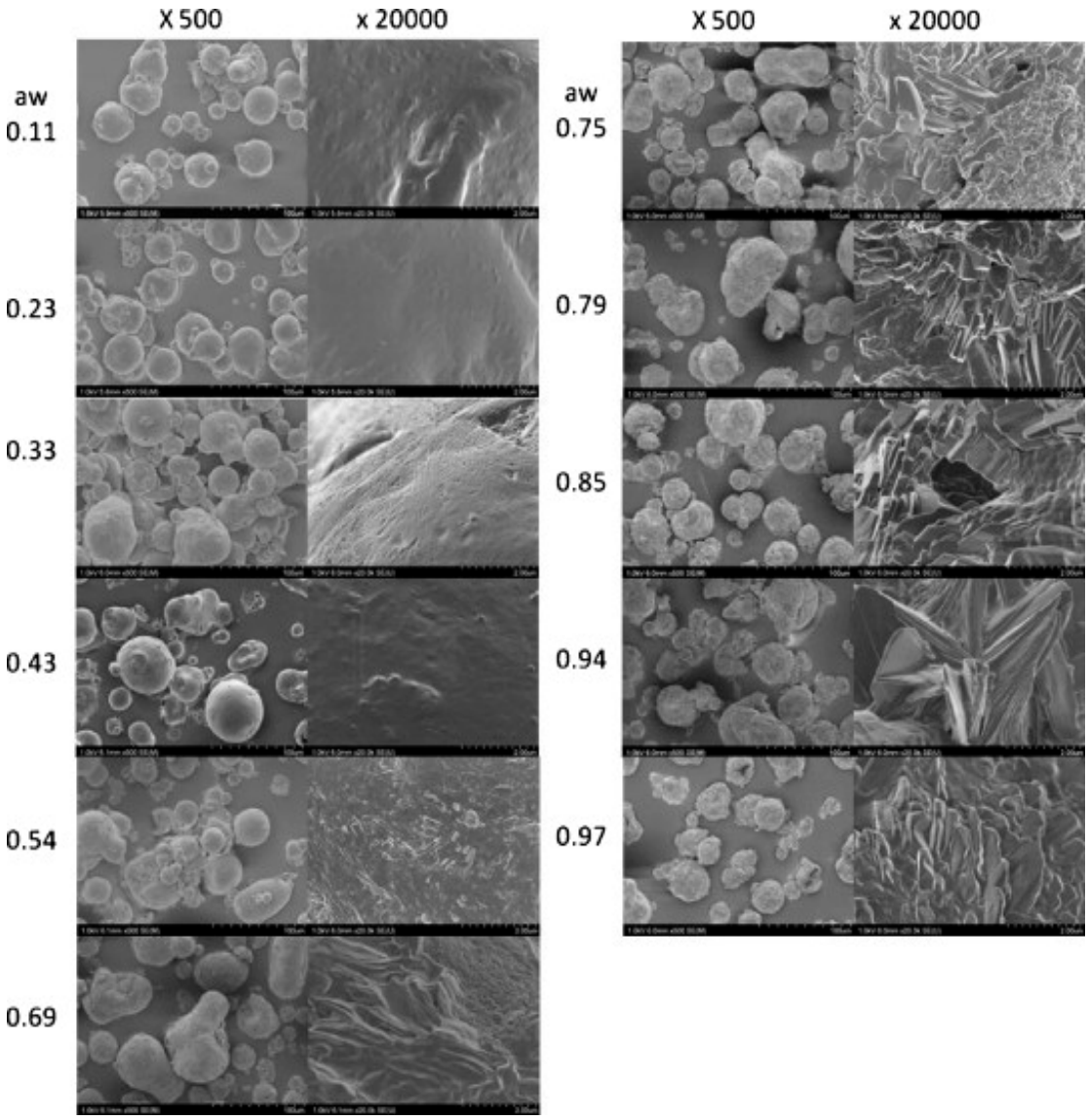

Figure 63. Surface characterization of skim milk particles observed by scanning electron microscopy at variable relative humidity (from 0.11 to 0.97).

c) Particle size

Particle size was followed during water uptake for WMP and SMP (figure 64).

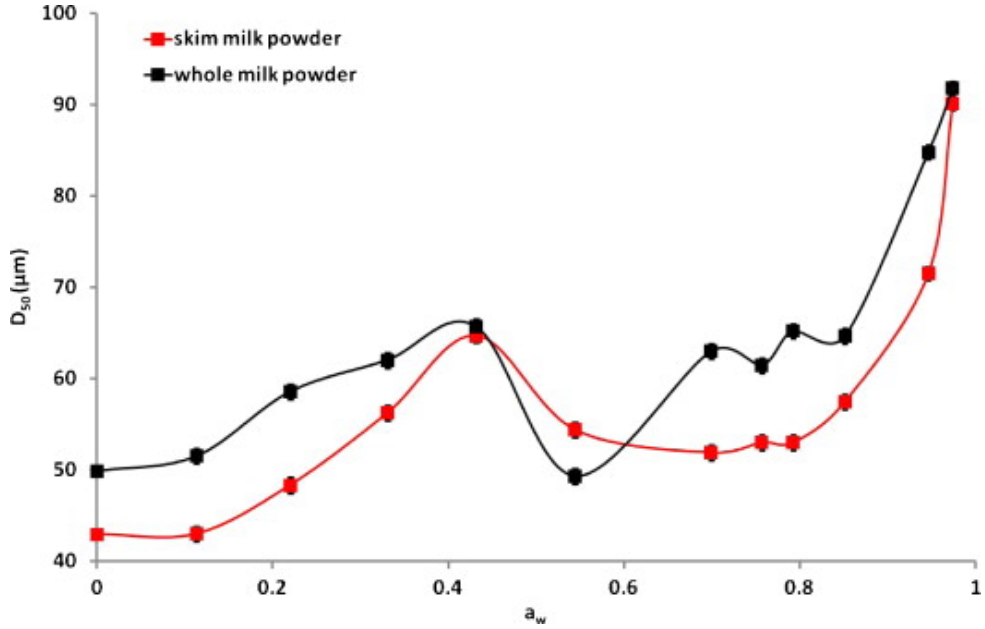

Figure 64. Evolution of particle size (d_{50}, µm) at 11 different a_w (from 0.11 to 0.97) for skim and whole milk powders determined with a Malvern apparatus. Mean of three independent analyses.

First, a significant size increase was observed for each powder between 11% and 43% RH (figure 64). Up to 43% RH, the d50 increases may be attributed to particle swelling due to water migration into the amorphous molecular matrix. Then, a particle size decrease was found around 54% RH and may be explain by the collapse of the amorphous matrix (lactose/proteins/lipids) triggered by crystallization of lactose. This relative humidity was well correlated with the apparition of crystals on microscopy images (figure 62 and figure 63). Finally, the particle size increases strongly from 54% RH. This phase, related to powder caking was already strongly documented (Fitzpatrick *et al.*, 2007; Hogan & O'Callaghan, 2010; Mathlouthi & Rogé, 2003; Nijdam & Langrish, 2006; Shrestha *et al.*, 2007; Silalai & Roos, 2010). For WMP, the caking may be mainly attributed to the presence of fat at the surface even if significant caking has been observed principally in powders containing a total fat content of at least 40% (Foster *et al.*, 2005). For SMP, lactose may be responsible of the caking phenomena even if lactose under its crystalline form is less sensitive to caking than amorphous lactose (Palzer, 2010).

IV.3.1.3. Water sorption isotherms

Kinetic data obtained during water adsorption of SMP and WMP at 20 ◦ C are given in figure 65. Extend of hydration was the lowest for whole milk powder particularly at high RH. Indeed, fat in whole milk powder is not a water-absorbing component. Consequently fat containing samples exhibit little moisture sorption (Palzer, 2010). If the moisture content was calculated on a non-fat basis, the isotherms of SMP and WMP are almost similar which was also observed in other studies (Foster *et al*., 2005; Jouppila & Roos, 1994; Lin *et al*., 2005). In agreement with electron microscopy images, lactose crystallization was observed. As crystalline form has a lower water capacity than amorphous form (Palzer, 2010), water is liberated and is characterized by a decrease in the sorption curve at around 50% RH.

The BET monolayer moisture content for SMP and WMP was calculated at 4.45 and 2.44 g 100 g^{-1} dry solid respectively (figure 66). These values were in agreement with the literature and are dependent of the powder chemical, composition, the temperature (Palzer, 2010).

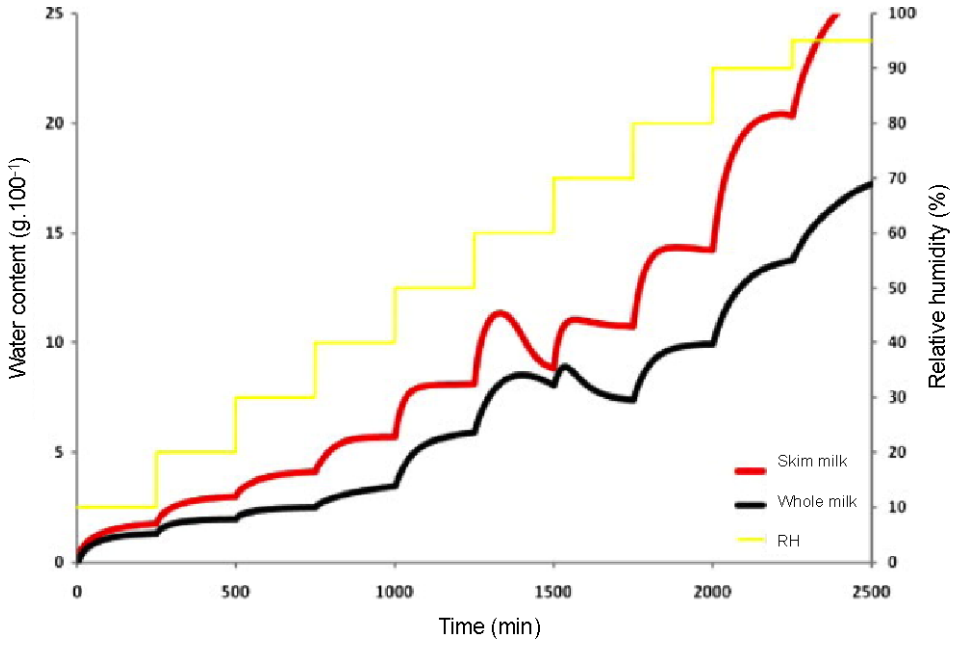

Figure 65. Example of kinetic data obtained during water adsorption of milk powders at 20 °C and measured by DVS automatic sorption analyzer (powders sieved at 50 µm).

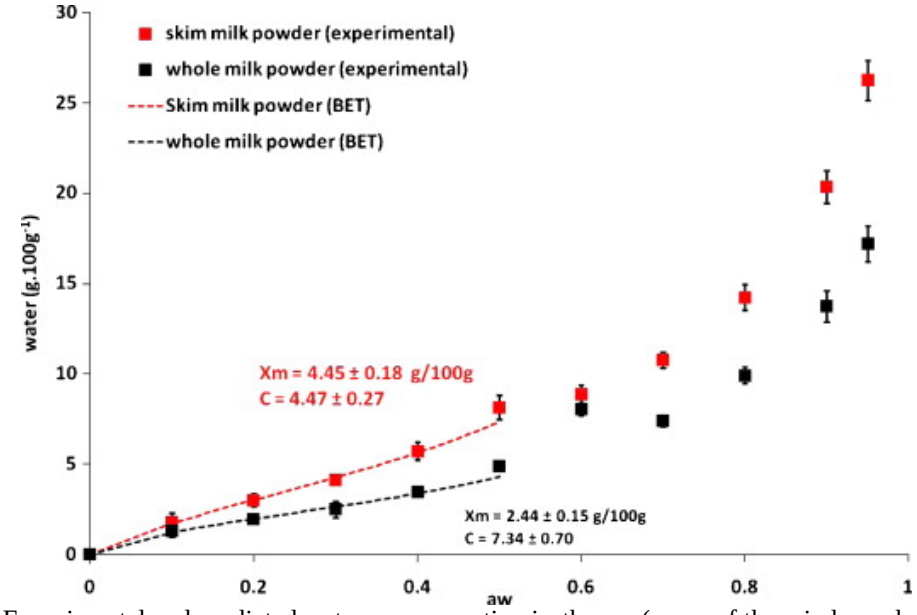

Figure 66. Experimental and predicted water vapor sorption isotherms (mean of three independent analyses). Determination of the monolayer moisture content (Xm) and constant C with the BET model for relative humidity ranging between 0% and 50%.

IV.3.1.4. Relationships between moisture diffusivity, powder structure and surfaces

Apparent moisture diffusion (called diffusivity in the continuation of the paper) as a function of relative humidity at 20 ◦ C is presented figure 67. This representation is based on the assumption that moisture sorption kinetic is limited by the diffusion. Water diffusivity in whole milk and skim milk powders was calculated for each RH level from the water sorption kinetic curve figure 65 measured using the DVS and the slope method developed by others (Yu *et al*., 2007). For this purpose, different hypothesis were formulated.

First, the diffusivity was assumed to be constant for each RH level and could change from one stage to another. Second, particles size is assumed to be homogeneous (average diameter apply to all particles) when placed in the DVS pan. Third, in this work, to improve the method, swelling during adsorption was considered. As indicated by figure 64, the powder size was variable upon water sorption and has been taken into account for a more accurate diffusivity determination (Chivrac *et al*., 2010). The resultant diffusivity values were plotted as a function of the average water activity of level for all the successive RH levels investigated (figure 67). A bell like curve was obtained for each powder in agreement with a great number of studies (Chivrac *et al*., 2010; Enrione *et al*., 2007; Roca *et al*., 2008a; Roca, Guillard *et al*., 2008; Yu *et al*., 2007). The maximum diffusivity value was observed at a_w = 0.41 for skim milk powder and aw between 0.41 and 0.53 for whole milk powder. D_{max} was respectively at 3.1 × 10−9 and 1.7 × 10−9 m2 s−1 for SMP and WMP. These calculated

values were in the range of those reported in literature for food products (Guillard *et al*., 2003; Labuza & Hyman, 1998). Comparison with dairy powders was impossible due to lack of data in this field up to now. As observed by others (Guillard *et al*., 2003), D_{max} values were not related to the moisture content corresponding to the monolayer value (4.45 and 2.44 g 100 g−1 for SMP and WMP respectively) but were slightly higher. Nevertheless, the amorphous-crystallized transition of lactose was estimated to be at about aw = 0.43 for WMP and 0.54 for SMP from MEB observation. This corresponds well to the point where the maximum in diffusion rate is observed in figure 67. The D_{max} was dependent on the state of the sample (Van Nieuwenhuijzen *et al*., 2008) and also on differences in the method used to determined the moisture diffusivity (Guillard *et al*., 2003; Labuza & Hyman, 1998) .

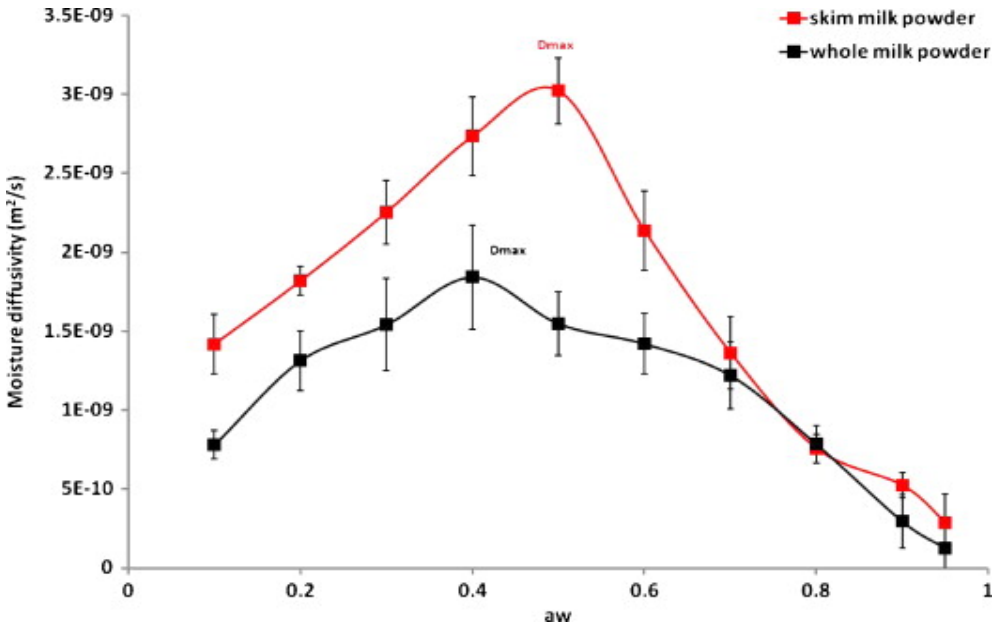

Figure 67. Moisture diffusivity of skim milk and whole milk powders as a function of aw. Mean of three independent analyses.

The bell like curves obtained may be explained by different processes occurring during water uptake. Comparison between curves obtained for WMP and SMP (figure 67) reveals that at low a_w, the moisture diffusivity was lower for WMP. During this first phase, water adsorbs to the surface of the particles. As expected, powders presenting important surface fat coverage (WMP) were less prone to adsorb water and the rate of sorption was lower than lactose containing powders (SMP). Water diffusion is known to be accelerated in polar hydrophilic matrices (Palzer, 2010). In addition, the average surface roughness of SMP particles was significantly higher (figure 60 and figure 61) increasing the effective area. Next

to the maximum, the diffusivity decrease may be attributed to change in lactose state. It is well established that the permeability of crystalline and amorphous substance differs significantly. As a consequence, crystalline lactose has a lower water capacity and a lower water diffusion than amorphous lactose (Palzer, 2010). This can be explained by differences in the free volume of these two types of matrices. The low free volume and the small hole size in crystalline structure may be responsible of a lower diffusion. As a consequence, when the quantity of crystallized lactose increases, the diffusivity decreases. Others incriminated the caking of the macroscopic structure (Roca *et al*., 2007) which in turn reduce the effective area exposed to the solvent and therefore decrease the sorption rate or changes in particle porosity (Guillard *et al*., 2003). Nevertheless, in this work, the evolution of particle size (swelling, collapse and caking) was taken into account in the mathematical calculation of the moisture diffusivity. Another possible phenomenon may be that at these humidities the transport of water vapor through the air may be a limiting factor. An important and unexpected decrease of the diffusivity value was observed for high relative humidity. Indeed, an additional phenomenon may occur and the Fickian model used to obtain the diffusivity value may be not entirely appropriate to represent this different diffusional mechanism. Indeed, water that migrates into the dry matrix (low RH) will probably do that at a different rate as compared to water migrating into the already hydrated matrix (Van Nieuwenhuijzen *et al*., 2008).

IV.3.2. Evolution of particle structure during water sorption in different size classes of durum wheat semolina.

IV.3.2.1. Raw and sieved semolina structure

Pictures (figure 68) show the general aspect of the powders at 50X and the surface aspect of the particles at 800X. At 50X, the size augmentation and the homogeny distribution of sieved powders were observed, opposed to raw powder. At 800X, the surface seems to present an evolution related to the particle size. More specifically in figure 68 G and H, particles present an irregular surface with some granule starch out from under the gluten matrix, whereas figure 68 J and K have a straight surface and starch granules can be observed. These grains are broken conserving a strait appearance. In figure 68 I, particle seems to be a transition from one texture to the other.

This evolution of the structure, can be related to wheat endosperm texture, this harder or softer structure of the endosperm is a consequence of gluten-starch bond, a stronger bond is proper to hard flours, whereas a weaker bond is proper to soft flours (Delcour & Hoseney,

2010), hence, hard flours as wheat durum (semolina) comes from hard endosperm. In spite of this claim, not all the particle seems to present the same texture, probably an heterogenic grain could contain zones with softer endosperm, then this parts would present a less resistance to milling producing finest particles. As a consequence, a less number of starch granules are fractured because the bond between protein and starch ruptures easily. On the other hand, harder zones would produce bigger particles and a big quantity of broken starch grains. These grains are fractured instead of stronger starch-gluten bond. Other factor to consider is the milling conditions applied to the grain kernel (Saad *et al.*, 2011a) proposed that the milling conditions could apply different forces trough the grain and produce some powders broken at the age and others broken through the starch particle.

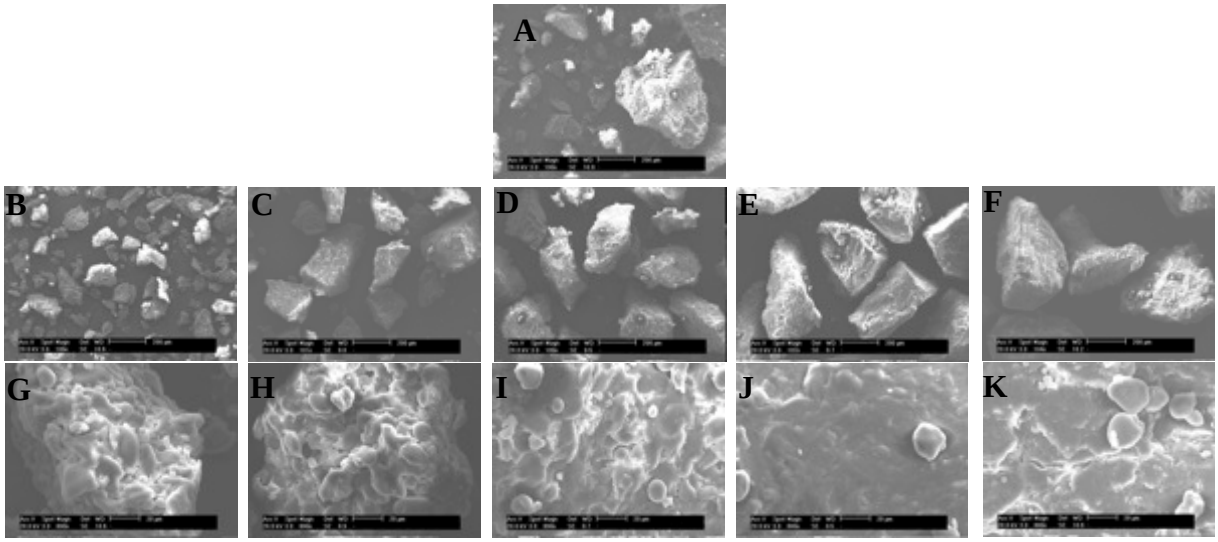

Figure 68. Scanning electron images of raw and sieved semolina particles at 50X (A-F) and 800X (G-K). Raw semolina at 50X (A). 0-160µm at 50X (B) 800X (G), 160-250 at 50X (C) 800X (H), 250-315 at 50X (D) 800X (I), 315-400 at 50X (E) 800X (J), 400-500 at 50X (F) 800X (K).

IV.3.2.2. Bulk Composition

Table 53 shows the physicochemical bulk composition of raw and sieved semolina. Since there is the possibility to have different characteristics according to particle size, the composition of fractions could be different; indeed, subtle but clear tendencies can be corroborated. A higher content of ashes in fine powders is measured (0-160 and 160-250 µm). Then, a decreasing tendency is observed when particle size increase. For proteins, differences are less clear, but an increasing tendency is present in all fractions with the particle size augmentation. The same increasing tendency is follow by lipids observing a clearest difference among the values. For the humidity, the tendency is not clear and values are in the same rank except for 400-500 µm fractions, this is the lowest value of humidity. Finally,

carbohydrates are deduced by difference from the total. It is also difficult to observe a tendency, a lower value is found for 400-500 μm fraction. These results disagree with those reported by Hébrard *et al*. (2003). These authors analyzed fractions of durum wheat sieved at 0-200, 200-400 and 400-600 μm, and a lower content of protein and lipids were related to the increment of size particle. Similar results where observed in different wheat flours compositions reported elsewhere (Ocieczek, 2007; Roman-Gutierrez *et al*., 2003). Hard flours present a higher content of protein and fat compared with soft flour semolina, this relation could support the hypothesis that fines particles are conformed by a softer material.

Table 53. Size particle by dry dispersion and bulk Chemical Composition (g/100 g dm) of raw semolina and fractions.

Fractions	D(50) μm	Ashes	Proteins	Lipids	Humidity	Total	Carb.*
Raw Semolina	298.31	0.91 ± 0.02	11.51 ± 0.36	1.52 ± 0.26	12.99 ± 0.05	26.93	73.07
0-160 μm	135.65	1.36 ± 0.03	10.62 ± 0.35	0.92 ± 0.18	12.40 ± 0.05	25.30	74.70
160-250 μm	218.67	0.94 ± 0.02	11.04 ± 0.2	0.97 ± 0.21	12.63 ± 0.02	25.58	74.42
250-315 μm	288.36	0.76 ± 0.01	11.05 ± 0.73	1.25 ± 0.12	12.21 ± 0.01	25.27	74.73
315-400 μm	373.76	0.70 ± 0.02	11.13 ± 0.34	1.16 ± 0.13	12.88 ± 0.14	25.87	74.13
400-500 μm	438.96	0.70 ± 0.03	11.92 ± 0.61	1.73 ± 0.22	11.76 ± 0.00	26.11	73.89

*Carbohydrates are calculated by difference from the total.

IV.3.2.3. Effect of water uptake on powder structure and particle size

a) Particule Structure

Fractions 0-160, 250-315 and 400-500μm were introduced in saturated atmospheres during 7 days allowing water exchanges between powder and relative humidity of the surrounding air. SEM was performed on powders equilibrated at the three highest RH's ranging (75, 85 and 97%). Pictures in figure 69 indicate that some changes in surface structure occurred. At 50X, powders seem to conserve the same structure until 85%RH, then an agglomeration took place at 97%RH. This agglomeration is remarkable in the fines particles and the effect decreases with a gain in the particle size.

At 800X, the aspect of surfaces at 75%RH is not very affected in comparison with powders at room RH, but a modification on the gluten matrix can be appreciated from 85%RH and it is really clear at 97%RH. Indeed, the moisture on the particles appears to affect the gluten matrix converting this firm component in a soft texture structure. This texture seems to get softer when RH increase, this change in the texture of gluten probably change their properties and gluten became sticky, hence, particles form bridges among them causing agglomeration. The structure of the starch not seems to change, nevertheless starch grains

appear to swell and gain in particle size. Pure wheat starch has demonstrated its capacity to gain until 17% of its volume with humidity (El-Khawas *et al*., 1966), these conditions could change in presence of semolina components, then this 17% would not be net, but an augmentation of the size still happen.

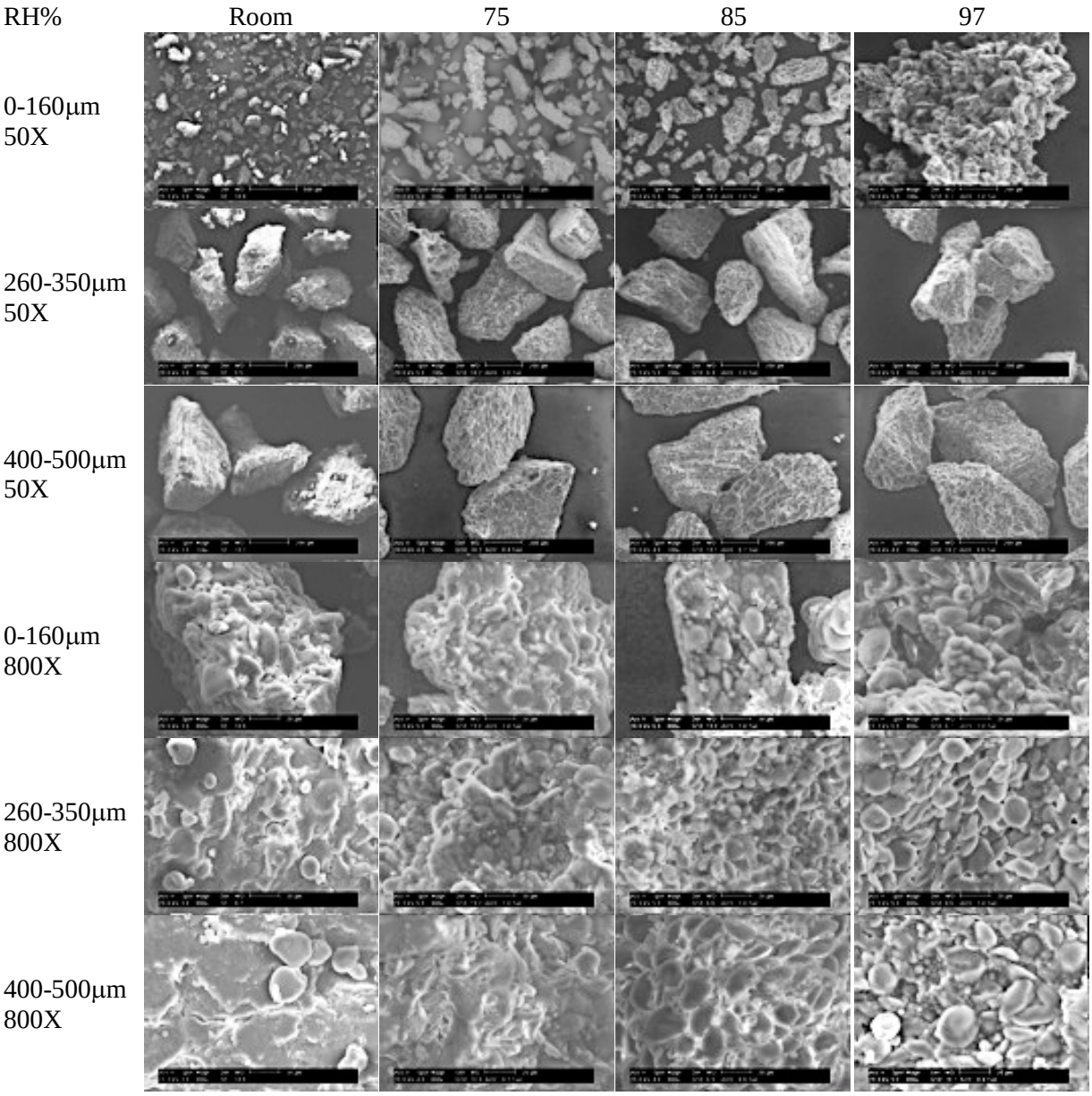

Figure 69. ESEM images at 50 and 800X of sieved semolina particles (0-160, 250-315 and 400-500µm) conditioned at different RH.

A clear modification of the gluten matrix allows starch to be more exposed and humidity can interact directly with these grains. The grain size as well as gluten matrix evolution get more evident at higher RH. Gluten-starch bond is really strong, but can be easily separated by water treatment (Delcour & Hoseney, 2010). Other interesting observation is the number of

broken starch grains that can be easier observed at 97% RH. It is visible that finest particles (0-160 μm) suffer a gluten-starch bond braking and the bigger particles present a fracture of the starch grains due to the difficulty to generate a gluten-starch bond braking. This observation supports the hypothesis that gluten structure of fine particles is not exactly the same than the rest of the powder. Indeed, 0-160 μm gluten matrix seems more viscous at 800X and this appearance disappears in 400-500 μm particles. An evolution in the properties of gluten matrix can be observed. Actually, large particles form agglomerates with difficulty in opposite to small particle that present a good agglomeration grade at 97 RH%. It could be also done to a difficulty in diffusion into the big particles, hence, the water takes more time to humidify the structure and this one becomes sticky.

b) Particle Size

Size of the three semolina fractions (0-160, 250-315, 400-500 μm) conditioned at different RH is shown in table 54.

Table 54. Particle size diameter by liquid dispersion of raw and sieved semolina after 7 days conditioned at different RH

		D(50) μm		
	RH%	0-160 μm	250-315 μm	400-500 μm
Room	-	105.60 ± 1.03	329.43 ± 6.24	546.71 ± 5.62
LiCl	11	103.53 ± 0.87	321.89 ± 4.70	525.78 ± 9.54
$MgNO_2$	54	101.30 ± 1.24	327.74 ± 4.75	539.08 ± 4.83
NaCl	75	112.02 ± 1.23	328.71 ± 2.25	543.38 ± 9.32
KCl	85	117.89 ± 2.12	335.20 ± 2.88	553.77 ± 10.69
$K2SO_4$	97	531.30 ± 46.42	386.07 ± 12.41	581.43 ± 12.79

Size is slightly altered by the effect of ethanol, a bigger size in original powder is observed. Despite the alteration the evolution in size can be observed. Size evolution of 0-160 μm particles appears not to be very important at low RH (11 and 54 %). An augmentation of some microns are observed for 75 % RH and some microns are also gained at 85 % RH. But a clear size augmentation is observed at 97 % RH, the particles at 250-315 μm present an evolution in size between 11 and 54 % RH but not between 54 and 75 % RH. A more considerable gain is observed at 85% RH and it is net at 97 % RH. Finally 400-500 μm particles observe the clearest evolution in size, around 10 microns by RH step, and these particles are less agglomerated at 97 % RH. The tendency in size increment as well as the microns gain by the particles is not exactly the same for all the fractions. This denotes some differences in the composition or structure of the particles. A tendency that describes an

augmentation in the size of the particles is remarked at RH inferior to 85%. A 97 % RH the agglomeration of particles is reflected in a really drastic augmentation of the size, this is not an augmentation due to the particle itself, but an agglomeration phenomena that is more evident in small particles.

After 7 days, the powders probably have not been 100% equilibrated at different RH's, consequently the water taken was measured. Results are presented in table 55. It is possible to conclude that the water taken is approximately the same for all the fractions, a little advantage is present by 400-500 μm, but it is not bigger enough to affect the interpretation of results. It can be considered that the water uptake is independent of the size fraction. This conclusion allows calculating the diffusion coefficient with a dynamic diameter for the three size fractions.

Table 55. Water taken by powders after 7 days at different RH's.

	Water uptake %		
RH%	0-160 μm	250-315 μm	400-500 μm
11	-5.9	-7.3	-6.6
54	0.24	0.17	0.30
75	2.82	2.86	2.27
85	7.20	6.40	7.67
97	25.03	24.19	25.15

IV.3.2.4. Sorption Isotherm

It can be observed in figure 70 (raw semolina) a type II curve according to the IUPAC classification. This curve is characteristic of finely divided non-porous solids (Delcour & Hoseney, 2010).

Three zones in the curve are observed I (0-20% RH), II (20-80% RH) and III (80-95% RH). Zone I represents the monolayer formation, zone II corresponds to the linear portion of the isotherm where the added water will bind with the components of the material forming layers. In zone III, the water presents a weakly bounding. In this state water is mobile. The "S" curve with a hysteresis after desorption is a classical behavior of natural high molecular weight polymers (Bushuk & Winkler, 1957; Hébrard *et al*., 2003).

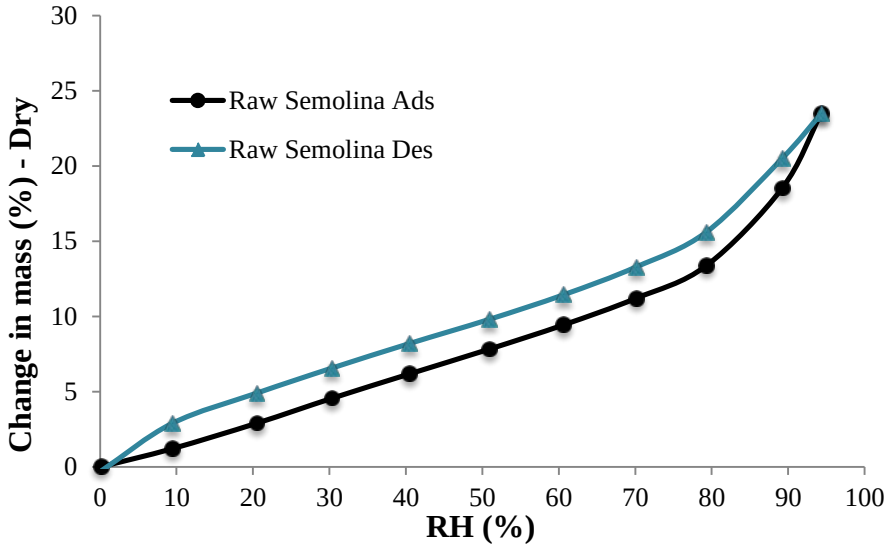

Figure 70. Isotherm for raw semolina absorption and desorption.

The same II type curve is observed in fractions isotherms (figure 71). The fractions display differences in the mass of water absorbed. Excepting the 315-400µm fraction, the differences in the curves happened in the zone I and III of the curve, between 20 and 80% RH the curves are parallels, thus, there is no difference in the absorptions of water at this point. Nevertheless, in zone I from 0-20% RH, fine particles absorb more and a clear tendency of decreasing values is observed whit the increment of size particle. In the particular case of 315-400 µm, the same tendency can be observed at the zone I, but this powder gain in mass also in the zone II, and this gain is more important in zone III, consequently, a little different curve is observed. Similar curves for hard flours have been reported elsewhere (Bushuk & Winkler, 1957; Hébrard *et al*., 2003; Ocieczek, 2007; Riganakos *et al*., 1997).

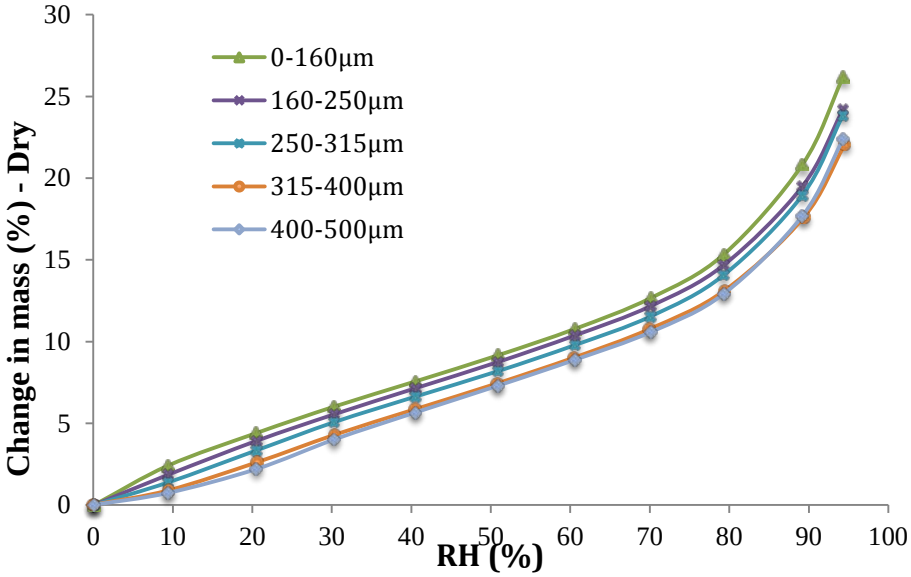

Figure 71. Isotherms for semolina fractions absorption.

Differences in mass gain for the fractions when particle size increases can be due to the fact that small particles offer a bigger contact surface. Raw semolina (not plotted in figure 71) appears at the center as an average of all behaviors.

IV.3.2.5. G.A.B. and Y&N models

a) G.A.B.

Relationship between water vapor sorption at equilibrium and RH's modeled by GAB equation (20) values are expressed in table 56. Model presents a good correlation, r_{GAB} values being over 0.92 for all the powders. G.A.B model present a limit ($0<K_{GAB}\leq 1$) imposed by the physics behind G.A.B. equation (20). This limit is respected for all the powders confirming the appropriate correlation. Monolayer value decreases inversely to the particle size. It means that a less quantity of water molecules is necessary to produce a monolayer. This is due to a smaller specific surface offered for bigger particle sizes, K_{GAB} shown a moisture capacity of multilayer with not a tendency in the values, then a similar interaction for all the powders is concluded. C_{GAB} values denote the interaction with the surface; a harder interaction is registered by 0-160 μm, the rest of powders present similar results among them.

Table 56. Equation parameters by GAB and Y&N equations

Semolina	G.A.B. X_m (Kg/Kgdm)	C_{GAB}	K_{GAB}	r_{GAB}	Y&N $A_{Y\&N}$ (Kg/Kgdm)	$E_{Y\&N}$	$B_{Y\&N}$ (Kg/Kgdm)	$r_{Y\&N}$
Raw	0.08	7.21	0.68	0.994	0.03	0.48	0.06	0.991
0-160 μm	0.09	11.30	0.67	0.997	0.04	0.26	0.04	0.991
160-250 μm	0.10	3.77	0.59	0.928	0.04	0.31	0.05	0.992
250-315 μm	0.08	4.24	0.68	0.942	0.03	0.40	0.06	0.992
315-400 μm	0.10	2.58	0.60	0.977	0.03	0.54	0.07	0.994
400-500 μm	0.08	5.85	0.65	0.997	0.03	0.58	0.08	0.992

c) Y&N

The Young and Nelson model shows good correlation with the experimental data for all the formulations, $r_{Y\&N}$ (table 56) of all fractions are between 0.991 and 0.992 in opposite with GAB model where r_{GAB} was variable among the samples. $A_{Y\&N}$, $E_{Y\&N}$ and $B_{Y\&N}$ terms are given in table 56. $A_{Y\&N}$ is a homologous of X_m in GAB equation and it represents the moisture capacity of a monomolecular layer; $B_{Y\&N}$ is related to the amount of moisture absorbed by the sample and it has not a similar term in the GAB model; finally, $E_{Y\&N}$ is an energy term relating the strength of water vapor interaction with the surface of the sample, this term is similar to C_{GAB}. Monolayer values present the same behavior than GAB calculation. The

moisture absorbed by the particle $(B_{Y\&N})$ increases with the augmentation of the particle size, as well as $E_{Y\&N}$. This last parameter expresses a stronger interaction of the water vapor with the surface of bigger particles and $B_{Y\&N}$ results represent a higher water absorption performed by big particles. It could be explained for the volume of big particles that can contain more water inside. A difference in the starch-gluten matrix structure could be also responsible.

IV.3.2.6. Diffusion Coefficient

By applying the model of Fickian law for spherical particles (equation 25), raw semolina and fractions coefficients can be obtained. Calculation where done with D(50) obtained by dry dispersion. Results are presented in figure 72. A similar bell-like curve was found for a semolina film by (Hébrard *et al.*, 2003) and other hydrophilic porous products such as cereal based (Guillard *et al.*, 2003; Roca *et al.*, 2007). This behavior has been explained as the mechanism of diffusion from vapor diffusion at low RH to liquid diffusion at high RH that produces an evolution of material's porosity (Chivrac *et al.*, 2010). In the case of semolina, there is an evolution of the starch-gluten matrix when it interact with moisture and water, as it has been demonstrated in this work, texture as well as porosity intra and inter-particle can change through diffusion process.

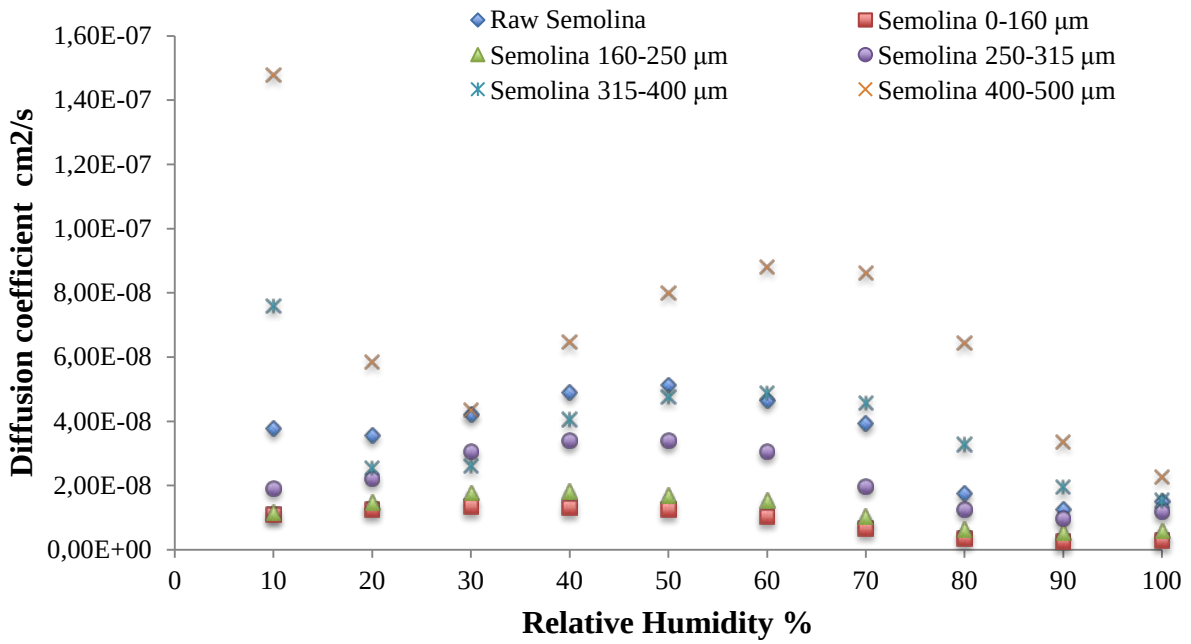

Figure 72. Influence of particle size in diffusion coefficient.

A tendency is remarked in figure 73, the bigger the particle the faster the diffusion. For big particles (315-400 and 400-500 µm fractions) the diffusion profiles start fast for the monolayer (10% RH), a deceleration is presented until 30% and it will accelerate until a

maximal speed observed at 60% RH, then a saturation of humidity reduces the speed at the next RHs. For small particles (0-160, 160-250 and 250-315 μm fractions) the diffusion profiles start slow for the monolayer (10% RH), a progressive acceleration is printed until a maximal speed observed at 40% RH, then a saturation of humidity reduce the speed at the next RHs. Raw powder follows a curve that result of the influence of all size behaviors, supporting the effect of the size in the diffusion coefficient. The evolution of the curve is clear and in agreement with the size evolution. One hypothesis explaining the behavior of big particles proposes a different structure of the gluten matrix based in the next information: big fraction (315-400 and 400-500 μm) are constituted of a bigger quantity of protein (11.13 and 11.92% respectively), higher weight proteins could explain this difference in protein content (table 53) as well as the harder texture corroborated in the ESEM images (figure 68). This harder texture not allowing the detachment of starches in milling could actually produce particles with more damaged starch that could accelerate the absorption of water.

IV.3.2.7. Dynamic Diffusion Coefficient

Diffusion coefficients where re-calculated by taking into account the evolution of particle size produced by humidification of samples (0-160, 250-315, and 400-500 μm). The diameter of size fractions obtained after conditioning at 11, 54, 75, 85 and 97 % RH were used to calculate 10, 50, 70, 80 and 95 % coefficients in DVS data. This coefficient is referred in this text as dynamic diffusion coefficient.

Due to the few quantity of sample available after conditioning at different RH, the measure of particle size was performed in liquid dispersion. Consequently, initial diffusion coefficients were also re-calculated for not-treated powders. Initial and dynamic diffusion results are shown in table 57 as well as graphic comparing both diffusions in figure 73. The diffusivity of fractions is few affected by change in particle size. There is just a little diminution of speeds at the initial points (10% RH), also an augmentation in the values at 95%. For 0-160 fraction, the value for 95 % is completely changed, this is a consequence of agglomeration that is clearly net for small particles.

A similar dynamic diffusion coefficient was determined for milk powders (Murrieta-Pazos *et al.* 2011). For these particles, the evolution of the diffusion coefficient was hard affected by particle size and particle structure, probably because there are more constraints related to their water diffusion. For example, milk powders are soluble in water whereas the

semolina is not, hence, the stability of curves even with a dynamic size particle could be explained by a not-soluble and more stable structure of semolina particles.

Table 57. Diffusion coefficient calculated with dynamic D(50) and initial-constant D(50) by liquid dispersion.

	Diffusion Coefficient cm^2/s					
	0-160µm		250-315µm		400-500µm	
RH%	Initial	Dynamic	Initial	Dynamic	Initial	Dynamic
10	5.68E-09	5.46E-09	4.61E-08	4.40E-08	2.29E-07	2.11E-07
50	7.33E-09	6.75E-09	4.24E-08	4.19E-08	1.23E-07	1.19E-07
70	5.74E-09	6.46E-09	3.84E-08	3.82E-08	1.38E-07	1.36E-07
80	3.74E-09	4.66E-09	2.47E-08	2.56E-08	1.03E-07	1.06E-07
95	1.43E-09	3.62E-08	1.21E-08	1.66E-08	3.79E-08	4.29E-08

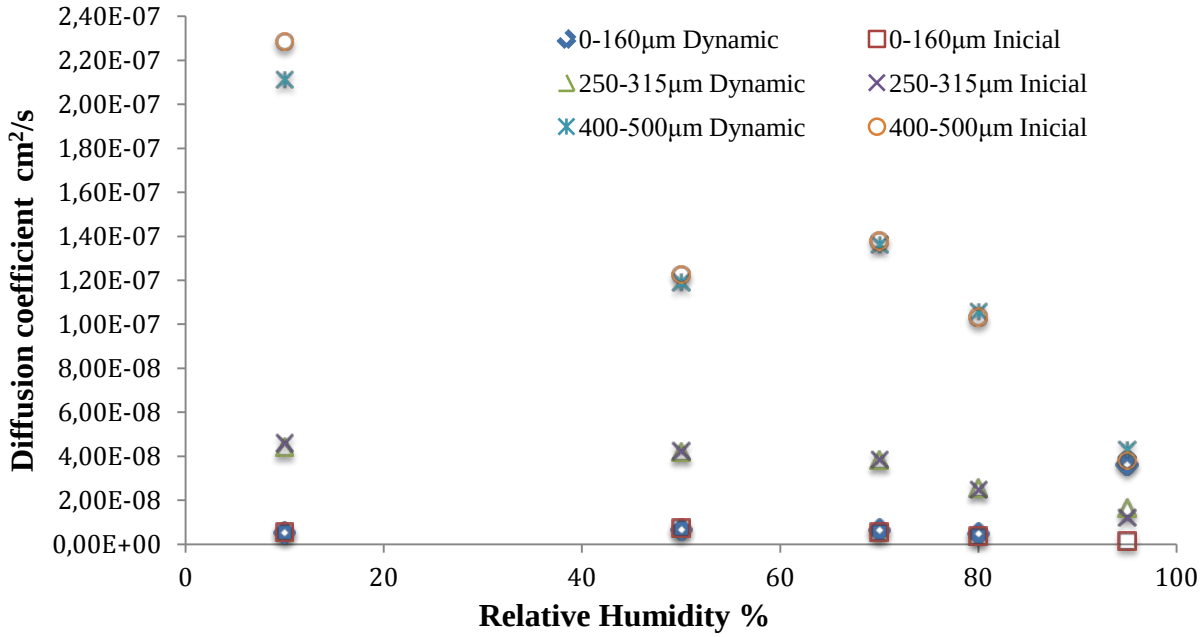

Figure 73. Initial and Dynamic coefficients

IV.3.3. SURFACE MODIFICATION ON FOOD POWDER BY DRY COATING

IV.3.3.8. Coating optimization on semolina.

The coating of powders is a useful process that is used in order to change certain characteristics such as flowability, color, wettability and many other applications. (Otles *et al*., 2011; Ouabbas, 2008; Ouabbas *et al*., 2009; Salazar-Banda *et al*., 2007). In the past, a wet coating method has typically been used to coat powders, but there are a number of drawbacks to this process, for example the need to use solvents and a drying stage. A more promising and innovative way to perform coatings on a large range of powders looks to be dry powder coating (Otles *et al*., 2011; Ouabbas *et al*., 2009; Thomas *et al*., 2009). This is because dry powder coating removes the need for solvents and a drying stage, thereby reducing the

processing time and making it more environmentally friendly process (Lefebvre *et al*., 2011). Dry powder coating is also less costly, it also has the added benefit of being easy to scale up into an industrial process because the equipment used in dry powder coating is already readily available (Otles, 2008; Ouabbas, 2008).

This part of the present work examined how semolina properties are affected when coated with gluten, arabinoxylan and starch, which are the principal components in wheat powders. The objective is to modify the surface of the particles in order to observe the effect of a strongly presence of each one of the principal components at the surface. Nevertheless coating conditions needs a big and carefully study to adequate the method to one powder, specially for food powder which use as hosts particle has never been performed. Unfortunately a such long investigation was not possible, thus the study of coating in semolina powders was focus into the rapid selection of coating conditions and characterization of the powders obtained. The proposal was to modify the surface to observe if any change in the powder could be observed by GCI. Coated powder was looked at ESEM; this observations helped to indicate, although not definitive, the strength of the powder coating. It shown the effectiveness of the coating and the kind of coating that was created. The coating was then examined in order to observe if a mono layer coating was created or a discrete coating was formed.

Initial tests were performed to find out the viability of semolina as a host powder. Semolina 315-400 was mixed in the cyclomix at different rotational speeds (500, 1000 and 1500 rpm), with each one mixed for 10 minutes with 60 % of the capacity filled at 600 ml (standard conditions). These were then analyzed too see if the semolina would have a large amount of breakage or change in surface morphology after mixing, since a large amount of semolina breaking would make it unusable as a host powder. First the semolina powders before and after Cyclomix were looked at using an ESEM (figure 74).

From the ESEM pictures (figure 74) it can be appreciated some small particles of powder mixed in with the larger particles. When comparing all four of the pictures there are similar numbers of small particles in the three cyclomixed powders (figure 74 B, C and D) as well as small particles in the non-cyclomixed powder (figure 74 A) showing there were particles present before cyclomixing. In the cyclomixed powders if the small particles were from breakage it would also be expected that at higher rotational speeds there would be more breakage. As there are similar numbers of small particles at all rotational speeds this would

suggest that these were already present, possibly remaining after sieving. These ESEM images indicate that the semolina had little breakage after being mixed in the cyclomix through the range of rotational speeds. After this essay, the criteria of speeds selection was based on non-breakage of the particles after cyclomix treatment. Nevertheless a breakage could occur and be not noted because of the presence of fine particles before the treatment, these particles would then hide the generation of new fine particles. Consequently in order to not ignore the possibility of breakage, 1000 rpm was selected as the speed of operation.

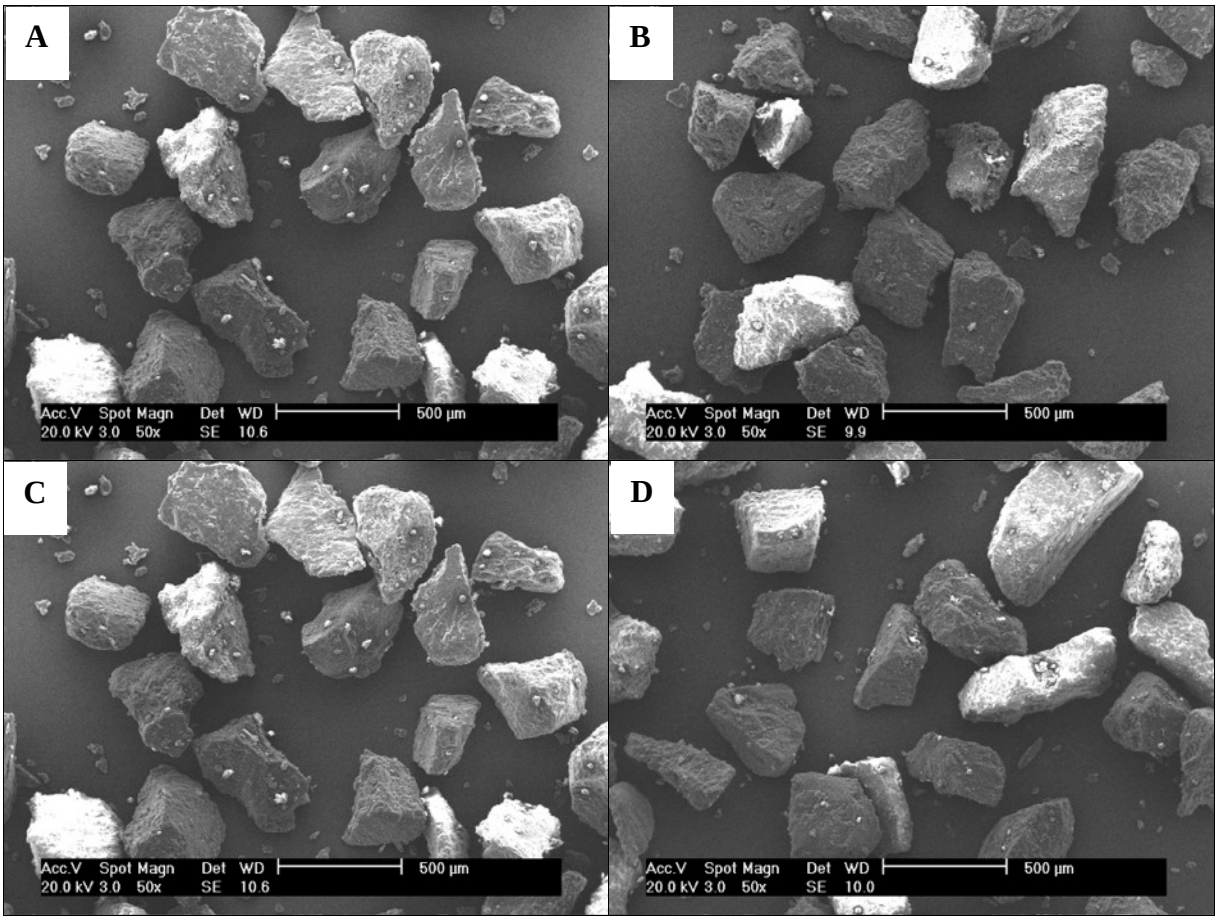

Figure 74. Photos of semolina observed by ESEM after a treatment in Cyclomix at 500 rpm (A), 1000 rpm (B) and 1500 rpm (C)

After establishing the viability of semolina powder the coating experiments could be started. The first coatings were done using semolina 315-400 at 1000 rpm, it was coated in gluten for 10 minutes at a 60% fill, thus 600ml (standard coating conditions). As it can be seen figure 75 and figure 76, the ESEM pictures of semolina coated in gluten, the micronized gluten has adhered to the surface of semolina particles. There is, however, some gluten that did not adhere to the semolina. This could be because too much gluten was used or because the coating that has been created is not a mono layer coating, so some gluten was left after

mixing which should have coated the semolina. It means that a discreet coating was produced with these powders. It is possible that conditions would not be the optimal, nevertheless, find the best conditions would involve a long study. However, the semolina particles are coated, and it was considered enough to test de surface modification in the powder.

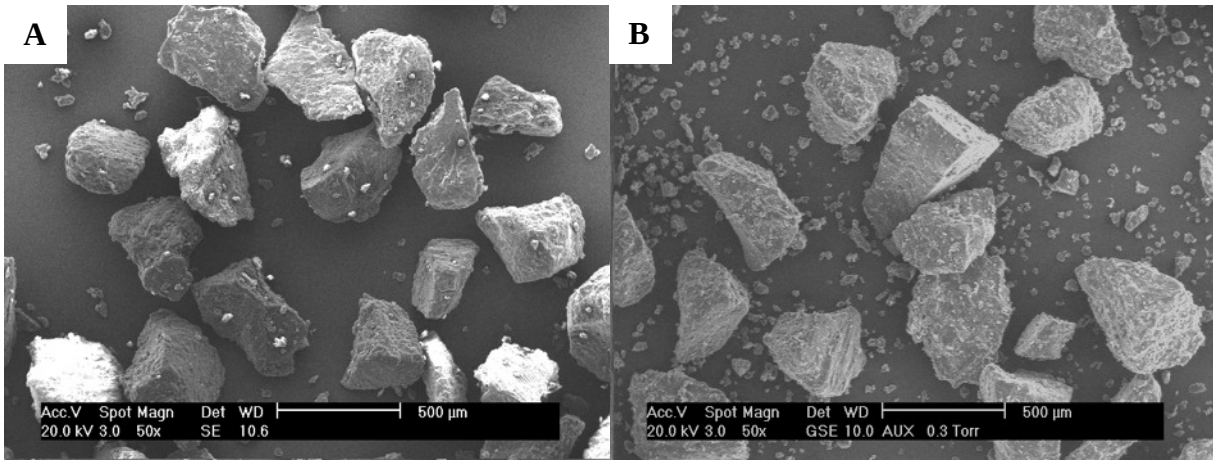

Figure 75. ESEM pictures of raw semolina (A) and semolina – micronized gluten coating (B) at 50X.

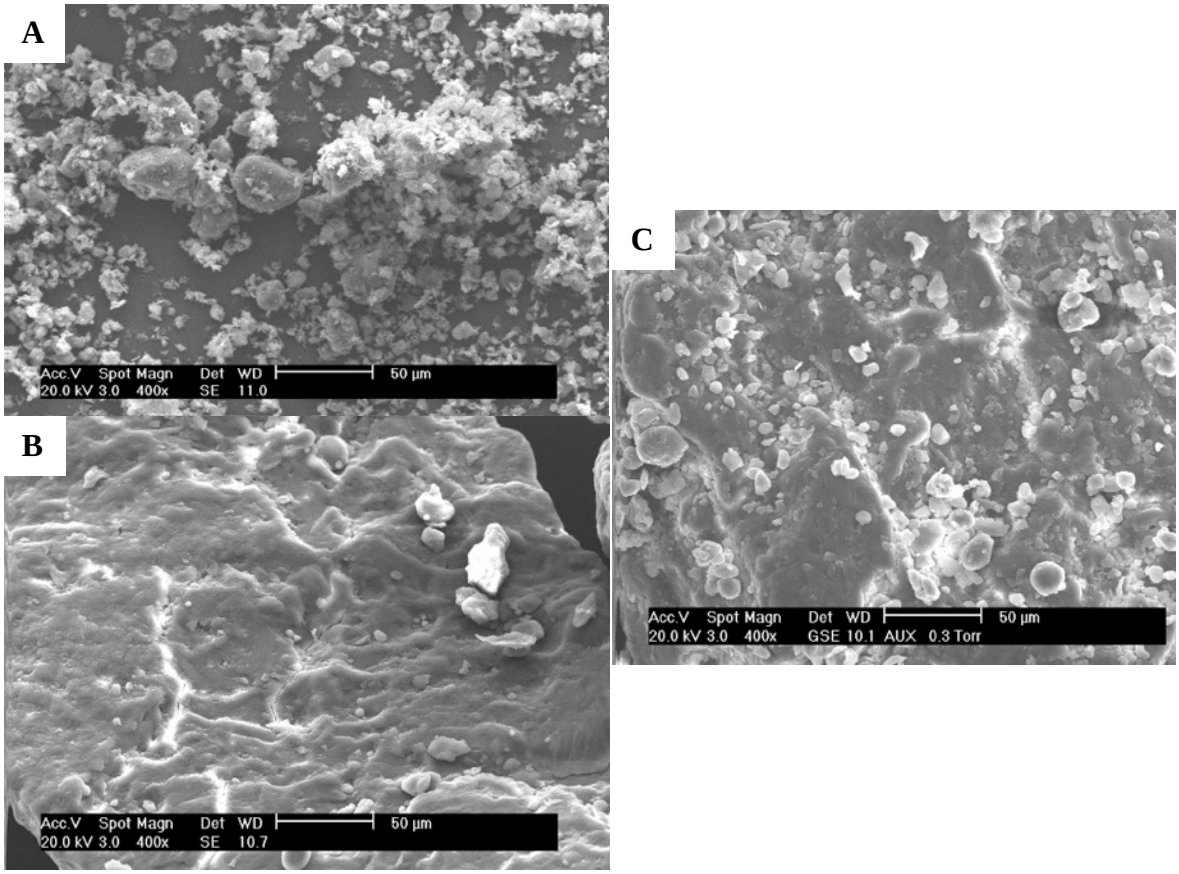

Figure 76. ESEM pictures of raw micronized gluten (A), raw semolina after cyclomix (B) and micronized gluten – arabinoxylan coating (C) at 400X.

The coating quality was then sized using a granulometer laser using a range of dispersion pressures to observe the effects on the powder. As the dispersion pressure increases it will separate the guest particles from the host particles, if the energy is sufficient. As the small guest particles break off from the host particles the particle number against particle size distribution will change along with the medium number distribution diameter, the D(0.5) at number of particle %.

For micronized gluten – semolina coating, it is shown in figure 77. In this figure it can bee seen that at the lower pressures a larger number of the particles are in the larger size range then as the pressure increases the larger number of particles moves towards a smaller particle size. This suggests that the gluten starts to break off from the semolina 315-400, this starts to happen between 1 bar of pressure with all the gluten being broken off at 2 bar.

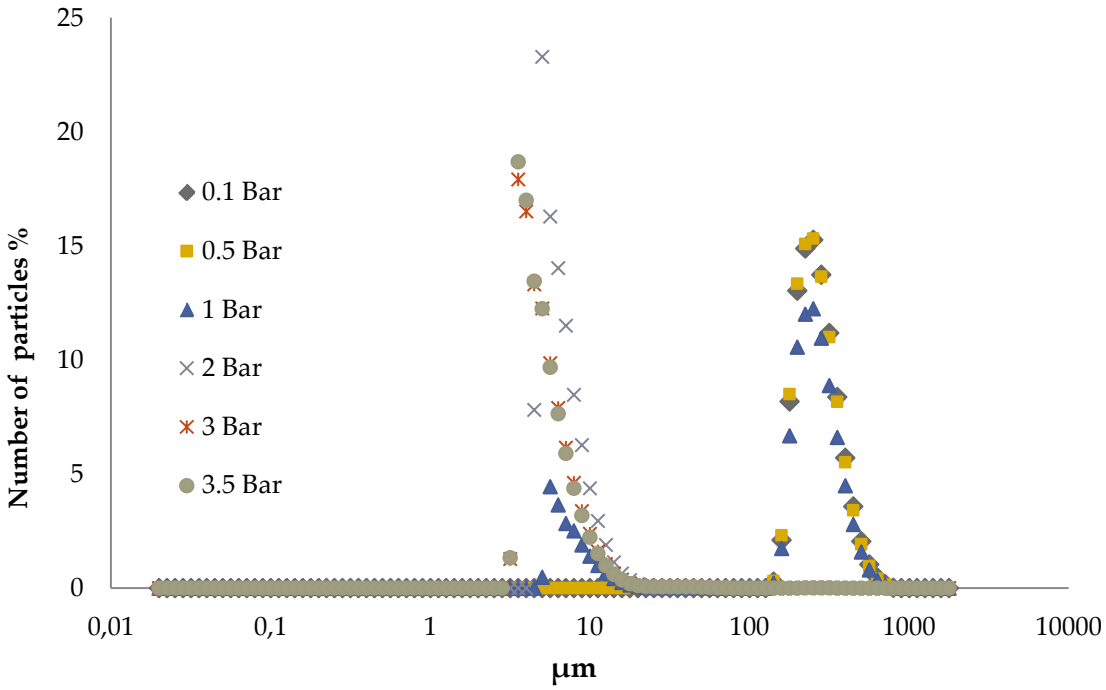

Figure 77. Size distribution (number %) in micronized gluten - semolina coating at different feeding pressures.

The starch and semolina coating (figure 78, figure 79) again left a large amounts of starch not attached to the semolina, it also left some of the semolina particles not very well coated but others well coated. This large amount of starch left was produce due to a not adequate ration of sizes. Indeed a difference 1:100 would be the optimal size for the guess and host particles respectively. Nevertheless the micronization of starch is quite difficult and it would change the properties of the powder because of the damage to the starch grains.

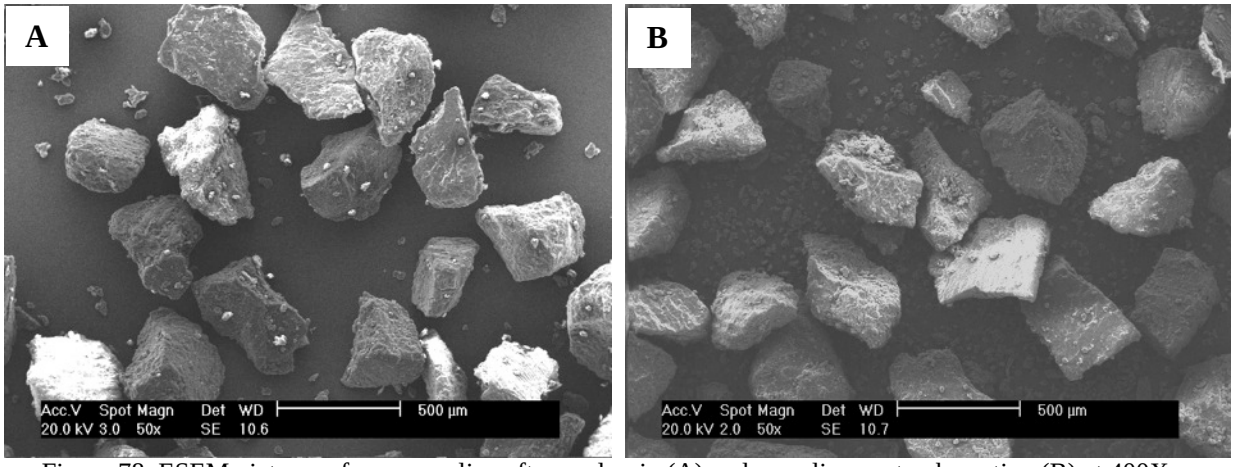

Figure 78. ESEM pictures of raw semolina after cyclomix (A) and semolina – starch coating (B) at 400X.

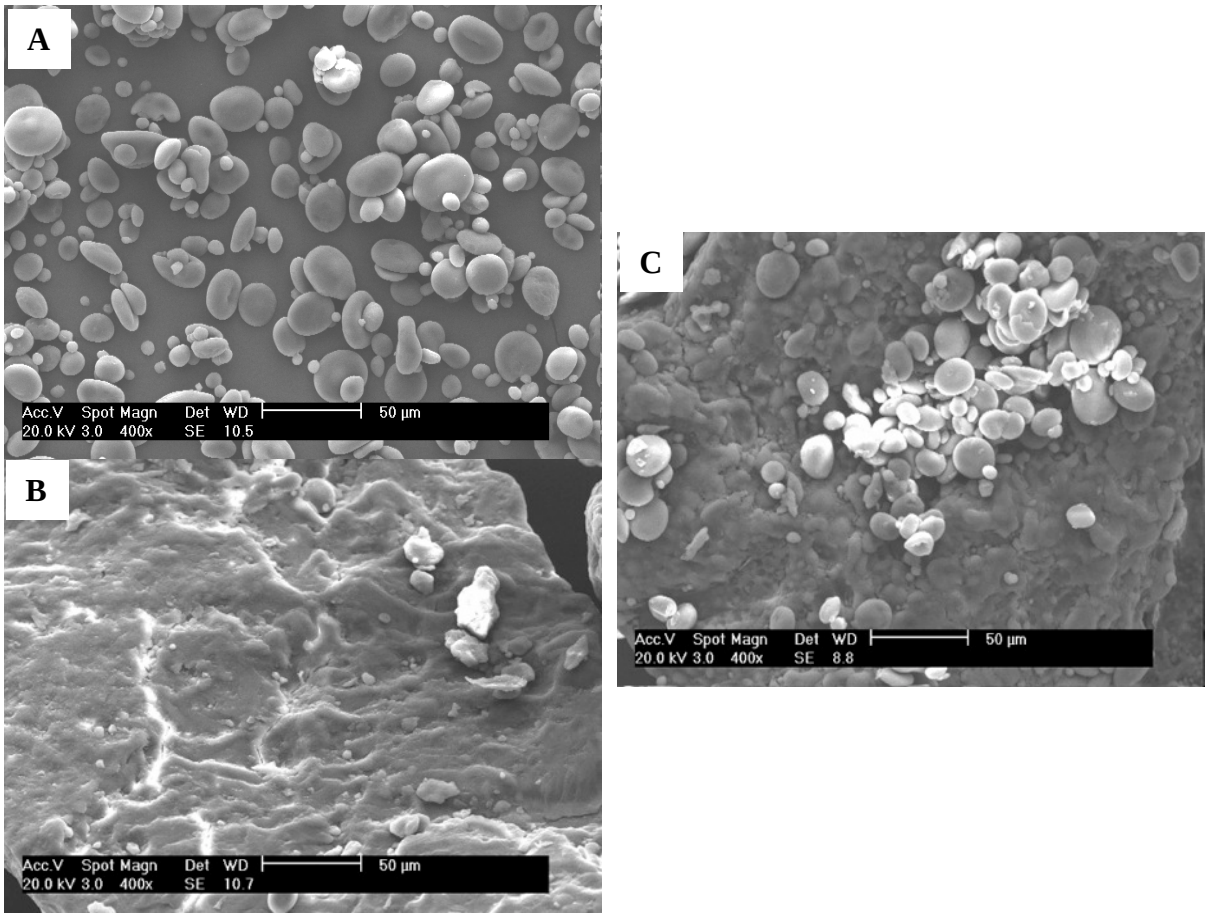

Figure 79. ESEM pictures of raw starch (A), raw semolina after cyclomix (B) and semolina – starch coating (C) at 400X.

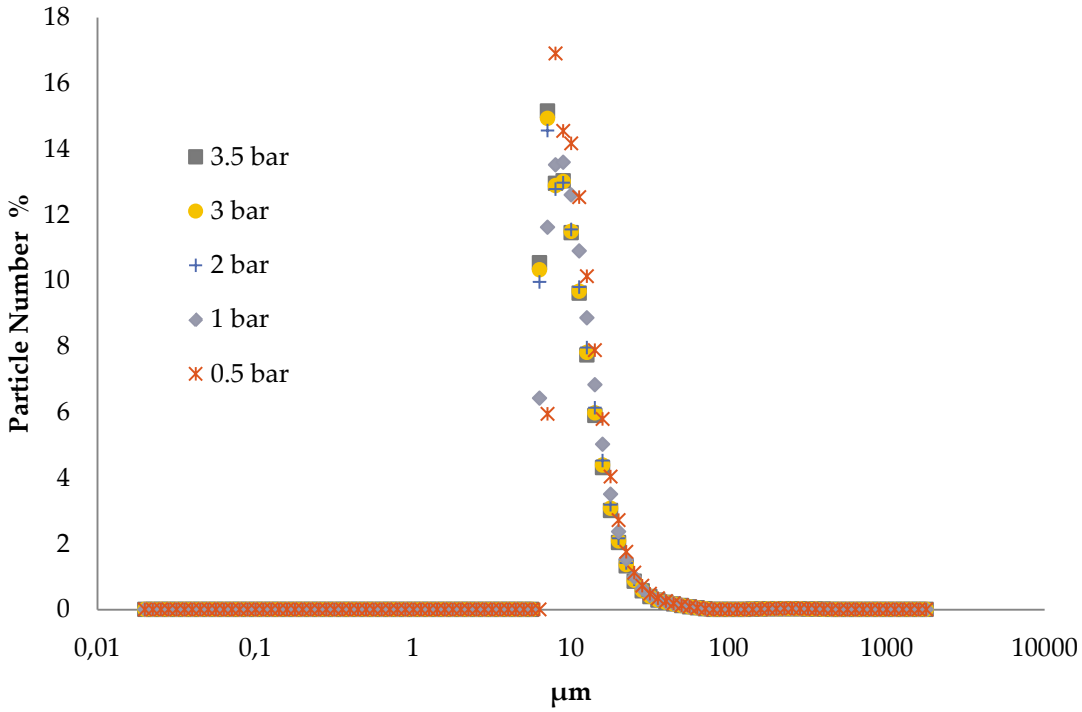

Figure 80. Size distribution (number %) in starch - semolina coating at different feeding pressures.

Figure 80 shows the quality of the starch semolina coating, a single peak of smaller particles is observed. This could be because the starch was not a very strong coating powder or because of the large amounts of starch powder that were left not coating the semolina after being treated in cyclomix, both of the possibilities are explained by the fact that starch is not small enough to coating a powder in the rank of 315-400 µm. However, the starch presented a better coating of expected, even when the difference of size is not enough, it seems that the surface of the starch permit the adhesion of the particles to the semolina surface. In this case we also considered that the coating was enough to measure differences in the surface modification.

Arabinoxylan was too small to be sized using the mastersizer 2000 and the ESEM images. Consequently, the quantity added to the coating was not calculated, but only simulated by considering a particle size of 1µm.

The arabinoxylan created a good coating (figure 81, figure 82 and figure 83) over the semolina with it smearing across the particles. Arabinoxylan can be seen smeared over the surface of some areas of the semolina, it means that arabinoxylan could form a film around the particle and form a continue coating (figure 83), if the quantity of arabinoxylan is well

estimated. However small amounts of the arabinoxylan were left not coating the powder (figure 81). Unfortunately, the arabinoxylan particles are not detected by granulometry laser, consequently the quality of coating was not measured.

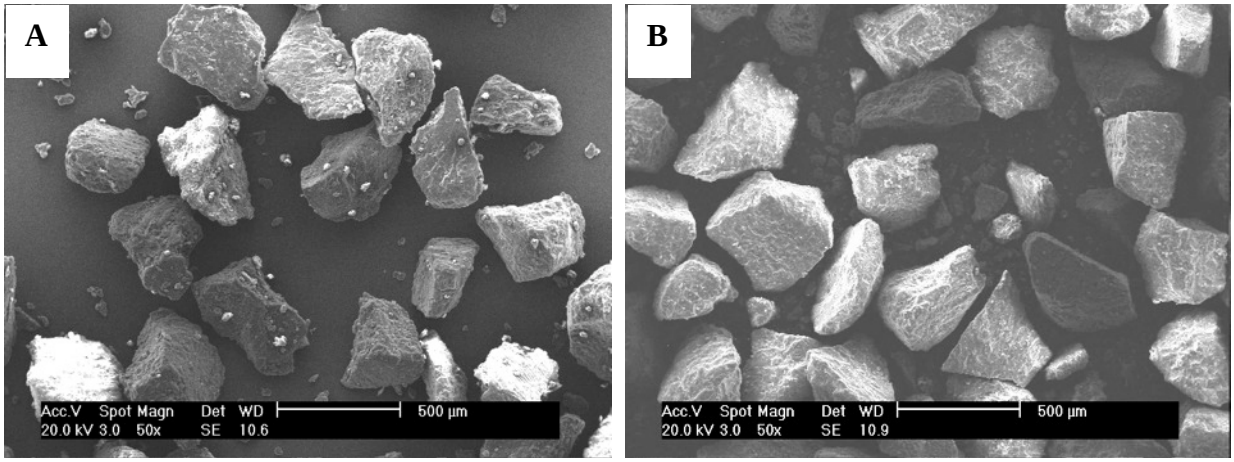

Figure 81. ESEM pictures of raw semolina after cyclomix (A) and semolina – arabinoxylan coating (B) at 50X.

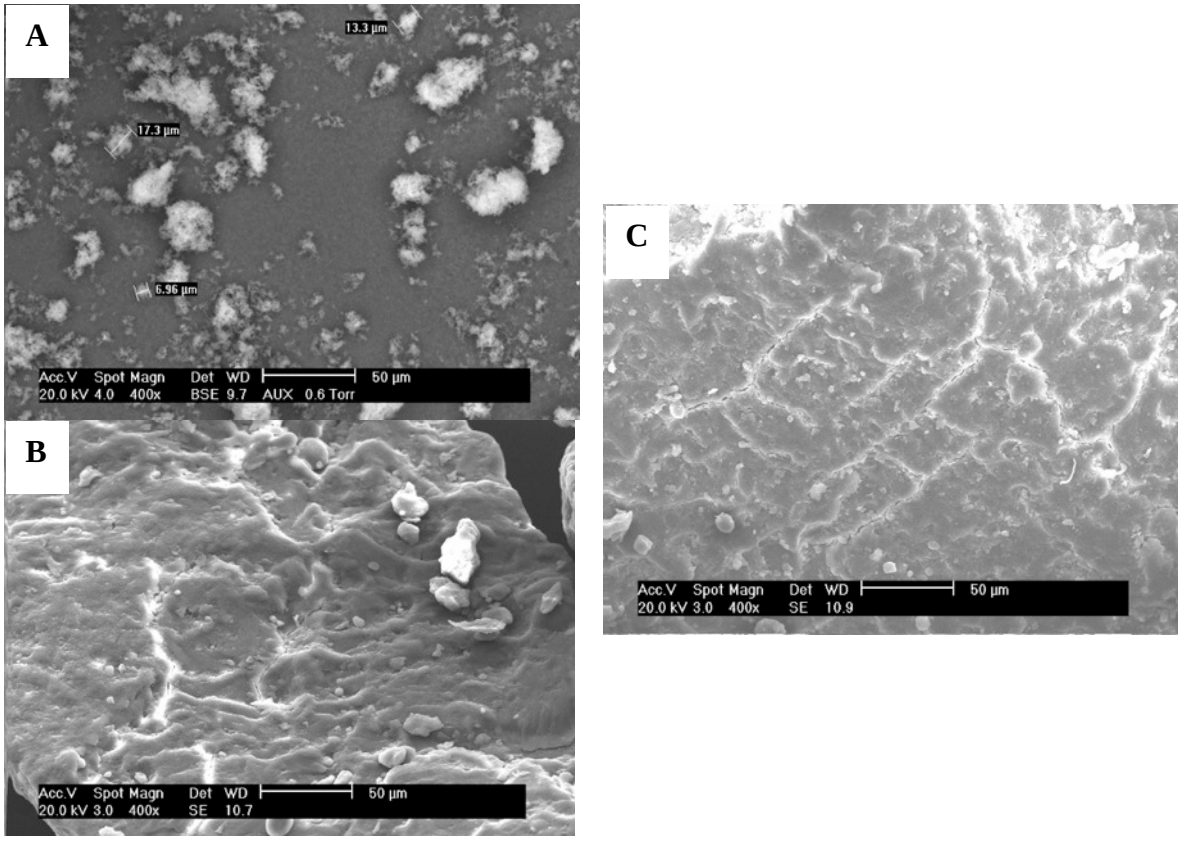

Figure 82. ESEM pictures of raw arabinoxylan (A), raw semolina after cyclomix (B) and semolina-arabinoxylan coating (C) at 400X.

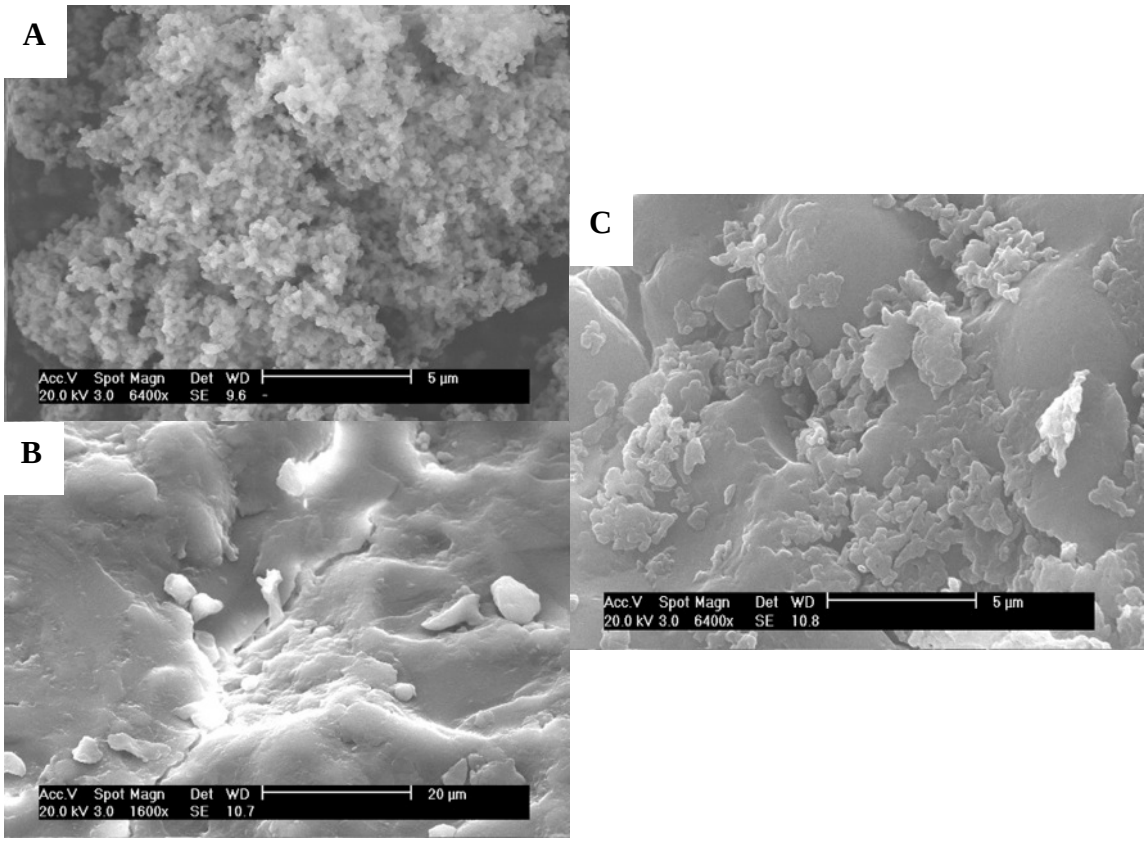

Figure 83. ESEM pictures of raw arabinoxylan (A), raw semolina after cyclomix (B) and semolina-arabinoxylan coating (C) at 1600X.

IV.3.3.9. Surface free energy of coated powders by IGC

The values obtained by IGC with the different coated powders as well as raw semolina fraction 315-400 µm, are presented in table 58.

Table 58. Values of γ_d^s and ΔG_{sp}^a of sieved semolina according to the nature of the coating.

	Probe		315-400	315-400 Gluten	315-400 Arab.	315-400 Starch
γ_s^d(mJ/m^2)	Alkanes	Linear	38	37	38	38
$-I_{sp}$ (kJ/mol)	Chloroform	Acid	10.1	10.8	10.7	9.8
	Acetone	Amphoteric	8.3	12.2	-	9.3
	Ethyl acetate	Amphoteric	4.2	5.3	5.3	4.2
	THF	Basic	5.5	7.0	6.9	6.4
	1,4-Dioxane	Basic	6.0	6.9	6.1	6.1

The coating with gluten and starch does not change significantly the retention capacity of the semolina surface by the polar or alkanes probes.

The coating with the gluten and arabinoxylan turns whatever the probe to an increase in the I_{SP}, both of them offer more energetic points on basic, amphoteric and acid probes. The coating with starch leads to a reduction of the I_{SP} registered with chloroform and acetone. These results can be interpreted as a limitation of the interaction between the probe and native gluten which is due to an excess of starch at the surface causing a reduction in the I_{SP} measurement with the acid probes.

From these results the gluten and arabinoxylan can be related whatever the probe with a higher energetic powder. Starch is less reactive and will reduce the interaction with acid probes.

Results are in agreement with those obtained in cellulose by (Rjiba et al., 2007), after coating, this affinity for the acid probes seams to be a characteristic in molecules of vegetal source such as arabinoxylan, gluten, starch or cellulose. Gluten and arabinoxylan present the higher affinity, this affinity is less strong with starch granules. Further investigation using lipids as a coating could complement the study. It would permit to know if lipids present also the same behavior.

It was noted an important point revealed by this study. Knowing that a very poor resolution of chromatographic peaks could cause a poor integration of chromatographic peaks, the shape of these peaks suggests that a diffusion phenomenon could take place inside the particles leading to forms of non-Gaussian chromatographic peaks.

IV.3.4. CONTRIBUTIONS OF THE FOOD POWDER SURFACE MODIFICATION TO THE FOOD POWDER KNOWLEDGE

The evolution of the surface after hydration was studied in both milk powders and semolina. It was possible to adapt the technique for both powders. From the results, different information was collected.

In the case of milk powders, an evolution of the surface as well as the particle size is observed from 40 % RH. The lactose crystallization occurs around 50 % RH in whole and skim milk powders and the growing of the crystals is visible at the particle surface. High RH strongly affects the surface, dissolution of the components is also observed. From the

dynamic diffusion coefficient, it was observed that skim milk powders present faster water diffusion than whole milk powder. These results are logical and linked to the presence or not of hydrophobic compounds like fat.

In the case of semolina, the humidity do not affect neither the surface nor the particle size until 70 % RH. At high HR (80-98 %) an evolution of the surface is observed, the gluten matrix gets softer and gelatinous and the starch swell up. However, there is no dissolution of the components. The dynamic diffusion coefficient is similar to the classic coefficient. This is logical because the particle size is not affected until HR reach high values. The use of the Y and N model can give information about differences in the water sorption in powder fractioned by size. The fractionation of the powder in different sizes relates the properties to the size particle, it permits a better understand of the effect of fines and big particles in the reactivity of the powder.

Finally, the dry coating is a very interesting technique to modify the surface of a food powder. Nevertheless, further investigation is necessary to optimize the coating process conditions and obtain a good quality of coated powders to permit a relation with the properties of the modified surface.

V. CONCLUSIONS ET PERSPECTIVES

Ce travail a permis de mettre en avant de nombreux résultats. De ces résultats une meilleure connaissance et explication de la surface des poudres alimentaires a été possible. Il est maintenant clair que pour une meilleure compréhension des relations entre les propriétés de surface et les propriétés fonctionnelles, il est absolument nécessaire de caractériser la surface de la poudre en détail. Pour ce faire, des méthodes analytiques spécifiques (physico-chimiques et physiques) capables d'évaluer les propriétés de surface des poudres alimentaires sont nécessaires. Ce travail de thèse a permis d'explorer des techniques innovantes, et de coupler ces techniques originales pour différentes poudres alimentaires. Les trois approches : atomique, moléculaire et microstructurale ont permis de mieux comprendre la réactivité de la surface et cette démarche a été originale et intéressante.

A l'échelle atomique…

Une étude approfondie avec les composants purs du lait et de la semoule a été faite pour valider l'utilisation de l'EDX dans le domaine des poudres alimentaires.

Pour les poudres de lait la technique a été validée. Même si les valeurs déduites à partir du système d'équations ne prédisent pas la quantité exacte des composants à la surface, une tendance sur la répartition des composants est clairement apparue. Le contenus en protéines est par contre correctement calculé, les valeurs des carbohydrates et des lipides sont toujours légèrement surestimées ou sous-estimées.

Du coté de la semoule, la technique semble plus compliquée à adapter. La surface hétérogène de la semoule ne permet pas des prédictions correctes, cela dépend beaucoup de la zone analysée. Toutefois, le couplage avec l'XPS permet de mieux comprendre la surface de la semoule. Les analyses effectuées par EDX sur des zones de semoule qui montrent une composition différente par ESEM, de même que les analyses par XPS à la semoule après extraction de la matière grasse, montrent que le modèle mathématique n'est pas toujours adapté. Par conséquence la prédiction des composants à la surface rend les valeurs aberrantes. Après agglomération de la semoule, c'est à dire, après l'obtention de couscous, les valeurs prédites par le système d'équations ne sont plus aberrantes. Cela peut s'expliquer par un réarrangement des composants à la surface des particules après hydratation, force mécanique et cuisson. La validation de l'EDX par mélanges binaires de composant purs n'a pas été faite parce que un mélange homogène des composants purs de semoule n'est pas possible à l'échelle de 5 µm.

A l'échelle moléculaire…

Pour la première fois sur des poudres de lait, une combinaison de techniques nouvelles (XPS, EDX, extractions de matières grasses) a été utilisée pour mieux comprendre la répartition des composants de la surface au cœur des particules. Des gradients de composition ont été validés par le couplage de techniques originales permettant l'analyse à des profondeurs variables. La technique EDX semble donc être un outil puissant qui peut parfaitement compléter l'analyse XPS, ce dernier étant maintenant bien documenté dans le domaine des produits laitiers en poudre.

Parallèlement, des gradients sur des poudres agglomérées en comparaison avec des poudres standards ont été étudiés. Il a été constaté que le processus d'agglomération n'a pas modifié les gradients de composition pour les poudres présentant la même composition chimique. La composition de la surface, les gradients de composition, ainsi que les fractions de matières grasses (la composition et les propriétés thermiques) sont similaires.

Pour la caractérisation des poudres réactives, la séparation de taille en différentes fractions permet de déterminer les particularités de la poudre à travers l'évolution de la taille des particules. Les fractions extrêmes 0-160 et 400-500 μm semblent avoir des caractéristiques différentes en comparaison avec le reste de la poudre au niveau de la morphologie, ce qui les rend plus réactives.

L'énergie libre de la surface est la même pour toutes les tailles de particules, mais des résultats plus intéressants sont attendus quand la nature de la sonde est acide ou basique. Le couplage avec la méthode XPS, permet de croiser l'information et de déduire les possibles composants qui interagissent avec la sonde. Néanmoins, l'obtention de ces données sont extrêmement compliquée. En effet, ces techniques ne sont pas complètement adaptées aux poudres alimentaires. L'énergie libre de surface obtenue par GCI et MC est un paramètre intéressant quand il est en rapport avec d'autres résultats. Toutefois, l'énergie libre de la surface des autres poudres alimentaires est quasiment inexistante dans la littérature. Une recherche plus approfondie est nécessaire pour adapter les deux techniques et pour obtenir des résultats plus fiables ainsi qu'une base de données permettant la comparaison des propriétés des surface dans le domaine alimentaire.

A l'échelle microstructurale…

Après une modification de la surface par l'intervention d'une contrainte externe hydrique, dans la poudre de lait entier et écrémée ainsi que pour la semoule; quelques conclusions se dessinent.

La diffusion de l'eau dans les poudres laitières a été étudiée et couplée à une étude structurale. Une relation entre l'état du lactose et la diffusivité de l'eau a été mise en évidence. L'évolution des composants à travers la diffusion de l'eau a mis en évidence la cristallisation du lactose à environ 54 % de HR et la dissolution des éléments aux fortes HR (> 80 %). Les différences observées ont été également liées à la composition de la surface (plus ou moins de lipides).

La diffusion de l'eau dans la semoule brute et tamisée, couplée avec l'évolution de la structure de la surface de semoule, a été étudiée. Une relation entre l'état de la matrice gluten-amidon et la diffusivité de l'eau a été mise en évidence. Les différences observées ont été liées à la taille des particules, la texture. Les propriétés de la matrice de gluten changent à travers la diffusion de l'humidité ; les petites particules présentent ainsi une prise plus élevée d'eau due à la présence d'une surface spécifique plus importante. Par conséquent, une structure plus mouillée a été observée. Ainsi, les particules de gluten apparaissent plus collantes permettant l'agglomération des particules à haute RH. Les grains d'amidon montrent une évolution de taille, c'est à dire un gonflement des grains.

Après insertion du diamètre réel dans le calcul du coefficient de diffusion, la poudre de lait écrémé présente une diffusion plus rapide que la poudre de lait entier. Dans le cas de la semoule, les courbes de coefficient dynamique de diffusion ne sont pas affectées par la taille des particules, le gonflement des particules est observé uniquement aux fortes HR, probablement dû aux propriétés non-solubles des composants formant le gluten.

Dans l'avenir, la connaissance de ces facteurs peut être utilisée pour un meilleur suivi de l'agglomération des poudres ainsi que l'amélioration de certaines propriétés fonctionnelles telles que la réhydratation ou encore les conditions de stockage. La combinaison de l'XPS et de l'EDX pour estimer la composition de surface des poudres à différentes profondeurs se complète avec le SEM qui permet d'étudier la structure des particules de poudre. Ces méthodes prometteuses peuvent aider à mieux comprendre la répartition des composants sous

la surface et leurs structures. Cette partie constitue une première étape à la compréhension du rôle de chaque constituant dans les propriétés des poudres alimentaires.

Dans le cadre d'une modification de la microstructure de surface de la semoule par enrobage à sec, la surface de la semoule a montré qu'elle peut être modifiée par enrobage à sec. La résistance de la semoule à la rupture lors d'un cisaillement élevé pendant l'utilisation du Cyclomix signifie qu'elle peut être recouverte sans être elle-même endommagée. Cette étude a également montré que le gluten, l'amidon et l'arabinoxylane peuvent recouvrir la surface en changeant légèrement les propriétés de surface. L'enrobage a été constaté par les images ESEM, le recouvrement est très faible mais il est considéré suffisant pour modifier la surface. Cependant, la quantité de force nécessaire pour séparer les particules de gluten au large de la semoule n'est pas très élevée (environ 0,5 bar de pression d'air). L'enrobage par gluten micronisée semble être le meilleur, cela était attendu car les particules de gluten ont été micronisées. Par conséquence, elles ont un rapport de taille plus adapté. L'arabinoxylane semble avoir un effet important dans les valeurs de CGI. En ESEM, l'enrobage semble avoir été effectivement déposé sur la surface de la semoule et semble former une couche unique. Cette propriété est liée aux propriétés physiques de l'arabinoxylane beaucoup plus malléables que les autres composants purs.

Conclusion générale et Perspectives…

Certaines techniques : modification de la surface par enrobage à sec, EDX, GCI et MC, ont rarement été utilisées sur des poudres alimentaires. Elles peuvent être un outil efficace pour évaluer les modifications des propriétés de surface d'une poudre. Malgré les difficultés pour adapter les techniques, elles semblent très prometteuses pour le domaine des poudres alimentaires. C'est toutefois indispensable d'approfondir les études pour obtenir des conditions optimales d'utilisation. Dans le cas de l'EDX, de nouveaux modèles mathématiques semblent nécessaires alors que pour la CGI et la MC, l'étude des poudres moins complexes comme des composant purs (amidon, lactose, gluten) semble prioritaire. Cela peut aider à mieux adapter les techniques et à mieux comprendre les phénomènes attendus pendant les analyses.

Parallèlement, d'autres investigations sont nécessaires pour lier les approches de base avec les applications technologiques, tout en intégrant la contribution de la surface des particules et les paramètres du procédé de fabrication. Les propriétés fonctionnelles

principales d'une poudre alimentaire peuvent être liées à des contraintes externes : hydriques, thermiques et/ou mécaniques et une évaluation fine de ces nouvelles propriétés doit être réalisée.

Finalement la détermination des propriétés de surface est d'une grande importance, cela peut être indispensable pour l'amélioration et l'optimisation de certaines propriétés fonctionnelles essentielles: le mouillage, la dispersibilité, la coulabilité, l'agglomération, notamment.

References

Adhikari, B., Howes, T., Bhandari, B. R., & Truong, V. (2001). Stickiness in Foods: A Review of Mechanisms and Test Methods. *International Journal of Food Properties*, *4*(1), 1-33.

ADPI. (2002). Determination of total ash - in standards for grades of dry milks including methods of analysis. *American Dry Product Institute, Elmhurst, IL, bulletin 916*, 40-41.

AFNOR. (1978). Détermination de la teneur en eau – méthode par étuvage, *No : V04-348*.

Al Mahdi, R., Nasirpour, A., Banon, S., Scher, J., & Desobry, S. (2006). Morphological and mechanical properties of dried skimmed milk and wheat flour mixtures during storage. *Powder Technology*, *163*(3), 145–151.

Ambarkhane, A. V., Pincott, K., & Buckton, G. (2005). The use of inverse gas chromatography and gravimetric vapour sorption to study transitions in amorphous lactose. *International Journal of Pharmaceutics*, *294*(1-2), 129–135.

An, H., Yang, H., Liu, Z., & Zhang, Z. (2008). Effects of heating modes and sources on nanostructure of gelatinized starch molecules using atomic force microscopy. *LWT - Food Science and Technology*, *41*(8), 1466–1471.

AOAC. (1984). *Official methods of analysis*. Association of Official Analytical Chemists (40.ª ed.). Washington DC.

Aspelund, T. G., & Wilson, L. A. (1983). Adsorption of off-flavor compounds onto soy protein: a thermodynamic study. *Journal of Agricultural and Food Chemistry*, *31*(3), 539–545.

Baldwin, P. M. (1995). *Studies on the surface chemistry, minor component composition and structure of granular starches* (PhD Thesis). University of Nottingham, UK.

Baldwin, P. M., Adler, J., Davies, M. C., & Melia, C. D. (1998). High Resolution Imaging of Starch Granule Surfaces by Atomic Force Microscopy. *Journal of Cereal Science*, *27*(3), 255–265.

Baldwin, P. M., Davies, M. C., & Melia, C. D. (1997). Starch granule surface imaging using low-voltage scanning electron microscopy and atomic force microscopy. *International Journal of Biological Macromolecules*, *21*(1-2), 103–107.

Barbosa-Canovas, G. V., Lopez, J. M., & Peleg, M. (1987). Density and compressibility of selected food powders mixtures. *Journal of Food Process Engineering*, *10*(1), 1–19.

Becker, H. A. (1959). A study of diffusion in solids of arbitrary shape, with application to the drying of the wheat kernel. *Journal of Applied Polymer Science*, *1*(2), 212–226.

Beleggia, R., Platani, C., Spano, G., Monteleone, M., & Cattivelli, L. (2009). Metabolic profiling and analysis of volatile composition of durum wheat semolina and pasta. *Journal of Cereal Science*, *49*(2), 301–309.

Bhaskar, A. R., Rizvi, S. S. H., Bertoli, C., Fay, L. B., & Hug, B. (1998). A comparison of physical and chemical properties of milk fat fractions obtained by two processing technologies. *Journal of the American Oil Chemists' Society*, *75*(10), 1249–1264.

Bosquillon, C., Rouxhet, P. G., Ahimou, F., Simon, D., Culot, C., Préat, V., & Vanbever, R. (2004). Aerosolization properties, surface composition and physical state of spray-dried protein powders. *Journal of Controlled Release*, *99*(3), 357–367.

Boutboul, A., Giampaoli, P., Feigenbaum, A., & Ducruet, V. (2000). Use of inverse gas chromatography with humidity control of the carrier gas to characterise aroma–starch interactions. *Food Chemistry*, *71*(3), 387–392.

Boutboul, A., Lenfant, F., Giampaoli, P., Feigenbaum, A., & Ducruet, V. (2002). Use of inverse gas chromatography to determine thermodynamic parameters of aroma-starch interactions. *Journal of Chromatography A*, *969*(1-2), 9–16.

Brendlé, E., & Papirer, E. (1997). A New Topological Index for Molecular Probes Used in Inverse Gas Chromatography. *Journal of Colloid and Interface Science*, *194*(1), 217–224.

Briggs, D. (1994). *Practical Surface Analysis: Auger and X-ray Photoelectron Spectroscopy v. 1* (2nd Edition.). Wiley-Blackwell.

Buchheim W. (1978). Distribution of extractable fat in particles spray dried whole milk. *XX International Dairy Congress*.

Buma, T. J. (1971). Free Fat in Spray-Dried Whole Milk. 10. A Final Report With a Physical Model for Free-Fat in Spray-Dried Milk. *Neth. Milk Dairy*, *25*, 159–174.

Bushuk, W., & Winkler, C. A. (1957). Sorption of water vapour on wheat flour, starch and gluten. *Cereal Chemistry*, *34*(2), 73–86.

Cavarretta, I. (2009). *The Influence of Particle Characteristics on the Engineering Behaviour of Granular Materials* (PhD Thesis). University of London, UK., London.

Chanvrier, H., Colonna, P., Della Valle, G., & Lourdin, D. (2005). Structure and mechanical behaviour of corn flour and starch–zein based materials in the glassy state. *Carbohydrate Polymers*, *59*(1), 109–119.

Chau, T. T., Bruckard, W. J., Koh, P. T. L., & Nguyen, A. V. (2009). A review of factors that

affect contact angle and implications for flotation practice. *Advances in Colloid and Interface Science*, *150*(2), 106–115.

Chivrac, F., Angellier-Coussy, H., Guillard, V., Pollet, E., & Avérous, L. (2010). How does water diffuse in starch/montmorillonite nano-biocomposite materials? *Carbohydrate Polymers*, *82*(1), 128–135.

Cliff, B., Lockyer, N., Jungnickel, H., Stephens, G., & Vickerman, J. C. (2003). Probing cell chemistry with time-of-flight secondary ion mass spectrometry: development and exploitation of instrumentation for studies of frozen-hydrated biological material. *Rapid Communications in Mass Spectrometry: RCM*, *17*(19), 2163–2167.

Coelho, U., Miltz, J., & Gilbert, S. G. (1979a). Water Binding on Collagen by Inverse Phase Gas Chromatography: Thermodynamic Considerations. *Macromolecules*, *12*(2), 284–287.

Coelho, U., Miltz, J., & Gilbert, S. G. (1979b). Application of inverse phase gas chromatography for determination of bound water in collagen. *Journal of Food Science*, *44*(4), 1150–1151.

Conder, J. R., & Young, C. L. (1979). *Physicochemical Measurement by Gas Chromatography*. John Wiley & Sons Ltd.

Crowther, A., Wilson, L. A., & Glatz, C. E. (1980). Effects of processing on adsorption of off-flavors onto soy protein1. *Journal of Food Process Engineering*, *4*(2), 99–115.

Cuq, B., Rondet, E., & Abecassis, J. (2011). Food powders engineering, between knowhow and science: Constraints, stakes and opportunities. *Powder Technology*, *208*(2), 244–251.

Deffense, E. (1993). Milk fat fractionation today: A review. *Journal of the American Oil Chemists' Society*, *70*(12), 1193–1201.

Delcour, J. A., & Hoseney, R. C. (2010). *Principles of Cereal Science and Technology, Third Edition* (3.ª ed.). Amer Assn of Cereal Chemists.

Demertzis, P. G., Riganakos, K. A., Giannakakos, P. N., & Kontominas, M. G. (1991). Study of water sorption behaviour of pectins using a computerised elution gas chromatographic technique. *Journal of the Science of Food and Agriculture*, *54*(3), 421–428.

Demertzis, P. G., Riganakos, K. A., & Kontominas, M. G. (1989). Water sorption isotherms of crystalline raffinose by inverse gas chromatography. *International Journal of Food Science & Technology*, *24*(6), 629–636.

Du, C.-J., & Sun, D.-W. (2004). Recent developments in the applications of image processing

techniques for food quality evaluation. *Trends in Food Science & Technology*, *15*(5), 230–249.

Dural, N. H., & Hines, A. L. (1993). Adsorption of water on cereal-bread type dietary fibers. *Journal of Food Engineering*, *20*(1), 17–43.

El-Khawas, F., Tawashi, R., & Von Czetsch Lindenwald, H. (1966). Water Vapor Sorption and Suction Potential of Starch Grains. *Journal of the Society of Cosmetic Chemists*, *17*(2), 103–114.

Enrione, J. I., Hill, S. E., & Mitchell, J. R. (2007). Sorption and Diffusional Studies of Extruded Waxy Maize Starch-Glycerol Systems. *Starch - Stärke*, *59*(1), 1–9.

Fäldt, P. (1995). *Surface composition of spray dried emulsions* (PhD Thesis). Department of Food Engineering, Lund University, Lund, Sweden.

Fäldt, P., Bergenstahl, B., Carlsson, G., Sloof, W. G., Colombo, V. E., & Driedonks, D. A. (1993). The surface coverage of fat on food powders analyzed by ESCA (electron spectroscopy for chemical analysis). Discussion. *Food structure*, *12*(2), 225–234.

Fäldt, P., & Bergenståhl, B. (1994). The surface composition of spray-dried protein—lactose powders. *Colloids and Surfaces A: Physicochemical and Engineering Aspects*, *90*(2–3), 183–190.

Fäldt, P., & Bergenståhl, B. (1996a). Spray-dried whey protein/lactose/soybean oil emulsions. 1. Surface composition and particle structure. *Food Hydrocolloids*, *10*(4), 421–429.

Fäldt, P., & Bergenståhl, B. (1996b). Changes in Surface Composition of Spray-Dried Food Powders due to Lactose Crystallization. *LWT - Food Science and Technology*, *29*(5–6), 438–446.

Fannon, J. E., Shull, J. M., & Bemiller, J. N. (1993). Interior channels of starch granules. *Cereal chemistry*, *70*(5), 611–613.

Farkas, J., & Mohácsi-Farkas, C. (1996). Application of differential scanning calorimetry in food research and food quality assurance. *Journal of Thermal Analysis*, *47*(6), 1787–1803.

Fitzpatrick, J. J., Hodnett, M., Twomey, M., Cerqueira, P. S. M., O'Flynn, J., & Roos, Y. H. (2007). Glass transition and the flowability and caking of powders containing amorphous lactose. *Powder Technology*, *178*(2), 119–128.

Focardi, S., Ristori, S., Mazzuoli, S., Tognazzi, A., Leach-Scampavia, D., Castner, D. G., & Rossi, C. (2006). ToF-SIMS and PCA studies of Seggianese olives and olive oil. *Colloids and Surfaces A: Physicochemical and Engineering Aspects*, *279*(1–3), 225–232.

Forny, L., Marabi, A., & Palzer, S. (2011). Wetting, disintegration and dissolution of agglomerated water soluble powders. *Powder Technology*, *206*(1–2), 72–78.

Foster, K. D., Bronlund, J. E., & Paterson, A. H. J. (Tony. (2005). The contribution of milk fat towards the caking of dairy powders. *International Dairy Journal*, *15*(1), 85–91.

Freudig, B., Hogekamp, S., & Schubert, H. (1999). Dispersion of powders in liquids in a stirred vessel. *Chemical Engineering and Processing*, *38*(4-6), 525–532.

Funami, T. (2010). Atomic force microscopy imaging of food polysaccharides. *Food Science and Technology Research*, *16*(1), 1–12.

Funami, T., Noda, S., Nakauma, M., Ishihara, S., Takahashi, R., Al-Assaf, S., Ikeda, S., et al. (2008). Molecular structures of gellan gum imaged with atomic force microscopy in relation to the rheological behavior in aqueous systems in the presence or absence of various cations. *Journal of Agricultural and Food Chemistry*, *56*(18), 8609–8618.

Fyfe, K. N., Kravchuk, O., Le, T., Deeth, H. C., Nguyen, A. V., & Bhandari, B. (2011). Storage induced changes to high protein powders: influence on surface properties and solubility. *Journal of the Science of Food and Agriculture*, *91*(14), 2566–2575.

Gaiani, C. (2006). *Étude des mécanismes de réhydratation des poudres laitières: influence de la structure et de la composition des poudres*, (PhD Thesis). University of Lorraine, Vandoeubre lès Nancy, France.

Gaiani, C., Banon, S., Scher, J., Schuck, P., & Hardy, J. (2005). Use of a Turbidity Sensor to Characterize Micellar Casein Powder Rehydration: Influence of Some Technological Effects. *Journal of Dairy Science*, *88*(8), 2700–2706.

Gaiani, C., Boyanova, P., Hussain, R., Murrieta Pazos, I., Karam, M. C., Burgain, J., & Scher, J. (2011a). Morphological descriptors and colour as a tool to better understand rehydration properties of dairy powders. *International Dairy Journal*, *21*(7), 462–469.

Gaiani, C., Ehrhardt, J. J., Scher, J., Hardy, J., Desobry, S., & Banon, S. (2006). Surface composition of dairy powders observed by X-ray photoelectron spectroscopy and effects on their rehydration properties. *Colloids and Surfaces B: Biointerfaces*, *49*(1), 71–78.

Gaiani, C., Morand, M., Sanchez, C., Tehrany, E. A., Jacquot, M., Schuck, P., Jeantet, R., et al. (2010). How surface composition of high milk proteins powders is influenced by spray-drying temperature. *Colloids and Surfaces B: Biointerfaces*, *75*(1), 377–384.

Gaiani, C., Mullet, M., Arab-Tehrany, E., Jacquot, M., Perroud, C., Renard, A., & Scher, J.

(2011b). Milk proteins differentiation and competitive adsorption during spray-drying. *Food Hydrocolloids*, *25*(5), 983–990.

Gaiani, C., Scher, J., Ehrhardt, J. J., Linder, M., Schuck, P., Desobry, S., & Banon, S. (2007a). Relationships between Dairy Powder Surface Composition and Wetting Properties during Storage: Importance of Residual Lipids. *Journal of Agricultural and Food Chemistry*, *55*(16), 6561–6567.

Gaiani, C., Schuck, P., Scher, J., Desobry, S., & Banon, S. (2007b). Dairy powder rehydration: Influence of protein state, incorporation mode, and agglomeration. *Journal of Dairy Science*, *90*(2), 570–581.

Gaiani, C., Schuck, P., Scher, J., Ehrhardt, J. J., Arab-Tehrany, E., Jacquot, M., & Banon, S. (2009). Native phosphocaseinate powder during storage: Lipids released onto the surface. *Journal of Food Engineering*, *94*(2), 130–134.

Galet, L., Vu, T. O., Oulahna, D., & Fages, J. (2004). The Wetting Behaviour and Dispersion Rate of Cocoa Powder in Water. *Food and Bioproducts Processing*, *82*(4), 298–303.

Gallant, D. J., Bouchet, B., & Baldwin, P. M. (1997). Microscopy of starch: evidence of a new level of granule organization. *Carbohydrate Polymers*, *32*(3-4), 177–191.

Gerin, P. A., Dengis, P. B., & Rouxhet, P. G. (1995). Performance of XPS analysis of model biochemical compounds. *Journal de chimie physique*, *92*(5), 1043–1065.

Grenha, A., Seijo, B., Serra, C., & Remuñan-López, C. (2007). Chitosan nanoparticle-loaded mannitol microspheres: structure and surface characterization. *Biomacromolecules*, *8*(7), 2072–2079.

Guillard, V., Broyart, B., Bonazzi, C., Guilbert, S., & Gontard, N. (2003). Moisture Diffusivity in Sponge Cake as Related to Porous Structure Evaluation and Moisture Content. *Journal of Food Science*, *68*(2), 555–562.

Gunning, A. P., Kirby, A. R., Parker, M. L., Cross, K. L., & Morris, J. (2010). Utilizing Atomic Force Microscopy in Food Research. *Food Technology*, *64*(12), 32–37.

Haque, M. K., & Roos, Y. H. (2006). Differences in the physical state and thermal behavior of spray-dried and freeze-dried lactose and lactose/protein mixtures. *Innovative Food Science & Emerging Technologies*, *7*(1-2), 62–73.

Hartmann, M., & Palzer, S. (2011). Caking of amorphous powders — Material aspects, modelling and applications. *Powder Technology*, *206*(1–2), 112–121.

Hassan, H. M., & Mumford, C. J. (1993). Mechanisms of Drying of Skin Forming Materials. III. Droplets of Natural Products. *Drying Technology: An International Journal*, *11*(7), 1765.

Hébrard, A., Oulahna, D., Galet, L., Cuq, B., Abecassis, J., & Fages, J. (2003). Hydration properties of durum wheat semolina: influence of particle size and temperature. *Powder Technology*, *130*(1–3), 211–218.

Hecht, J. P., & King, C. J. (2000). Spray Drying: Influence of Developing Drop Morphology on Drying Rates and Retention of Volatile Substances. 2. Modeling. *Industrial & Engineering Chemistry Research*, *39*(6), 1766–1774.

Helen, H. J., & Gilbert, S. G. (1985). Moisture Sorption of Dry Bakery Products by Inverse Gas Chromatography. *Journal of Food Science*, *50*(2), 454–458.

Hentschel, M. L., & Page, N. W. (2003). Selection of Descriptors for Particle Shape Characterization. *Particle & Particle Systems Characterization*, *20*(1), 25–38.

Hogan, S. A., & O'Callaghan, D. J. (2010). Influence of milk proteins on the development of lactose-induced stickiness in dairy powders. *International Dairy Journal*, *20*(3), 212–221.

IDF. (1987). Dried milk, dried whey, dried butter-milk & dried butter-serums determination of fat contents Röse-Gottlieb reference method. International Dairy Federation: Brussels, Belgium, 9C.

Iijima, M., Shinozaki, M., Hatakeyama, T., Takahashi, M., & Hatakeyama, H. (2007). AFM studies on gelation mechanism of xanthan gum hydrogels. *Carbohydrate Polymers*, *68*(4), 701–707.

ISO. (2006). Representation of results of particle size analysis. Part 1-6. Part 6: Descriptive and quantitative representation of particle shape and morphology. *Draft International Standard ISO/DIS 9276, Geneva., International Organization for Standardization*.

James, B. J., & Smith, B. G. (2009). Surface structure and composition of fresh and bloomed chocolate analysed using X-ray photoelectron spectroscopy, cryo-scanning electron microscopy and environmental scanning electron microscopy. *LWT - Food Science and Technology*, *42*(5), 929–937.

Jayasundera, M., Adhikari, B., Adhikari, R., & Aldred, P. (2011a). The effect of protein types and low molecular weight surfactants on spray drying of sugar-rich foods. *Food Hydrocolloids*, *25*(3), 459–469.

Jayasundera, M., Adhikari, B., Aldred, P., & Ghandi, A. (2009). Surface modification of spray dried food and emulsion powders with surface-active proteins: A review. *Journal of Food Engineering*, *93*(3), 266–277.

Jayasundera, M., Adhikari, B., Adhikari, R., & Aldred, P. (2010). The Effect of Food-Grade Low-Molecular-Weight Surfactants and Sodium Caseinate on Spray Drying of

Sugar-Rich Foods. *Food Biophysics*, *5*(2), 128–137.

Jayasundera, M., Adhikari, B., Adhikari, R., & Aldred, P. (2011b). The effects of proteins and low molecular weight surfactants on spray drying of model sugar-rich foods: Powder production and characterisation. *Journal of Food Engineering*, *104*(2), 259–271.

Jayasundera, M., Adhikari, B., Howes, T., & Aldred, P. (2011c). Surface protein coverage and its implications on spray-drying of model sugar-rich foods: Solubility, powder production and characterisation. *Food Chemistry*, *128*(4), 1003–1016.

Jenni, K. (2007). *Caractérisation des propriétés de surface de poudres alimentaires: farine de blé.* (Master report). Université de Monpellier, France.

Jouppila, K., Kansikas, J., & Roos, Y. H. (1997). Glass Transition, Water Plasticization, and Lactose Crystallization in Skim Milk Powder. *Journal of Dairy Science*, *80*(12), 3152–3160.

Jouppila, K., & Roos, Y. H. (1994). Water Sorption and Time-Dependent Phenomena of Milk Powders. *Journal of Dairy Science*, *77*(7), 1798–1808.

Kentish, S., Davidson, M., Hassan, H., & Bloore, C. (2005). Milk skin formation during drying. *Chemical Engineering Science*, *60*(3), 635–646.

Kim, E. H. J. (2008). *Surface composition of industrial spray-dried dairy powders and its formation mechanisms* (PhD Thesis). The University of Auckland, Auckland, Nueva Zelanda.

Kim, E. H. J., Chen, X. D., & Pearce, D. (2002). Surface characterization of four industrial spray-dried dairy powders in relation to chemical composition, structure and wetting property. *Colloids and Surfaces B: Biointerfaces*, *26*(3), 197–212.

Kim, E. H. J., Chen, X. D., & Pearce, D. (2005a). Effect of surface composition on the flowability of industrial spray-dried dairy powders. *Colloids and Surfaces B: Biointerfaces*, *46*(3), 182–187.

Kim, E. H. J., Chen, X. D., & Pearce, D. (2005b). Melting characteristics of fat present on the surface of industrial spray-dried dairy powders. *Colloids and Surfaces B: Biointerfaces*, *42*(1), 1–8.

Kim, E. H. J., Chen, X. D., & Pearce, D. (2009a). Surface composition of industrial spray-dried milk powders. 1. Development of surface composition during manufacture. *Journal of Food Engineering*, *94*(2), 163–168.

Kim, E. H. J., Chen, X. D., & Pearce, D. (2009b). Surface composition of industrial spray-dried milk powders. 2. Effects of spray drying conditions on the surface composition. *Journal of Food Engineering*, *94*(2), 169–181.

Kim, E. H. J., Chen, X. D., & Pearce, D. (2009c). Surface composition of industrial spray-dried milk powders. 3. Changes in the surface composition during long-term storage. *Journal of Food Engineering*, *94*(2), 182–191.

Kim, E. H. J., Dong Chen, X., & Pearce, D. (2003). On the Mechanisms of Surface Formation and the Surface Compositions of Industrial Milk Powders. *Drying Technology*, *21*(2), 265–278.

Kingshott, P., Andersson, G., McArthur, S. L., & Griesser, H. J. (2011). Surface modification and chemical surface analysis of biomaterials. *Current opinion in chemical biology*, *15*(5), 667–676.

Kirby, A. R., MacDougall, A. J., & Morris, V. J. (2008). Atomic force microscopy of tomato and sugar beet pectin molecules. *Carbohydrate Polymers*, *71*(4), 640–647.

Knowlton, T. M., Carson, J. W., Klinzing, G. E., & Yang, W. C. (1994). The importance of storage, transfer and collection. *Chemical Engineering Progress*, *90*(4), 44–54.

Konopka, I., Rotkiewicz, D., & Tańska, M. (2005). Wheat endosperm hardness. Part II. Relationships to content and composition of flour lipids. *European Food Research and Technology*, *220*(1), 20–24.

Labuza, T. ., & Hyman, C. . (1998). Moisture migration and control in multi-domain foods. *Trends in Food Science & Technology*, *9*(2), 47–55.

Lagoudaki, M., & Demertzis, P. G. (1994). Equilibrium moisture characteristics of dehydrated food constituents as studied by a modified inverse gas chromatographic method. *Journal of the Science of Food and Agriculture*, *65*(1), 101–109

Lagoudaki, M., Demertzis, P. G., & Kontominas, M. G. (1993). Moisture Adsorption Behaviour of Pasta Products. *Lebensmittel-Wissenschaft und-Technologie*, *26*(6), 512–516.

Larousse.fr - Types de broyeurs. Encyclopédie. Recuperado noviembre 30, 2012, a partir de http://www.larousse.fr/encyclopedie/image/Laroussefr_-_Article/1001454

Laskin, A., & Cowin, J. P. (2001). Automated Single-Particle SEM/EDX Analysis of Submicrometer Particles down to 0.1 μm. *Analytical Chemistry*, *73*(5), 1023–1029.

Lefebvre, G., Galet, L., & Chamayou, A. (2011). Dry coating of talc particles with fumed silica: Influence of the silica concentration on the wettability and dispersibility of the composite particles. *Powder Technology*, *208*(2), 372–377.

Lévy, R., & Maaloum, M. (2002). Measuring the spring constant of atomic force microscope cantilevers: thermal fluctuations and other methods. *Nanotechnology*, *13*(1), 33–37.

Lin, S. X. Q., Chen, X. D., & Pearce, D. L. (2005). Desorption isotherm of milk powders at

elevated temperatures and over a wide range of relative humidity. *Journal of Food Engineering*, *68*(2), 257–264.

Lukasiewicz, M., Ptaszek, A., Koziel, L., Achremowicz, B., & Grzesik, M. (2007). Carboxymethylcellulose/polyaniline blends. Synthesis and properties. *Polymer Bulletin*, *58*(1), 281–288.

Lyn, M. E., Burnett, D., Garcia, A. R., & Gray, R. (2010). Interaction of Water with Three Granular Biopesticide Formulations. *Journal of Agricultural and. Food Chemistry*, *58*(3), 1804–1814.

Marabi, A., Raemy, A., Bauwens, I., Burbidge, A., Wallach, R., & Saguy, I. S. (2008). Effect of fat content on the dissolution enthalpy and kinetics of a model food powder. *Journal of Food Engineering*, *85*(4), 518–527.

Mathlouthi, M., & Rogé, B. (2003). Water vapour sorption isotherms and the caking of food powders. *Food Chemistry*, *82*(1), 61–71.

McKenna, A. B. (1997). Examination of whole milk powder by confocal laser scanning microscopy. *Journal of Dairy Research*, *64*(3), 423–432.

McKenna, A. B., Lloyd, R. J., Munro, P. A., & Singh, H. (1999). Microstructure of whole milk powder and of insolubles detected by powder functional testing. *Scanning*, *21*(5), 305–315.

McMullin, S. L., Bernhard, R. A., & Nickerson, T. A. (1975). Heats of adsorption of small molecules on lactose. *Journal of Agricultural and Food Chemistry*, *23*(3), 452–458.

Millqvist-Fureby, A. (2003). Characterisation of spray-dried emulsions with mixed fat phases. *Colloids and Surfaces B: Biointerfaces*, *31*(1–4), 65–79.

Millqvist-Fureby, A., Elofsson, U., & Bergenståhl, B. (2001). Surface composition of spray-dried milk protein-stabilised emulsions in relation to pre-heat treatment of proteins. *Colloids and Surfaces B: Biointerfaces*, *21*(1–3), 47–58.

Millqvist-Fureby, A., & Smith, P. (2007). In-situ lecithination of dairy powders in spray-drying for confectionery applications. *Food Hydrocolloids*, *21*(5–6), 920–927.

Mistry, V. V., Hassan, H. M., & Robinson, D. J. (1992). Effect of lactose and protein on the microstructure of dried milk. *Food Structure*, 11(1), 73-82.

Murrieta-Pazos, I., Gaiani, C., Galet, L., Calvet, R., Cuq, B., & Scher, J. (2012a). Food powders: Surface and form characterization revisited. *Journal of Food Engineering*, *112*(1-2), 1–21.

Murrieta-Pazos, I., Gaiani, C., Galet, L., Cuq, B., Desobry, S., & Scher, J. (2011). Comparative study of particle structure evolution during water sorption: Skim and

whole milk powders. *Colloids and Surfaces B: Biointerfaces*, *87*(1), 1–10.

Murrieta-Pazos, I., Gaiani, C., Galet, L., & Scher, J. (2012b). Composition gradient from surface to core in dairy powders: Agglomeration effect. *Food Hydrocolloids*, *26*(1), 149–158.

Nasirpour, A., Landillon, V., Cuq, B., Scher, J., Banon, S., & Desobry, S. (2007). Lactose Crystallization Delay in Model Infant Foods Made With Lactose, β-Lactoglobulin, and Starch. *Journal of Dairy Science*, *90*(8), 3620–3626.

Newell, H. E., Buckton, G., Butler, D. A., Thielmann, F., & Williams, D. R. (2001a). The use of inverse phase gas chromatography to measure the surface energy of crystalline, amorphous, and recently milled lactose. *Pharmaceutical research*, *18*(5), 662–666.

Newell, H. E., Buckton, G., Butler, D. A., Thielmann, F., & Williams, D. R. (2001b). The use of inverse phase gas chromatography to study the change of surface energy of amorphous lactose as a function of relative humidity and the processes of collapse and crystallisation. *International Journal of Pharmaceutics*, *217*(1-2), 45–56.

Nguyen, T., & Johns, W. E. (1978). Polar and dispersion force contributions to the total surface free energy of wood. *Wood Science and Technology*, *12*(1), 63–74.

Nijdam, J. J., & Langrish, T. A. G. (2006). The effect of surface composition on the functional properties of milk powders. *Journal of Food Engineering*, *77*(4), 919–925.

Ocieczek, A. (2007). Comparison of sorption properties of semolina and farina. *Acta Agrophysica*, *9*(1), 135–145.

Ohtani, T., Yoshino, T., Hagiwara, S., & Maekawa, T. (2000a). High-resolution Imaging of Starch Granule Structure using Atomic Force Microscopy. *Starch - Stärke*, *52*(5), 150–153.

Ohtani, T., Yoshino, T., Ushiki, T., Hagiwara, S., & Maekawa, T. (2000b). Structure of rice starch granules in nanometre scale as revealed by atomic force microscopy. *Journal of Electron Microscopy*, *49*(3), 487 –489.

Olivares, M. L., Passeggi Jr., M. C. G., Ferrón, J., Zorrilla, S. E., & Rubiolo, A. C. (2010). Study of milk/[kappa]-carrageenan mixtures by atomic force microscopy. *Food Hydrocolloids*, *24*(8), 776–782.

Ortega-Rivas, E. (2009). Bulk properties of food particulate materials: An appraisal of their characterisation and relevance in processing. *Food and Bioprocess Technology*, *2*(1), 28–44.

Otles, S. (2008). *Modification of surface properties of biopowders by dry particle coating.* (PhD Thesis). Université de Toulouse., France.

Otles, S., Lecoq, O., & Dodds, J. A. (2011). Dry particle high coating of biopowders: An energy approach. *Powder Technology*, *208*(2), 378–382.

Ouabbas, Y. (2008). *Procédés mécaniques d'élaboration à sec de particules composites à propriétés d'usage contrôlées. Caractérisation et stabilité d'un gel de silice.* (PhD Thesis). Ecole Nationale Supérieure des Mines de Saint-Etienne. Saint-Etienne, France.

Ouabbas, Y., Dodds, J., Galet, L., Chamayou, A., & Baron, M. (2009). Particle-particle coating in a cyclomix impact mixer. *Powder Technology*, *189*(2), 245–252.

Özkan, N., Walisinghe, N., & Chen, X. D. (2002). Characterization of stickiness and cake formation in whole and skim milk powders. *Journal of Food Engineering*, *55*(4), 293–303.

Palzer, S. (2010). The relation between material properties and supra-molecular structure of water-soluble food solids. *Trends in Food Science & Technology*, *21*(1), 12–25.

Paramita, V., Iida, K., Yoshii, H., & Furuta, T. (2010). Effect of Feed Liquid Temperature on the Structural Morphologies of *d*-Limonene Microencapsulated Powder and Its Preservation. *Journal of Food Science*, *75*(1), E39–E45.

Parker, M. L., Kirby, A. R., & Morris, V. J. (2008). In situ imaging of pea starch in seeds. *Food Biophysics*, *3*(1), 66–76.

Perea, M. J., Arzate, I., Terres, E., Alamilla, L., Calderon, G., Guttierrez, G. F., Garibay, V., *et al*. (2009). Morphological characterization of powder milk and their relationship with rehydration properties. *Proceedings of the 5th CIGR section IV international symposium on food 439 processing, monitoring technology in bioprocesses and food quality management.* Potsdam, Germany.

Písecký, J. (1997). *Handbook of Milk Powder Manufacture*. Niro A/S.

Prego, I., Maldonado, S., & Otegui, M. (1998). Seed Structure and Localization of Reserves inChenopodium quinoa. *Annals of Botany*, *82*(4), 481–488.

Prom-u-thai, C., Huang, L., Rerkasem, B., Thomson, G., Kuo, J., Saunders, M., & Dell, B. (2008). Distribution of Protein Bodies and Phytate-Rich Inclusions in Grain Tissues of Low and High Iron Rice Genotypes. *Cereal Chemistry*, *85*(2), 257–265.

Qi, P. X. (2007). Studies of casein micelle structure : the past and the present. *Review Literature And Arts Of The Americas*, *87*(4-5), 363–383.

Quiroga, C. C., & Bergenståhl, B. (2007). Characterization of the microstructure of phase segregated amylopectin and β-lactoglobulin dry mixtures. *Food Biophysics*, *2*(4), 172–182.

Rayas-Duarte, P., Robinson, S. F., & Freeman, T. P. (1995). In situ location of a starch granule protein in durum wheat endosperm by immunocytochemistry. *Cereal Chemistry*, *72*(3), 269–274.

Refstrup, E. (2003). Drying of milk. *Encyclopedia of Dairy Science* (H. Roginsky., pp. 860–871). London: Academic Press.

Ridout, M. J., Parker, M. L., Hedley, C. L., Bogracheva, T. Y., & Morris, V. J. (2004). Atomic Force Microscopy of Pea Starch: Origins of Image Contrast. *Biomacromolecules*, *5*(4), 1519–1527.

Riganakos, K.A., Demertzis, P. G., & Kontominas, M. G. (1989). Gas chromatographic study of water sorption by wheat flour. *Journal of Cereal Science*, *9*(3), 261–271.

Riganakos, K.A., Demertzis, P. G., & Kontominas, M. G. (1994). Water Sorption by Wheat and Soy Flour: Comparison of Three Methods. *Journal of Cereal Science*, *20*(1), 101–106.

Riganakos, K. A, Demertzis, P. G., & Kontominas, M. G. (1997). Study of water sorption of flours (wheat and soy) using a hygrometric method: effect of relative humidity during heat treatment. *Zeitschrift für Lebensmitteluntersuchung und Forschung A*, *204*(5), 369–373.

Rjiba, N., Nardin, M., Dréan, J.-Y., & Frydrych, R. (2007). A study of the surface properties of cotton fibers by inverse gas chromatography. *Journal of Colloid and Interface Science*, *314*(2), 373–380.

Roca, E., Broyart, B., Guillard, V., Guilbert, S., & Gontard, N. (2007). Controlling moisture transport in a cereal porous product by modification of structural or formulation parameters. *Food Research International*, *40*(4), 461–469.

Roca, E., Broyart, B., Guillard, V., Guilbert, S., & Gontard, N. (2008a). Predicting moisture transfer and shelf-life of multidomain food products. *Journal of Food Engineering*, *86*(1), 74–83.

Roca, E., Guillard, V., Broyart, B., Guilbert, S., & Gontard, N. (2008b). Effective moisture diffusivity modelling versus food structure and hygroscopicity. *Food Chemistry*, *106*(4), 1428–1437.

Roman-Gutierrez, A. D., Mabille, F., Guilbert, S., & Cuq, B. (2003). Contribution of Specific Flour Components to Water Vapor Adsorption Properties of Wheat Flours. *Cereal Chemistry*, *80*(5), 558–563.

Rousset, P., Sellappan, P., & Daoud, P. (2002). Effect of emulsifiers on surface properties of sucrose by inverse gas chromatography. *Journal of Chromatography A*, *969*(1–2),

97–101.

Rouxhet, P. G., Misselyn-Bauduin, A. M., Ahimou, F., Genet, M. J., Adriaensen, Y., Desille, T., Bodson, P., *et al*. (2008). XPS analysis of food products: toward chemical functions and molecular compounds. *Surface and Interface Analysis*, *40*(3-4), 718–724.

Rouxhet, Paul G., & Genet, M. J. (2011). XPS analysis of bio-organic systems. *Surface and Interface Analysis*, *43*(12), 1453–1470.

Russell, P. L., Gough, B. M., Greenwell, P., Fowler, A., & Munro, H. S. (1987). A study by ESCA of the surface of native and chlorine-treated wheat starch granules: The effects of various surface treatments. *Journal of Cereal Science*, *5*(1), 83–100.

Saad, M. (2011). *Étude des mécanismes d'agglomération des poudres céréaliers: contribution des caractéristiques physiques et chimiques des particules sur leur réactivité. Application pour la fabrication de couscous.* (PhD Thesis). SupAgro Montpellier, Montpellier.

Saad, M., Gaiani, C., Mullet, M., Scher, J., & Cuq, B. (2011a). X-ray Photoelectron Spectroscopy for Wheat Powders: Measurement of Surface Chemical Composition. *Journal of Agricultural and Food Chemistry*, *59*(5), 1527–1540.

Saad, M., Gaiani, C., Scher, J., Cuq, B., Ehrhardt, J. J., & Desobry, S. (2009). Impact of re-grinding on hydration properties and surface composition of wheat flour. *Journal of Cereal Science*, *49*(1), 134–140.

Saad, M., Sadoudi, A., Rondet, E., & Cuq, B. (2011b). Morphological characterization of wheat powders, how to characterize the shape of particles? *Journal of Food Engineering*, *102*(4), 293–301.

Salazar-Banda, G. R., Felicetti, M. A., Gonçalves, J. A. S., Coury, J. R., & Aguiar, M. L. (2007). Determination of the adhesion force between particles and a flat surface, using the centrifuge technique. *Powder Technology*, *173*(2), 107–117.

Sanyal, B., Chawla, S. P., & Sharma, A. (2009). An improved method to identify irradiated rice by EPR spectroscopy and thermoluminescence measurements. *Food Chemistry*, *116*(2), 526–534.

Schuck, P., Jeantet, R., & Dolivet, A. (2012). Analytical Methods for Food and Dairy Powders (1.ª ed.). Wiley-Blackwell.

Shrestha, A. K., Howes, T., Adhikari, B. P., Wood, B. J., & Bhandari, B. R. (2007). Effect of protein concentration on the surface composition, water sorption and glass transition temperature of spray-dried skim milk powders. *Food Chemistry*, *104*(4), 1436–1444.

Silalai, N., & Roos, Y. H. (2010). Roles of water and solids composition in the control of glass transition and stickiness of milk powders. *Journal of Food Science*, *75*(5), E285–296.

Sindayikengera, S., & Xia, W. (2006). Nutritional evaluation of caseins and whey proteins and their hydrolysates from Protamex. *Journal of Zhejiang University. Science. B*, *7*(2), 90–98.

Sissons, M. (2008). Role of durum wheat composition on the quality of the pasta and bread. *Food*, *2*(2), 75–90.

Smith, D. S., Mannheim, C. H., & Gilbert, S. G. (1981). Water Sorption Isotherms of Sucrose and Glucose by Inverse Gas Chromatography. *Journal of Food Science*, *46*(4), 1051–1053.

Stevens, J. S., & Schroeder, S. L. M. (2009). Quantitative analysis of saccharides by X-ray photoelectron spectroscopy. *Surface and Interface Analysis*, *41*(6), 453–462.

Ten Grotenhuis, E., van Aken, G., van Malssen, K., & Schenk, H. (1999). Polymorphism of milk fat studied by differential scanning calorimetry and real-time X-ray powder diffraction. *Journal of the American Oil Chemists' Society*, *76*(9), 1031–1039.

Thomas, G., Ouabbas, Y., Grosseau, P., Baron, M., Chamayou, A., & Galet, L. (2009). Modeling the mean interaction forces between powder particles. Application to silica gel–magnesium stearate mixtures. *Applied Surface Science*, *255*(17), 7500–7507.

Ticehurst, M. D., York, P., Rowe, R. C., & Dwivedi, S. K. (1996). Characterisation of the surface properties of [alpha]-lactose monohydrate with inverse gas chromatography, used to detect batch variation. *International Journal of Pharmaceutics*, *141*(1-2), 93–99.

Tomoaia-Cotisel, M., Cioica, N., Cota, C., Racz, C., Petean, I., Bobos, L. D., Mocanu, A., *et al*. (2010). Structure of starch granules revealed by atomic force microscopy. *Studia Universitatis Babes-Bolyai Chemia*, *2*(2), 313–324.

Ulusoy, U. (2008). Application of ANOVA to image analysis results of talc particles produced by different milling. *Powder Technology*, *188*(2), 133–138.

Van Nieuwenhuijzen, N. H., Meinders, M. B. J., Tromp, R. H., Hamer, R. J., & van Vliet, T. (2008). Water uptake mechanism in crispy bread crust. *Journal of Agricultural and Food Chemistry*, *56*(15), 6439–6446.

Vega, C., Kim, E. H. J., Chen, X. D., & Roos, Y. H. (2005). Solid-state characterization of spray-dried ice cream mixes. *Colloids and Surfaces. B, Biointerfaces*, *45*(2), 66–75.

Vignolles, M. L., Jeantet, R., Lopez, C., & Schuck, P. (2007). Free fat, surface fat ad dairy

powders: interactions between process and product. A review. *Le Lait*, *87*(3), 50.

Vignolles, M. L., Lopez, C., Ehrhardt, J.-J., Lambert, J., Méjean, S., Jeantet, R., & Schuck, P. (2009a). Methods' combination to investigate the suprastructure, composition and properties of fat in fat-filled dairy powders. *Journal of Food Engineering*, *94*(2), 154–162.

Vignolles, M. L., Lopez, C., Madec, M. N., Ehrhardt, J. J., Méjean, S., Schuck, P., & Jeantet, R. (2009b). Fat properties during homogenization, spray-drying, and storage affect the physical properties of dairy powders. *Journal of Dairy Science*, *92*(1), 58–70.

Wadell, H. (1933). Sphericity and roundness of rock particles. *Journal of Geology*, *41*(3), 310–331.

Waduge, R. N., Xu, S., & Seetharaman, K. (2010). Iodine absorption properties and its effect on the crystallinity of developing wheat starch granules. *Carbohydrate Polymers*, *82*(3), 786–794.

Walton, D. E. (2000). The morphology of spray dried particles a qualitative view PB-Taylor & Francis. *Drying Technology: An International Journal*, *18*(9), 1943.

Washburn, E. W. (1921). The Dynamics of Capillary Flow. *Physical Review*, *17*(3), 273–283.

Whistler, R. L., & Turner, E. S. (1955). Fine structure of starch granule sections. *Journal of Polymer Science*, *18*(87), 153–156.

Wrolstad, R. E., Decker, E. A., Schwartz, S. J., Sporns, P., Decker, E. A., & Schwartz, S. J. (2004). *Handbook of Food Analytical Chemistry, Water, Proteins, Enzymes, Lipids, and Carbohydrates* (1.ª ed.). Wiley-Interscience.

Wuttisela, K., Triampo, W., & Triampo, D. (2009). Chemical force mapping of phosphate and carbon on acid-modified tapioca starch surface. *International Journal of Biological Macromolecules*, *44*(1), 86–91.

Yu, X., Schmidt, A. R., Bello-Perez, L. A., & Schmidt, S. J. (2007). Determination of the Bulk Moisture Diffusion Coefficient for Corn Starch Using an Automated Water Sorption Instrument. *Journal of Agricultural and Food Chemistry*, *56*(1), 50–58.

Zhou, Q., & Cadwallader, K. R. (2004). Inverse Gas Chromatographic Method for Measurement of Interactions between Soy Protein Isolate and Selected Flavor Compounds under Controlled Relative Humidity. *Journal of Agricultural and Food Chemistry*, *52*(20), 6271–6277.

Zhou, Q., & Cadwallader, K. R. (2006). Effect of flavor compound chemical structure and environmental relative humidity on the binding of volatile flavor compounds to dehydrated soy protein isolates. *Journal of Agricultural and Food Chemistry*, *54*(5),

1838–1843.

Zimm, B. H., & Lundberg, J. L. (1956). Sorption of Vapors by High Polymers. *The Journal of Physical Chemistry*, *60*(4), 425–428.

ANNEX A

ANNEX B

ANNEX C

SCIENTIFIC PRODUCTION

National Events

Poster

I. Murrieta-Pazos, C. Gaiani, J. Scher. Cristallisation du lactose à la surface de poudres laitières à différentes humidités relatives. (2011), Colloque RP2E, Nancy, France.

Oral Communications

I. Murrieta Pazos, S. Patry, L. Galet, C. Gaiani, J. Scher. Comparative Study Of Particles Structure Evolution During Water Sorption In Different Size Class Of Durum Wheat Semolina, 2012, STP2012 – 7ème colloque Science et Technologie des Poudres 4 -6 juillet 2012- Toulouse (France).

International Congress

Poster

R. Hussain, C. Gaiani, P. Boyanova, **I. Murrieta Pazos**, P. Schuck and J. Scher, Relationships between morphology and rehydratation properties of milk powders, 2010, *Colloque de la FIL, Nouvelle Zélande*.

C. Gaiani, **I. Murrieta Pazos**, L. Galet and J. Scher, Relationships between surface composition and functional properties of food powders, 2011, *Colloque granulation, Suisse*

Oral Communications:

C. Gaiani, **I. Murrieta Pazos**, R. Hussain, P. Boyanova and J. Scher, Relationship between milk powders morphology and its rehydratation properties, 2011, *Colloque granulation, Suisse*.

I. Murrieta-Pazos, S. Patry, L. Galet, C. Gaiani, J. Scher. Development of a methodology to determine the gradient distribution of lactose, fat and proteins in milk powder particles. International Symposium on Spray Dried Dairy Products (IDF/INRA) 19-21 June 2012 in St Malo, France.

Written communications in international journals

C. Gaiani, P. Boyanova, R. Hussain, **I. Murrieta Pazos**, M.C. Karam, J. Burgain and J. Scher (2011), Morphological descriptors as a tool to better understand rehydratation properties of dairy powders, *International Dairy Journal*, 21:7, 462–469.

Murrieta-Pazos, I., Gaiani, C., Galet, L., Cuq, B., Desobry, S., Scher, J., (2011). Comparative study of particle structure evolution during water sorption: Skim and whole milk powders. *Colloids and Surfaces B: Biointerfaces* 87:1, 1–10.

Murrieta-Pazos I., Gaiani C., Galet L., Calvet R., Scher J. (2012). Composition gradient from surface to core in dairy powders: Agglomeration effect, *Food Hydrocolloids*, 26:1, 149-158.

Murrieta-Pazos, I., Gaiani, C., Galet, L., Calvet, R., Cuq, B., Scher, J., (2012). Food powders: Surface and form characterization revisited. *Journal of Food Engineering* 112:1-2, 1–21.

Murrieta-Pazos I., Galet L., Calvet R., Kaouach F., Gaiani C., Scher J. How to characterize reactive food powders: Particle shape and surface characterization of durum wheat semolina. Submission on December 2012.

Murrieta-Pazos I., Rolland C., Laurence G., Scher J. and Gaiani C. Energy Dispersive X-ray: Validation of the technique to characterize the surface composition of milk powders, Food Hydrocolloids. Development of a methodology to determine the gradient distribution of lactose, fat and proteins in milk powder particles by coupling EDX and XPS. Submission on December 2012.

Caractérisation de la forme et de la surface de poudres laitières et céréalières : Relations entre propriétés et réactivité des particules

Les travaux réalisés dans le cadre de la présente thèse se positionnent dans le contexte de la caractérisation des propriétés de surface des particules. La forme ainsi que les propriétés de surface sont fortement reliées aux propriétés fonctionnelles et à la réactivité des poudres alimentaires. Toutefois, le nombre de techniques disponibles pour l'étude et la caractérisation de la surface d'une particule alimentaire sont très réduites. Ainsi, l'objectif de ce travail a été de développer de nouvelles techniques et protocoles de caractérisation de la forme et de la surface des particules de poudre de lait et de semoule. L'objectif ultime est de mettre en relation les propriétés de surface et la réactivité des particules. Le fil conducteur de ce travail est une approche multi-échelle mettant en jeu différentes techniques d'analyse et de caractérisation. A l'échelle atomique, des techniques pour caractériser la surface et le cœur des particules par EDX ont été développées (permettant de sonder la particule à 1 µm de profondeur). L'adaptation de l'EDX couplé à l'XPS (5 nm de profondeur) permet de remonter à des valeurs de composition de surface (lactose, lipides, protéines) à partir des pourcentages atomiques. A l'échelle moléculaire, les gradients de composition par couplage de l'EDX et l'XPS ainsi que les différentes fractions de matière grasse (matière grasse libre, encapsulée et totale) ont été étudiés. En parallèle, un protocole de caractérisation a permis d'évaluer les propriétés de forme à l'aide d'un granumorpholomètre. L'énergie libre de surface a été déterminée par la CGI et la Monté Capillaire. Ces techniques novatrices dans le domaine des poudres alimentaires ont démontré leur intérêt. Finalement, à l'échelle de la microstructure, la modification de la surface par des contraintes externes a été étudié. Ainsi, les interactions particule/eau et la modification de la surface par enrobage à sec ont été étudiés Pour cela, des composants purs comme enrobant (carbohydrates ou protéines) ont été utilisés.

Mots clés : Réactivité, caractérisation de la surface, poudres de lait, semoule, XPS, EDX, CGI, Monté Capillaire.

Shape and surface characterization of milk and wheat powders: Relation between properties and reactivity of the particles

The work carried out on this PhD thesis is positioned in the context of the characterization of the food particle surface properties. The shape and surface characteristics are strongly related to the functional properties and reactivity of food powders. However, the number of techniques available, to perfrome the study and characterization of food particles surface is reduced. Thus, the objective of this work was to develop new techniques and protocols in order to characterize the shape and surface of milk powder and semolina particles. The ultimate goal is to relate the particle surface properties and reactivity. A multi-scale approach raised in this work involves different analytical techniques and characterization. At the atomic scale, techniques to characterize the surface and the heart of particles by EDX were developed (exploration of the particle at 1 micron depth). The adaptation of the EDX coupled to the XPS (5 nm depth) permit figure out the values of surface composition (lactose, fat, protein) from atomic percentages. At the molecular level, the composition gradients studied by coupling the EDX and XPS as well as different fractions of fat (fat free, encapsulated and total) were studied. In parallel, a characterization protocol was used to evaluate the shape properties using a granumorpholometer. The surface free energy was determined by IGC and Capillary rise. These innovative techniques in the field of food powders have demonstrated to be of interest. Finally,a at the microstructural scale, the surface modification by external contraints was studied. Thus, interactions particle / water and surface modification by dry coating, to do it, pure components as coating (carbohydrates or proteins) were used.

Keywords: reactivity, surface characterization, milk powder, semolina, XPS, EDX, IGC, Capillary Rice.

LIST OF EQUATIONS